

Finite element modelling of open longitudinal stiffener to crossbeam connection in OSD bridges for hot-spot stress determination

Sayantana Pandit

Student number: 4770455

Master thesis: CIE 5060-09

Key words: Fatigue, Hot-spot stress, FEM, OSD

Cover Image - Haringvlietbrug: <http://www.haringvlietbrug.nl/>



Finite element modelling of open longitudinal stiffener to crossbeam connection in OSD bridges for hot-spot stress determination

by

Sayantan Pandit

to obtain the degree of Master of Science in Structural Engineering
at the Delft University of Technology,
to be defended publicly on Monday August 17, 2020 at 2:00 PM.

Student number: 4770455
Thesis duration: November 1, 2019 – August 17, 2020
Thesis committee: Prof. dr. ir. M. Veljkovic, TU Delft, Chairman Steel and Composite Structures
Dr. ir. J. H. den Besten, TU Delft, Committee Member
W. Wu, MSc TU Delft, Supervisor
Prof. dr. J. Maljaars, TNO, Committee Member
ir. B. Wijnbeld, Rijkswaterstaat, Supervisor

An electronic version of this thesis is available at <http://repository.tudelft.nl/>.



Rijkswaterstaat
Ministry of Infrastructure
and Water Management



TNO innovation
for life

Preface

The following report serves as a representation of the outcome of 10 months of work towards completion of the master thesis project (CIE 5060-09). It encapsulates the graduation research to finish my master study in structural engineering with steel structure specialisation at the Delft University of Technology, Netherlands. The phenomenon of fatigue is an on-going problem for a lot of bridges in The Netherlands. Thus, I developed an interest to investigate this topic further during my master thesis. This report consists of a research investigation on fatigue behaviour of one of the important details of orthotropic steel deck (OSD) bridges. This detail is a longitudinal open stiffener to crossbeam joint at the location of a cope hole. The satisfaction and euphoria on the successful completion of any task would be incomplete without mentioning the names of people who made it possible to do so. All the members of my graduation committee have been extremely supportive during my entire journey. Their constant guidance and encouragement crowned my efforts with success. I would like to use this brief section as an opportunity to express my sincere gratitude.

I am grateful to the Department of Civil Engineering and Geo-sciences, TU Delft, for giving me the opportunity to execute this research, which is an integral part of the curriculum of master of science program. I want to extend my deepest sense of gratitude to the chairman of Steel and Composite Structures, Prof. dr. ir. Milan Veljkovic, who despite being extraordinarily busy with his duties, took out the time to guide me on the right path throughout this project. His critical reviews have enormously assisted this research.

I would like to thank ir. Bas Wijnbeld for giving me the opportunity to work with Rijkswaterstaat on such an amazing research project. His knowledge and experience regarding fatigue has helped me learn a lot from his guidance. I am also very thankful to all the employees of the Steel Department of Rijkswaterstaat (GPO) for their constant encouragement, invaluable advice and inspiration. I am indebted to Prof. dr. Johan Maljaars from TNO, for the valuable time which he has spared for me during his work. His comments and feedback have helped me understand the critical aspects of fatigue and finite element modelling. I am also thankful to the employees of TNO for their advice and support throughout the duration of the graduation project. Overall, it was a great experience for learning and professional development. I am grateful for having a chance to work and meet with wonderful professionals who led me through this task.

It is my radiant sentiment to place on record my best regards to Weijian Wu, who was my daily supervisor from TU Delft, for his continuous encouragement and active supervision. He was always available to discuss about past research and intricate details of finite element modelling during the ideation phase of the thesis. Furthermore, I would like to thank Dr. ir. Henk den Besten who has also been extremely supportive throughout the course of the project with his creative suggestions. He always made sure that I am able to defend my work which has been instrumental to my growth as a professional. I am also grateful to work together with two other MSc students, Dennis van der Ende from TU Delft and Navid Nikraftar from TU Eindhoven. Their guidance and support regarding finite element modelling had a positive impact on my research.

I take this opportunity to express my regards to my mother Mrs. Sangita Pandit and my father Mr. Paritosh Pandit for educating me in all aspects. I will never forget the unconditional love and support from all the members of my family. I would also like to thank all my friends for their constant encouragement and motivation. Last but not the least, I would like to thank my good friend Srishti for making my masters journey a memorable one.

*Sayantana Pandit
Delft, August 2020*

Nomenclature

2D	Two-dimensional
3D	Three-dimensional
ABS	American Bureau of Shipping
CAFL	Constant Amplitude Fatigue Limit
CV	Coefficient of variation
DNVGL	Det Norske Veritas Germanischer Lloyd
DNV	Det Norske Veritas
FEA	Finite Element Analysis
FEM	Finite Element Method
FE	Finite Element
HAZ	Heat Affected Zone
HCF	High Cycle Fatigue
IIW	International Institute of Welding
LCF	Low Cycle Fatigue
LEFM	Linear Elastic Fracture Mechanics
OSB	Orthotropic Steel Bridge
OSD	Orthotropic Steel Deck
PDE	Partial Differential Equations
RP	Reference Point (ABAQUS®)
RWS	Rijkswaterstaat
SCF	Stress Concentration Factor
SD	Standard Deviation
SHSS	Structural Hot-Spot Stress
TNO	Toegepast Natuurwetenschappelijk Onderzoek (English: Netherlands Organisation for Applied Scientific Research)

Summary

The phenomenon of fatigue in orthotropic steel deck (OSD) bridges is a predominant problem because of complexity of the prediction methods. In the past, many researchers have studied the fatigue behaviour of various details in OSDs via both experiments and Finite Element Modelling (FEM). In the present research, the connection of open stiffener to crossbeam at the location of cope hole in OSDs has been studied. Structural hot-spot stress method using surface stress extrapolation has been used to investigate the cracks in stiffener in the longitudinal direction and cracks in crossbeam.

FEM is extensively used for analysing OSDs. In engineering applications, 2D shell elements are widely used instead of 3D solid elements for analysis due to less computational cost. The welds are generally not modelled with shell elements for fatigue assessment of welded structures. In this study, large difference of SHSS is obtained by shell and solid elements for both simple and complex fillet welded details and also for the OSD. This difference in structural hot-spot stress (SHSS) is reduced by the application of three weld modelling techniques with shell elements: (i) the IIW approach [28], (ii) the Eriksson's approach [20] and (iii) a combination of IIW and Eriksson's approaches. All the three methods are based on increasing the thickness of shell elements at the weld region which are easy to be applied in practice. The dependence of SHSS on mesh size and element type is also investigated in this thesis.

A parametric study is performed first on simple and then on complex fillet welded details to check whether the weld modelling technique can be applied to different geometries, loading and boundary conditions. The solid element model of the complex detail is first validated with experimental strain measurements. Then, SHSS values from other numerical models are compared with the solid model. Representative load cases are investigated initially followed by load combinations. The weld modelling method with shell elements gives good consistency in the ratio of hot-spot stress compared to the solid element model for these details. The deformations are also investigated for all load cases and load combinations. The combined weld modelling technique (iii) with shell elements replicated the weld stiffness of the solid model for both in-plane and out-of-plane load cases.

As a final step in checking the consistency of SHSS ratios between shell elements with welds and solid elements in the application of OSD, a parametric investigation is performed. This study involved two geometric variants of OSD with different load positions. These two variants were based on the design of existing bridges in The Netherlands with relatively thin plate and newly designed ones with thicker plates. The parametric study is divided into two parts. The first part is based on representative load cases. The second part is based on SHSS influence lines for determination of critical loading positions having maximum and minimum hot-spot stress. For both these studies, the weld modelling approaches with shell elements gave a good match of SHSS compared to the solid models. The SHSS results from the shell model with weld are more consistent compared to the regular shell model without weld. From the preliminary parametric study on OSD, it is found that after weld modelling with shell elements using the combined approach of IIW [40] and Eriksson [20], less scatter is observed in the SHSS ratios. The coefficient of variation (CV) in SHSS ratio for crossbeam is **6.8%** and that for stiffener is around **5.1%** which is low. The SHSS values are computed based on the stress perpendicular to weld toe. From the detailed parametric study, the mean value of SHSS ratio is **1.07** (range: **0.99-1.15**) for the crossbeam and **1.02** (range: **0.98-1.10**) for the stiffener. The CV of SHSS ratio is **5.4%** for the crossbeam and **4%** for the stiffener. The stress profiles are also investigated at the critical locations of OSD. The shell model with the combined weld modelling approach is in good agreement with not only SHSS but also with the stress at a distance far away from the stress concentration when compared to the solid model. The deformations are also very similar for both the numerical models. Thus, it is concluded that the combined weld modelling technique using the IIW [40] and the Eriksson's [20] approach with shell elements could be used for accurate fatigue life assessment using hot-spot stress method where the measure of accuracy is with respect to the solid element model.

Contents

Summary	iii
1 Introduction	1
1.1 Background	2
1.2 Problem statement	2
1.3 Motivation	3
1.4 Aim of the thesis	4
1.5 Research question and research objectives	4
1.6 Scope and limitations.	5
1.7 Methodology	5
1.8 Thesis outline	6
2 State-of-the-art (Literature Review)	7
2.1 Behaviour of OSD with open stiffeners	8
2.2 Introduction to fatigue	9
2.3 S-N curves	10
2.4 Detail categories	12
2.5 Stress based fatigue assessment methods	15
2.5.1 Nominal stress method.	16
2.5.2 Structural hot-spot stress (SHSS) method	16
2.5.3 Effective notch stress method	24
2.6 Comparison of the fatigue assessment methods	24
2.7 Finite element method (FEM)	27
2.8 Past research on shell and solid element modelling of OSDs	32
2.9 Fatigue load models (FLM) according to EN 1991-2	35
2.10 Residual stresses.	36
2.11 Fatigue life prediction.	37
2.12 Partial safety factors	37
3 Simple fillet welded details	38
3.1 Single side fillet welded longitudinal plate joint (T-joint)	39
3.1.1 Numerical investigation from the research of Śledziewski (2018)	39
3.1.2 Geometry	39
3.1.3 Material properties	40
3.1.4 Stress extraction path and coordinate system	40
3.1.5 Loading and boundary conditions	40
3.1.6 Numerical modelling	41
3.1.7 Mesh sensitivity study for tension load case	44
3.1.8 Element type study for tension load case	46
3.1.9 Linear and quadratic extrapolation for tension load case.	46
3.1.10 Numerical model validation for tension load case.	47
3.1.11 Parametric study for tension load case	48
3.1.12 Mesh sensitivity for bending load-case	48
3.1.13 Element type study for bending load-case	49
3.1.14 Linear and quadratic extrapolation for bending load case	50
3.1.15 Parametric study for bending load case.	51
3.2 Double side fillet welded transverse plate joint (cruciform joint)	52
3.2.1 Experimental investigation of Karabulut and Lombaert (2020).	52
3.2.2 Numerical investigation of Karabulut and Lombaert (2020)	52
3.2.3 Numerical modelling in the current report	53

3.3	General findings	57
4	Complex fillet welded details in steel bridges	58
4.1	Experimental investigation of complex detail from the research of Akhlaghi (2009)	59
4.2	Numerical investigation of complex detail from the research of Akhlaghi (2009)	60
4.3	Geometry	61
4.4	Strain gauge location and placement	61
4.5	Material properties	62
4.6	Loading and boundary conditions	62
4.7	Finite element modelling	63
4.8	Modelling with solid elements	63
4.9	Measurement of SHSS from the experiments.	66
4.10	Calculation of SHSS from the solid element model.	66
4.11	Modelling with shell elements	67
4.12	Comparison of SHSS with numerical results of Akhlaghi (2009).	69
4.13	Shell elements including weld geometry	69
4.14	Numerical models subjected to different load cases	70
5	Parametric analysis of fillet welded transverse and longitudinal cruciform joint	74
5.1	Motivation	75
5.2	Weld modelling with increased thickness method	75
5.3	Numerical models of fillet welded cruciform joint	75
5.4	Parametric study on transverse fillet welded cruciform joint based on the dimensions of OSD	77
5.5	Parametric study on fillet welded longitudinal cruciform joint based on the dimensions of OSD	82
6	Parametric analysis of OSD	86
6.1	Motivation	87
6.2	Geometrical variants for the parameter model	87
6.3	Material properties and boundary conditions	87
6.4	Load cases for preliminary parametric study	88
6.5	Global shell model	89
6.6	Sub-solid model	90
6.7	Global mesh - shell	91
6.8	Local mesh - shell and solid	91
6.9	Procedure for parametric study including influence lines.	94
6.10	Weld modelling with shell elements for the OSD	96
6.11	Mesh sensitivity study of the OSD variants	97
6.12	Multi-axial stress state in fatigue assessment.	98
6.13	Numerical analysis of OSD	100
6.13.1	Nominal stress determination using three axle loads (six load patches).	100
6.13.2	Preliminary parametric study on OSD	102
6.13.3	Main parametric study (Influence lines of SHSS for light OSD variant)	106
6.13.4	Main parametric study (Influence lines of SHSS for heavy OSD variant)	109
6.14	Determination of critical points based on axle load paths 1, 2 and 3.	111
6.14.1	Critical points for light OSD variant based on S11	112
6.14.2	Critical points for heavy OSD variant based on S11	113
6.15	Calculation of statistical parameters.	117
7	Results and Discussion	119
7.1	Results and discussion.	120
8	Conclusions and Recommendations	123
8.1	Conclusions.	124
8.2	Recommendations	125

A	Deformed mesh for shell and solid element models	126
A.1	Deformed mesh for shell models for different load cases	127
A.2	Deformed mesh for solid models for different load cases	128
B	Mesh and element sensitivity study for simple fillet welded details	129
B.1	Fillet welded T-joint	130
B.2	Fillet welded cruciform joint	133
C	Mesh and element sensitivity study for complex fillet welded details	134
C.1	Detail of open-stiffener to crossbeam connection with a cope hole	135
D	Mesh and element sensitivity study of the OSD	137
D.1	Mesh sensitivity study on geometry variant-1 (based on old/light OSD)	138
D.2	Mesh sensitivity study on geometry variant-2 (based on new/heavy OSD)	139
E	Validation of numerical models	141
E.1	Strain validation of detail of open stiffener-crossbeam with a cope hole.	142
F	Verification of finite element models	143
F.1	Calculation of stresses and beam deflections for verification of FE model of the complex welded detail	144
F.2	Verification of finite element model	147
G	Calculations for nominal stress method	148
G.1	Fatigue life assessment based on nominal stress method for complex welded joint	149
H	SHSS based on maximum principal stress for OSD	155
H.1	Study on reference load cases LC1, LC2, LC3a and LC3b	156
H.2	Critical points for light OSD variant based on maximum principal stress	158
H.3	Critical points for heavy OSD variant based on maximum principal stress	160
I	Contour plots	163
I.1	Fillet welded T-joint loaded in tension	164
I.2	Fillet welded T-joint loaded in bending	165
I.3	Fillet welded cruciform joint loaded in tension.	166
I.4	Detail with deck plate, crossbeam and open-stiffener with a cope-hole	168
I.4.1	Stress contour plots of the numerical models	168
I.4.2	Deformation contour plots of the numerical models	169
I.5	Fillet welded transverse and longitudinal cruciform joint	170
I.5.1	Transverse cruciform joint	170
I.5.2	Longitudinal cruciform joint.	171
I.6	Orthotropic steel deck parameter model variant - 1 (based on old OSD)	172
I.6.1	Deformed mesh of shell and solid models	172
I.6.2	Stress contour plots of shell and solid elements	173
I.6.3	Deformation contour plots of shell and solid elements	173
J	Further investigation of out-of-plane bending	175
J.1	Double side fillet welded transverse cruciform joint.	176
J.2	OSD.	178
K	Other weld modelling approaches with shell elements	180
K.1	New approach of weld modelling with shell elements	181
K.2	Tabulated results	184
	Bibliography	185

1

Introduction

“You have to learn the rules of the game. And then you have to play better than anyone else.”

Albert Einstein

This chapter comprises the introduction to orthotropic steel deck (OSD) bridges, fatigue and the challenges in finite element modelling (FEM) due to the complex geometry and load carrying mechanism of such bridges. It also encapsulates the motivation behind this MSc thesis. Moreover, the problem definition, goal, research questions, scope, methodology and outline of the thesis are also described in this chapter.

1.1. Background

Orthotropic Steel Deck (OSD) bridges consist of a thin deck plate, supported by main girders, longitudinal stiffeners and transverse stiffeners. All these components are connected to each other by welding. The deck plate thus performs both the function of bearing the loads from the vehicles and contributing to the entire load-bearing behaviour of the bridge. The orthotropic steel deck is generally supported on cross girders which in turn are supported on main girders. In general, OSDs have different stiffness characteristics in two different directions - transverse and longitudinal [15]. Thus they are also known as an orthogonal anisotropic steel deck or in short ortho-tropic steel deck [5]. The longitudinal stiffeners, also known as longitudinal ribs, provide support to the deck plate. They also increase the flexural rigidity of the cross section of the OSD and help in distributing the load to the transverse crossbeams. The longitudinal stiffeners can be classified as continuous and discontinuous in terms of placing. The continuous longitudinal stiffener passes through the crossbeam whereas the discontinuous longitudinal stiffener ends at the crossbeam. The longitudinal stiffeners can be categorised as of two types based on shape. These are open stiffeners and closed stiffeners as displayed in Figure 1.1.

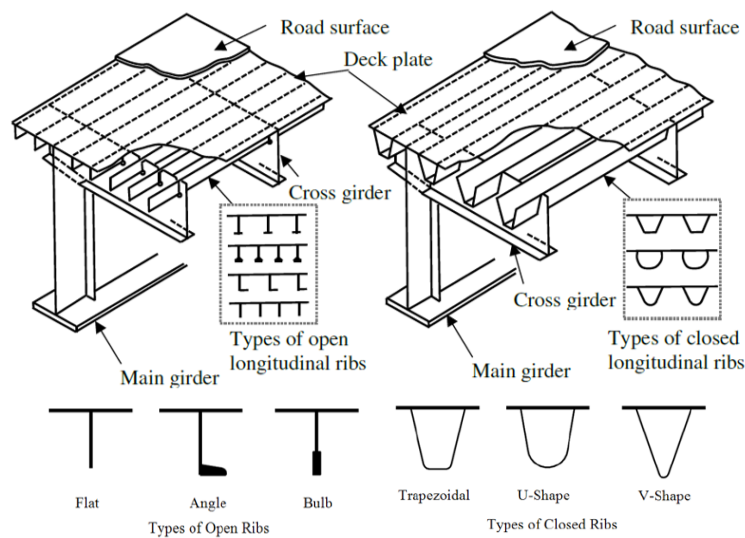


Figure 1.1: Types of longitudinal stiffeners [32]

The crossbeam acts as a transverse stiffener. It is an inverted T-section, which is welded to the deck plate. The crossbeam does not have a separate top flange as the deck plate acts as its top flange. The load is transferred by the crossbeam transversally to the main girders. The crossbeam also provides support to the longitudinal stiffeners and often have cut-outs for the continuous longitudinal stiffeners [5].

OSDs have several advantages like low weight, speedy erection and high load carrying capacity and thus it makes them suitable for movable and long-span bridges. Nowadays, all the bridges are designed using computer softwares containing finite element packages. However, analysis of orthotropic steel deck bridges implies some understanding especially since it involves finite element modelling (FEM). The complex geometry and load transfer mechanism of OSD bridges results in difficulties in estimation of correct fatigue resistance of certain connections. Moreover, bridge deck connections having cut-out holes increases the complexity of OSDs [14]. Despite all the advantages, there are some limitations in the use of an OSD. The main reason is due to its fabrication cost and also due to the amount of welding it involves which results in high manufacturing cost. These deck connections have been prone to fatigue problems.

1.2. Problem statement

In the early years of development of OSD, open-stiffener decks were used widely on highway bridges in Europe. After the Second World War (1945), an increase in the production of OSD started in The Netherlands [34]. The open stiffener or open-ribbed decks generally have simple connections. The stiffeners are easy to fabricate, install and weld.

In The Netherlands, fatigue cracks have been observed in the deck plate at the intersection with the trough stiffener and the cross-beam web in a number of the bridges that were constructed between 1960 and 1990 [35]. Cracks have also been observed at the connection of the stiffener and crossbeam with a cope hole [34]. Since then, the traffic load has increased in terms of weight and number of vehicles. In addition, the wheel configuration has changed due to the use of single, heavily loaded wheels instead of twin-wheel systems. This was not anticipated in the design. Several cracks have been found in many OSD bridges in The Netherlands like Galecopperbrug and Van Brienoordbrug [32]. These cracks have occurred due to the fatigue phenomenon. The cracks in OSD which are most representative and the ones which are widely investigated are present in the following locations [34]:

- The deck-stiffener connection, between or at the crossbeams.
- The connection of the stiffener with the crossbeam, with or without cope holes.
- The splice welded joint of the stiffeners.

This thesis focuses on the connection between the open stiffener and crossbeam at the location of a cope hole. Only the cracks which can occur at this location are further investigated in the following chapters. The objective of this thesis is to find the structural hot-spot stress (SHSS) in the vicinity of the longitudinal open stiffener to crossbeam connection of OSDs using Finite Element Method (FEM), in order to find an accurate approach for engineering calculations. Figure 1.2 shows the critical crossbeam-stiffener locations which are prone to fatigue cracking in OSDs.

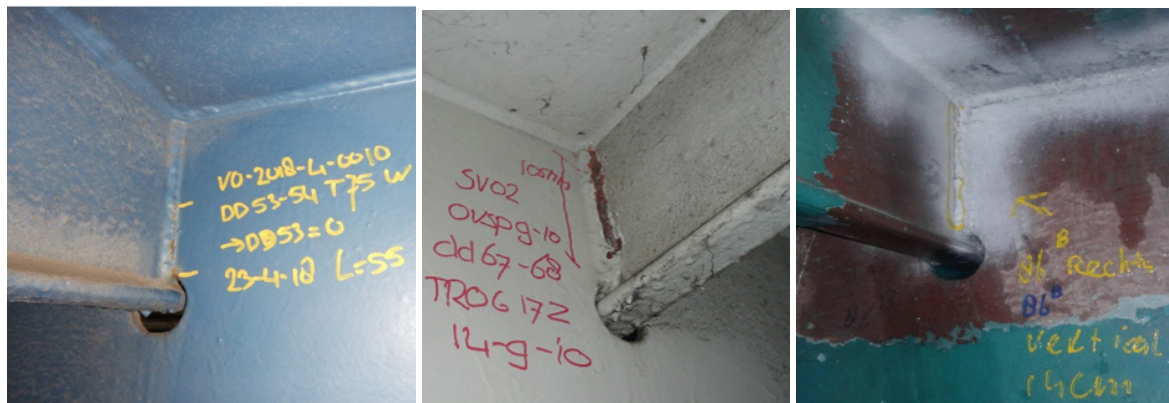


Figure 1.2: Fatigue cracks at intersection between longitudinal open stiffeners and crossbeams (Picture: Rijkswaterstaat)

Currently, Rijkswaterstaat and TNO are doing research to improve the current version of the Eurocode 3 (EN 1993-1-9, fatigue design of steel structures) [2]. Specific attention is paid to Table 8.8 and 8.9 in which the different detail categories of the orthotropic steel deck with open and closed stiffeners are given. Their goal is to provide an updated version of these tables at the next Eurocode revision. The requirements for shell and solid element modelling will be given in the new version of Eurocode 3.

1.3. Motivation

In engineering applications, shell elements are most widely used. This is because the modelling effort and computational power required by application of shell elements is less than that compared to solid or volume elements. The use of solid elements for modelling give more accurate results as they replicate the real structural behaviour better than shell elements. However, the computational effort will increase significantly if the entire numerical model has to be made by using volume elements as illustrated by Zhang and Shao [53]. Thus, there is an urgent need to find the SHSS in the vicinity of the longitudinal open stiffener to crossbeam connection of OSDs using shell elements, in order to find an accurate approach for engineering calculations. It is recommended in Eurocode 3 [2] that the calculation of stress for fatigue assessment using nominal stress approach should be based on combination of direct and shear stresses in the web of the crossbeam considering the net cross section of the beam. According to EN 1993-1-9, Table 8.9 [2], a nominal stress range of 56 MPa is recommended for the connection between continuous longitudinal open stiffeners and crossbeam.

However, recent fatigue tests performed by Aygül, Al-Emrani and Urushadze [14] have shown that test results produced by the structural hot-spot stress (SHSS) and effective notch stress approach had a good agreement with the recommended S–N curves. According to their research, the nominal stress approach overestimated the fatigue life of the test specimens, thereby producing results that were on the unsafe side. For the investigation of the fatigue behaviour of complex details in OSD, a more accurate method to find SHSS with shell elements should be proposed. Since SHSS approach involve FEM, there is a concern regarding the reliability of the use of 2D shell finite elements against 3D solid finite elements for accurate stress prediction in the critical welded connections.

Different design standards and research studies have different approaches to determine the SHSS for fatigue assessment. In all the design standards, t is taken as the thickness of the investigated plate. The DNV (2011) [3] and DNVGL (2016) [6] recommend the use of 20-node quadratic solid elements having size of $(t/2 \times t/2)$ or 8-node quadratic shell elements having size of $(t \times t)$ for finding SHSS. The maximum principal stress is to be linearly extrapolated from two reference points ($t/2$ and $3t/2$) in order to calculate the SHSS (DNV (2011) [3]). Fricke, Petershagen and Paetzold (1998) [24] recommend the use of 20-node quadratic solid elements having size equal to the plate thickness (t) at the hot-spot region. They also recommend using at least three elements of equal length in the region where stress increases. The component stresses normal to the weld are to be quadratically extrapolated using the three elements to determine the SHSS. The ABS (1992) [1] recommends 20-node quadratic solid elements or 8-node quadratic shell elements to be used with a size of $(t \times t)$ for finding SHSS. The maximum principal stress is to be linearly extrapolated from two reference points ($t/2$ and $3t/2$), to find the hot-spot stress. The recommendations of the IIW (Hobbacher (Ed) 2009) [28] covers the current method of using SHSS approach involving the most economic and coarser meshing in the numerical model. A. Hobbacher [28] recommends using the maximum principal stress for calculating the SHSS in uni-axial stress condition.

1.4. Aim of the thesis

The goal of this thesis is to find a consistent method to obtain the stress range from shell element model with good agreement with values from solid element models which is attractive in practical design and analysis. The aim of the research is summarised in the following points:

- To find the parameters which affect the hot-spot stress of open rib to crossbeam joint in OSDs.
- To find simple, yet accurate modelling techniques with shell elements for finding the SHSS.
- To find the critical positions of the open stiffener-crossbeam connection in an OSD based on maximum and minimum hot-spot stress.
- To investigate the influence of loading and geometry on the hot-spot stress at the critical locations of OSD.

The outcome of this thesis can be helpful for developing a suitable methodology for hot-spot stress calculation of open rib-to-crossbeam welded connections using shell elements. The foreseen deliverable to be presented at the end of the thesis are some recommendations for numerical modelling with shell elements at the investigated connection. This will be followed by a discussion on the accuracy of the developed shell element modelling.

1.5. Research question and research objectives

The main objective of this research is to develop a numerical model with shell elements such that it can give a consistent ratio of hot-spot stress compared to solid elements for complex details of OSD. In order to investigate suitable ways of approaching the complexity of determining SHSS using shell elements, an effort is made to answer the following research question:

What is the most consistent method for finding the stress range for fatigue assessment using shell elements compared to the hot-spot stress range using solid elements in modelling the connection between the open stiffener and crossbeam with a cope hole in OSD bridges?

While answering the main research question, several sub-research questions should be answered which are as follows:

- Where are the critical positions of the open stiffener-crossbeam connection in an OSD?
- What is the influence of the effect of loading (load positions) and geometry (thickness of the components) on the stress ranges at the hot-spot location of the open stiffener to crossbeam welded connections?
- What is the difference between the ratio of SHSS obtained from the solid elements and the SHSS obtained from shell element models in the investigated connection, based on the different loading positions and plate thicknesses?
- How can the accuracy of shell element modelling be improved in terms of hot-spot stress calculation?

1.6. Scope and limitations

The scope of this master thesis centres around the connection between open longitudinal stiffener and crossbeam at the location of a cope hole. The fatigue life assessment will be based on the structural hot-spot stress (SHSS) method calculated by surface extrapolation. The fatigue cracks observed in the following locations have been studied in detail: crack longitudinally in open stiffener and crack in crossbeam [14] both starting from weld toe. Two geometrical variants will be investigated: one based on old OSD design which is light and the other based on new OSD design which is heavy. The dimensions of these two variants will be different. This report limits in surface stress extrapolation approach for calculation of SHSS in the aforementioned connections. It is believed that solid element modelling with welds included, is the most accurate modelling approach with surface stress extrapolation. Different shell element modelling techniques are used and the SHSS results are compared with the corresponding solid element model. The idea is to find a consistent method for getting the stress range from a shell element model and relate it to the structural stress range from a sub-solid element model.

1.7. Methodology

In the first part of this thesis, two different simple fillet welded details are investigated with different type of elements (linear and quadratic; full and reduced integration) and mesh densities. The first welded detail modelled is a single side fillet welded longitudinal plate joint (also called a longitudinal T-joint) subjected to tension and bending load cases. The second one is a double side fillet welded transverse cruciform joint. Numerical models with shell and solid elements are developed for these details. The stress gradients are studied for all the numerical models. The goal of this study is to find consistency in the ratio of SHSS of shell to that of solid for simple details. Another goal is to find specific cases where the shell element model is not feasible for calculating the SHSS.

In the second part, some complex welded details are investigated with different types of elements (linear and quadratic; full and reduced integration) and mesh densities. The solid model made for this reference detail is first validated with experimental strain measurements. After validation, the solid model is chosen as a reference for comparison of SHSS with other the numerical models.

In the third part, the aspect of weld modelling with shell elements is investigated in the form of a detailed parametric study. This study is performed on a double side fillet welded transverse and longitudinal cruciform joint. The increased thickness method of weld modelling with shell elements from the IIW guidelines [28], the Eriksson's method [20] and the combined approach is studied for some reference load cases. The comparison is made based on the ratio of SHSS of shell to that of solid. The investigation is also extended for a combination of load cases in later sections.

In the final part, a parametric analysis is performed on an OSD based on realistic bridge dimensions. The influence of geometry and position of loading are investigated to check its effect on the ratio of SHSS. The critical locations are determined from SHSS influence lines using the DLOAD subroutine in ABAQUS. The objective is to find a consistent ratio of SHSS of shell to that of solid for two geometric variants of OSD using weld modelling with shell elements.

1.8. Thesis outline

In order to approach the main goal of this research project, it is essential to divide the workflow into distinctive parts. Hence, the chapters are categorised based on the numerical models and their contents are discussed below.

- **Chapter-1** consists of an overall introduction to the master thesis.
- **Chapter-2** encapsulates the state-of-the-art (literature study) for this master thesis. It highlights the past research related to the fatigue behaviour of an open-ribbed OSD subjected to loading. The background of fatigue and fatigue crack initiation is also provided. It also gives an overview of different approaches to calculate the hot-spot stress at the critical locations.
- **Chapter-3** highlights the behaviour and working with shell and solid element models for some simple fillet welded details. It mainly focuses on numerical modelling of simple fillet welded details. Also, some aspects regarding the details which cannot be modelled properly with shell elements have been provided. Two types of details have been investigated in this chapter: single side fillet welded longitudinal plate joint (detail type a) and double side fillet welded transverse cruciform joint (detail type b). The details of geometry for these two joints have been obtained from literature.
- **Chapter-4** covers the behaviour and working with shell and solid element models for some complex fillet welded details in steel bridges. The solid element model of the reference detail is first validated with respect to the experimental strain measurements. The hot-spot stresses are then obtained using the solid element models. Furthermore, shell element models with welds are also developed and investigated. The main focus is on the ratio between the hot-spot stress obtained from the shell and solid elements. Some more numerical models have been developed and these models are investigated with different load cases in order to study the behavioural difference between shell and solid elements in terms of stresses and deformations.
- **Chapter-5** highlights an elaborate parametric study of a fillet welded longitudinal and transverse cruciform joint. In addition to the shell and solid models, the shell model incorporating welds using the increased thickness method is investigated. The increase of thickness of plate along the weld region is done using three different approaches: the Eriksson's approach [20], the approach given by the IIW recommendations [40] and a combination of these two approaches. The purpose of this study is to obtain consistency in the ratio of calculated SHSS values from shell elements to that from solid elements for this particular detail.
- **Chapter-6** provides a complete parametric study of a bridge deck based on realistic dimensions of bridges in The Netherlands. This chapter contains a preliminary and a detailed parametric investigation on two geometric variants of OSD. The main regions of interest is based on two types of cracks on the investigated detail: crack in crossbeam and crack in open stiffener as had been discussed in Chapter-1. In the first section, a preliminary parametric investigation is performed on the OSD for some reference load cases. The SHSS is calculated based on the stress perpendicular to weld toe and then compared between the numerical models. In the detailed parametric study, SHSS influence lines are computed for six different numerical models which are investigated in this study. The same procedure is applied both for the light and heavy OSD variants. In addition to this, the critical points having maximum and minimum SHSS are investigated for all the numerical models. The statistical components like the mean and coefficient of variation are also obtained for the SHSS ratios from the parametric study.
- **Chapter-7** presents the explanation of results obtained from the numerical analyses.
- **Chapter-8** contains a set of conclusions drawn from this research and corresponding answers to the research questions. In addition, some recommendations for further research are presented.
- **Appendices A-K** contain all the additional work encompassing detailed explanation of the chapters in this thesis.

2

State-of-the-art (Literature Review)

“Learn from yesterday, live for today, hope for tomorrow. The important thing is not to stop questioning.”

Albert Einstein

This chapter highlights the past research related to the fatigue behaviour of an open-stiffener OSD subjected to loading. At first, the background of fatigue and fatigue crack initiation is given. Previous studies on various stress based fatigue assessment methods are included and critically synthesised. More emphasis is given to the hot-spot stress method and the available recommendations from codes or standards. An overview of different approaches to calculate the hot-spot stress at the critical locations having maximum stress concentration is provided. Past research on the application of shell and solid elements, have been compiled elaborately. At the end of this chapter, some insights regarding fatigue damage calculation and residual stresses have been presented. Thus, an encapsulation of all the information retrieved from the literature research is documented in this chapter.

2.1. Behaviour of OSD with open stiffeners

The orthotropic steel deck (OSD) is composed of different parts. Each of these parts behave in a different manner when they are subjected to traffic loading. Thus, a design check of each and every component is very important. The OSDs deform during traffic loading. This results in occurrence of axial forces, bending moments and shear forces in the system as shown in Figure 2.1 [13]. For such a system, the loads are generally transferred from deck plate to crossbeams and finally to main girders. The load transfer in the crossbeam develops internal forces: shear forces and bending moments, under the in-plane crossbeam behaviour. The out-of-plane crossbeam behaviour is caused due to local bending and torsion as the stiffeners rotate with the deformation of the crossbeam under traffic loads [13]. The in-plane and out-of-plane behaviour strictly depends on the position of the traffic loads. A cope hole is usually present in the crossbeam to make the manufacturing process easier.

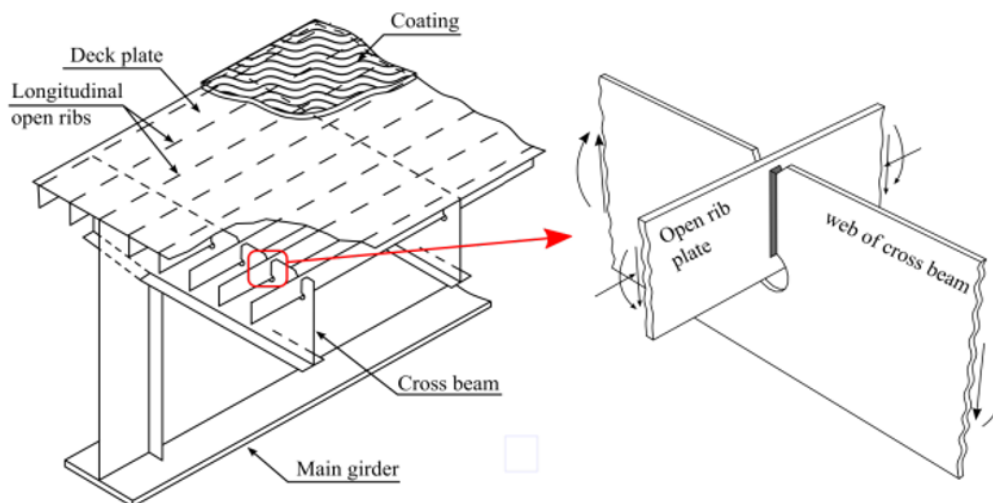


Figure 2.1: Left: Different parts of an OSD with open stiffeners, Right: Internal forces in the web of crossbeam and stiffener [13]

The longitudinal stiffeners can be open or closed shaped. There are many reasons for the application of closed stiffeners. For example, the cost also plays an integral role in the choice of stiffener type. Closed stiffeners are sometimes used when there is a requirement of torsional rigidity in bridges. Open stiffeners generally have a height of a maximum of 200-220 mm and a thickness of 8-12 mm. In The Netherlands, most bridges with open stiffeners generally have a height of 160 mm with a thickness of 8 mm. Newer bridges are designed in with thicker open stiffeners having a height of 220 mm and a thickness of 10 mm. The stiffener webs are generally connected to the deck plate with fillet welds along both sides. They are aligned in the longitudinal direction and can be continuous or dis-continuous through the crossbeam. The spacing between the webs is usually around 300 mm for open stiffeners [34]. This is the required criteria of having accessibility for welding, leading to easier maintenance and a good quality of work. The strength of the deck plate assembly with open stiffeners is sufficient to allow the crossbeams to have a spacing of 2000 mm [34].

Bulb and flat stiffeners pass the crossbeam through a slot with a cope hole. Angle stiffeners pass through a cut-out [34]. Misalignment is an important issue which stiffeners placed between crossbeams usually suffer from. This makes them more susceptible to fatigue [34]. Open-ribbed OSDs were originally used in the ship building industry. Open-ribbed decks without cope-holes have better fatigue performance compared to closed-ribbed decks as was revealed from the studies of Wolchuk [45] and Wolchuk and Ostapenko [46]. However, open-ribbed decks with cope-holes have a different behaviour as these cause high local stress concentrations which was observed from the study of Miki [37].

Cope holes are usually provided for the joints between crossbeams and longitudinal ribs in order to get accessibility to the crossing welds. However, from the study of Miki and Tateishi [37], it was found that shear deformation resulted in high local stress concentration in these cope hole regions of details in

I-section beams which were loaded in-plane. This caused reduction of the fatigue strength. According to the research of Miki [37], the local stresses were greatly increased when the shear deformation was induced in the gap of flange plate inside a cope hole. The crack locations observed by Miki and Tateishi [37] from their study are shown in Figure 2.2. Thus, it was established that the assessment of fatigue strength of such welded details with cope holes involve the consideration of shear stresses. Kolstein [32] stated that a cope hole in the crossbeam at the stiffener-to-deck plate connection should be avoided. Yokozeki and Miki [50] [51] concluded that the elimination of the cope holes in the crossbeam reduced the hot-spot stress ranges at the intersection between longitudinal stiffeners and crossbeam. In this thesis however, the details with cope holes is investigated further. This is because most the existing bridges in The Netherlands have cope holes.

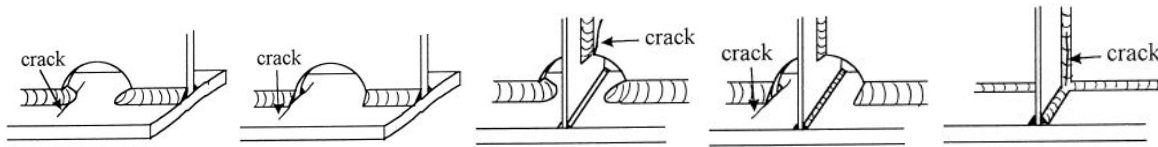


Figure 2.2: Fatigue cracks observed for cope hole details existing in I-beam sections [37]

The numerical study of Śledziewski [55] suggested that as the ratio of shear stress to bending stress (τ/σ) increases, there is a rise in local stress concentration within the cope hole region. Change of shape and dimensions of hole also affect the improvement of fatigue strength of such a joint [55]. From the fatigue tests performed by Fryba and Gajdos [25] on open stiffener OSDs, it was concluded that apple-shaped cut-outs have better stress distribution compared to normal cut-outs when the detail is subjected to bending load. For specimens loaded under tension apple-shaped openings had better resistance to fatigue than circular openings as was seen from the experiments of Jent and Bez [30].

2.2. Introduction to fatigue

The phenomenon of fatigue in steel structures occurs when they are exposed to cyclic loading. Fatigue is the progressive, localized and permanent structural change that occurs in a material subjected to repeated or fluctuating strains at nominal stresses, that have maximum values less than the tensile strength of the material [11]. It is known that loads occurring due to traffic lead to stress variation in the structure during its lifetime. One important factor for fatigue life is the magnitude of this stress variation. The damages due to high cycle fatigue are normally caused by the stress states within the yield criteria of the material. Thus, elastic stresses are generally considered in the fatigue strength calculations.

The lifetime of the structure in the context of fatigue can be divided into three phases: crack initiation phase, crack propagation phase and final fracture (Figure 2.3 [16]). Phase 1 or crack initiation phase is more important in case of high cycle fatigue (HCF). HCF is characterized by elastic deformation. In this case, most of the time is spent in the initiation of the crack. Phase 2 or crack propagation period is important in case of low cycle fatigue (LCF). LCF is characterized by repeated plastic deformation. In this case, most of the time is spent in crack growth and stresses usually are higher than the yield strength of the material. The number of cycles to failure is low for LCF and high for HCF, hence the terms low and high cycle fatigue. The total number of cycles to fatigue failure is the sum of number of cycles for crack initiation and number of cycles for crack propagation.

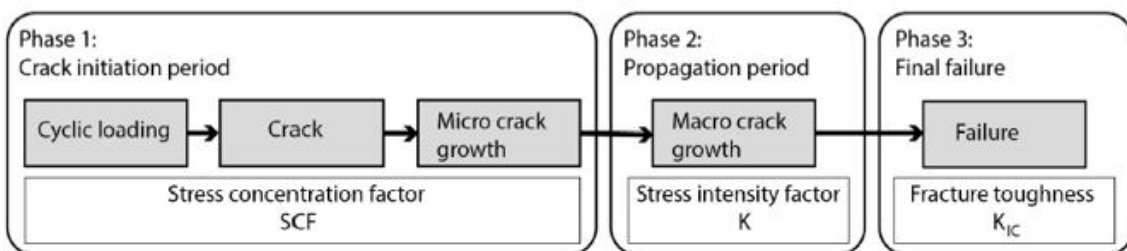


Figure 2.3: The three phases in fatigue [16]

The nucleation of a crack is regarded as the period from an initial defect to the formation of a crack which is detectable. This stage can be further sub-divided into micro-structural and mechanical nucleation as shown in Figure 2.4 [52]. At points where the stress range is large, the initiation of a crack takes place at such regions. The reason for local increase in stress range is due to stress concentration effects which occur because of geometric discontinuities in the detail like misalignment, the shape and size of the weld and local weld defects [13]. The fatigue life is dependent on the stress range, fatigue detail class and the intensity of load cycles. More heavy traffic is found in highway bridges compared to normal bridges. This results in large stress range and high load cycles. The fatigue design of highway steel bridges plays a dominant role for its service life.

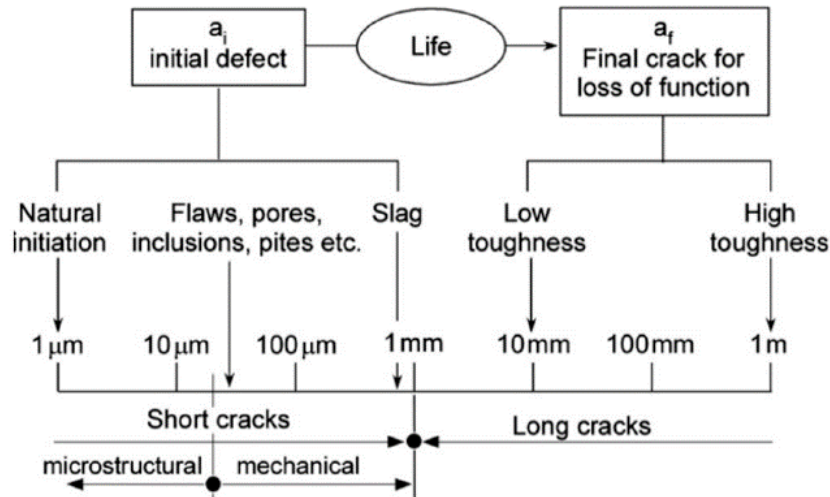


Figure 2.4: Scale of lengths of the life cycle of a component which is subjected to cyclic loading [52]

2.3. S-N curves

The relation between stress range (S) and number of load cycles to failure (N_f) is described by S-N curves. The stress ranges determined from the stress-based fatigue assessment procedures can be assessed according to the S-N curves. EN 1993-1-9 [2] provides a set of 14 equally spaced fatigue resistance S-N curves for the nominal stress approach. For each S-N curve, a group of details are associated. The S-N curve describes the limit of fatigue resistance. It is determined for each specific welded detail separately. A detail category provides the stress range which causes fatigue failure at 2×10^6 number of load cycles. For each specific joint, the detail category should be determined from experiments.

Figure 2.5 shows a typical S-N curve. Curve fitting is performed with the results obtained from experiments. From the figure it can be observed that this line is the mean value of the fatigue test data. However, for the design purposes, an acceptable safety margin should be provided.

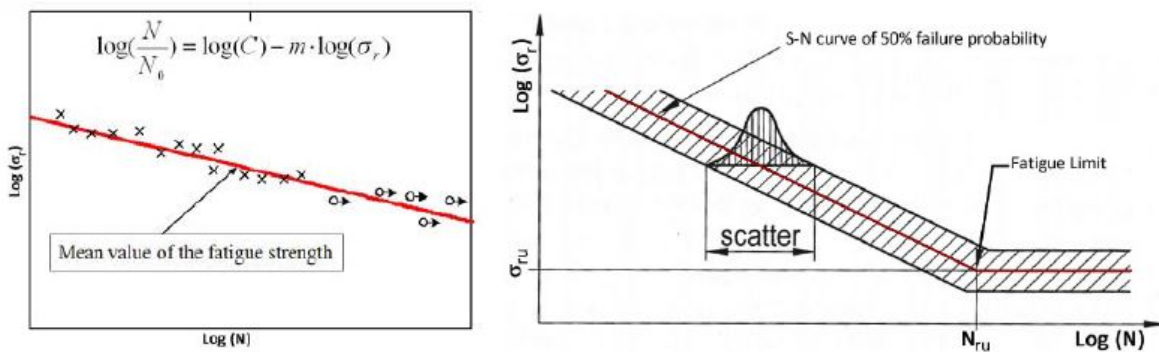


Figure 2.5: Left: S-N curve fitted on test results, Right: Mean S-N curve and the scatter band [27]

All the influencing parameters which are not included in the stress range for fatigue assessment are taken into account in the detail category. These influencing factors arise due to welding, for example weld imperfections and residual stresses. The S-N curves do not give a lot of information about the progress of fatigue damage. They only provide the total fatigue life. The stress range at constant amplitude fatigue limit (CAFL) ($\Delta\sigma_D$) corresponds to $N_D = 5 \times 10^6$ load cycles. The stress range at cut-off limit ($\Delta\sigma_L$) should be determined at $N_L = 10^8$ load cycles. The stress ranges can be calculated according to the following equations:

$$\Delta\sigma_D = \left(\frac{2}{5}\right)^{1/3} \cdot \Delta\sigma_C \qquad \Delta\sigma_L = \left(\frac{5}{100}\right)^{1/5} \cdot \Delta\sigma_D$$

Figure 2.6 shows the standard S-N curves from EN 1993-1-9 [2]. Point 1 is the detail category, point 2 is the constant amplitude fatigue limit (CAFL) and point 3 is the cut-off limit.

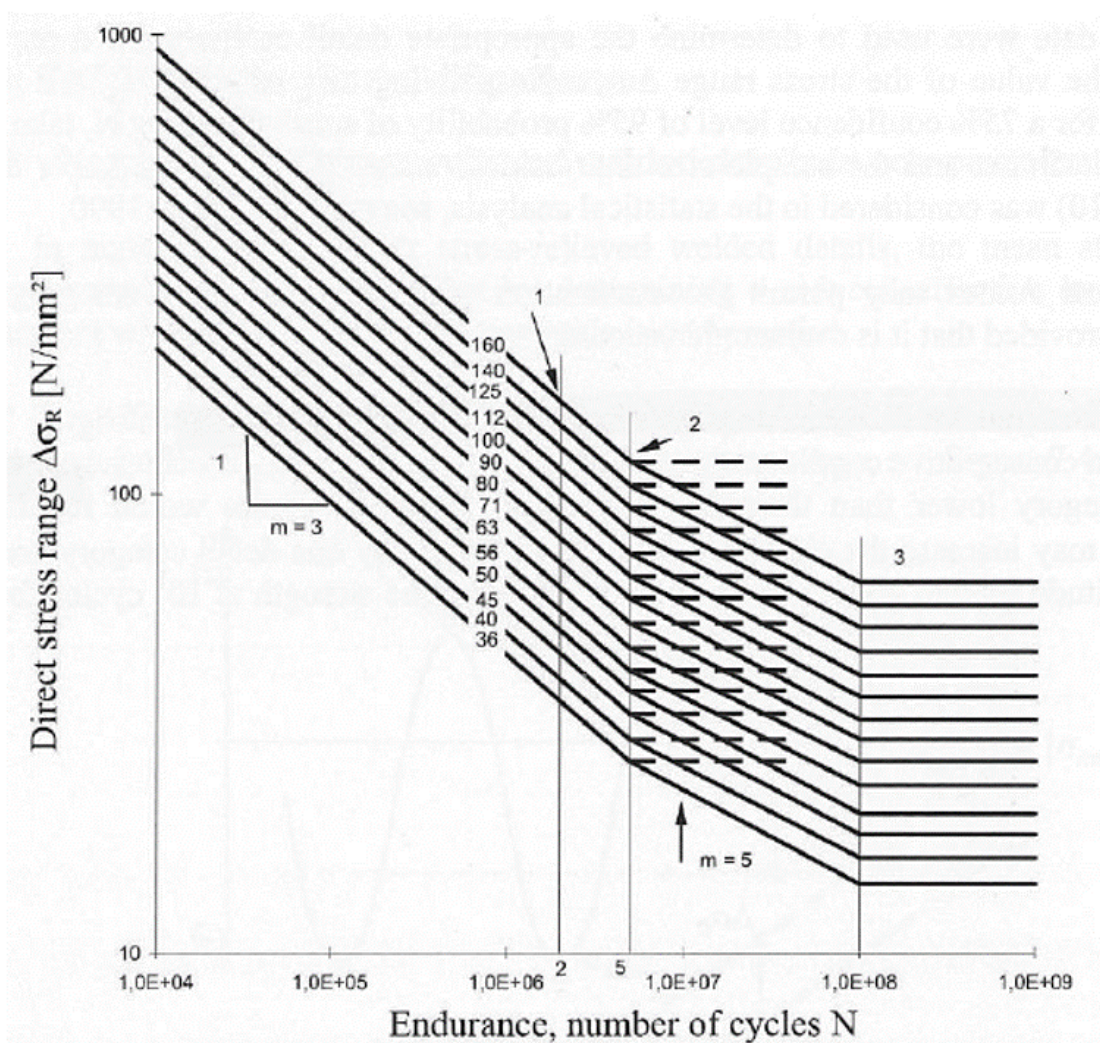


Figure 2.6: The standard S-N curves according to Eurocode 3 Part 1-9 (EN 1993-1-9) [2]

The fatigue life is infinity if the stress range is below the stress value at constant amplitude fatigue limit (CAFL). For a stress range with variable amplitude, the fatigue life is infinity if that stress range is less than the cut-off limit and the value of m changes from $m = 3$ to $m = 5$ after the CAFL is reached. The S-N curve is also known as a Wöhler Curve. The progression of the S-N curve can be influenced by

many parameters. These parameters are: ratio of stress (mean stress), frequency of loading, corrosion, temperature, residual stresses and the occurrence of notches. The design fatigue life N_R corresponding to the design stress range $\Delta\sigma_R$ is determined according to the following equations:

$$N_R = \min \left\{ \begin{array}{l} \left(\frac{\Delta\sigma_C}{\Delta\sigma_R} \right)^3 \cdot N_C \quad \Delta\sigma_R \leq \Delta\sigma_D \\ \left(\frac{\Delta\sigma_D}{\Delta\sigma_R} \right)^5 \cdot N_D \quad \Delta\sigma_D < \Delta\sigma_R \leq \Delta\sigma_L \\ \infty \quad \Delta\sigma_R \geq \Delta\sigma_L \end{array} \right.$$

2.4. Detail categories

EN 1993-1-9 [2] provides information regarding the detail categories of OSDs with open and closed stiffeners. Figure 2.7 [2] shows a part of Table 8.9 of EN 1993-1-9 which corresponds to the detail categories for OSDs with open stiffeners according to **nominal stress approach**. It is known that an equivalent stress range should be found by combination of the direct (normal) stress range and shear stress range at the stiffener. The next step is to use this equivalent stress range as nominal stress range in the appropriate S-N curve (detail category 56 as shown in Figure 2.7).

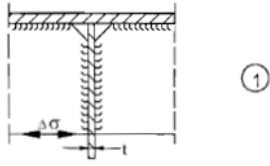
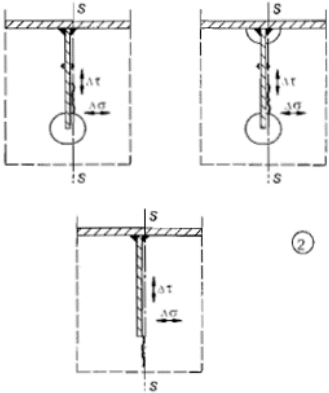
Detail category	Constructional detail		Description	Requirements
80	$t \leq 12\text{mm}$		1) Connection of longitudinal stringer to cross girder.	1) Assessment based on the direct stress range $\Delta\sigma$ in the stringer.
71	$t > 12\text{mm}$			
56			2) Connection of continuous longitudinal stringer to cross girder. $\Delta\sigma = \frac{\Delta M_x}{W_{nat,s}}$ $\Delta\tau = \frac{\Delta V_x}{A_{w,nct,s}}$	2) Assessment based on combining the shear stress range $\Delta\tau$ and direct stress range $\Delta\sigma$ in the web of the cross girder, as an equivalent stress range: $\Delta\sigma_{eq} = \frac{1}{2} \left(\Delta\sigma + \sqrt{\Delta\sigma^2 + 4\Delta\tau^2} \right)$
			Check also stress range between stringers as defined in EN 1993-2.	

Figure 2.7: Detail categories for OSDs having open stiffeners (Table 8.9 EN 1993-1-9 [2]) based on nominal stress approach

The Eurocode (EN 1993-1-9) [2] and IIW guidelines [28] [40] recommend detail categories for steel plated joints based on the **hot-spot stress approach** as shown in Figure 2.8.

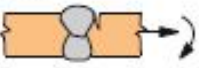
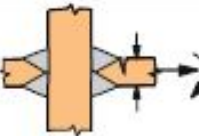
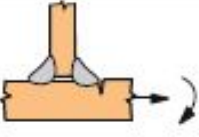
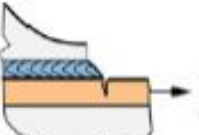

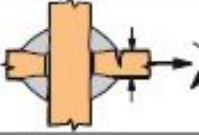
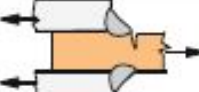
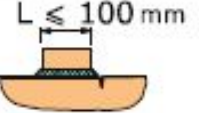
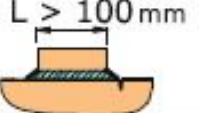
No	Joint	Description	Quality	FAT _{St}	FAT _{A1}	<i>n</i>
1		Butt joint	As-welded, proved free from significant flaws by NDT	100	40	0.2
2		Cruciform or T-joint with full penetration K-butt welds	K-butt welds, no lamellar tearing	100	40	0.3
3		Non-load carrying fillet welds				
4		Bracket or stiffener ends, welds either welded around or not				
5		Cover plate ends and similar joints	Fillet weld(s) as-welded	90	36	0.3
6		Cruciform joint with load-carrying fillet welds				
7		Lap joint with load-carrying fillet welds	Fillet or full penetration weld, as-welded	100	40	0.1
8		Type "b" joint with short edge attachment				
9		Type "b" joint with long edge attachment	Fillet or full penetration weld, as-welded	90	36	0.1

Figure 2.8: Detail categories recommended by Eurocode [2] and IIW [40] based on SHSS approach

A detail category is classified in a simplified form with the requirements of FAT class - for example FAT100, which is the same as detail category C100 in the Eurocode (EN 1993-1-9) for **hot-spot stress approach**. This shown as detail 3 in Figure 2.8, which is a non-load carrying fillet weld according to both the Eurocode (EN 1993-1-9) [2] and IIW recommendations [40].

The same detail is again classified as detail category FAT80 (detail 1) according to the DNVGL recommendations [6] for **hot-spot stress approach** as shown in Figure 2.9 [6].

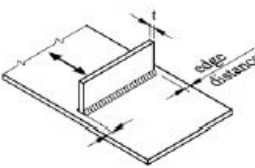
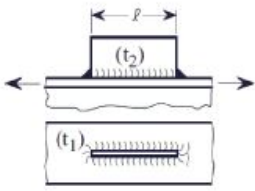
No.	Geometry	Description of joint	K factor	FAT N/mm ²
1		Transverse attachment on unsupported plate. Edge distance, if any, to be minimum 10mm.		
		$t \leq 25 \text{ mm}$ ($K_{ms}=1.2$):	1.13	80
		$t > 25 \text{ mm}$ and $t_p > 25 \text{ mm}$ ($K_{ms}=1.2$):	1.27	71
		$t_p > 50 \text{ mm}$ and $t_p > 2t$ ($K_{ms}=1.12$):	1.19	76
		$t_p = \text{Base plate thickness}$		
		For transverse attachment supported below, see detail no. 4 in Table 8		
2		Longitudinal attachment welded on beam flange, bulb or supported plate:		
		$l \leq 50 \text{ mm}$	1.13	80
		$50 \text{ mm} < l \leq 150 \text{ mm}$	1.27	71
		$150 \text{ mm} < l \leq 300 \text{ mm}$	1.43	63
		$l > 300 \text{ mm}$	1.61	56
		For $t_2 \leq 0.5t_1$, FAT class (K factors) may be improved by a factor of 1.125, but not better than FAT 80 (K=1.13) (not valid for bulb profiles)		

Figure 2.9: Proposed detail categories according to DNVGL [6] for attachments welded to a plate or stiffener based on SHSS approach

The DNVGL [6] is used in offshore engineering and they recommend a lower detail class for the investigated joint. Each design code or standard is based on different experiments for different types of connections. The detail categories are based on simple or standard connections. According to the DNVGL recommendations [6], the fatigue strength of welded details depend on the direction of the principal stress relative to the weld toe. The detail categories intended for **nominal stress method** and **hot-spot stress method** are shown in Figure 2.10 [6].

Angle ϕ in Figure D-3	Detail classified as F for stress direction normal to the weld	Detail classified as E for stress direction normal to the weld	S-N curve when using the hot spot stress methodology
0 - 30	F	E	D
30 - 45	E	D	C2
45 - 60	D	C2	C2
60 - 75	C2	C2	C2*
75 - 90	C2*	C2*	C2*

* A higher S-N curve may be used in special cases. See Table A-3 for further information.

Figure 2.10: Classification of details and selection of S-N curve by DNVGL [6]

These detail categories depend on the angle which the principal stress makes with the normal to the weld toe which is shown in Figure 2.11 [6]. The DNVGL [6] also recommends the design hot-spot stress S-N curve which also depends on the angle which the principal stress makes with the normal to the weld. This is also shown in Figure 2.11 [6] and the detail categories associated are D and C2.

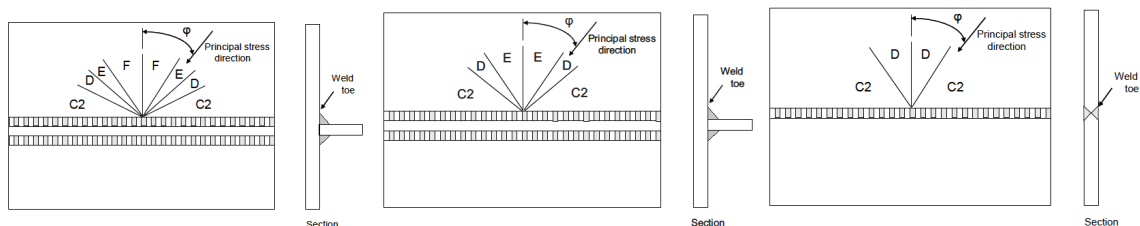


Figure 2.11: Classification of details depending on the angle of the principal stress with the normal to the weld toe by DNVGL [6]

It is to be noted that the correspondence between S-N curves in DNVGL standard [6] and IIW recommendations [40] relate only to number of cycles less than 5×10^6 in Eurocode 3 (EN 1993-1-9) [2]. The relationship between the S-N curves in DNVGL [6] and those in IIW [40] and EN 1993-1-9 [2] is given in Figure 2.12 [6].

<i>DNV notation</i>	<i>IIW and Eurocode 3 notation</i>
B1	160
B2	140
C	125
C1	112
C2	100
D	90
E	80
F	71
F1	63
F3	56
G	50
W1	45
W2	40
W3	36

Figure 2.12: Relationship between the notations according to DNVGL [6]

2.5. Stress based fatigue assessment methods

The stress ranges at the critical locations (like the weld toe and weld root) have to be identified for investigation of the fatigue life based on the S-N curve. In this thesis, the fatigue crack starting from weld toe is studied in detail. There are several methods for calculating the stress range for evaluation of the fatigue life. The fatigue strength assessment methods can be broadly divided into two categories: **global** and **local** approaches. The nominal stress method is a global approach. Whereas both the hot-spot stress method and the effective notch stress method are local approaches.

EN 1993-1-9 [2] provides a description of the two methods for fatigue assessment. These are the nominal stress method and the hot-spot stress method. The nominal stress method is generally used for simple welded joints which are classified in various detail categories in EN 1993-1-9 [2]. When the geometry of a detail is complex, the structural hot-spot stress (SHSS) method is recommended. Another method is the effective notch stress method which is described by the International Institute of Welding (IIW) recommendations [28][40][38]. Figure 2.13 shows the stress distribution close to the weld toe. Depending on which approach is followed, the shape and geometry of the welds and welding defects are generally considered in the calculation of stress or in the design S-N curve.

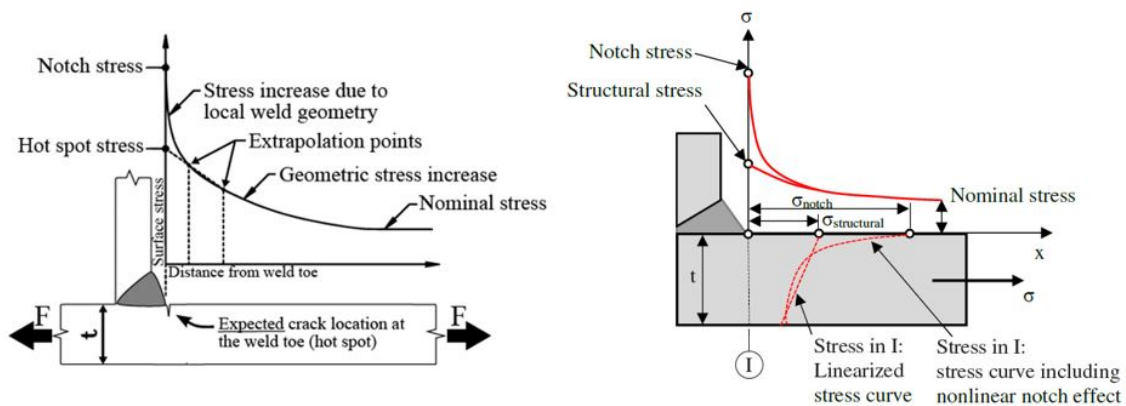


Figure 2.13: Stress distribution near the weld toe on the surface and through the thickness [12]

2.5.1. Nominal stress method

The nominal stress can be described as the undisturbed far-field stress. The nominal stress method is defined according to EN 1993-1-9 [2]. This approach incorporates nominal stress in the weld or nominal stress in the parent material of the joint to evaluate fatigue life of the detail. In this method, the local stress increasing effect at notches is excluded from the stress range. The stress concentrations due to the local weld profile and weld imperfections are also not considered in this approach. Thus, these should be included in the detail category.

There are some drawbacks of the nominal stress method. They are as follows: (i) it is not applicable when the investigated detail geometry is so complex that it is difficult to assign a detail category; (ii) it is unable to represent complex loading conditions and, (iii) it is not possible to capture size effect of dimensional differences [31]. The main drawback of this method is that if the investigated detail is not available in the tables of standard details provided by the code, then it cannot be designed. In such cases it can only be designed if laboratory fatigue tests are carried out and the data from test results are consolidated into a single S-N curve for that detail.

The modified nominal stress method is used when the stress raising effects or macro-geometric effects are considered. The stress raising factors are eccentricities, geometric discontinuities and misalignment. The stress concentration factor k_f is used in order to incorporate the stress raising effects. The modified nominal stress is determined by multiplying the nominal stress by the stress concentration factor. The difference between modified nominal stress method and SHSS method is that the latter includes the stress raising effects due to geometric complexity only. The discontinuities in the local weld geometry and imperfections in the weld are excluded in determination of SHSS and therefore, it is included in the hot-spot stress S-N curve [22].

$$\sigma_{nom,mod} = SCF \cdot \sigma_{nom}$$

2.5.2. Structural hot-spot stress (SHSS) method

The structural hot-spot stress (SHSS) approach has already shown its reliability and efficiency for the fatigue strength assessment of welded details in the offshore industry for many years [9]. The SHSS is an abstract or pseudo stress which includes stress concentration effects caused due to the geometrical variations of the detail at the expected fatigue crack initiation area which is also known as a 'hot-spot'. The SHSS is aimed at considering all the geometric parameters but it does not include the notch effect caused by the weld profile. This notch stress is illustrated in Figure 2.14 [40]. The non-linear component is excluded from the SHSS. Hence, one hot-spot stress S-N curve can be associated to several details. The SHSS can be determined by surface stress extrapolation to the weld toe from reference points. This approach is limited to the fatigue assessment of the weld toe.

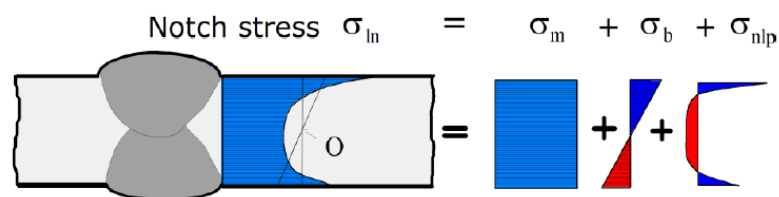


Figure 2.14: Non-linear stress distribution along the thickness of the plate [40]

The concept of SHSS was introduced years ago for fatigue design of tubular structures. Swierstra [43] had investigated fatigue design of tubular joints using the SHSS approach. It was found that the mesh size and element type have a large impact on the stress range to be calculated. Swierstra [43] also found that the hot spot stress method results in a more accurate solution if solid elements were used instead of shell elements for tubular joints.

In the experimental and numerical study of Akhlaghi [9], a detail of an open stiffener to crossbeam joint was investigated under a 3-point bending test. He had investigated three full-scale experiments under constant amplitude fatigue loading (CAFL). The assessment of accuracy of the numerical models using SHSS approach was done by comparison with the results from experiments. He found that the SHSS values calculated from the numerical solid model using fine mesh was **14%** higher than the average values obtained from the experiments. This deviation of **14%** was regarded as acceptable considering the effect of misalignment in the real specimen. It was concluded from this research that the predicted fatigue lives for all the specimens were lower than the actual fatigue lives which meant that the results from SHSS method were on the safe side. More details about the numerical research of Akhlaghi [9] is provided in Chapter-4.

Figure 2.15 shows the hot-spot types according to the available design standards. The classification of hot-spot types depend on the design code which is given as follows:

- According to IIW [28] [40], there are two types of hot-spots depending on their location on the plate and their orientation with respect to the weld toe: type-“a” and type-“b”. Hot-spot type-“a” occur when the weld is located on the surface of the plate. Hot-spot type-“b” occur when the weld is located at the edge of the plate.
- According to DNVGL [6], however, there are three types of hot-spots: type-“a”, type-“b” and type-“c”. Hot-spot type-“a” occur at the weld toe on the plate surface at an ending attachment. Hot-spot type-“b” occur at the weld toe around the plate edge of an ending attachment. Hot-spot type-“c” occur along the weld of an attached plate (weld toes on both the plate and attachment surface).

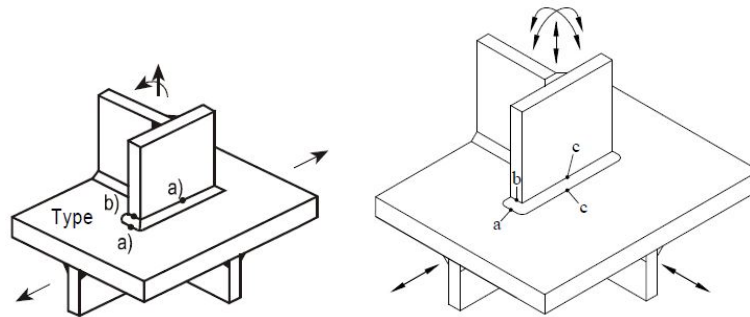


Figure 2.15: Types of hot-spots according to IIW [28] (left) and DNVGL [6] (right)

In type-“b” hot-spots the stress distribution approaching the weld toe does not depend on the plate thickness, which is in contrast to type-“a” hot-spots [40]. The calculation of SHSS based on FEM according to the IIW recommendations involves determination of stresses from specific points away from the weld toe. These are known as reference points. The reference points for surface stress extrapolation are different for different types of hot-spots. From these reference points, stress values are extracted, and hot-spot stress is determined according to the type of hot-spots and following equations:

Type-“a” hot-spots: For a fine mesh with element length not more than $0.4t$ at the hot spot, the evaluation of SHSS from nodal stresses at two reference points $0.4t$ and $1.0t$ away from the weld toe, is obtained according to the following equation -

$$\sigma_{hs} = 1.67 \cdot \sigma_{0.4t} - 0.67 \cdot \sigma_{1.0t}$$

Type-“b” hot-spots: For a fine mesh with element length of not more than 4 mm at the hot spot, the evaluation of SHSS from nodal stresses at three reference points 4 mm, 8 mm and 12 mm away from the weld toe, is obtained according to the following equation -

$$\sigma_{hs} = 3 \cdot \sigma_{4 \text{ mm}} - 3 \cdot \sigma_{8 \text{ mm}} + \sigma_{12 \text{ mm}}$$

Type-“c” hot-spots: For this type, the same calculation procedure is followed as for Type-“a” hot-spot.

$$\sigma_{hs} = 1.67 \cdot \sigma_{0.4 \cdot t}^{-0.67} \cdot \sigma_{1.0 \cdot t}$$

It is also important to note that the equations used for hot-spot stress extrapolation also depend on the element size (coarse/fine). For welded joints, the stress distribution over the thickness of a plate near a weld toe is non-linear. The notch effect of the weld results in this non-linear stress distribution. The structural stress is defined as the stress taking into account the geometrical variations of the detail at the expected fatigue crack initiation area which is also known as a hot-spot, excluding the effect of notch [40]. According to the IIW [40], the structural hot-spot stress (SHSS) method is applicable for welded joints having the following conditions: (i) the fluctuating principal stress acts predominantly transverse to the weld toe or the ends of a discontinuous longitudinal weld; (ii) the potential fatigue crack will initiate at the weld toe or weld end.

The potential fatigue-critical points as was revealed from the study by Aygül and Al-Emrani [13] are shown in Figure 2.16 [13]. The governing stress direction is also shown. The potential crack locations are as follows:

- **Crack A:** The fatigue crack observed in the web of the crossbeam which started at the weld toe under in-plane loading. This crack started from the edge of the cope hole and propagated along the weld. The detail was defined as a type-“b” hot-spot for this type of crack, as weld was located at the edge of the plate and stress distribution through the thickness of crossbeam is uniform. The stresses were extracted along the direction perpendicular to the weld line along the crossbeam.
- **Crack B:** The root crack of the fillet weld at the intersection between the rib and the crossbeam. For cracks originating from weld roots, the SHSS cannot be classified as type-“a” or type-“b”. The force transfer takes place from the stiffener to the crossbeam through the weld.
- **Crack C:** The fatigue cracking in the open rib plate which also started from the weld toe. In this case, stresses were extracted in the direction perpendicular to the weld line along the stiffener. The detail was defined as a type-“a” hot-spot point for this type of crack as the weld was located on the surface of the plate.
- **Cracks D and E:** The fatigue cracking in the deck plate which started either from the toe of weld or along the fillet weld between the rib and the deck plate. These cracks were derived by the normal stresses in the deck plate and both points were defined as type-“a” hot-spot points.
- **Crack F:** The fatigue crack in the web plate of the cross beam which started from the edge of the cut-out hole and was generated by the multi-axial stress condition at this location. A preliminary study on multi-axial stress state has been provided in the later sections.

Crack location	Type of hot spot point	Detail category
A	b	90
B	N/A	N/A
C	a	90
D	a	100
E	a	100
F	N/A	N/A

Figure 2.16: The critical points subjected to fatigue in OSD with open stiffeners and fatigue classes based on SHSS method [13]

Determination of SHSS by surface extrapolation

The approach of extrapolation of stress at the surface considers the stress distribution along the top or bottom surface of a plate near the weld toe. The reference points for surface stress extrapolation are located in front of a weld toe at certain specific distances. These distances are dependent on the thickness of the plate for type-“a” and type-“c” hot-spots. The approach of linear surface stress extrapolation involve determination of the nodal stresses at two reference points located at specific distances away from the weld toe. After that the SHSS is found by extrapolation of these stress values to the weld toe. The structural stress distribution is generally taken as linear (Figure 2.17). For the linear case two reference points are used which are located at distances $0.4t$ and $1.0t$ away from the weld toe. For more coarse meshes, it is recommended to use extrapolation points which are located at $0.5t$ and $1.5t$ distance from the weld toe. The notch stress due to the weld itself is not included by using linear extrapolation of surface stress from the two reference points. This is because these reference points are located far away from the region which is influenced by the local weld geometry [40].

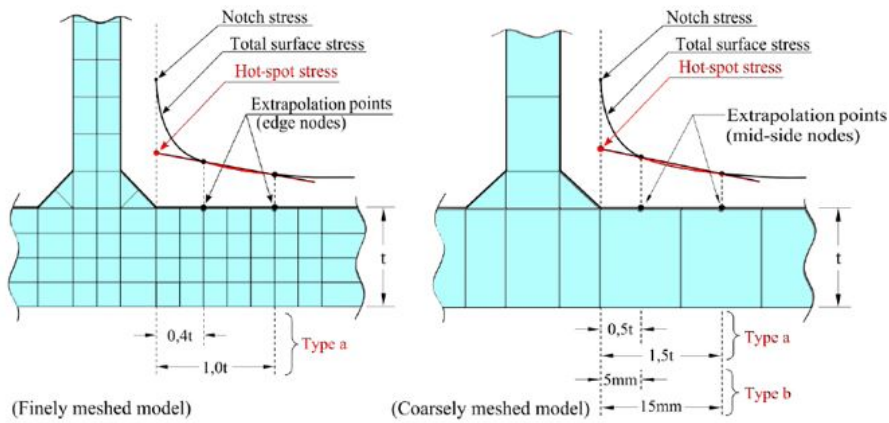


Figure 2.17: Linear surface stress extrapolation [28]

There are some exceptions in using linear extrapolation for special cases like for example a pronounced non-linear increase of structural stress towards the hot-spot or a sharp change of direction of the applied force or a thick-walled structure. For such cases, the linear extrapolation method may give results which are not conservative. Thus, for these cases, quadratic (non-linear) surface stress extrapolation procedure is recommended as shown in Figure 2.18 [28][40]. Quadratic surface stress extrapolation may also be used if the stress gradient is very steep near the weld toe [28]. For type-“b” hot-spots, quadratic extrapolation method is recommended from the reference points located at 4 mm, 8 mm and 12 mm away from the weld toe for fine meshed model. For coarse meshing, the reference points are located at 5 mm and 15 mm away from weld toe and linear extrapolation is recommended. In case of coarse meshing, the stresses are sometimes extracted from the mid-side-node of elements.

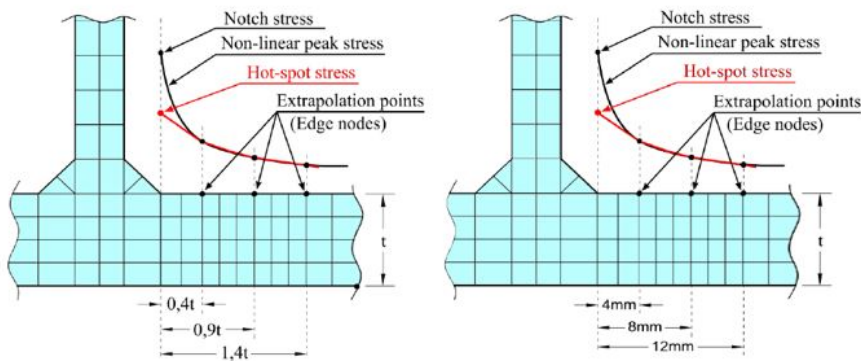


Figure 2.18: Quadratic surface stress extrapolation [28]

The equations used for the determination of SHSS at the weld toe using linear and quadratic stress extrapolation techniques are summarised in Table 2.1 [40].

Table 2.1: Different types of hot-spots and quadratic and linear stress extrapolation procedure according to IIW guidelines [40]

Type of Hot-spot	Parameters	Relatively Coarse Mesh		Relatively Fine Mesh	
		Shell	Solid	Shell	Solid
Type-a Hot-spot	Element Size	t	t x t	$\leq 0.4t$	$\leq 0.4t \times t$
	Reference Points	0.5t and 1.5t		0.4t and 1.0t	
	Hot-spot stress	$\sigma_{hs} = 1.5\sigma_{0.5t} - 0.5\sigma_{1.5t}$		$\sigma_{hs} = 1.67\sigma_{0.4t} - 0.67\sigma_{1.0t}$	
	Extrapolation	Linear Extrapolation		Linear Extrapolation	
Type-b Hot-spot	Element Size	10mm	10mm x 10mm	4mm	4mm x 4mm
	Reference Points	5mm & 15mm		4mm, 8mm & 12mm	
	Hot-spot stress	$\sigma_{hs} = 1.5\sigma_{5mm} - 0.5\sigma_{15mm}$		$\sigma_{hs} = 3\sigma_{4mm} - 3\sigma_{8mm} + \sigma_{12mm}$	
	Extrapolation	Linear Extrapolation		Quadratic Extrapolation	

Determination of SHSS by through thickness linearization

The stress linearization through the thickness or through thickness at the weld toe (TTWT) approach is the linear formulation of the non-linear stress distribution directly at the weld toe [28][40]. In this procedure, the SHSS is evaluated from the stresses in the cross-section of the plate in the thickness direction. The origin of the stress profiles are from the weld toe as shown in Figure 2.19 [42]. This concept involves a 3-step procedure. In the first step, the non-linear stress distribution is integrated over the plate thickness. In the second step, a linear stress distribution is generated from the outcome. In the last step, there is a summation of the resulting linear distribution which produces the bending and membrane stress components. The SHSS is found by adding the membrane and bending stress components.

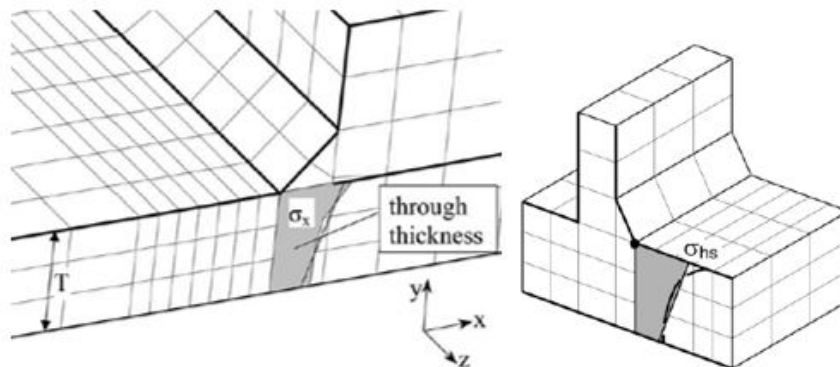


Figure 2.19: Though thickness stress linearization [42]

For application of the through thickness linearization method, use of finite elements which are situated in front of the weld toe is recommended. This is to be done along with turning off the nodal averaging function [27]. The reason for turning off the stress averaging function is that the weld region undergoes lower stresses due to the presence of extra material. But, the elements which are situated in front of the weld toe, withstand higher stresses. The nodal averaging function reduces the stresses at the weld toe. Thus, the calculated SHSS can be underestimated because of nodal averaging [27]. For cruciform type of joints loaded in tension, stresses through half of the thickness of the plate is used. The through thickness linearization method is mesh sensitive just like the surface stress extrapolation method. However, according to Poutiainen [42], the TTWT method is more forgiving compared to surface stress extrapolation when it comes to mesh requirements. When quadratic solid elements are used to calculate the SHSS by the TTWT method, it is recommended to use at least three isoparametric solid elements in the thickness direction [28]. This is done so as to have an acceptable amount of accuracy in the non-linear stress calculation at the weld toe.

Determination of SHSS by Dong method

The stress in the element adjacent to the weld toe is generally affected by the stress singularity at the notch. Thus, several elements (at least three recommended by IIW [28]) in the thickness direction are required to avoid any influence of the notch effect and so obtain reasonable results. Dong [17] proposed a special procedure to derive the linear part of the stress distribution in the through-thickness direction. The Dong method has two different approaches:

1. **Stress based approach** - According to this approach, the structural stress has to be calculated using local stress outputs from solid elements at a certain distance (δ) away from the weld toe (Figure 2.20 [17]). After this step, equilibrium conditions should be imposed in terms of stress resultants between two adjacent cut sections.

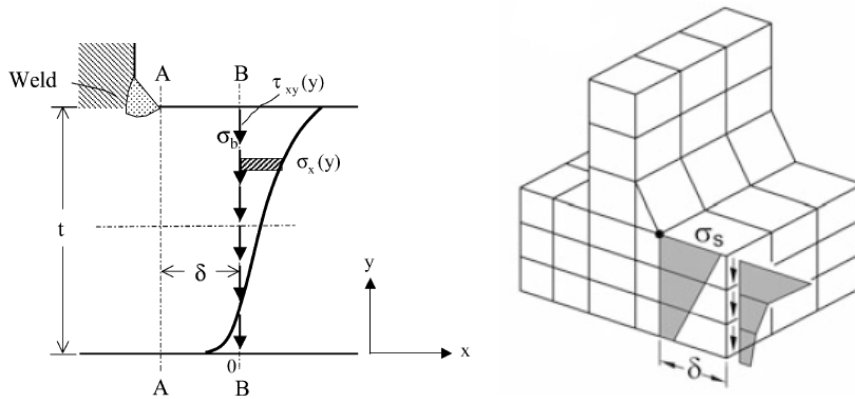


Figure 2.20: Structural stress from a distance δ for solid elements with monotonic stress distribution (Dong method) [17]

The local stresses near the notch increases with the reduction of element sizes and thus they are mesh sensitive. According to Dong [17], the approach is mesh insensitive since it uses of the stresses through the thickness at a certain distance away from the weld toe. The SHSS is determined by establishing equilibrium conditions for normal and shear stress components at the distance δ away from the weld toe. Using equilibrium conditions between sections A-A' and B-B', it can be seen that the structural stress components must satisfy the following conditions [17].

$$\sigma_m = \frac{1}{t} \int_0^t \sigma_x(y) \cdot dy$$

$$\sigma_m \cdot \frac{t^2}{2} + \sigma_b \cdot \frac{t^2}{6} = \int_0^t \sigma_x(y) \cdot y \cdot dy + \delta \int_0^t \tau_{xy}(y) \cdot dy$$

2. **Nodal force based approach** - Another approach is by using nodal forces at the weld toe plane to calculate line forces and line moments along the weld toe line, from which membrane and bending stress can be derived [18] (Figure 2.21). With nodal forces and moments, greater accuracy can be achieved compared to procedures using element stresses.

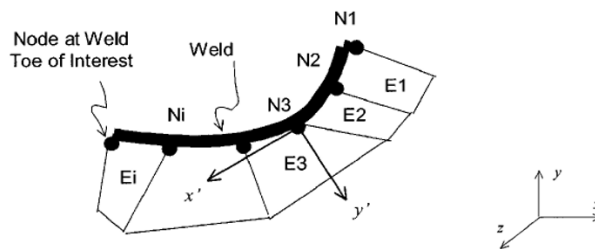


Figure 2.21: Structural stress calculation procedure for curved weld with distorted mesh [18]

Shell elements can also be used for the determination of SHSS using Dong method (Figure 2.22). The stress distribution along the weld toe can be calculated directly from the nodal forces and moments in the elements in front of the weld toe considering the element shape functions [27]. This is done with the help of a transformation matrix which relates the nodal forces/moments to line forces and moments. Finally, the membrane stress and bending stress is calculated at each nodal position along the weld toe line [27].

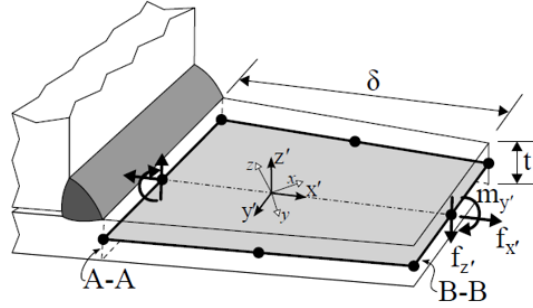


Figure 2.22: Structural stress from a distance δ for shell elements (Dong method) [27]

By using the following simultaneous equation, the line forces and moments along the entire weld line obtained from the transformed element nodal forces [33][18].

$$\begin{Bmatrix} F_1 \\ F_2 \\ F_3 \\ \vdots \\ F_n \end{Bmatrix} = \begin{bmatrix} \frac{l_1}{3} & \frac{l_1}{6} & 0 & 0 & \cdots & 0 \\ \frac{l_1}{6} & \frac{(l_1+l_2)}{3} & \frac{l_2}{6} & 0 & \cdots & 0 \\ 0 & \frac{l_2}{6} & \frac{(l_2+l_3)}{3} & \frac{l_3}{6} & 0 & 0 \\ 0 & 0 & \ddots & \ddots & \ddots & 0 \\ \vdots & \ddots & \ddots & \ddots & \frac{(l_{n-2}+l_{n-1})}{3} & \frac{l_{n-1}}{6} \\ 0 & \cdots & \cdots & 0 & \frac{l_{n-1}}{6} & \frac{l_{n-1}}{3} \end{bmatrix} \begin{Bmatrix} f_1 \\ f_2 \\ f_3 \\ \vdots \\ f_n \end{Bmatrix}$$

In the nodal forces approach of Dong method, an important aspect is converting the global coordinate system to a local coordinate system in which the local axes x' and y' should be perpendicular to weld toe [42] if the crack is parallel to weld line. The line forces and moments derived from the nodal forces and moments can be converted to the structural stress components and thus the SHSS can be obtained using the following equation:

$$\sigma_s = \sigma_m + \sigma_b = \frac{f_{x'}}{t} + \frac{6(m_{y'} + \delta \cdot f_{z'})}{t^2}$$

Some researchers claim that the Dong method [33] is mesh insensitive even for hot-spots with steep stress gradients. However, Poutiainen [42] has proved a considerable mesh sensitivity in this approach in case of solid elements [42]. Not regarding the influence of shear stresses acting in the lateral faces of elements was the reason for this observation. This resulted in inaccuracies depending on the element size. According to this research, at $\delta = 0.4t$, the influence of these extra shear forces was negligible.

Determination of SHSS at a single point close to the weld toe

There has already been a lot of approaches for the simplification of SHSS evaluation by using the surface stress far away from the region which is affected by the weld toe notch. Fricke [23] suggested a simpler approach where the value of the SHSS was directly read out from one point which was situated at a distance of $0.5 \times t$ away from the weld toe (Figure 2.23 [28]). The IIW guidelines [28] also suggested using this approach to find the SHSS. This approach involved neither any extrapolation technique nor any integration. Since the stress distribution generally contains a stress gradient, the SHSS at a distance of $0.5 \times t$ was smaller than that at the weld toe for specific cases like the one shown in Figure 2.23 [13].

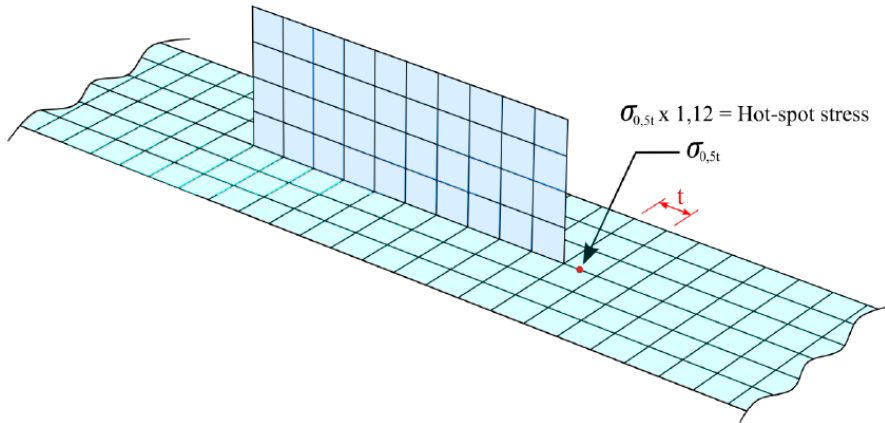


Figure 2.23: One point structural hot-spot stress determination [28] [13]

Therefore, it was used with a lower design S-N curve (a lower FAT class as compared to the FAT class used for SHSS with stress extrapolation). In order to have a good fit to fatigue test results, the SHSS obtained from the one-point stress determination approach should be multiplied with a factor of 1.12 (Figure 2.23) [13]. For a finite element model having an element size of $t \times t$ (where t = plate thickness), the reference point situated at a distance of $0.5 \times t$ away from weld toe is a useful validation [13]. The stress at this point located at the element mid-side for a second order element can be directly obtained from the FE-model.

Haibach [40] made an alternative proposal for the one-point SHSS approach by using absolute distances from the weld toe. Haibach’s method involves the utilization of strain on the surface of plate at a certain distance which is 2 mm away from weld toe and finding from measurements a common strain-life curve for various welded details having different geometry.

Determination of SHSS according to Xiao and Yamada

Xiao and Yamada [48] had developed an approach to determine the SHSS based on the calculated stress at a depth 1 mm below the weld toe. The IIW [28] also has some guidelines regarding this approach. This concept was founded on analysis results of a reference structural detail which was a non-load carrying cruciform joint with plate thickness of 10 mm as shown in Figure 2.24 [48].

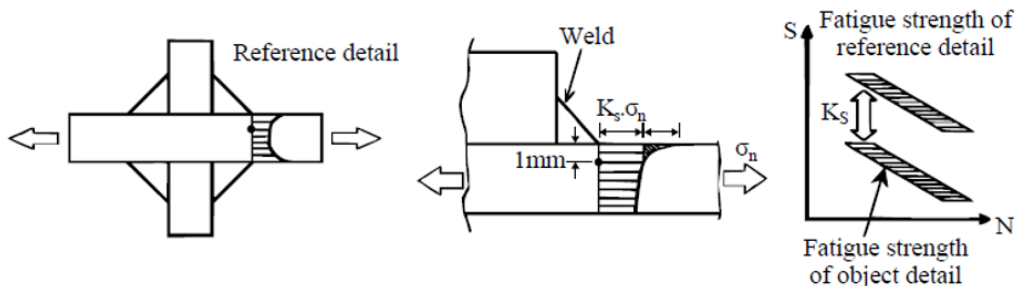


Figure 2.24: Structural stress according to Xiao and Yamada [48]

From the FEA of this reference detail it was observed that irrespective of the weld shape and size, the stress value through the thickness drops to approximately the nominal stress at 1 mm depth from the plate surface. However, this method can only be applied for membrane stresses. It was not applicable for details subjected to a combination of membrane and bending stresses. The stress obtained from this method was also correlated with early crack propagation phase. In order to obtain the SHSS according to Xiao and Yamada [48], the FE model has to be developed with a very fine mesh that is capable of providing the stress at 1 mm in depth along crack path with an acceptable amount of accuracy. This approach showed a good correlation between this stress at 1 mm in depth and fatigue life to the extent that it could be considered to be equivalent to the SHSS. Thus, it was used with the same hot-spot stress design S-N curves [40].

2.5.3. Effective notch stress method

The geometrical discontinuities present in welded details are cope holes, sharp and local changes in shapes and mis-alignments. The stress raisers or notches emanating from these geometrical discontinuities are very common and cannot be avoided for such details in structures. These notches have a large amount of influence on the fatigue resistance of welded details. The stress at these localized stress raisers is often referred to as the “notch stress” [28]. The notch stress in welded joints is the total local stress caused by both the component geometry and the local stress raiser, for example the shape and local geometry of the weld itself and the surrounding local region [13]. For very sharp notches where the radius is approaching to zero, the theoretical elastic notch stress tends to infinity. For such cases, the stress is referred to as being “singular” and the phenomenon is called “stress singularity”. Singular stresses which are tending to infinity cannot be used for fatigue assessment. Hence, to overcome this problem, the effective notch stress is defined as the average stresses over a certain distance for 2D or over a certain volume for 3D.

The concept of the effective notch stress method states that if the local stress at the point of crack initiation in a welded detail is calculated by assuming a predefined reference notch radius, then the fatigue strength of this detail can be related to a single fatigue strength S-N curve. This method is restricted to the assessment of welded joints with respect to potential fatigue failures from the weld toe or weld root. A disadvantage of this method is that it is more time consuming in terms of computation than the SHSS method. Due to the stress singularities which appear at the weld root and toe of the FE model, a realistic stress at these points is difficult to determine by computation. In order to prevent stress singularities, a notch at these points was applied as shown in Figure 2.25 [28]. The effective notch stress includes the local stress raising effects due to geometry of the detail and of the weld. Stress concentrations due to welding defects and misalignment are incorporated in the detail category.

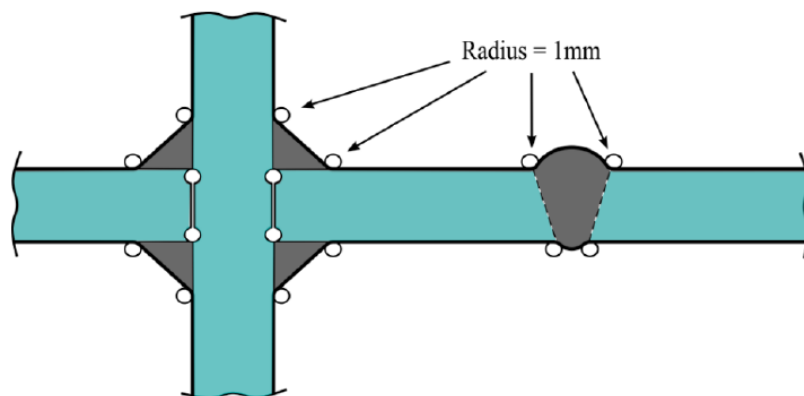


Figure 2.25: Fictitious rounding of weld toes and roots by effective stress method (IIW recommendations [28])

2.6. Comparison of the fatigue assessment methods

Marquis and Samuelsson [36] gave a qualitative comparison of the accuracy and computational effort for different fatigue assessment methods as shown in Figure 2.26 [36]. In OSD bridges, the intersection between crossbeam and longitudinal open stiffeners is sensitive to fatigue. Several researchers have

tried to explain the fatigue behaviour of this detail with different stress assessment methods. According to the research of Wang [44], the analysis of the fatigue strength of fillet welds lead to similar results for both the effective notch stress method and the SHSS method.

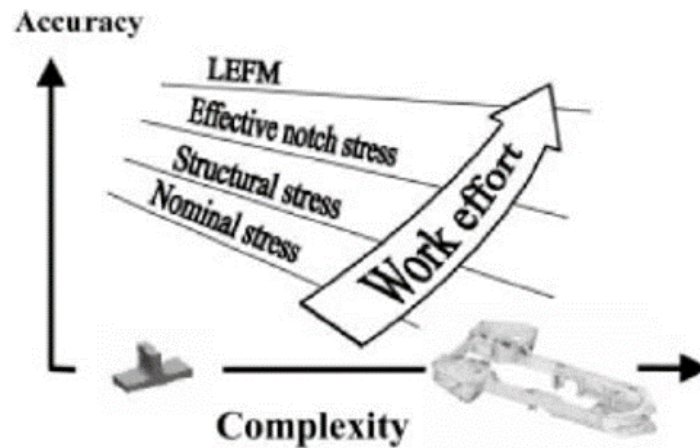


Figure 2.26: The comparison of accuracy vs. computational effort for fatigue strength assessment methods in welded joints [36]

It is known that the stress concentration factor (SCF) is the ratio of SHSS to nominal stress. There is no SCF for nominal stress. The SCF for SHSS is non-uniform because of the sensitivity of finite element types, element size, classification of welded joints, and different extrapolation techniques. The SCF for effective notch stress is not accurate due to indeterminate notch size and localized stresses around the notch [49].

Aygul, Al-Emrani and Urushadze [14] investigated the applicability of fatigue strength assessment methods using FEA. The detail investigated was a welded rib-to-cross-girder connection with a cope hole. Ten full-scale fatigue tests were conducted by them. During the fatigue experiment, each specimen was supported vertically on two roller supports at the ends of the crossbeam. They were subjected to a vertical load which was provided by an actuator and applied via a loading beam. The loading beam was used to divide the load from the actuator into two equal loads at the end of the rib [14]. Three specimens were first subjected to a static load. This was done to measure the strain distribution at predetermined locations, including the hot spot points where it was expected that crack would start. The fatigue tests were performed under constant amplitude fatigue loading (CAFL). The total number of load cycles to the detection of crack for different crack locations was recorded. Each specimen was tested with a different load range and the load frequency for the specimens varied between 2 and 3 Hz [14].

This study of Aygül, Al-Emrani and Urushadze [14] was performed to simulate the behaviour fatigue crack at the intersection between the longitudinal open ribs and cross girder. It was observed that the cracks appeared at the weld toe and then propagated along the weld line in the web of the crossbeam in most of the test specimens. However, in some specimens the cracks changed their path and propagated through the weld into the longitudinal rib.

EN 1993-1-9 [2] (Table 8.9) recommends a detail category "Category 56" when considering the **nominal stress** for the fatigue design of orthotropic bridge decks with open ribs. The nominal stress at the mid-section considering the net-section due to the cut-out hole of the web of the crossbeam was calculated following recommendations from the EN 1993-1-9 [2]. The equivalent stress, i.e. the resultant stress of the normal stress and shear stress, was used as the governing stress for the fatigue strength capacity of the welded joints. The fatigue life of the test specimens was computed using the equivalent nominal stress range and the results were plotted in Figure 2.27 [14] using linear regression analysis with a slope of 3 to compare with the recommended fatigue design class C56. It was observed that the calculated nominal stress did not yield appropriate results (Figure 2.27) [12].

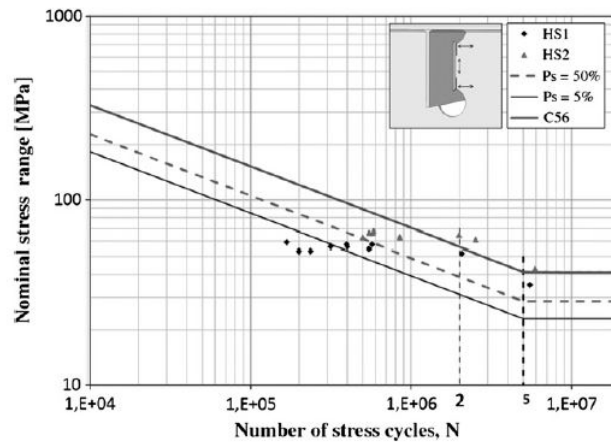


Figure 2.27: Fatigue test results when considering the nominal stress approach according to EN 1993-1-9 [14] [12]

However, as can be seen from Figure 2.28 (a) [14], almost **90%** of the load was carried through shear by the part of the web between the two cut-outs [12]. When only this part of the web was considered to carry the shear force, the equivalent nominal stress was found to be higher. Thus, the nominal stress method provided good agreement with the experimental results only when the distribution of shear stress over the welded region and the distribution of normal stress over the girder region were considered correctly. The results from the equivalent nominal stress approach for determining the fatigue life were in good agreement with the recommended design curve of C56 as shown in Figure 2.28 [14]. The calculated amount of load cycles to failure was **20%** lower compared to the hot spot stress method.

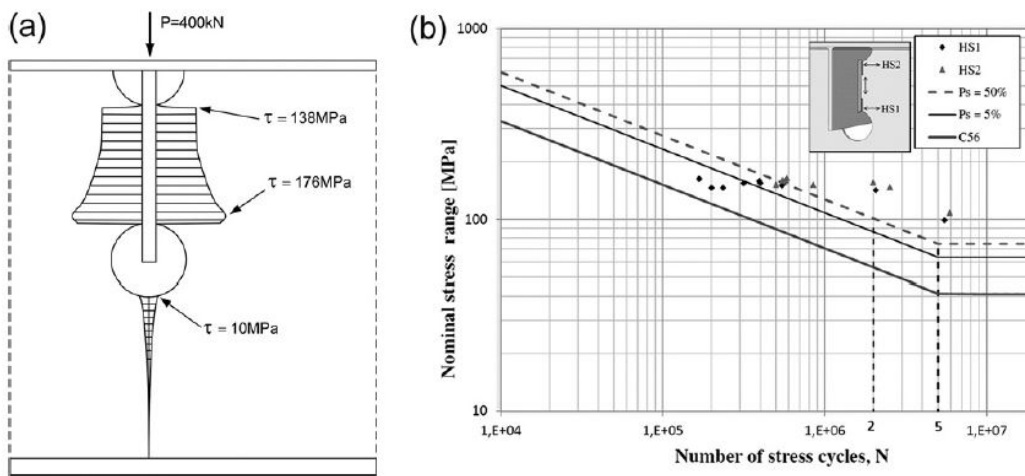


Figure 2.28: (a) Shear stress distribution and (b) S-N diagram using equivalent nominal stress considering the welded section.[12] [14]

The **structural hot-spot stress (SHSS) approach** (Figure 2.29 [14]) was more accurate in prediction of fatigue life for the studied detail. It was recommended to use solid element models including the welds for evaluating the structural hot spot stresses for the details with cut-out holes. For finding SHSS from FEM using mid-plane shell elements, the most important and crucial aspect was modelling the welds in the investigated section [12]. It was also concluded from their research, that shell element models without modelling the welds yielded unrealistic stress values for the investigated detail. From this study it was also found that around the cut-out holes, the curved stress evaluation path did not show reliable results and so the straight stress evaluation path was used to calculate the hot-spot stresses. The results from the SHSS based evaluation of the fatigue life were in good agreement with the recommended design curve of C90 as shown in Figure 2.29 [14] [12].

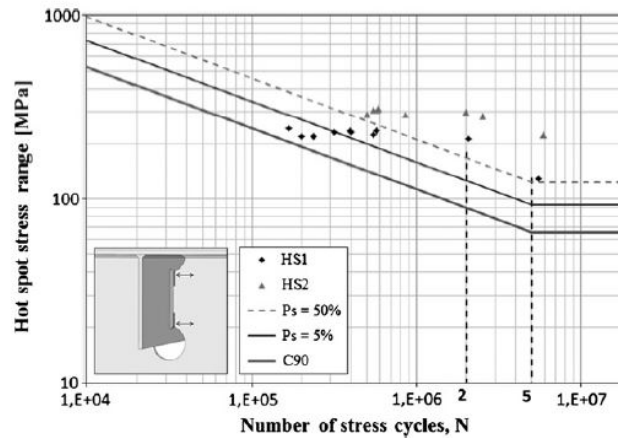


Figure 2.29: Fatigue test results when considering the structural hot spot stress approach [14] [12]

Evaluating the fatigue life according to the **effective notch stress method** was only possible from finite element analysis. Since very fine meshed models around the critical points were required, the sub-modelling technique was utilized in their study to determine the effective notch stress. This approach (Figure 2.30) [14] showed that the root geometry did not have a significant effect on the stresses at the weld toe as the stress distribution was mainly influenced by the cut-out hole. The detail category was FAT225. The results for the effective notch stress from this study, were conservative as shown in Figure 2.30 [14]. The determined value of load cycles (fatigue life) was less than half of the cycles which was determined with the hot spot stress method (with quadratic extrapolation) [14].

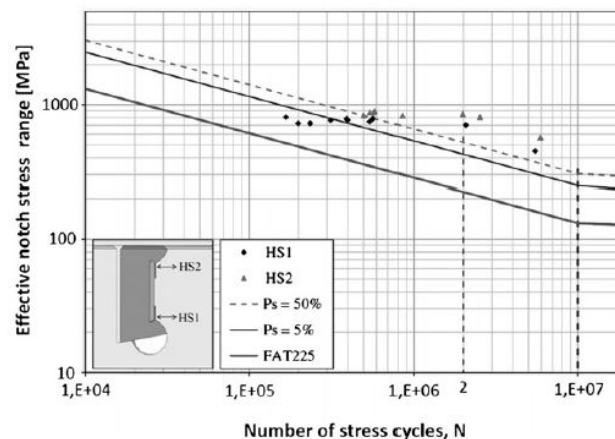


Figure 2.30: Fatigue test results for an orthotropic bridge deck based on effective notch stresses according to the IIW [14] [12]

2.7. Finite element method (FEM)

Finite Element Analysis (FEA) is defined as the simulation of a physical phenomenon using the numerical technique called Finite Element Method (FEM). FEM divides a large system into smaller and simpler parts which are known as finite elements (FE). This is achieved by discretisation in the space dimension, which is implemented by meshing of the object. FEM is used to understand, quantify and approximate any physical phenomena for example structural behaviour. Generally, these processes are described using Partial Differential Equations (PDEs). There are different FE programs which can be used to solve these physical phenomena using PDEs. In order to compute displacements, stresses or strains it is important to solve these PDEs. There is an increasing demand for reducing the computational power and effort to calculate the SHSS in the practical field. For this reason, simple models with coarse mesh sizes are generally preferred for analysis. In addition, the numerical models have to be able to capture the formation of steep stress gradients at the hot-spot locations. There are two types of elements which can capture plate bending: shell elements and solid elements, Figure 2.31 [28].

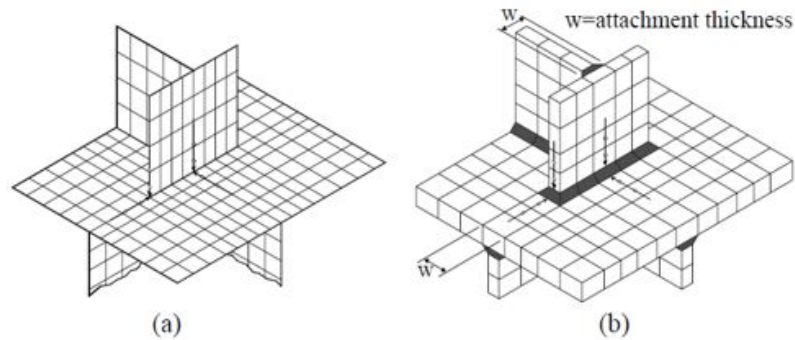


Figure 2.31: Numerical models for welded joints and stress evaluation paths: (a) shell elements excluding welds, (b) solid elements including welds [28]

In numerical modelling using FEA, shell elements can be used for getting effective results for some specific details. There is a possibility of huge computational time savings with shell elements. This is because it is possible to model thin features with fewer mesh elements. On one hand, thin shells do not consider the stress in the direction perpendicular to the shell surface which is through the thickness direction. On the other hand, thick shells can consider stresses in through-thickness direction or in the direction normal to the middle surface and account for shear deformation. The thin shell theory has some important assumptions which allow shell structures to be analysed in an efficient way by effectively simplifying a 3D problem to a 2D problem. The thin shell theory considers that the strains are small compared with unity and that the shell thickness does not change. This means that the changes in Poisson out-of-plane thickness can be ignored for thin shells. The main assumptions of the thin shell or first-order shell theory which is also known as the 'Kirchhoff-Love theory' are as follows:

1. The normal to the shell surface remain straight after deformation.
2. The normal to the shell surface remain normal after deformation.
3. The transverse normal stress is negligible.

A thick shell or second-order shell theory is obtained by discarding Assumption 2, taking transverse shear deformation into account. This known as 'Mindlin-Reissner theory'. Progressively, higher-order theories are obtained by additionally discarding Assumption 1 and then Assumption 3, leading to a full three-dimensional (3D) continuum theory with explicit modelling of all stress and strain components and changes of thickness. The theory manual of ABAQUS [8] has a shell element library divided into three categories consisting of general-purpose, thin, and thick shell elements.

- Thin shell elements provide solutions to shell problems that are adequately described by classical Kirchhoff shell theory [8].
- Thick shell elements yield solutions for structures that are best modelled by shear flexible Mindlin-Reissner shell theory. The manual recommends the application of transverse shear-flexible thick shell elements when the thickness is more than about 1/15 of a characteristic length on the surface of the shell [8].
- General-purpose shell elements provide solutions to both thin and thick shell problems [8].

The simplest modelling technique which is used in practice is by using 2D shell or plate elements. Generally, these elements are modelled using the mid-plane of the associated plate with no offsets. In engineering applications, shell elements are most widely used. This is because the modelling effort and computational power required by application of 1D shell elements is less than that compared to 2D solid or volume elements. Unlike the solid element models, the welds are generally not modelled with shell elements for the evaluation of welded structures. This is a general simplification for shell element models which cannot be applied for all details. The main problem is that shell elements are not suitable for the determination of structural hot-spot stresses (SHSS) for certain complex welded details. It can underestimate the stiffness of the weld for such details.

Solid elements 3D: Solid elements (Figure 2.31) provide a three-dimensional visual representation of the structure which needs to be modelled. They are modelled with tetrahedral (4-noded), hexahedral (8-noded) or iso-parametric (20-noded) elements [28] (Figure 2.32). More accurate approximation of stresses with solid elements is achieved compared to shell elements and thus they are closer to the real behaviour of the structure. With solid elements, the geometry of the weld can be fully modelled which provide more accurate results when compared to shell elements. Solid elements have 3 degrees of freedom per node all of which are translational degrees of freedom [28].

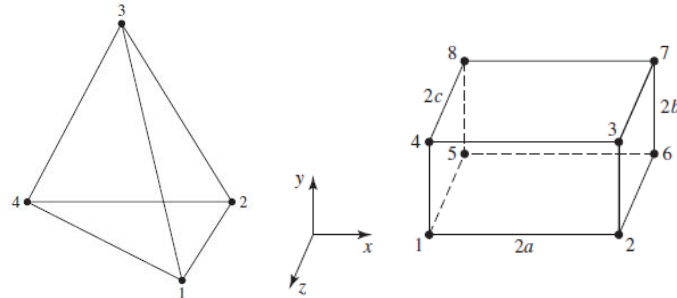


Figure 2.32: Solid elements with tetrahedral and brick shapes (4- and 8-noded respectively) [29]

Solid elements are particularly recommended in case of complex structures. One layer of iso-parametric 20-node elements in thickness direction yields reasonably accurate results due to the quadratic displacement function and linear stress distribution. The linear distribution of stress in thickness facilitates the SHSS determination directly at the weld toe. However, when multi-layer solid element models are used, the stress distribution through the thickness becomes non-linear. Subsequently, to obtain the SHSS, the through thickness stress should be linearized or alternative SHSS determination methods should be used. Moreover, using several solid elements through thickness drastically increase the computational time.

Shell elements 2D: Shell elements (Figure 2.31) give a good approximation of stresses if the thickness of the element is much smaller than the length and width of the element. The inner, outer or middle planes of the structural elements are modelled using shell elements. The welds are generally not modelled when shell elements are used for modelling a connection. For lower order linear elements, different types of geometrical shapes are possible: triangular or rectangular (Figure 2.33).

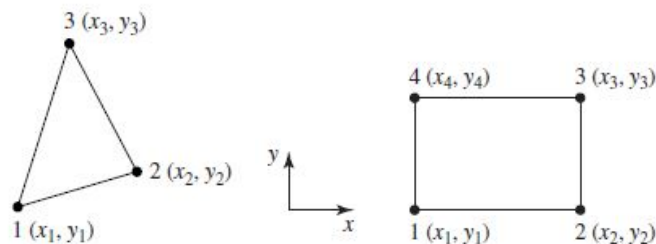


Figure 2.33: Shell elements with triangular and rectangular shapes (3- and 4-noded respectively) [29]

Triangular elements are generally used when the geometry is irregular or curved. The degrees of freedom are calculated at the nodes of an element in which the triangular element has 3 nodes and the rectangular element has 4 nodes. The rectangular element has more degrees of freedom than the triangular element and this generally results in a more accurate approximation of the results when used correctly. With shell element modelling, it is also possible to use higher order elements. When quadratic elements are used the number of nodes for the triangular and rectangular elements are respectively 6 and 8 [28]. Higher accuracy is obtained with higher order elements, but the computational time also increases. Thus, care should be taken if higher order elements are relevant and needed for obtaining the results. Shell elements have 5 degrees of freedom per node and is composed of translational and rotational degrees of freedom [28].

Different approaches for modelling of welds with shell elements

Weld modelling with oblique shell elements: The welds can be modelled by oblique shell elements. This method was initially proposed by Niemi [39]. (Figure 2.34).

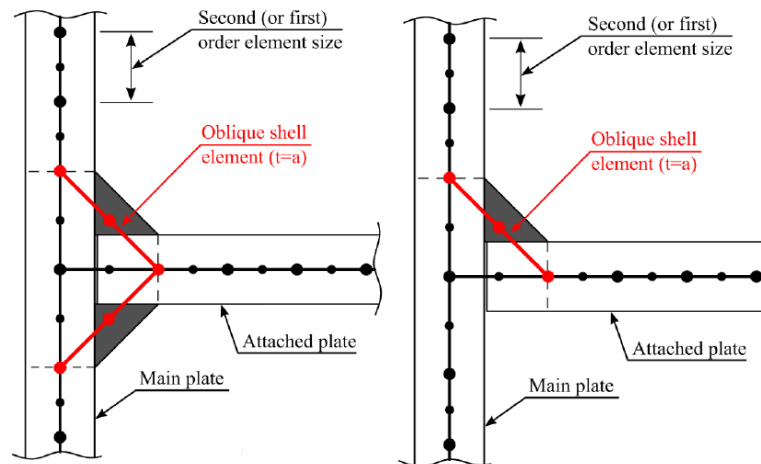


Figure 2.34: Weld modelling with inclined shell elements [39] [40]

The application of oblique or inclined elements is also listed in IIW guidelines [40]). There are some drawbacks of this method. The shell model made with such type of elements exaggerate the area of cross section close to the intersection of the plates. These oblique elements do not provide accurate stress at the weld itself. Therefore, this method can only be used for fatigue assessment at weld toe. The thickness of oblique shell elements is taken as equal to the weld throat thickness as shown in Figure 2.34. The mid-planes of the plates are modelled.

Weld modelling with shell elements having increased thickness of plate in weld region: The stiffness of the weld in the shell element model can be incorporated by increasing the thickness of the elements in the vicinity of the weld. This method was proposed by Niemi et al. [39] in which it is suggested to increase the thickness of the intersection, but there was no recommendation regarding the length and thickness of the adapted elements. Eriksson [20] has recommended using elements with increased thickness both in the attached plate and the parent plate for a double-sided fillet weld.

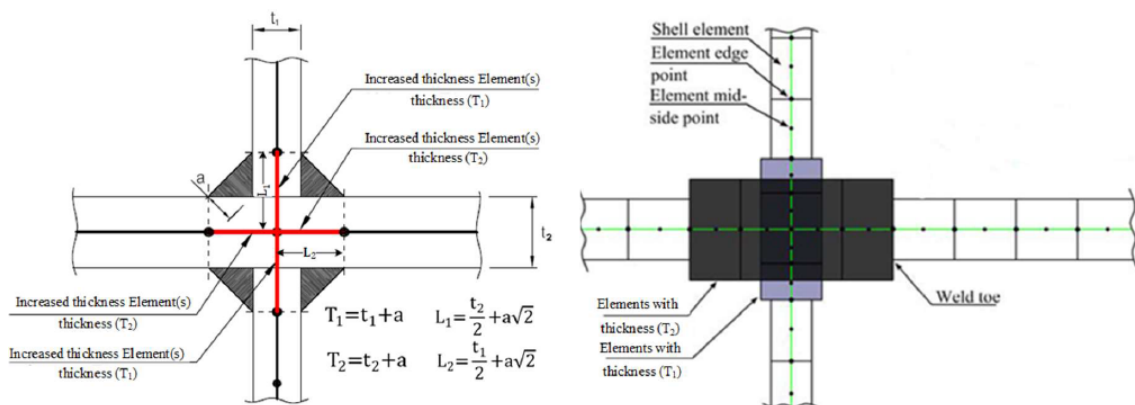


Figure 2.35: Weld modelling using increased thickness [20]

The application of increased thickness in the intersection of welded joints is also listed in the IIW guidelines [28] (Figure 2.36). But, in this approach an inclined strip is made which is different from the Niemi approach. The shell model developed using this approach depends on two geometrical properties: the increased thickness and the length of the elements (Figure 2.36).

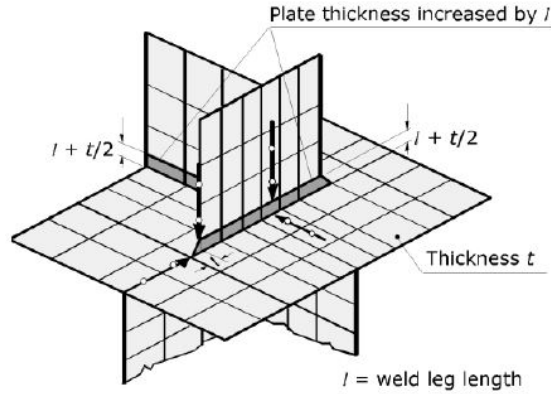


Figure 2.36: Weld modelling using increased thickness [40]

Weld modelling with shell elements using rigid links: The application of rigid links to the shell elements in the mid-surface of the plates. This approach was introduced by Fayard et al. [21] to find the SHSS at the weld toe. The area of cross section of the shell elements correspond to the actual area. This approach is also recommended by the IIW [40] (Figure 2.37).

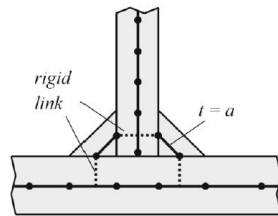


Figure 2.37: Weld modelling with rigid links [40]

According to IIW, it is proposed that the stress at the weld toe can be directly read out at the elements' centre of gravity (Figure 2.38). This means that there is no need for any extrapolation when determining the SHSS at weld toe. The basis of this approach is to model the local rigidity of a joint resulting from the weld stiffness. It is done by connecting the two adjacent shell elements using rigid links each connecting a pair of nodes located along the whole weld length. The stiffness and geometry of the welds can be considered in the shell element models using the above mentioned approaches. This is done because sometimes it is important to make the welds in a shell element model for specific details where the shell elements are not feasible for use.

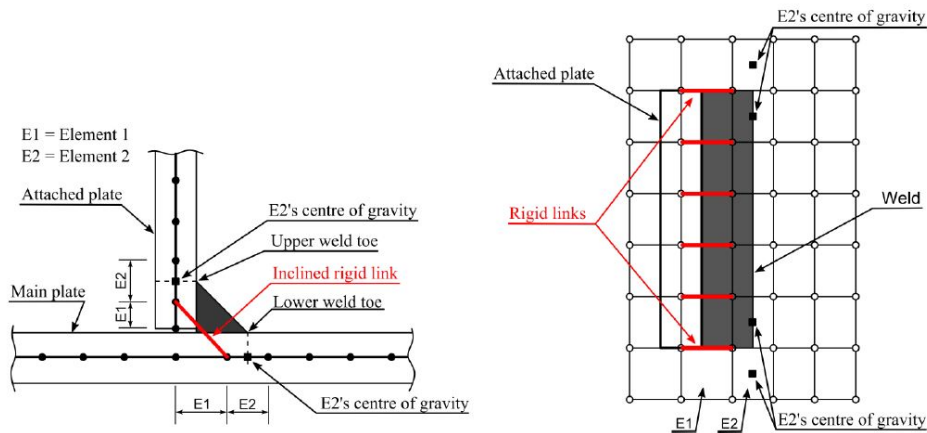


Figure 2.38: Weld modelling with rigid links [13]

2.8. Past research on shell and solid element modelling of OSDs

In the calculations of FEM, the Gaussian Quadrature approach is generally used. This approach is developed to give appropriate results for polynomials of degree $2n - 1$ or less by a suitable choice of the nodes x_i and weights w_i for $i = 1, \dots, n$. For the function to be integrated, a number of points are calculated and their positions are optimised. These points are known as Gaussian co-ordinates. The function is then multiplied by an optimised weight function for each of the Gaussian coordinates. In the final step, they are added together to calculate the integral.

When big scale structures have to be analysed, modelling the complete structure with solid elements is not often feasible as it involves a large computational time. On the other hand, the application of shell elements reduces the computational time to a great extent when compared with the full model made with solid elements. Thus, FEA of big structures with a lot fatigue critical points can be conducted in two steps. In the first step, the complete model can be developed with shell elements having a coarse mesh in order to find the location of the potential hot-spot regions. In the second step, two different approaches can be followed. The first approach is the sub-modelling technique with solid elements which involves higher accuracy of results. An important aspect is to provide adequate rotational stiffness at the interface between shell and solid elements. This is because the shell elements normally cannot transfer any moment to the solid elements. The second approach is to refine the mesh locally at the hot-spot regions of the global shell model with the help of partitioning.

In the method of developing solid element sub-models for large scale structures, at first, a shell element model with coarse mesh is recommended to calculate the global deformation of the structure. This model is called global model. Having obtained the global stresses, a local sub-model is developed with solid elements to model the investigated region with an appropriate mesh size needed to obtain the stress accurately. The appropriate mesh size is obtained after a mesh sensitivity study on the region of interest. The deformations obtained from the global shell model is generally used as boundary conditions for the local solid model or solid sub-model. Another way is to couple the solid element sub-model with the global shell model using tie constraints at the interface. However, small scale structures can be built completely with solid elements. It is true that with solid elements, the computational time increases when a fine mesh is applied at the weld toe region. Thus, for such structures also two approaches are generally recommended. The first approach is to make sub-models with solid elements to locally increase the mesh density. For the remaining part of the structure, solid elements with coarse mesh is recommended for increasing efficiency. The deformations obtained from the global solid model is used as boundary conditions for the local solid sub-model. The second approach is to refine the mesh locally at the hot-spot regions of the solid model using partitions.

Numerical investigation of P. Beld (2019): Beld [16] in her numerical analysis had used the measured strain values from the experiment of Wu et al [47] for validation of both the shell and solid element models. The experiment was performed on one of the troughs and measurements were done on two trough-deck joints. The experimental strain measurements from both the joints are shown in Figure 2.39 [16]. In addition, an average value of strain from these two trough-deck joints was used for the validation of the numerical models [16]. The FE model strain results were considered to be acceptable if the deviation from the experimentally measured strains were within **10%** according to Beld [16].

Figure 2.39 represents the strain results of two types of solid element models with linear and quadratic elements having a mesh size of 2 mm, a shell element model with a mesh size of 4 mm and a shell element model with a mesh size of 20 mm. The solid models were having full weld penetration as it was found from this research that the lack of weld penetration did not have any effect on the strain values. Due to the occurrence of stress singularity in all the numerical models, it was impossible to determine the strain value at the root of the weld directly from the FEM output. So, the strain gradients and the strain profiles were investigated for all the different numerical models to compare the accuracy of results. It was observed that the shell element model with a relatively fine mesh had a similar trend with the measured strains of the first specimen. But at a distance of 4 mm from the weld root, the strain range was found to be higher than the **10%** deviation (Figure 2.39 [16]). The coarse mesh (20 mm) shell element model gave higher strain range in comparison to the fine mesh (4 mm) model. For the coarse mesh shell model, the strain range was comparable to all the other numerical

models at a distance of 20 mm away from the weld root. The strain was higher in the region close to the weld root. Therefore, the slope of the curve was larger compared to the other numerical models.

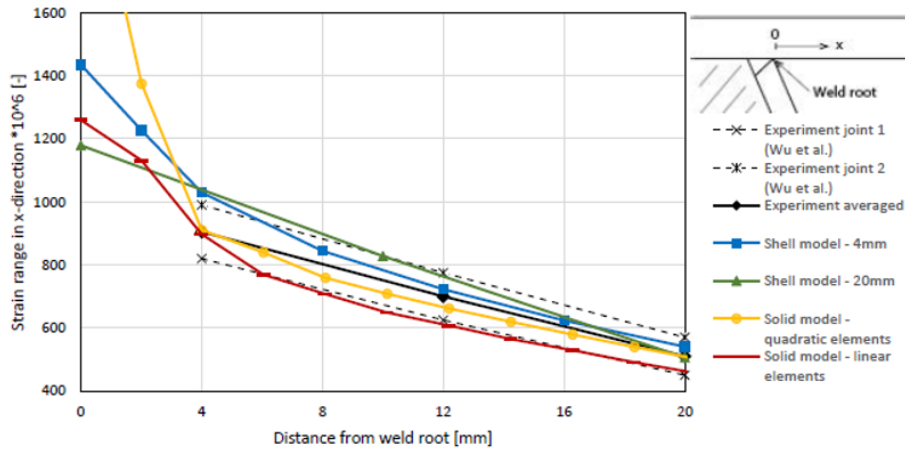


Figure 2.39: Comparison of strains between the finite element models and experimental measurements at the lower surface of deck plate [16]

In this research, solid and shell elements with reduced integration were used. On one hand, the solid model with quadratic elements (C3D20R) agreed well with the experimental results [16]. On the other hand, the solid model with linear elements (C3D8R) gave strain range which was lower than the strains obtained from the experiments. Beld [16] stated in her conclusion that the application of solid elements for the SHSS method resulted in a longer fatigue life in comparison to the application of shell elements for the investigated detail (Figure 2.40). The fatigue life determined from calculation with solid elements was **44%** higher than that compared to the shell element model with a relatively fine mesh.

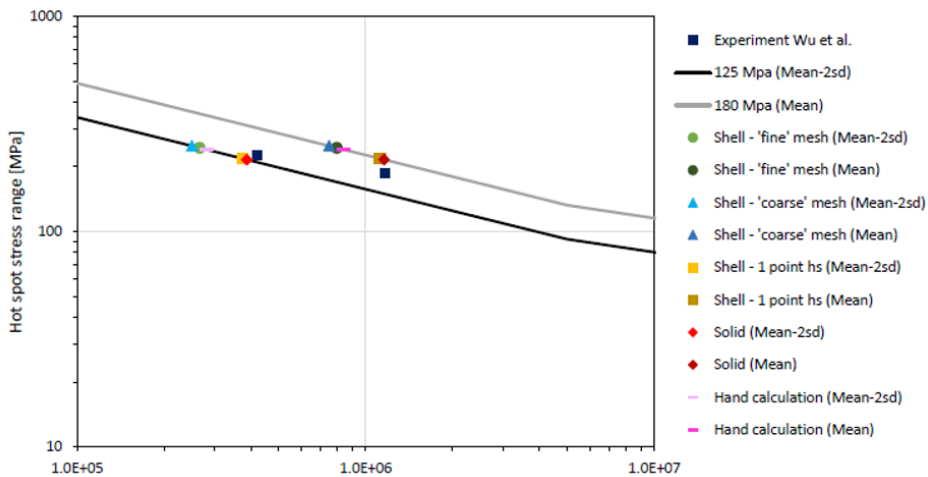


Figure 2.40: Hot-spot stress design S-N curve plots for numerical models and results from experiments [16]

Numerical investigation of M. Aygül, M. Al-Emrani and S. Urushadze (2011): In the research of Aygül [14], a series of fatigue tests were performed under constant amplitude fatigue loading (CAFL) and the number of cycles to crack detection for different cracking locations was registered. At first, a three point bending test was performed where a static load was applied initially to three test specimens (Figure 2.41). The static loading was applied such that the stresses were below the yield strength of the specimens. The strain distribution was measured at pre-determined locations, which included the hot-spot regions where it was expected that the crack would initiate. These locations were 'HS1' and 'HS2' as shown in Figure 2.41.

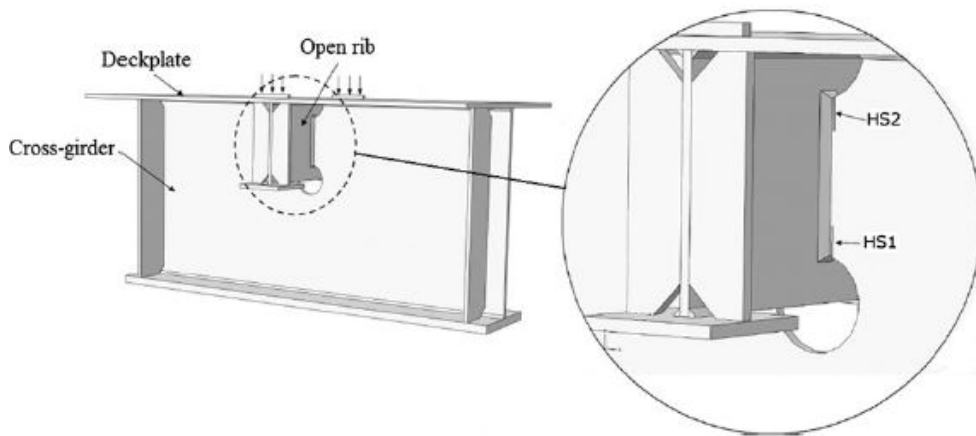


Figure 2.41: Application of load for fatigue testing of the specimen and the regions of interest (hot-spots) [14]

The same locations were also investigated by Akhlaghi [9][10] in his research with another test specimen having similar detail. The point 'HS1' corresponds to point 'wb' and the point 'HS2' corresponds to point 'wt' in the thesis of Akhlaghi [9]. A comparison study was made between the SHSS values calculated from the numerical analysis of Aygül [14] using shell and solid elements as shown in Figure 2.42. It was observed that solid elements with an element size of 4 mm complied best with the experimental strain measurements. The solid element models estimated the SHSS really well at the investigated points of the specimen [14]. The shell element model where the welds were modelled using oblique/inclined shell elements also gave good results compared with the normal shell element models without welds. The SHSS values obtained from the shell models without welds had a large difference with the SHSS values obtained from solid models and also from measurements [14].

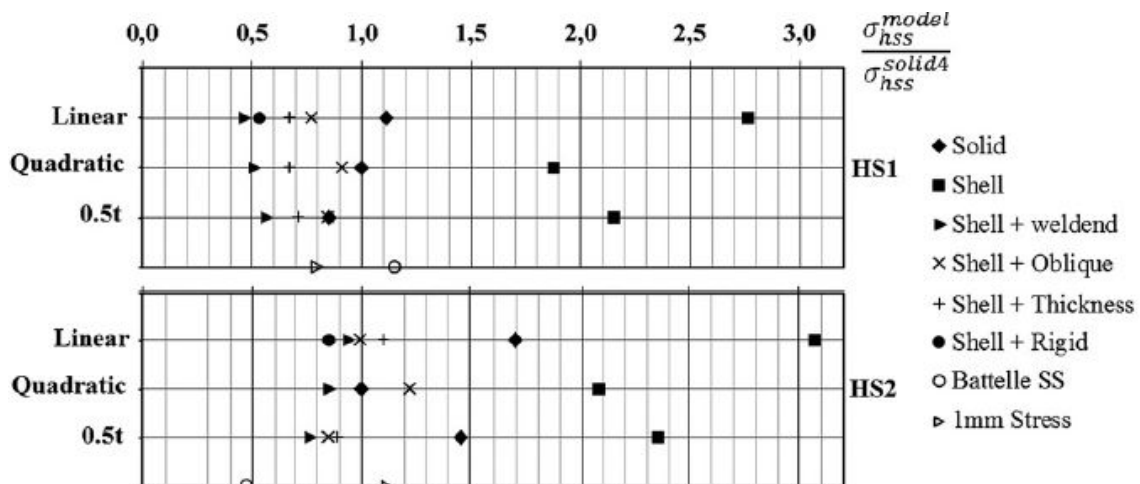


Figure 2.42: Comparison of the results from FE analyses [14]

In the research of Aygül [14], it was stated that shell elements were not suitable for the representation of the actual behaviour of the structure for such joints as the one investigated. Thus, including welds in the shell element models using the IIW guidelines [28] is strongly recommended when analysing welded joints with cut-out holes. It was also concluded that the stress evaluation path around the hole (curved stress evaluation path) did not have good agreement with the experimental results. The Battelle structural stress method [17] produced a good result for 'HS1', while the method underestimated the stress concentration at 'HS2' [14]. However, the approach of Xiao and Yamada [48] which was the 1 mm stress method gave good results for both investigated points 'HS1' and 'HS2' as shown in Figure 2.42. In this research, a large scatter in fatigue assessment as shown in Figure 2.43 was observed when different fatigue assessment procedures were used [12][13][14].

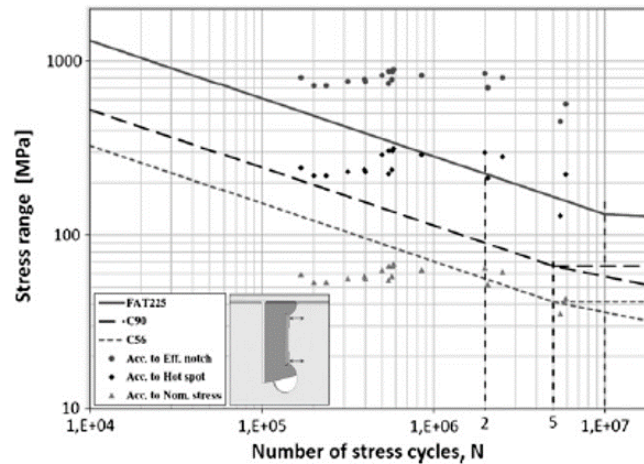


Figure 2.43: The S–N curves for an orthotropic bridge deck based on nominal stress approach, SHSS approach and effective notch stress approach [14] compared with fatigue experiments

Numerical study of N. Osawa (2011): Osawa [41] in his study, proved that solid elements have a lower curvature than shell elements in a connection or intersection between two elements. In Osawa's research, he obtained a difference in stress results when modelling the connection between two plates with shell and solid element types. The transverse curvature of a solid element might be restrained to some extent by the element it is intersected by. But this was not observed for shell elements. This is explained in Figure 2.44 [41].

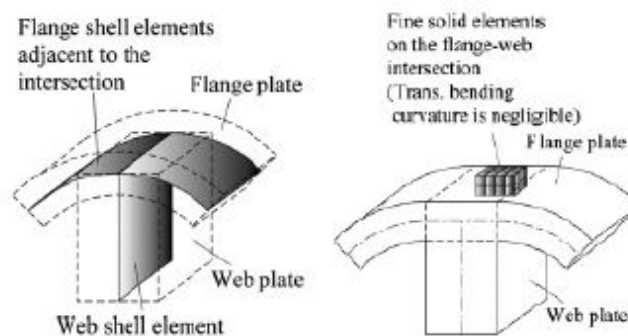


Figure 2.44: Visible difference between the curvature for shell element model and the curvature for solid elements [41]

2.9. Fatigue load models (FLM) according to EN 1991-2

For the application of the nominal stress concept, the fatigue load model FLM 3 according to Eurocode 1 (EN 1991-2) [4] with its fictitious four-axle vehicle and the damage equivalent factors λ is generally used. For the fatigue assessment at the very local details on an OSD, FLM 3 does not deliver appropriate results because of the fictitious wheel patch areas for each axle. The occurring stresses in the details are dependent on the axle loads of the heavy vehicles as well as the wheel load geometries within an axle. Thus, a more accurate load model with more realistic wheel geometries and axle loads is necessary for the assessment of local details of OSD.

The fatigue load model FLM 4 includes 5 different lorry types and within a single vehicle 3 different axle types are indicated. This load model FLM 4 is much more detailed than FLM 3, so that it is appropriate for fatigue assessment of the very local details on an orthotropic bridge deck. FLM 4 has also the possibility to adapt the axle loads and gross weights with weigh in motion measurements (called FLM 4*). The fatigue load model FLM 2 is based on the same lorry and axle types as FLM 4, but they have higher axle load and gross weights. Fatigue load models FLM 4, FLM 4* and FLM 2 are presented in Figure 2.45 [4]. There are 5 different lorry types (T1 to T5) according to EN 1991-2 [4].

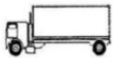

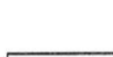


type	lorry type	axle spacing [m]	wheel type resp. axle type	lorry percentage \bar{n}_i [%]	FLM 4*		FLM 4		FLM 2	
					A_i	G_{tot}	A_i	G_{tot}	A_i	G_{tot}
T1		4.50	A B	20	49,7 92,3	142 (71%)*	70 130	200	90 190	280
T2		4.20 1.30	A B B	5	61,6 105,7 105,7	273 (88%)*	70 120 120	310	80 140 140	360
T3		3.20 5.20 1.30 1.30	A B C C	50	51,4 110,2 66,1 66,1 66,1	360 (73%)*	70 150 90 90 90	490	90 180 120 120 120	630
T4		3.40 6.00 1.80	A B B B	15	52,1 104,1 66,9 66,9	290 (74%)*	70 140 90 90	390	90 190 140 140	560
T5		4.80 3.60 4.40 1.30	A B C C C	10	49,9 92,7 64,2 57,1 57,1	321 (71%)*	70 130 90 80 80	450	90 180 120 110 110	610

Figure 2.45: Fatigue load models FLM 4, FLM 4* and FLM 2 (* percentage of FLM 4) (EN 1991-2 [4])

2.10. Residual stresses

When the weld metal contracts during cooling phase, the stresses which get locked in result in the development of residual stresses. These stresses can be generated during the manufacturing process or during welding. Figure 2.46 [26] shows the manufacturing residual stresses which develop during the cooling process of hot-rolled sections. The outer part of flanges and middle part of web is in compression and the remaining part of the section is in tension. A tensile residual stress reduces fatigue life and a compressive residual stress increases fatigue life. The residual stresses may also relax with time, especially if there are peaks in the load spectrum that cause local yielding effect at stress concentration points. The other method to reduce residual stress is by re-heating which is not always possible to implement. Complete relief of residual stress is not possible to achieve. The detail category used for fatigue assessment with the S-N curve includes the residual stresses.

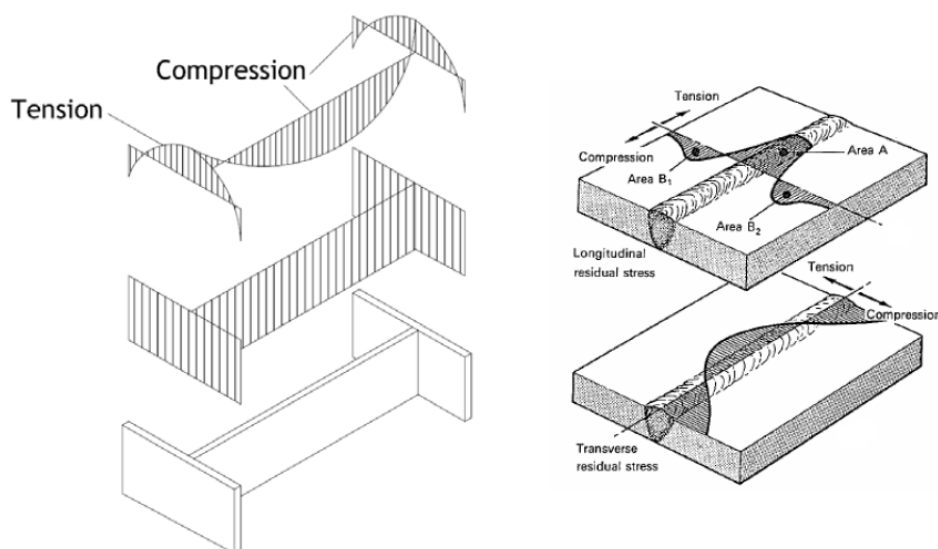


Figure 2.46: Residual stresses in a hot rolled element (left) and due to welding (right) [26]

2.11. Fatigue life prediction

The fatigue damage is generally evaluated using Palmgren-Miner Damage Model. According to Palmgren and Miner, failure occurs when the cumulative damage caused by each loading cycle equals one.

$$D = \sum_{i=1}^k \frac{n_i}{N_i}$$

Where, k is the different stress levels, N_i is the average number of load cycles to failure, n_i is the number of load cycles accumulated and D is damage ratio (failure occurs when D reaches 1).

When both direct/normal and shear stresses occur in the region which is prone to cracking, the EN 1993-1-9 [2] recommends the damage ratios due to each stress effect being calculated. In this case, it is assumed that total fatigue damage caused by combination of different types of stresses is the summation of damages caused by each individual type of stress. The damage ratio for each source is the total number of load cycles that the particular detail is exposed to during its service life divided by the total number of cycles to failure at that stress level which is evaluated from the S-N curve. This is represented in the following equation:

$$D_{\sigma} + D_{\tau} = \left(\frac{n}{N} \right)_{\sigma} + \left(\frac{n}{N} \right)_{\tau} \leq 1$$

Where, D_{σ} is the damage due to normal stress and D_{τ} is the damage due to the shear stress.

2.12. Partial safety factors

From Eurocode (EN 1993-2), the consequence of failure for OSD should be taken as low consequence and the fatigue assessment method should be considered as safe life as shown in Table 2.2 (EN 1993-2-NB, 2011).

Table 2.2: Partial safety factor for fatigue strength (EN 1993-2-NB, 2011)

Assessment method	Consequence of failure	
	Low consequence	High consequence
Damage tolerant	1.00	1.15
Safe life	1.15	1.35

This means that the partial safety factor for fatigue strength (γ_{Mf}) is 1.15. A distinction is made between the fatigue strength factor (γ_{Mf}) and the fatigue load factor (γ_{Ff}) in fatigue design. The fatigue load factor (γ_{Ff}) is equal to 1. The fatigue strength factor depends on the assessment method and the consequence of failure (Table 2.2).

After a brief study on past research in this chapter, it is observed that various researchers have tried to bridge the gap between the calculation of hot-spot stress with shell and solid elements. Some of them have suggested using weld modelling methods with shell elements for improving both the global and local behaviour in terms of deformation. From the numerical investigation of Akhlaghi [10], it was observed that there is a huge scatter of hot-spot stress between the regular shell and solid model. This scatter was reduced after modelling welds with shell elements using the increased thickness method. Moreover, the stress gradients obtained after weld modelling with shell elements were more in-line with the stress gradients obtained from the solid model. Thus, among the weld modelling methods with shell elements, the increased thickness approach according to IIW [28] and according to Eriksson [20] has been elaborately explored in the present research for the connection of open stiffener to crossbeam at the location of cope hole in OSD.

3

Simple fillet welded details

“The only source of knowledge is experience.”

Albert Einstein

This chapter focuses on numerical modelling of simple fillet welded details. The hot-spot stress is computed using finite element modelling in order to gain some insight regarding the difference in behaviour between shell and solid elements. Also, some aspects regarding the details which cannot be modelled properly with shell elements have been provided. Two types of details have been investigated in this chapter: (a) single side fillet welded longitudinal plate joint and (b) double side fillet welded transverse cruciform joint. The geometrical details of these two joints have been obtained from literature.

3.1. Single side fillet welded longitudinal plate joint (T-joint)

The first studied detail is a single side fillet welded longitudinal plate joint (detail type a) which is also known as a T-joint (section 3.1.2). This detail is numerically investigated under tension and bending load cases and the structural hot-spot stress (SHSS) is determined.

3.1.1. Numerical investigation from the research of Śledziewski (2018)

In the research of Śledziewski [54], a unit stress (1 MPa) was applied on the FEM models, the output was interpreted as the stress concentration factor (SCF). Linear and quadratic extrapolation methods were used to find the hot-spot stress. Based on the statistical assessment of the test data, the course of the regression curve was determined and in consequence the standard fatigue for 2 million cycles (N_c) was determined. The analysis was carried out according to the requirements of the Eurocode 3 (EN 1993-1-9 [2]). Table 3.1 summarises the test results of the longitudinal attachments subjected to tensile loading [54].

Table 3.1: Numerical results on fatigue for longitudinal plate joint according to nominal stress approach [54]

Test data	N	Nominal stress range (MPa)	Hot-spot stress range (MPa)		SCF	
			Linear Extrapolation	Quadratic Extrapolation	Linear Extrapolation	Quadratic Extrapolation
1	1.96E+05	181.3	213.9	217.5	1.18	1.20
2	2.46E+05	180.2	212.6	216.2	1.18	1.20
3	3.40E+05	149.8	176.7	179.7	1.18	1.20
4	4.17E+05	139.9	165.1	167.9	1.18	1.20
5	4.93E+05	139.9	165.1	167.9	1.18	1.20
6	7.72E+05	119.9	141.5	143.9	1.18	1.20
7	9.29E+05	109.4	129.0	131.2	1.18	1.20
8	1.14E+06	110.7	130.6	132.8	1.18	1.20
9	1.29E+06	100.3	118.4	120.4	1.18	1.20
10	1.43E+06	100.3	118.4	120.4	1.18	1.20

It was also concluded from the literature that the assumed detail category FAT71 is appropriate. But on the other hand, the recommended fatigue detail category FAT100, from SHSS method is conservative. Thus, it was recommended from the literature, to be replaced by the category FAT90 [54].

3.1.2. Geometry

Steel plates of 16 mm thickness are used in this study. The longitudinal rib is 50 mm high and 60 mm long, whereas the main plate is 300 mm long and 90 mm wide. The weld throat thickness is 5 mm [54].

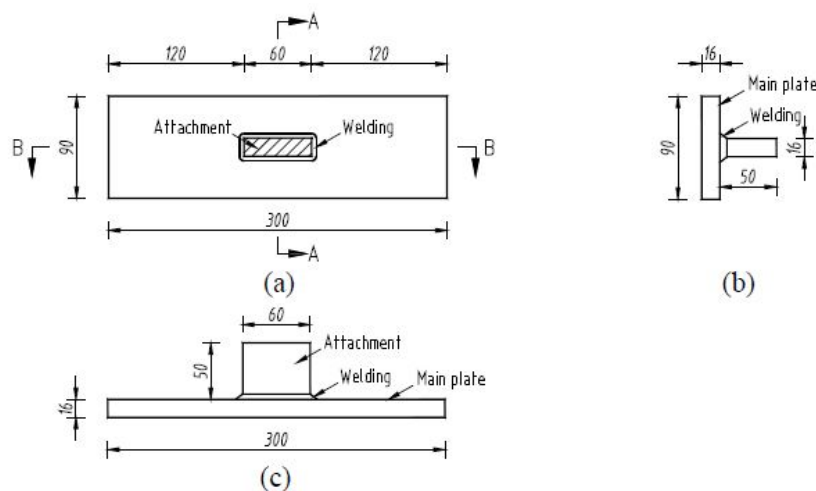


Figure 3.1: Geometry of the investigated welded steel joint (all dimensions in millimetre): (a) top view of the specimen (b) section A-A (c) section B-B [54]

3.1.3. Material properties

Steel with elastic modulus of $E = 210$ GPa and Poisson's ratio of $\nu = 0.3$ is used for the entire geometry including the welds. Since elastic material behavior is assumed for the fatigue analysis, only elastic material properties are defined.

3.1.4. Stress extraction path and coordinate system

The coordinate system is chosen to be consistent for both solid and shell finite element models. The plate surface stresses along a line perpendicular to the weld toe are used to compare both the numerical models. The same path and direction are used for both the numerical models as shown in Figure 3.2. The assembly orientation is also chosen to be consistent in both the models.

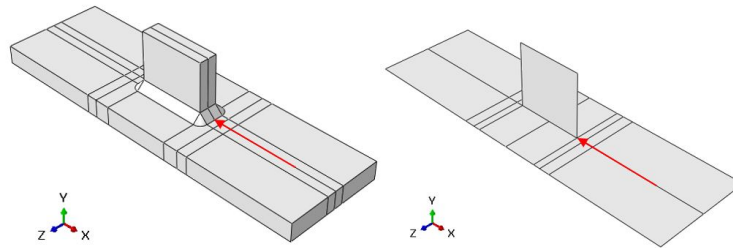


Figure 3.2: Coordinate system for the numerical models: solid (left) and shell (right)

3.1.5. Loading and boundary conditions

Tension: Tensile stress of 1 MPa is applied on both ends of main plate. The tensile load is applied in longitudinal (x) - direction following the coordinate system shown in Figure 3.2. The models are not restrained in width and thickness directions. Thus, lateral contraction is not prevented in the numerical models. Full geometry is used for developing the models in order to maintain consistency in modelling as is also done by Śledziwski [54]. All other numerical models in this thesis are made using full geometry. The loading and boundary condition is shown in Figure 3.3.

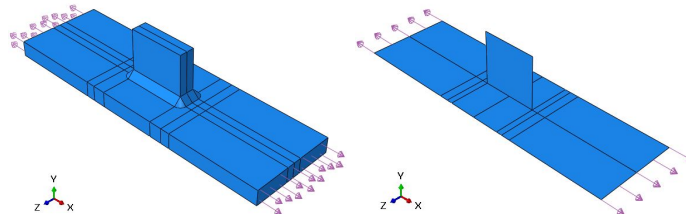


Figure 3.3: Solid (left) and shell (right) element models under tension

Bending: A uniform pressure of 1 MPa is applied over the top plate. The bottom plate is simply supported at the ends. Both edges at the end of the plate is restrained against vertical - (y) direction according to the coordinate system shown in Figure 3.2. For the solid model, the bottom edge is used for applying the boundary conditions as shown in Figure 3.4.

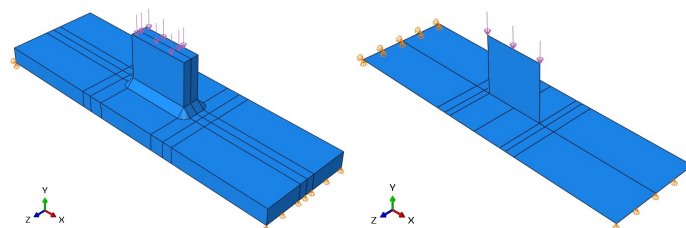


Figure 3.4: Solid (left) and shell (right) element models under bending

3.1.6. Numerical modelling

The solver used for numerical modelling is set to Static - General in the step module of ABAQUS as linear analysis is performed. The plates in the numerical model are partitioned to create nodes at the reference points 0.4 t and 1.0 t for linear surface stress extrapolation. The same is done at points 0.4 t, 0.9 t and 1.4 t for quadratic surface stress extrapolation. The weld throat thickness is 5 mm. Here, t is the plate thickness. The stress concentration in longitudinal attachments is observed on the base plate surface at the weld toe for tensile load (Figure 3.5). Therefore, it is classified as type-“a” hot-spot. To find the SHSS, the stress distribution orthogonal to the weld toe is plotted for both the models (Figure 3.5). The figure shows the stress paths for extrapolation of the solid and shell numerical models at the plate surface. The origin of the stress profile is taken at the weld toe for solid element model and at the plate intersection for shell element model. For all the numerical models, average stress over the finite element boundaries are considered by using the stress averaging option in ABAQUS. The stress profiles are also investigated with the stress averaging turned off. It is observed that there is no effect of stress averaging on the hot-spot stress as the reference points are far away from the affected nodes.

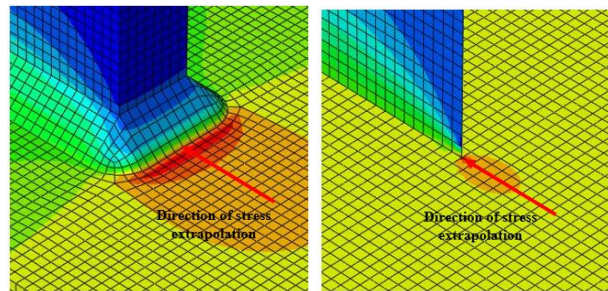


Figure 3.5: Stress path orthogonal to the weld line at the base plate surface for tension load

Development of solid element models: The solid element reference model is developed using dimensions from Figure 3.1 [54]. The weld is modelled using chamfering and solid sweep function in ABAQUS. The curvature of the weld at the corner of the stiffener is modelled using sweep edge tool. This is done so that the weld looks as close to reality as possible. The effect of element sizes are studied for the solid element models. They are made such that a cubic block could be generated having dimensions $A \times A \times A$ mm³ where A is the mesh size in mm. Since the thickness of the main and stiffener plates is 16 mm, for a mesh size of 2 mm (t/8), the number of elements in the thickness direction is 8. The mesh sizes investigated are $A = t/2$, $t/4$, $t/8$ and $t/16$ (8 mm, 4 mm, 2 mm and 1 mm respectively). The stress contour plot of the solid model loaded in tension is shown in Figure 3.6.

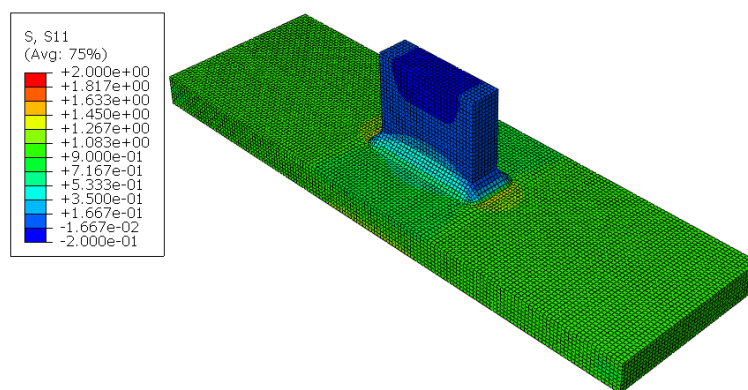


Figure 3.6: Contour plot of stress (S11) for solid element model loaded under tension

For the solid model, the middle path of the attachment plate is considered (Figure 3.5) because it showed maximum stress concentration compared to the corner path of the attachment plate. The stress perpendicular to the weld toe is extracted along the path shown in Figure 3.5. The crack - assign seam tool in ABAQUS is used to model the gap between the plates inside the weld region. This is done to

model a load carrying weld connecting the two plates. The effect of non-load carrying weld is checked. It is observed that the stress values did not change more than 1% if the seam is not incorporated in the solid model (Figure 3.7). The extraction of stress perpendicular to weld toe is done according to the path shown in Figure 3.5. For both the load cases tension and bending, there is no significant difference between the solid models with and without seam crack. The number of elements at the weld for solid model are the same as the global mesh size in the mesh refinement study.

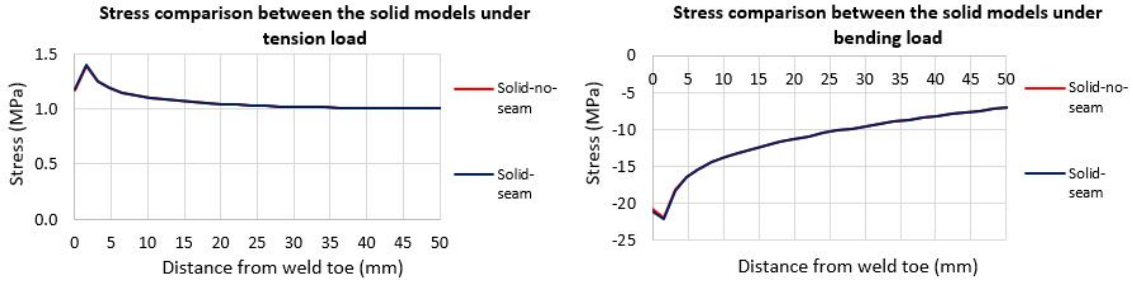


Figure 3.7: Stress perpendicular to weld toe for solid model with and without seam for tension load (left) and bending load (right)

Development of shell element models: Initially, the shell element model is developed using mid-plane geometry according to IIW [28]. The mid-plane sections are incorporated in the property module as shown in Figure 3.8. The total height of stiffener plate is the sum of height of stiffener plate and half of thickness of base plate. Thus, the total height of the shell element model after extrusion remained same as that of the solid element model. The weld is not modelled with shell elements for any of the approaches at first. In later sections, the weld modelling concept using shell elements has been investigated in detail. For the shell model however, there is only one path as shown in Figure 3.5.

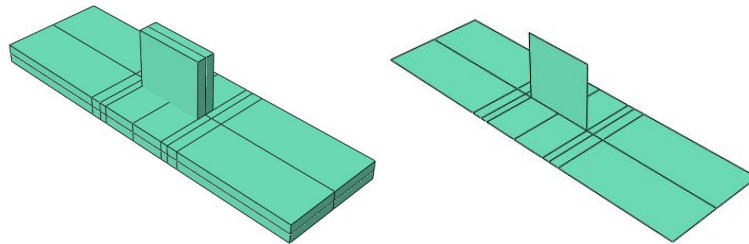


Figure 3.8: The shell element model with and without rendered shell thickness using mid-plane sections for both the plates

In order to study the effect of offsetting the plate, the base plate is modelled with bottom surface approach. The height of the stiffener is taken to be the reference height of 50 mm without any additions of thickness. This can be visualized in Figure 3.9.

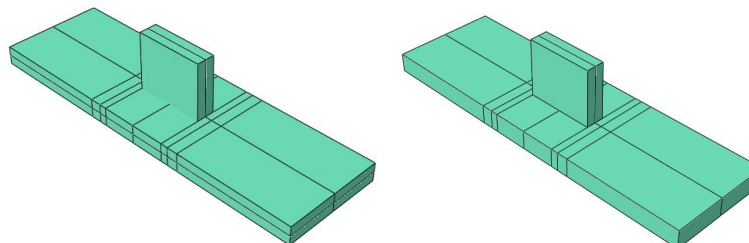


Figure 3.9: Shell model with different modelling approaches, left: shell offset - mid-surface, right: shell offset - bottom-surface

The meshing of the shell element models is made such that a square plate could be generated having dimensions $A \times A \text{ mm}^2$ where A is the mesh size in mm. The mesh sizes investigated are $A =$

$t/2$, $t/4$, $t/8$, and $t/16$, where t is the thickness of plate. Both these approaches are analysed for tension and bending load cases as shown in Figure 3.10.

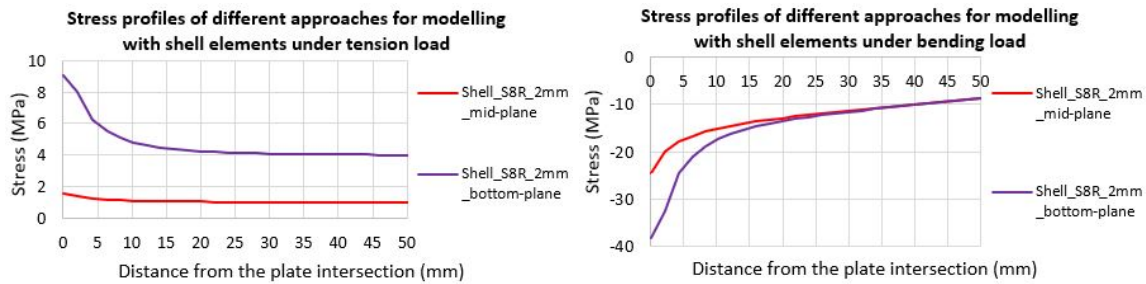


Figure 3.10: The stress profiles of shell element model with different approaches for modelling under tension load (left) and bending load (right)

On one hand, the difference in stress results for tension load case is mainly due to the eccentricity which is present in the offset - bottom surface approach. This eccentricity is not present with the offset - mid-surface approach. Due to this eccentricity, additional moments develop on the base plate ends at the time of tensile loading. This is also the reason why the nominal stress values are different for the shell models loaded in tension (Figure 3.10). The gap in nominal stress values between the numerical models is approximately **3 MPa**. On the other hand, for bending load, the nominal stress is found to be same for both the approaches of shell modelling. The difference is observed in the stress gradient in the vicinity of the hot-spot (Figure 3.10). The stress profiles converged at a distance of 25 mm away from the weld toe for both the approaches of shell modelling in bending load case.

In addition to the stresses, the deformations are also investigated for both load cases (Figure 3.11). The graphs show that the deformation behaviour is more or less similar for both the shell models under bending but the same is not observed for tension.

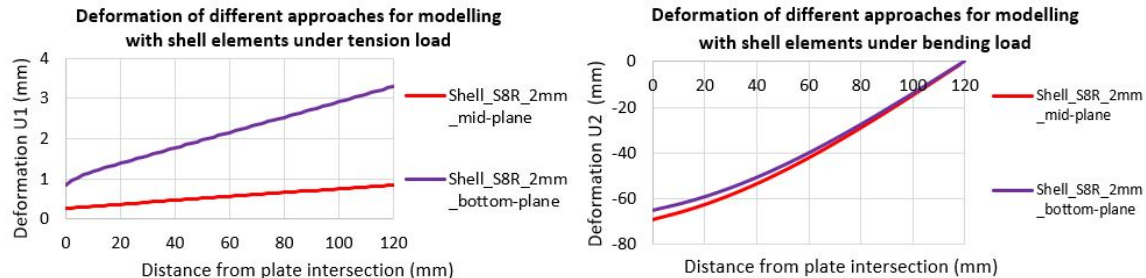


Figure 3.11: The deformation of shell models subject to tension load (left) and bending load (right)

Thus, the SHSS values are different for both the approaches of modelling shell elements as shown in Table 3.2. The shell model with shell offset-bottom surface showed a very large hot-spot stress value for tensile loading (**6.26 MPa**). The SHSS obtained from the numerical investigation of Śledziewski [54] was **1.18 MPa** for linear extrapolation (Table 3.1) [54] for tension loading. The mid-surface approach of shell model gave a SHSS value of **1.24 MPa** which is closer to that obtained from the research of Śledziewski [54] with an overestimation of **5%** which is acceptable.

Table 3.2: SHSS obtained from two different approaches using shell elements

Tensile load			Bending load		
SHSS (MPa)		Percentage Difference in SHSS (%)	SHSS (MPa)		Percentage Difference in SHSS (%)
Shell offset: Mid-surface	Shell offset: Bottom surface-plane		Shell offset: Mid-surface	Shell offset: Bottom surface-plane	
1.24	6.26	404%	-18.61	-25.15	35%

The mid-surface offset approach is chosen as an appropriate modelling strategy with shell elements for further analysis as the bottom surface offset is giving a higher value compared to the numerical results Śledziewski [54] (Table 3.1 and 3.2). Thus, the development of the shell model with mid-surface offset is recommended as a better strategy for such details. The stress contour plot (S11) of the shell element model using mid-plane approach and loaded in tension is shown in Figure 3.12.

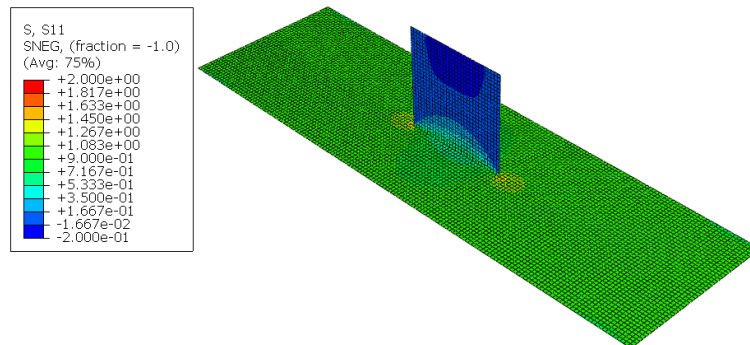


Figure 3.12: Contour plots for shell element model loaded under tension

Shell element model with welds modelled using the local increase in thickness approach:

The welds are modelled using the approach mentioned in the IIW guidelines [40]. Figure 2.36 in Chapter-2 illustrates this approach. This increases the stiffness of the welded region and it will result in higher value of SHSS compared to the shell elements without welds. This has been investigated in a parametric study in later sections. The details of the stress contour plots are shown in Appendix-I for shell element model, solid element model and shell element model with welds. From deformation contours shown in Appendix-I for bending, it can be seen that all the numerical models have more or less same deformation in the middle of the base plate.

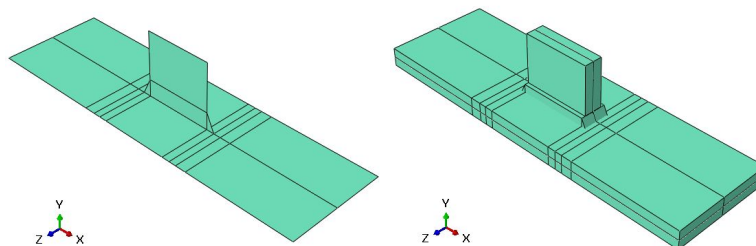


Figure 3.13: Weld modelling with shell elements with increase of thickness at the weld location: (Left - normal view) (Right - rendered view)

3.1.7. Mesh sensitivity study for tension load case

A mesh sensitivity study for tensile loading is performed for this welded detail. At first, FE models meshed using elements with reduced integration is studied. Later on, the elements with full integration are also investigated. The thickness of the base and top plates is $t = 16$ mm. The following global mesh sizes are investigated: 8 mm, 4 mm, 2 mm and 1 mm respectively ($t/2$, $t/4$, $t/8$ and $t/16$). The description of the investigated element types is shown in Table 3.3 [8]. The figures for the stress profiles obtained from mesh sensitivity analysis for tension load case are shown in Appendix-B.

Table 3.3: Description of the elements [8]

Element type	Description	Integration points
C3D8R	An 8-node linear brick element with reduced integration and hourglass control	1x1x1
C3D8	An 8-node linear brick element	2x2x2
C3D20R	A 20-node quadratic brick element with reduced integration	2x2x2
C3D20	A 20-node quadratic brick element	3x3x3
S4R	A 4-node doubly curved thin or thick shell element with reduced integration, hourglass control and finite membrane strains	1x1
S4	A 4-node doubly curved general-purpose shell element with finite membrane strains	2x2
S8R	An 8-node doubly curved thick shell element with reduced integration	2x2

The SHSS value is calculated from the numerical models using linear extrapolation for all the mesh sizes. The SHSS values and SCF are shown in Table 3.4. For the quadratic solid elements (C3D20R) loaded in tension, it is observed that the SHSS values are converging to **1.177 MPa** for mesh size of 2 mm. For the linear solid elements (C3D8R), it is observed that the SHSS value for 2 mm mesh and that for 1 mm mesh is very close to each other. However, for obtaining full convergence with C3D8R elements, a mesh size of 0.5 mm is required. But this involved a lot of computational time as a mesh size of 0.5 mm is very small. Thus, a mesh size of 2 mm is selected as a proper mesh size for further numerical investigation with solid elements under tensile load. For the linear shell elements (S4R) loaded in tension, it is observed that the SHSS values are converging for mesh size of 2 mm to a value of **1.215 MPa**. This behaviour is also observed for quadratic shell elements (S8R). Thus, for the shell elements also a mesh size of 2 mm is selected for further numerical analysis with tensile loading.

Table 3.4: SHSS of solid and shell elements with reduced integration for tension

Tensile load - Linear Extrapolation					
Element Type	Mesh	$\sigma_{0.4t}$ (MPa)	$\sigma_{1.0t}$ (MPa)	SHSS (MPa)	SCF
Solid - C3D8R	8mm	1.102	1.058	1.132	1.132
	4mm	1.128	1.061	1.172	1.172
	2mm	1.134	1.063	1.182	1.182
	1mm	1.136	1.065	1.184	1.184
Solid - C3D20R	8mm	1.127	1.092	1.150	1.150
	4mm	1.138	1.087	1.173	1.173
	2mm	1.137	1.078	1.177	1.177
	1mm	1.137	1.078	1.177	1.177
Shell - S4R	8mm	1.139	1.058	1.192	1.192
	4mm	1.140	1.057	1.196	1.196
	2mm	1.151	1.056	1.215	1.215
	1mm	1.151	1.056	1.214	1.214
Shell - S8R	8mm	1.215	1.066	1.315	1.315
	4mm	1.184	1.064	1.264	1.264
	2mm	1.170	1.060	1.243	1.243
	1mm	1.169	1.058	1.244	1.244

A separate mesh sensitivity study for tensile loading is also performed using elements with full integration with the above mentioned mesh sizes 8 mm, 4 mm, 2 mm and 1 mm. Appendix-B also shows the figures of mesh sensitivity study with full integration. The SHSS values and the SCF obtained with full integration has been summarized in Table 3.5.

Table 3.5: SHSS of solid and shell elements with full integration

Tensile load - Linear Extrapolation					
Element Type	Mesh	$\sigma_{0.4t}$ (MPa)	$\sigma_{1.0t}$ (MPa)	SHSS (MPa)	SCF
Solid - C3D8	8mm	1.112	1.068	1.142	1.142
	4mm	1.128	1.071	1.165	1.165
	2mm	1.130	1.060	1.177	1.177
	1mm	1.131	1.060	1.179	1.179
Solid - C3D20	8mm	1.189	1.061	1.275	1.275
	4mm	1.149	1.065	1.206	1.206
	2mm	1.134	1.066	1.179	1.179
	1mm	1.136	1.070	1.180	1.180
Shell - S4	8mm	1.262	1.084	1.380	1.380
	4mm	1.186	1.064	1.267	1.267
	2mm	1.165	1.058	1.236	1.236
	1mm	1.164	1.057	1.236	1.236

For a mesh size of 2 mm, the difference in SHSS values for C3D8R and C3D8 is within 1%. For the same mesh size, the difference in SHSS for C3D20R and C3D20 is almost negligible. For 4-noded shell elements, the difference in SHSS values between reduced and full integration is 1%. Thus, for further investigation, shell and solid elements with reduced integration are used for tension loading. This is because, sufficient amount of accuracy is achieved with reduced integration in lesser computation time.

3.1.8. Element type study for tension load case

At first, different element types for shell and solids are investigated for the same mesh size. The final mesh size for almost all the numerical models is obtained as 2 mm based on mesh sensitivity study. The SHSS values are calculated using linear extrapolation and the SCF is found. This is summarised in Table 3.6. It is observed that the maximum variation of SHSS values for the solid models with different element types is within 1% and that for the shell model within 2% for the same mesh size of 2 mm. This variation is expected and can be considered as acceptable. The details of the stress profiles are shown in Appendix-B.

Table 3.6: SHSS of different element types for tension

Tensile load, Linear Extrapolation, Mesh - 2mm					
Element	Element Type	$\sigma_{0.4t}$ (MPa)	$\sigma_{1.0t}$ (MPa)	SHSS (MPa)	SCF
Solid	C3D8R	1.135	1.063	1.182	1.182
	C3D20R	1.137	1.078	1.177	1.177
	C3D8	1.131	1.060	1.177	1.177
	C3D20	1.134	1.066	1.179	1.179
Shell	S4R	1.151	1.056	1.215	1.215
	S8R	1.170	1.060	1.243	1.243
	S4	1.165	1.058	1.236	1.236

Secondly, the stress profiles for different solid and shell element types with reduced integration is investigated for different mesh sizes (Appendix-B). The stress profiles of 2 mm quadratic solid elements (C3D20R) are compared with 1 mm linear solid elements (C3D8R). Also, the stress profiles of 2 mm quadratic shell elements (S8R) are compared with 1 mm linear shell elements (S4R). The SHSS values are also compared as shown in Table 3.7.

Table 3.7: SHSS of solid and shell elements with different element types

Tensile load, Linear Extrapolation						
Element	Element Type	Mesh	$\sigma_{0.4t}$ (MPa)	$\sigma_{1.0t}$ (MPa)	SHSS (MPa)	SCF
Solid	C3D8R	1mm	1.136	1.065	1.184	1.184
	C3D20R	2mm	1.137	1.078	1.177	1.177
Shell	S4R	1mm	1.15	1.06	1.214	1.214
	S8R	2mm	1.17	1.06	1.243	1.243

From the table, it is observed that the maximum variation of SHSS values between the linear and quadratic solid element types is within 1% and between the linear and quadratic shell element types is 2%. This difference can be considered as acceptable for the current study.

3.1.9. Linear and quadratic extrapolation for tension load case

The SHSS values are found from quadratic solid and shell elements using both linear and quadratic extrapolation methods. This is shown in Table 3.8. Also, the ratio between the SHSS of solid and shell is obtained. It is also important to state that the origin of the stress profile for the solid model is taken at the weld toe. But for the shell model the origin or starting point of stress extraction is the intersection of mid-plane of plates. The IIW [40] also recommends to take the origin for shell element model as the intersection of the mid-planes of the connecting plates.

Table 3.8: Linear and quadratic extrapolation for tension

Tensile load	Linear Extrapolation				Quadratic Extrapolation				
Elements Types	$\sigma_{0.4t}$ (MPa)	$\sigma_{1.0t}$ (MPa)	SHSS (MPa)	Ratio SHSS shell/solid	$\sigma_{0.4t}$ (MPa)	$\sigma_{0.9t}$ (MPa)	$\sigma_{1.4t}$ (MPa)	SHSS (MPa)	Ratio SHSS shell/solid
Solid_2mm (C3D20R)	1.137	1.078	1.177	1.056	1.138	1.076	1.040	1.206	1.077
Shell_2mm (S8R)	1.170	1.060	1.243		1.169	1.069	1.039	1.300	

3.1.10. Numerical model validation for tension load case

The SCF obtained from numerical analyses in this thesis is compared to the SCF obtained from the numerical investigation of Śledziewski [54] for validation of the solid model subjected to tension. The SHSS of the solid model (C3D20R) with 2 mm mesh showed good agreement with numerical study of Śledziewski [54] for both linear and quadratic stress extrapolation methods. However, the SHSS from the S8R model with 2 mm mesh is **5%** higher compared to the results of Śledziewski [54] for linear extrapolation and **8%** higher for quadratic extrapolation as shown in the Table 3.9.

Table 3.9: Comparison of SHSS values from the numerical models with results from Śledziewski [54]

Tensile Load	SCF - FEM		SCF - Numerical Śledziewski		Percentage Difference (%) with Experiment	
	Linear Extrapolation	Quadratic Extrapolation	Linear Extrapolation	Quadratic Extrapolation	Linear Extrapolation	Quadratic Extrapolation
Solid_2mm (C3D20R)	1.177	1.206	1.18	1.20	-0.25%	0.51%
Shell_2mm (S8R)	1.243	1.300			5.32%	8.30%

The stress distribution perpendicular to the weld toe for the solid model and the shell model are shown in Figure 3.14. The stress distribution of the solid and shell models are first plotted separately and then together in one plot. The figure shows that for this specific detail, the shell and solid model has the same nominal stress value far away from the stress concentration at for example at 50 mm away from weld toe. However, the stress gradient is different and thus it gives different hot-spot stress values when the stresses are extrapolated from reference points.

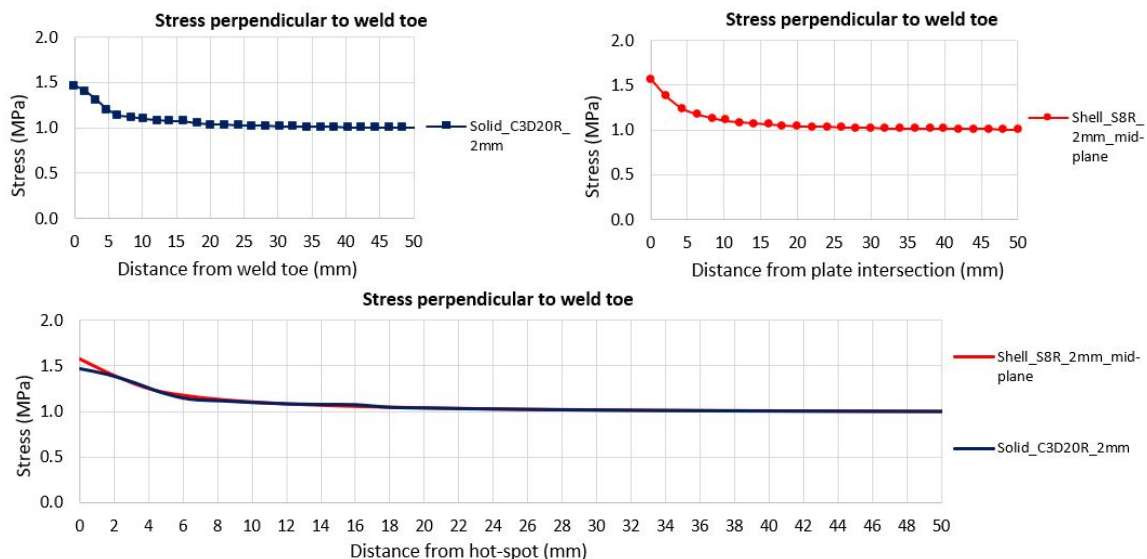


Figure 3.14: Stress distribution perpendicular to weld toe for the numerical models under tension

3.1.11. Parametric study for tension load case

At first, a parametric study of the weld throat thickness for tension load case is performed as shown in Table 3.10. The weld throat thicknesses investigated are (a) = 4 mm, 5 mm and 6 mm. It is observed that the SHSS decreased with increase of throat thickness for this specific detail under tension.

Table 3.10: SHSS values for different weld throat thicknesses

Loading	Tension		
Element type and mesh	Solid_2mm_C3D20R		
Extrapolation Method	Linear Extrapolation		
Throat thickness (a)	a = 4mm	a = 5mm	a = 6mm
SHSS (MPa)	1.223	1.177	1.164

The main parametric study is performed for the detail with varying thickness of the stiffener (t_s) and base plate (t_p). The stiffener and base plate thickness of the reference detail is 16 mm. The SHSS values are obtained for $t_s = 8$ mm, 12 mm, 20 mm and 24 mm and $t_p = 8$ mm, 12 mm, 20 mm and 24 mm respectively using linear extrapolation as shown in Table 3.11. The nominal stress in tension is 1 MPa and thus the SCF is the same as the SHSS. The percentage difference of SHSS with respect to the reference model is also shown.

Table 3.11: Parametric study of T-joint under tensile load

Tension Load	Solid_2mm_(C3D20R)			Shell_2mm_(S8R)		Shell+weld I/W_2mm_(S8R)		Ratio	
SHSS -Linear Interpolation	SHSS (MPa)	Percentage difference with reference model (%)	SHSS (MPa)	Percentage difference with reference model (%)	SHSS (MPa)	Percentage difference with reference model (%)	SHSS shell/solid	SHSS shell+weld I/W/solid	
Stiffener thickness t_s (mm)	8	1.23	4.4%	1.18	-5.1%	1.24	-5.9%	0.96	1.01
	12	1.20	2.2%	1.21	-2.5%	1.28	-2.8%	1.01	1.07
	16	1.18	0.0%	1.24	0.0%	1.32	0.0%	1.06	1.12
	20	1.17	-0.3%	1.28	3.0%	1.35	2.5%	1.09	1.15
Base plate thickness t_p (mm)	24	1.16	-1.3%	1.32	6.0%	1.38	4.8%	1.13	1.19
	8	1.35	14.8%	1.48	19.2%	1.72	30.7%	1.10	1.28
	12	1.27	8.1%	1.36	9.1%	1.49	12.7%	1.07	1.17
	16	1.18	0.0%	1.24	0.0%	1.32	0.0%	1.06	1.12
	20	1.16	-1.1%	1.17	-5.9%	1.27	-3.8%	1.01	1.09
	24	1.15	-2.0%	1.14	-8.5%	1.17	-11.3%	0.99	1.01

For the single side fillet welded longitudinal plate joint (T-joint) loaded in tension a parametric study is performed (Table 3.11). When the thickness of the stiffener (t_s) is varied, all other parameters are kept constant. Similarly, when the thickness of the base plate (t_p) is varied, all other parameters are kept constant. On one hand, it is found that the SHSS values obtained from the solid element model increased on decreasing the thickness of the stiffener plate. On the other hand, the SHSS values from the shell element model decreased on decreasing the thickness of the stiffener plate. The SHSS values increased with the reduction of the base plate thickness for both solid and shell elements. Since, the shell element model is initially developed without modelling the welds, there is a lot of scatter in the ratio of the SHSS of shell to that of solid subjected to tension. This scatter in SHSS did not get reduced after modelling the weld with shell elements using increased thickness approach from I/W [40].

3.1.12. Mesh sensitivity for bending load-case

A mesh sensitivity study is also performed for bending load case. At first, elements with reduced integration are used to develop the FE model. The thickness of the base and top plates are $t = 16$ mm. The following mesh sizes are investigated: $t/2$, $t/4$, $t/8$ and $t/16$ i.e. 8 mm, 4 mm, 2 mm and 1 mm respectively. The stress profiles are shown in Appendix-B. The same element types are used: C3D8R, C3D20R, S4R and S8R as is done for the tension load case. The SHSS values and SCF are also computed as shown in Table 3.12. For the quadratic solid elements (C3D20R) loaded in bending, it is observed that the SHSS values are converging for mesh size of 2 mm to a value of **-19.08 MPa**. For the linear solid elements (C3D8R), it is observed that the SHSS value for 2 mm mesh and that for 1 mm mesh is very close to each other. However, for obtaining full convergence with C3D8R elements, a mesh size of 0.5 mm is required. But this involved a lot of computational time as a mesh size of 0.5

mm is very small. Thus, a mesh size of 2 mm is selected as a proper mesh size for further numerical investigation with solid elements under bending. For the linear shell elements (S4R) loaded in bending, it is observed that the SHSS values are converging for mesh size of 2 mm to a value of **-18.41 MPa**. This behaviour is also observed for quadratic shell elements (S8R). Thus, for the shell elements also a mesh size of 2 mm is selected for further numerical analysis.

Table 3.12: SHSS of solid and shell elements with reduced integration for bending

Bending load - Linear Extrapolation				
Element Types	Mesh size	$\sigma_{0.4t}$ (MPa)	$\sigma_{1.0t}$ (MPa)	SHSS (MPa)
Solid - C3D8R	8mm	-11.81	-9.70	-13.23
	4mm	-13.98	-11.12	-15.90
	2mm	-15.36	-12.62	-17.19
	1mm	-15.37	-12.62	-17.21
Solid - C3D20R	8mm	-17.15	-13.43	-19.64
	4mm	-16.87	-13.54	-19.11
	2mm	-16.85	-13.53	-19.08
	1mm	-16.85	-13.53	-19.08
Shell - S4R	8mm	-16.61	-13.79	-18.49
	4mm	-16.33	-13.66	-18.12
	2mm	-16.48	-13.60	-18.41
	1mm	-16.43	-13.59	-18.44
Shell - S8R	8mm	-16.97	-13.69	-19.17
	4mm	-16.78	-13.68	-18.85
	2mm	-16.62	-13.64	-18.61
	1mm	-16.61	-13.61	-18.61

A separate mesh sensitivity study for bending is also performed using full integration with the above mentioned mesh sizes 8 mm, 4 mm, 2 mm and 1 mm (Appendix-B). At first, the SHSS values are calculated using linear extrapolation method. Later, the quadratic extrapolation method is also investigated. The SHSS values are calculated using linear extrapolation (Table 3.13).

Table 3.13: SHSS of solid and shell elements with full integration for bending

Bending load - Linear Extrapolation				
Element Type	Mesh Size	$\sigma_{0.4t}$ (MPa)	$\sigma_{1.0t}$ (MPa)	SHSS (MPa)
Solid - C3D8	8mm	-13.46	-10.59	-15.39
	4mm	-14.47	-11.41	-16.52
	2mm	-15.19	-11.98	-17.34
	1mm	-15.20	-11.98	-17.35
Solid - C3D20	8mm	-17.42	-13.35	-20.15
	4mm	-16.49	-13.51	-18.49
	2mm	-16.47	-13.50	-18.45
	1mm	-16.47	-13.50	-18.45
Shell - S4	8mm	-17.76	-13.89	-20.34
	4mm	-16.61	-13.68	-18.57
	2mm	-16.57	-13.61	-18.55
	1mm	-16.47	-13.59	-18.39

3.1.13. Element type study for bending load-case

At first, different element types for shell and solids are investigated for bending load for the same mesh size. The stress profiles of these elements are shown in Appendix-B. The SHSS values are calculated using linear extrapolation. This is summarised in Table 3.14.

Table 3.14: SHSS of different element types for bending

Bending load, Linear Extrapolation, Mesh - 2mm				
Element	Element Type	$\sigma_{0.4t}$ (MPa)	$\sigma_{1.0t}$ (MPa)	SHSS (MPa)
Solid	C3D8R	-15.36	-12.62	-17.19
	C3D20R	-16.85	-13.53	-19.08
	C3D8	-15.19	-11.98	-17.34
	C3D20	-16.47	-13.50	-18.45
Shell	S4R	-16.48	-13.60	-18.41
	S8R	-16.62	-13.64	-18.61
	S4	-16.57	-13.61	-18.55

Secondly, the stress profiles for different solid and shell element types with different mesh sizes and reduced integration are investigated (Appendix-B). The stress gradients of 2 mm quadratic solid elements (C3D20R) are compared with 1 mm linear solid elements (C3D8R). Also, the stress gradients of 2 mm quadratic shell elements (S8R) are compared with 1 mm linear shell elements (S4R). These are shown in the figures in Appendix-B. The SHSS values are calculated using linear extrapolation as shown in Table 3.15.

Table 3.15: SHSS of different element types for bending

Bending load, Linear Extrapolation					
Element	Element Type	Mesh	$\sigma_{0.4t}$ (MPa)	$\sigma_{1.0t}$ (MPa)	SHSS (MPa)
Solid	C3D8R	1mm	-15.37	-12.62	-17.21
	C3D20R	2mm	-16.85	-13.53	-19.08
Shell	S4R	1mm	-16.43	-13.59	-18.34
	S8R	2mm	-16.62	-13.64	-18.61

It is found that the maximum variation of SHSS values between the 1 mm linear and 2 mm quadratic solid element types is **10%**. It is also observed that the variation between the linear and quadratic shell element types is negligible for bending load case.

3.1.14. Linear and quadratic extrapolation for bending load case

The SHSS values are found from quadratic solid and shell elements using both linear and quadratic extrapolation method. This is shown in Table 3.16. Also, the ratio between the SHSS of solid to that of shell is obtained as shown in the table.

Table 3.16: SHSS using linear and quadratic extrapolation for bending

Bending Load	Linear Extrapolation				Quadratic Extrapolation				
	$\sigma_{0.4t}$ (MPa)	$\sigma_{1.0t}$ (MPa)	SHSS (MPa)	Ratio SHSS shell/solid	$\sigma_{0.4t}$ (MPa)	$\sigma_{0.9t}$ (MPa)	$\sigma_{1.4t}$ (MPa)	SHSS (MPa)	Ratio SHSS shell/solid
Solid_2mm (C3D20R)	-16.85	-13.53	-19.08	0.976	-16.87	-13.96	-12.10	-19.96	0.978
Shell_2mm (S8R)	-16.62	-13.64	-18.61		-16.62	-13.99	-12.47	-19.52	

The stress distribution perpendicular to the weld toe and deformation in the direction of load for solid and shell models are shown in Figure 3.15. For this load case as well, the shell and the solid models have the same nominal stress far away from the weld toe. However, the stress gradient is different near the weld toe which results in a small difference in SHSS values between the numerical models. Since, the solid element model has a higher stress gradient, it gives higher hot-spot stress value compared to the shell element model.

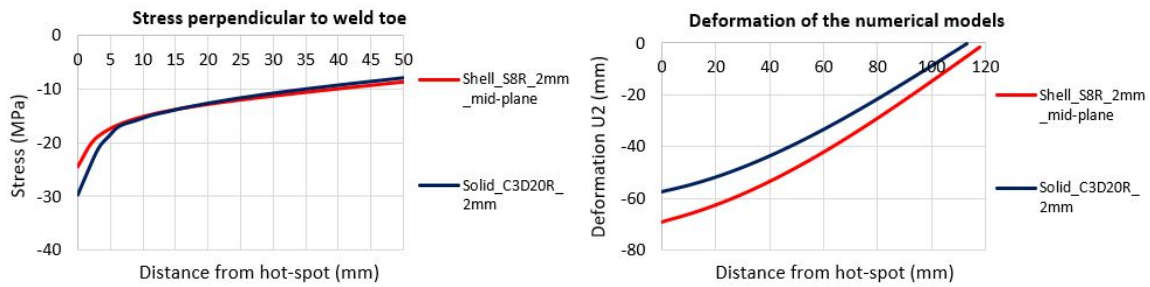


Figure 3.15: Stress distribution perpendicular to weld toe and deformation for shell and solid model under bending load

3.1.15. Parametric study for bending load case

At first, a parametric study of the weld throat thickness for bending load case is performed as shown in Table 3.17. The weld throat thicknesses investigated are (a) = 4 mm, 5 mm and 6 mm. Again, it is found that the SHSS reduced in magnitude with the increase of weld throat thickness just like for the tension load case.

Table 3.17: SHSS values for different weld throat thicknesses

Type of loading	Bending		
Element type and mesh	Solid_2mm_C3D20R		
Extrapolation Method	Linear Extrapolation		
Throat thickness (a)	a = 4mm	a = 5mm	a = 6mm
SHSS (MPa)	-19.42	-19.08	-18.78

The main parametric study is performed for the specimen with varying thickness of the stiffener (t_s) and base plate (t_p). The stiffener and base plate thickness of the reference specimen is 16 mm. The SHSS values are calculated for $t_s = 8$ mm, 12 mm, 20 mm and 24 mm and $t_p = 8$ mm, 12 mm, 20 mm and 24 mm using linear extrapolation as shown in Table 3.18. When the thickness of the stiffener (t_s) is varied, all other parameters are kept constant. Similarly, when the thickness of the base plate (t_p) is varied, all other parameters are kept constant. The percentage difference of SHSS with respect to the reference model having $t_s = 16$ mm and $t_p = 16$ mm is also shown.

Table 3.18: Parametric study of T-joint under bending load

Bending Load		Solid_2mm_(C3D20R)		Shell_2mm_(S8R)		Shell+weld IIW_2mm_(S8R)		Ratio	
SHSS -Linear Interpolation	SHSS (MPa)	Percentage difference with reference model (%)	SHSS (MPa)	Percentage difference with reference model (%)	SHSS (MPa)	Percentage difference with reference model (%)	SHSS shell/solid	SHSS shell+weld IIW/solid	
Stiffener thickness t_s (mm)	8	-9.7	49%	-8.8	53%	-8.8	52%	0.91	0.91
	12	-14.3	25%	-13.6	27%	-13.5	26%	0.96	0.95
	16	-19.1	0%	-18.6	0%	-18.3	0%	0.97	0.96
	20	-23.0	-20%	-23.7	-27%	-23.2	-27%	1.03	1.01
Base plate thickness t_p (mm)	24	-27.8	-45%	-28.9	-55%	-28.2	-54%	1.04	1.02
	8	-93.6	-391%	-107.2	-476%	-98.3	-436%	1.15	1.05
	12	-54.6	-186%	-58.7	-215%	-55.2	-201%	1.08	1.01
	16	-19.1	0%	-18.6	0%	-18.3	0%	0.98	0.96
	20	-13.1	31%	-12.6	32%	-12.4	32%	0.96	0.95
	24	-7.6	60%	-7.3	61%	-7.1	61%	0.95	0.93

The same welded longitudinal plate joint is loaded in bending for another parametric study (Table 3.18) and a different behaviour is observed. The magnitude of SHSS obtained from the shell element reference model is lower compared to that obtained from the solid element reference model. From the parametric study it is found that there is again a considerable amount of variation in the ratio of SHSS of shell to that of solid when subjected to bending. However, this variation is reduced to some extent from a coefficient of variation (CV) of 7.0% to 4.6% for bending, by modelling the welds with shell elements using increased thickness at the welded region according to IIW [28].

3.2. Double side fillet welded transverse plate joint (cruciform joint)

The second simple welded detail analysed is a double side fillet-welded cruciform joint (detail type b) loaded in tension. The welded detail from the study performed by Karabulut and Lombaert [31] is numerically investigated with solid and shell elements.

3.2.1. Experimental investigation of Karabulut and Lombaert (2020)

In the research of Karabulut and Lombaert [31], a uniform pressure type load of 80 MPa is applied on the two ends of a non-load-carrying cruciform welded joint. The measurements are performed using strain gauges SG1(0.4t) and SG2(1.0t) [31]. The strain gauges are installed after the plate surface is cleaned both mechanically (de-greasing, grinding, polishing with abrasive sand paper) and chemically (with conditioner and neutralizer) as shown in Figure 3.16 [31].

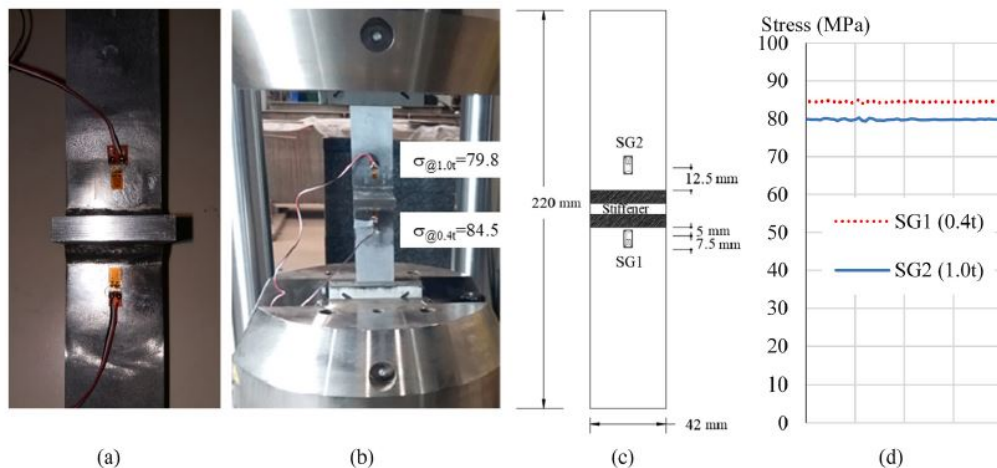


Figure 3.16: Test with strain gauges: (a) bonded strain gauge; (b) test setup – stresses are in MPa; (c) placement scheme of strain gauges; (d) stress readout [31]

The thickness of the base plate is 12.5 mm. The hot-spot stress in the test specimen is measured using strain gauges at 0.4t (5 mm) and 1.0t (12.5 mm) from the weld toe. The measured stresses are **84.5 MPa** and **79.8 MPa** at a distance of 5 mm and 12.5 mm from the weld toe respectively. According to Karabulut and Lombaert [31], by using linear surface stress extrapolation, the measured value of SHSS is **87.6 MPa**. The measured stress values at 0.4t and 1.0t are also shown in Figure 3.16 [31].

3.2.2. Numerical investigation of Karabulut and Lombaert (2020)

The analysis of the test specimen was performed via FEM using ABAQUS [8]. In the numerical model of Karabulut and Lombaert [31], the boundary conditions were chosen such that the specimen is subjected to uniform tension, resulting in a nominal stress range in the flange corresponding to the detail category FAT 80 [31]. The linear 8-noded solid elements with reduced integration (C3D8R) were used in their analysis. The element size was limited to 0.4 t and the material exhibited a linear elastic behaviour ($E = 200$ GPa). The stress field obtained from the FEM is shown in Figure 3.17 [31].

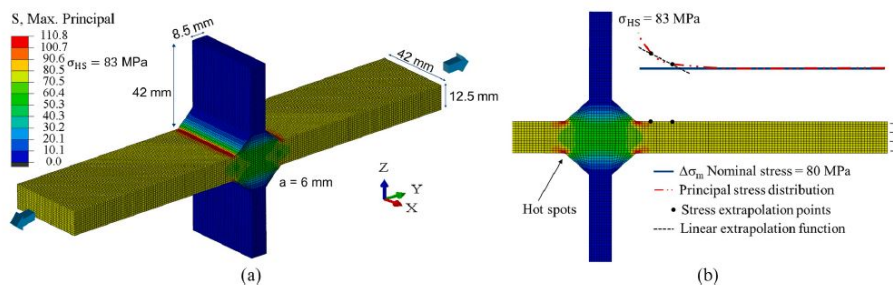


Figure 3.17: FEM of the test specimen: (a) principal stress results; (b) calculation of SHSS [31]

The thickness of the base plate was 12.5 mm. The top and bottom stiffeners had a thickness of 8.5 mm. The width of all the plates are 42 mm. The length of the detail was 200 mm and the weld throat thickness was 6 mm. The SHSS calculated for this model was found to be **83 MPa** using linear surface stress extrapolation as shown in Figure 3.17 [31]. A sensitivity analysis of the computed SHSS were performed and the results are summarized in Figure 3.18 [31]. It was concluded that there is a very little influence of the sensitivity study on the magnitude of SHSS [31], a maximum variation within **10%**.

Sensitivity analysis on computational parameters		HSS	Maximum variation
Mesh size	< 1 mm	82.19 MPa	5.5%
	< 2.5 mm	82.69 MPa	
	< 5 mm	86.91 MPa	
	< 12.5 mm	87.59 MPa	
Element type	Linear 8-node	84.96 MPa	5%
	Quadratic 20-node	80.94 MPa	
Shell vs. solid	Shell	81.38 MPa	3%
	Solid	84.09 MPa	
Integration method	Reduced	84.96 MPa	7.7%
	Full	91.51 MPa	
Extrapolation method	Linear	84.96 MPa	3.3%
	Quadratic	87.87 MPa	

Figure 3.18: Sensitivity analysis of the computed SHSS [31]

3.2.3. Numerical modelling in the current report

The same loading and boundary conditions are applied in the current numerical models for comparison with the experimental and numerical results of Karabulut and Lombaert [31]. This is shown in Figure 3.19. However, the coordinate system is chosen to be consistent with the model shown in section 3.1. Thus, the tensile loading of **80 MPa** is applied at the two ends of the main plate along longitudinal - (x) direction. A structured mesh is used in all the numerical models.

Development of solid element models: The solid element model is developed using the dimensions from [31]. The weld is modelled using the same technique as for the T-joint in section 3.1 i.e by chamfering and sweep tools. A small gap between the plates is also modelled using the assign seam tool in ABAQUS. The origin of the stress profiles is taken at the weld toe. The global meshing of the solid element models is performed such that a cubic block of size $A \times A \times A$ mm³ is generated where A is the mesh size in mm. A structured meshing approach is used in the solid element model (Figure 3.19). A mesh and element sensitivity study is performed, the details of which are given in Appendix-B.

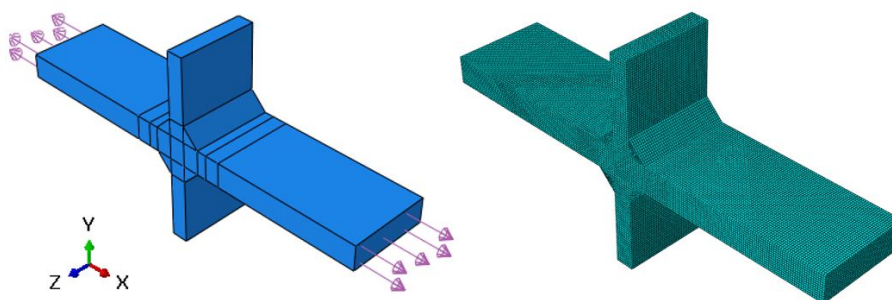


Figure 3.19: The coordinate system, loading and mesh of the solid model [31]

Development of shell element models: The shell element models are developed using mid-plane geometry (Figure 3.20). The top plate is modelled with a height including half the thickness of the base plate. The bottom plate is modelled using a similar approach. Thus, the top and bottom plates are made such that the total height is same as that of the solid model. The welds are not modelled in

the shell element model for this detail. The global meshing with the shell model is done such that a square plate of size $A \times A$ mm² can be generated where A is the mesh size in mm. A mesh and element sensitivity analysis is performed with shell and solid elements as shown in Appendix-B.

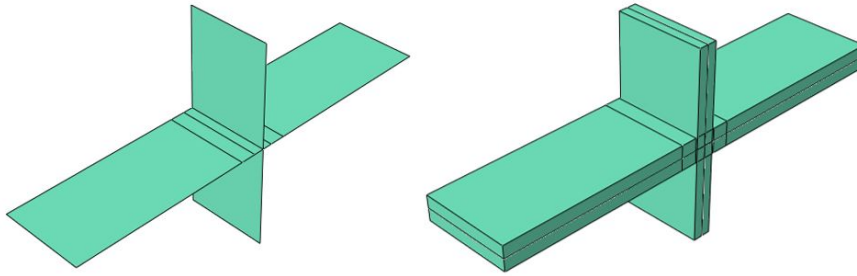


Figure 3.20: Mid-plane approach in modelling with shell elements

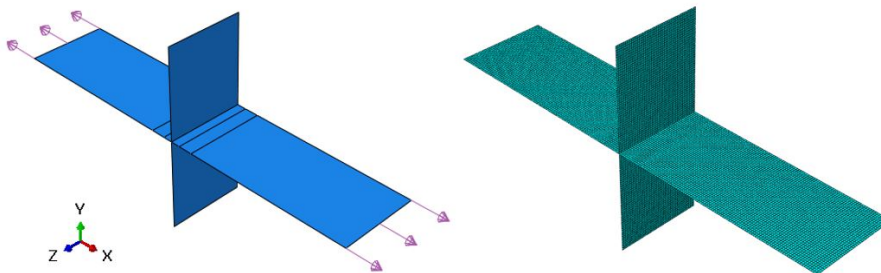


Figure 3.21: The coordinate system and loading of the shell model [31]

The contour plot of the maximum principal stress for this detail with the solid element model is shown in Figure 3.22. From the contour plot it is observed that the exact similar stress distribution was obtained from the numerical investigation by Karabulut and Lombaert [31] as given in Figure 3.17. The contour plots of the stress component perpendicular to the weld toe for shell and solid elements is provided in Appendix-I.

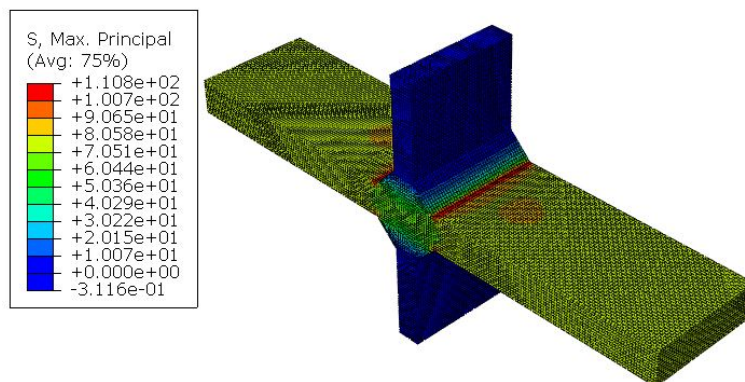


Figure 3.22: Contour plot for solid element model having a mesh size of 1mm

From the mesh sensitivity study (Appendix-B) it is found that there is no significant difference between the coarse and fine meshed linear shell models. Linear and quadratic elements with reduced and full integration are also used for a particular mesh size and the stress profiles are shown in Appendix-B. The SHSS values are calculated using linear extrapolation as is recommended by Karabulut and Lombaert [31]. Table 3.19 summarizes the SHSS values obtained for different mesh sizes and element types using linear surface stress extrapolation. The solid elements in general gave higher hot-spot stress values compared to shell elements.

The maximum variation of SHSS values for different mesh sizes using C3D20R elements is within **6%** compared to **5.5%** obtained by Karabulut and Lombaert [31]. Moreover, the SHSS values converged for mesh sizes smaller than 2.5 mm for both linear and quadratic solid elements. Thus, 2.5 mm is recommended as an appropriate mesh size for further analysis with solid elements for this detail.

Table 3.19: SHSS values for all the numerical models of the transverse cruciform joint

Number	Element type	ABAQUS Nomenclature	Mesh size (mm)	SHSS (MPa)
1	Linear solid with reduced integration	C3D8R	12.5	87.53
2	Linear solid with reduced integration	C3D8R	5	85.11
3	Linear solid with reduced integration	C3D8R	2.5	82.11
4	Linear solid with reduced integration	C3D8R	1	82.11
5	Quadratic solid with reduced integration	C3D20R	12.5	81.94
6	Quadratic solid with reduced integration	C3D20R	5	80.94
7	Quadratic solid with reduced integration	C3D20R	2.5	86.49
8	Quadratic solid with reduced integration	C3D20R	1	86.06
9	Linear shell with reduced integration	S4R	12.5	79.31
10	Linear shell with reduced integration	S4R	5	78.14
11	Linear shell with reduced integration	S4R	2.5	78.24
12	Linear shell with reduced integration	S4R	1	78.24
13	Quadratic shell with reduced integration	S8R	12.5	77.79
14	Quadratic shell with reduced integration	S8R	5	78.07
15	Quadratic shell with reduced integration	S8R	2.5	78.24
16	Quadratic shell with reduced integration	S8R	2.5	78.27
17	Linear solid with full integration	C3D8	2.5	83.54
18	Quadratic solid with full integration	C3D20	2.5	86.49
19	Linear shell with full integration	S4	2.5	78.22

The maximum variation of SHSS values for different mesh sizes using S8R elements is within **1%**. Moreover, the SHSS values converged below a mesh size of 2.5 mm for both linear and quadratic shell elements. Thus, 2.5 mm mesh is also recommended as an appropriate mesh size for further analysis with shell elements. Figure 3.23 shows the SHSS values from Table 3.19 where the measured value of SHSS is **87.6 MPa**, shown by a red line.

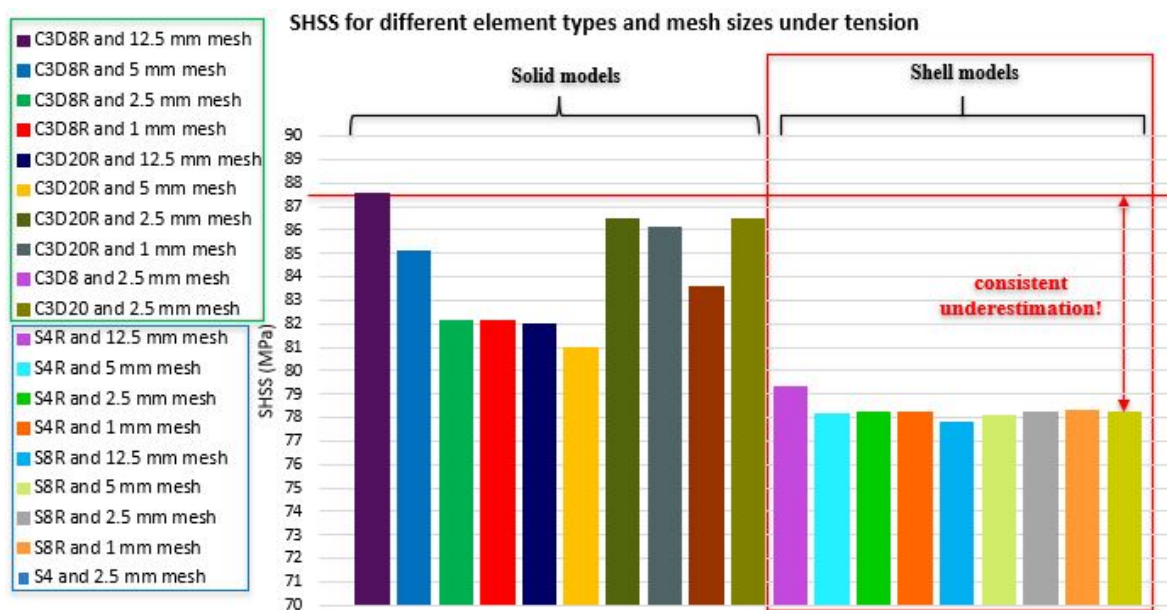


Figure 3.23: Comparison of SHSS values from different element types under tension load case

Finally, a comparison study is made between the SHSS obtained using linear and quadratic extrapolation techniques with a mesh size of 2.5 mm. In this study, C3D20R and S8R elements are used. This is shown in Table 3.20. The SHSS results from the solid model with linear extrapolation is **4.2%** lower than the measured SHSS of **87.6 MPa**. The SHSS results from the solid model with quadratic extrapolation is **1.6%** lower than the measured SHSS. This difference in results is considered as acceptable and thus the solid model gave good results of SHSS. The SHSS results from the shell model with linear extrapolation is **10.7%** lower than the measured SHSS. The SHSS results from the shell model with quadratic extrapolation is **11.3%** lower than the measured SHSS. This difference in results cannot be acceptable as the underestimation is large. The maximum variation with linear and quadratic extrapolation methods is **2.5%** for solid models and **1%** for shell models. Karabulut and Lombaert [31] had obtained a maximum variation of **3.3%** between SHSS from linear and quadratic extrapolation methods as shown in Figure 3.18 of section 3.2.2.

Table 3.20: Comparison of hot-spot stresses between the numerical models with different extrapolation techniques

Tensile load	Linear Extrapolation				Quadratic Extrapolation					
	Elements	$\sigma_{0.4t}$ (MPa)	$\sigma_{1.0t}$ (MPa)	SHSS (MPa)	Ratio SHSS shell/solid	$\sigma_{0.4t}$ (MPa)	$\sigma_{0.9t}$ (MPa)	$\sigma_{1.4t}$ (MPa)	SHSS (MPa)	Ratio SHSS shell/solid
Solid_2.5mm (C3D20R)		82.67	80.74	83.96	0.93	82.67	80.54	80.90	86.16	0.90
	Shell_2.5mm (S8R)	79.10	80.39	78.24		79.10	80.24	80.68	77.68	

In this case, it can be said that the shell element model is not feasible to be used for finding the hot-spot stress. This can be explained by observing the maximum principal stress distribution of the shell and solid model (Figure 3.24 (left)). Since, this detail is loaded in pure tension, the stress perpendicular to the weld toe is almost equal to the maximum principal stress. Thus the stress distribution perpendicular to weld toe for both the solid and shell models have also been plotted in Figure 3.24 (right). From the stress profiles, it can be clearly observed that the shell model does not show any stress concentration. Even after application of weld modelling with shell elements, there will be no effect on stress concentration for this detail loaded in tension. Thus, there will always be a consistent underestimation of hot-spot stress with shell elements as shown in Figure 3.23.

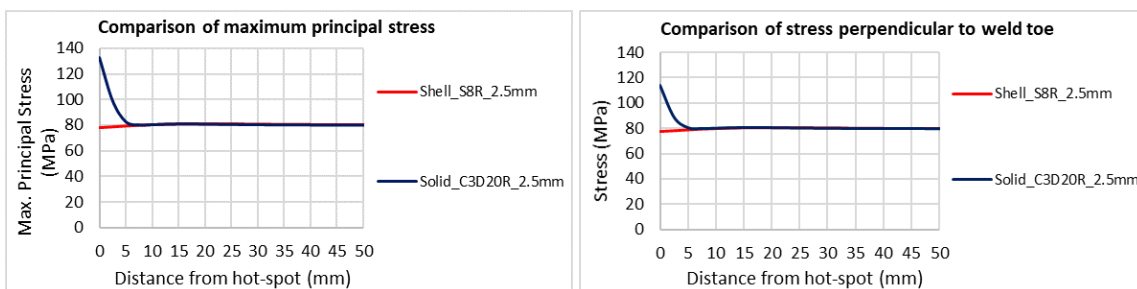


Figure 3.24: Maximum principal stress and stress perpendicular to weld toe between shell and solid models of cruciform joint

It can be concluded that for such details loaded in tension, the SHSS values are lower for the shell element model compared to the solid element model (Table 3.19). This behaviour was also observed from the numerical results of Karabulut and Lombaert [31]. From Figure 3.23, it can be observed that there is no hot-spot in the shell element model. This is because the stress concentration at weld toe cannot be captured using shell elements and hence, it is not suitable to use shell elements for hot-spot stress calculation for this detail using surface extrapolation. The numerical results of the SHSS from solid element model agreed well with the fatigue test results of Karabulut and Lombaert [31].

3.3. General findings

The main parameters affecting the hot-spot stress using surface extrapolation from the FEM models are as follows: geometry (thickness of components), throat thickness of weld, definition of type of hot-spot (type-“a”, “b” or “c”), type of extrapolation (linear and quadratic), type of element (linear and quadratic) and element size. This explicitly means that the calculation of hot-spot stress depends on the reference points and how these reference points are defined in the numerical model.

The stress profiles of the single side fillet welded longitudinal plate joint and the transverse cruciform joint are also investigated with the stress averaging option in ABAQUS being turned off. However, it is observed that there is no effect of stress averaging on the hot-spot stress as the reference points are far away from the affected nodes. For this detail, both the linear and quadratic extrapolation methods gave SHSS values which were quite close to each other with a difference within **4%** for the solid model and within **5%** for the shell element model for tension and bending load cases. The throat thickness of the weld has some influence on the structural hot-spot stress (SHSS) for this detail. However, this variation of SHSS is within **5%** for a tolerance of +/- 1 mm throat thickness, which is considered acceptable.

The SHSS value is also computed without modelling the gap using weld-seam from the crack-assign seam tool in ABAQUS. But the difference in results from the numerical model with gap is within **1%**. For the single side fillet welded longitudinal plate joint, the shell element model developed using shell offset - bottom surface gave SHSS values which are not in good agreement with the SHSS values obtained by Śledziewski [54]. This is because of eccentricity which results in additional moments in the shell models with bottom surface approach. These moments lead to additional stresses in the model. Thus, the shell element geometry developed using mid-planes is recommended as a better approach for modelling. For the double side fillet welded transverse cruciform joint, the solid elements with full integration yielded higher values of SHSS compared to reduced integration. This was also observed in the FE results of Karabulut and Lombaert [31]. However, this difference is less than **3%**. So, it is considered as acceptable to use the solid elements with reduced integration because it involves lower computation time.

Reduced integration uses a lesser number of Gaussian co-ordinates when solving the integral. With full integration there are more gaussian co-ordinates for each element and thus more accuracy is achieved and also more is the computational time taken. However, sufficient amount of accuracy is achieved with reduced integration and thus this makes it a recommended choice for elements in such details for the calculation of hot-spot stress.

With reduced integration, the number of elements through the thickness of the base plate plays a critical role for specimens loaded in bending. For the linear 8-node brick (C3D8R) model loaded in bending, four elements through the thickness failed to provide enough accuracy compared to the quadratic 20-node brick (C3D20R) element model and numerical results. A very fine mesh with element size 0.5 mm is required for the linear solid elements for having better accuracy in SHSS compared to the quadratic elements when subjected to bending. But the computational time taken by linear 8-node brick (C3D8R) elements with a very fine mesh size of 0.5 mm is larger than C3D20R and thus it is not feasible to use the linear solid elements for numerical modelling of such details loaded in bending. Also, the convergence rate of C3D20R elements is higher than C3D8R elements subject to bending load. In conclusion, it is recommended to use the quadratic 20-node brick (C3D20R) with a mesh size of 2 mm ($t/8$, where $t = 16$ mm is the thickness of the base plate) for the fillet welded T-joint and 2.5 mm ($t/5$, where $t = 12.5$ mm is the thickness of the base plate) for the welded cruciform joint. For the shell model, the 8-node quadratic elements (S8R) is recommended to be used as it gave better SHSS results compared to the 4-node linear (S4R) elements. Also, the convergence rate of S8R elements is higher than S4R elements subject to bending load. Thus, it can be concluded that with linear elements, a smaller mesh size is required which increases the computational time.

4

Complex fillet welded details in steel bridges

“Once we accept our limits, we go beyond them.”

Albert Einstein

In this chapter, finite element modelling is performed on a complex fillet welded detail in steel bridges. Some numerical models are developed based on previous fatigue tests in the literature. All these models are investigated for different load cases in order to study the behavioural difference between shell and solid elements in terms of stresses and deformations. The solid element model of the reference detail is first validated with the experimental strain measurements. The hot-spot stresses are then obtained using the solid element models. Furthermore, the weld modelling approach using increased thickness of plates according to IIW [40] has been investigated for standard load cases. The main focus is on the differences between the hot-spot stresses obtained from the shell and solid element modelling.

4.1. Experimental investigation of complex detail from the research of Akhlaghi (2009)

The experimental study performed by Akhlaghi [9][10] dealt with a three-point bending test on a crossbeam-stiffener welded connection with a cope hole. The test specimen was held on two roller supports at the crossbeam ends. The load was applied in a vertical plane passing through the mid-span of crossbeam by a loading beam. This is shown in Figure 4.1 [9][10]. The loading beam divided the load into two equal parts and applied each part to one stiffener end.

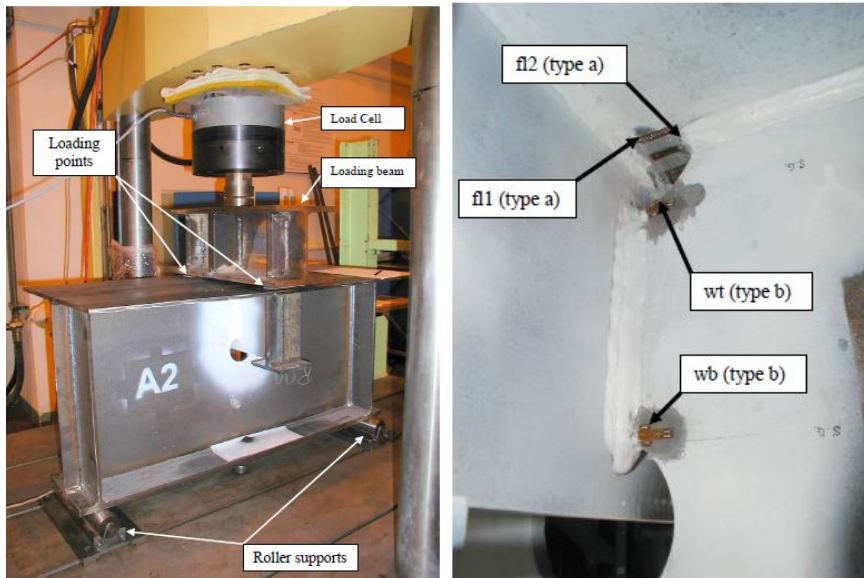


Figure 4.1: The test specimen mounted on the fatigue test machine and associated hot-spot locations [9]

The specimens were first loaded statically with a small load to carry out elastic strain measurements with strain gauges. Then, a high cycle fatigue test was performed with constant amplitude fatigue load (CAFL). Two hot-spot points were identified on the web of the crossbeam ('wb' and 'wt' as shown in Figure 4.1) and two hot-spot points on the deck plate ('fl1' and 'fl2' as shown in Figure 4.1) on each side of the symmetry plane [9]. In this thesis, the point 'wb' has been further investigated. At this point, the crack started from the weld toe at the corner of the crossbeam plate as shown in Figure 4.2. For all specimens, the first crack in the joint was observed at the hot-spot points [9]. The details of the crack locations are shown in Figure 4.2 [9].

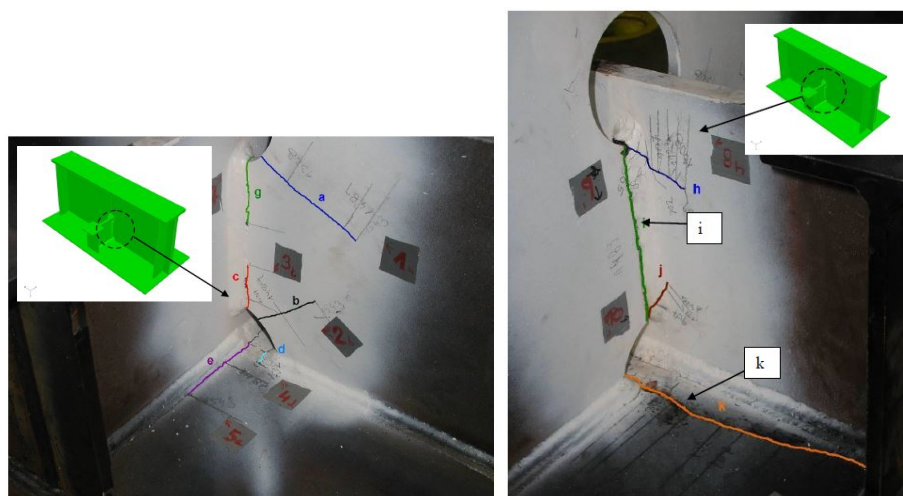


Figure 4.2: Fatigue cracks in the specimen (left and right sides respectively) [9]

4.2. Numerical investigation of complex detail from the research of Akhlaghi (2009)

In the analytical part of the study by Akhlaghi [10], various finite element models were made. Different modelling techniques to incorporate the weld into shell element models were also investigated and compared to the results from the experiments and to those obtained from the solid element models.

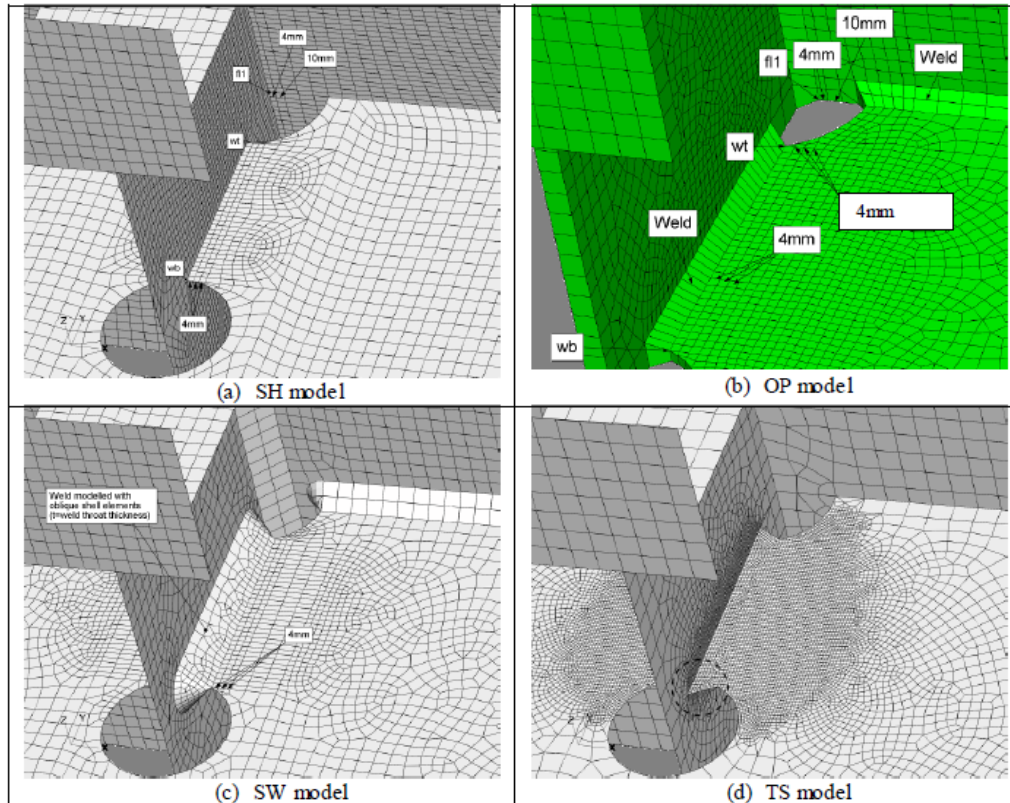


Figure 4.3: FEM models developed by Akhlaghi [10]

Four numerical models were investigated in the study of Akhlaghi [9][10] (Figure 4.3):

1. **SH model:** A quadratic shell element model with a mesh size of 4 mm at the hot-spot regions. The geometry was based on the mid-planes of the plates in the physical part. Welds were not modelled. Stress extrapolation was carried out to the intersection of mid-planes of the plates [10].
2. **OP model:** A quadratic solid element model with a mesh size of 4 mm at the hot-spot regions. The welds were modelled [10].
3. **SW model:** A quadratic shell element model with a mesh size of 4 mm. Geometry and stiffness of the welds were incorporated into the FE model by means of oblique shell elements with a thickness equal to weld throat thickness. Stress extrapolation was carried out upto the weld toe for the SW model [10].
4. **TS model:** A quadratic shell element model with mesh size of 2 mm. The weld was modelled by increasing the thickness of the elements in the weld region. The stress extrapolation was carried out to the transition point, where the thickness of shell elements changed for the TS model [10].

It was observed from the research of Akhlaghi [10] that the shell element model (SH) resulted in unrealistically high SHSS values which were not acceptable (the difference in ratios). The measured hot-spot stress was closer to the hot-spot stress obtained from the solid element model with a difference smaller than 15%. Thus, the solid element model (OP) had sufficient accuracy to be used as a reference for comparing the results from the other models. This is shown in Figure 4.4 [10].

Model	'wb' hot spot			'wt' hot spot		
	SHSS for 400kN loading [MPa]	Ratio of SHSS value to solid element model	Ratio of SHSS value to measurement	SHSS for 400kN loading [MPa]	Ratio of SHSS value to solid element model	Ratio of SHSS value to measurement
SH	873	3.80	4.32	848	3.16	4.51
OP	230	1.00	1.14	268	1.00	1.43
SW	126	0.55	0.62	72	0.27	0.38
TS	158	0.69	0.78	223	0.83	1.19
Measured	202	-	-	188	-	-

Figure 4.4: SHSS from FEA obtained by Akhlaghi [10]

4.3. Geometry

The dimensions of the investigated detail with a cope hole are shown in Figure 4.5 and 4.6 [10][9].

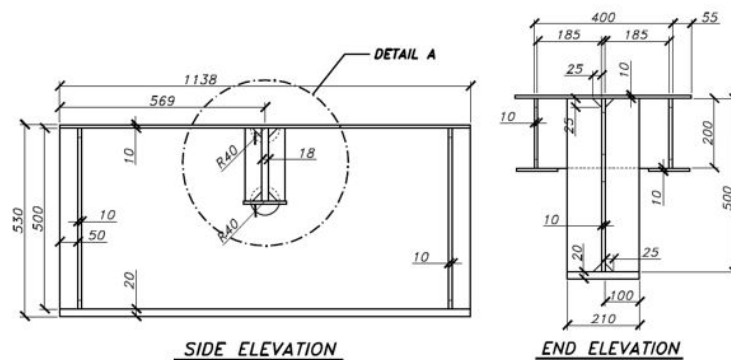


Figure 4.5: Left: Side elevation and Right: End elevation of the test specimen [10] [9]

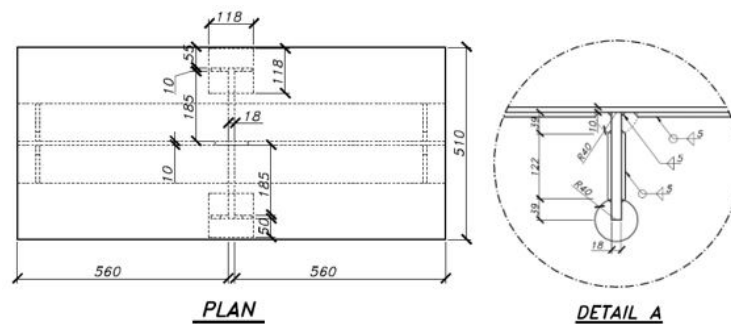


Figure 4.6: Left: Plan view of the test specimen and Right: Detail view of the investigated connection [10] [9]

From the study of Akhlaghi [10], it was reported that using symmetry condition to reduce the model size was affecting the stresses in the numerical models. Thus, in this thesis, the whole geometry of the specimens was numerically modelled using both shell and solid elements.

4.4. Strain gauge location and placement

The detailed placement of the strain gauges used in the experiment is shown in Figure 4.7 [9]. The numbers in red colour indicate the channel number in the strain data output. The range of numbers (for example 10-21) denotes the strain gauges [9]. The first critical location of hot-spot which is denoted as 'HS1' in this thesis, ('wb' according to Akhlaghi [9]) is investigated for the purpose of validating the numerical models. The placement of the strain gauges 31-40 in SIDE 1 is also shown in an enlarged view in Figure 4.7[9].

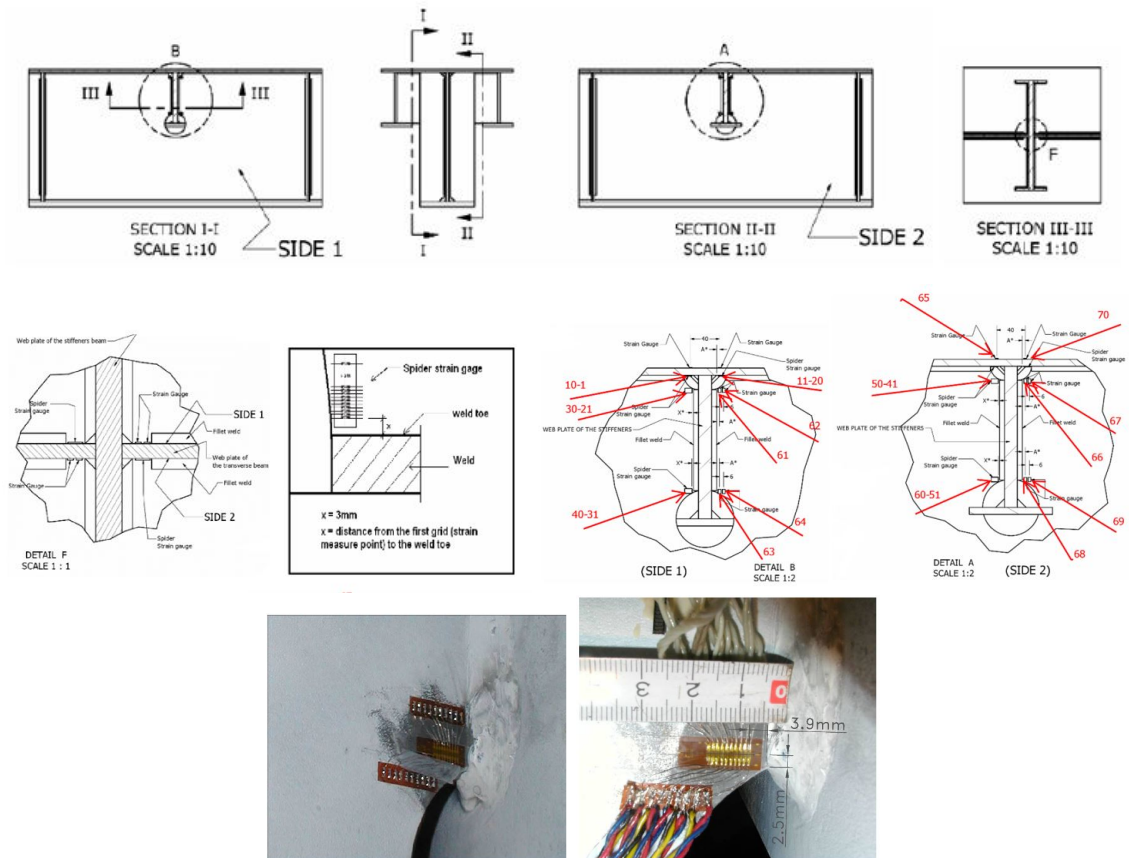


Figure 4.7: Placement of strain gauges and location of hot-spots [9]

4.5. Material properties

The Young's modulus of steel used in the numerical models is $E = 210$ GPa and the poisson's ratio of steel $\nu = 0.3$. Elastic properties were considered in the numerical analysis [9].

4.6. Loading and boundary conditions

The specimens were tested in a way similar to the three-point bending test. They were supported on one pin and one roller at either ends of the crossbeam. In the experiment, the load was applied by a loading beam passing through the mid-span of the crossbeam (Figure 4.1). In the numerical models, the load is applied by distributing it symmetrically into two equal parts and each part to one end of the stiffeners. The loading and boundary conditions are shown in Figure 4.8, similar to Akhlaghi [9].

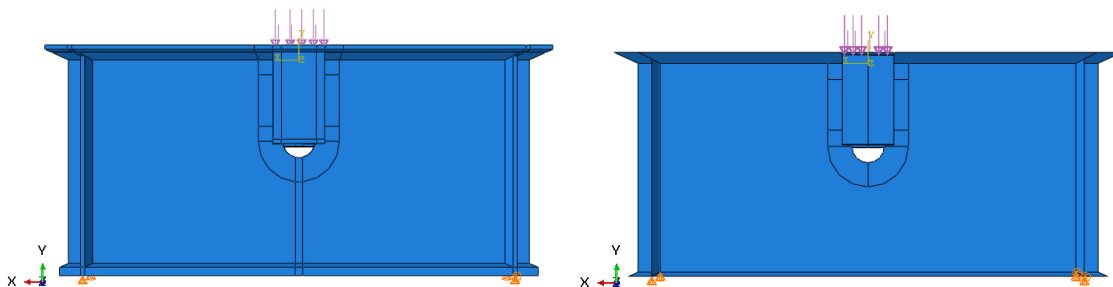


Figure 4.8: Loading and boundary condition for the test specimen (Left: solid model, Right: shell model)

4.7. Finite element modelling

Before starting with the development of the FE models, some preliminary calculations regarding the stresses and deflections are performed. These are summarised in Appendix-F. This is done to have more insight regarding the verification of the FE models. All the FE models are verified with the deflections at the mid-span and equilibrium checks. Also, the nominal stress is calculated by doing some hand calculations as shown in Appendix-G. From the case study on the single side fillet welded transverse plate joint (detail type a) loaded in tension and bending and from the cruciform joint (detail type b) loaded in tension (Chapter-3), some facts on the feasibility of using shell elements for modelling are reported.

For details having a notch or a cope hole, it is expected that SHSS values computed from shell element models without welds will be significantly larger than the values from the solid element model. This is because with the shell model there is an underestimation of stiffness in the welded region. This is also observed in the numerical results of Akhlaghi [9] as shown in Figure 4.4. Also, shell elements being modelled with mid-plane geometry will have a different behaviour than the ones where offsets are applied at the top and bottom plates. This is due to the eccentricities from the offsets which will create additional moments. These additional moments will result in additional stresses which will affect the stress gradient and also SHSS values.

4.8. Modelling with solid elements

A full-scale solid model is made using the dimensions from Figure 4.5. In order to place the nodes exactly at the stress extrapolation points, the solid model is partitioned. The fillet weld geometry is generated by chamfering two intersecting edges of crossbeam web plate and stiffener plate, using 'solid sweep' function around the curved edges. The curved corner of the weld can also be generated by 'extrude' and 'revolve' operations available in the part module of ABAQUS. All these operations provide better control and accuracy in generating the weld geometry. The gap between the connected plates inside the weld is modelled using the crack - assign seam tool. The fillet weld geometry is shown in Figure 4.9. The weld geometry is modelled as close to reality as possible.

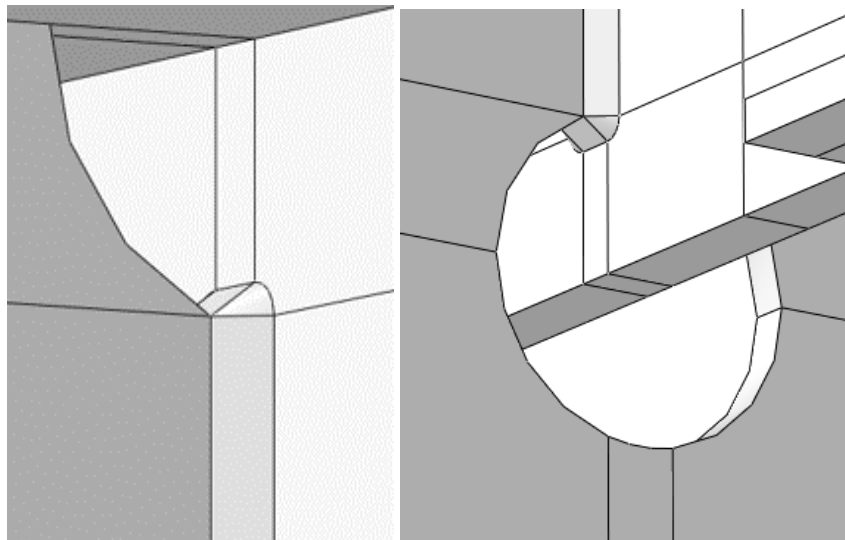


Figure 4.9: Modelling of fillet weld geometry in solid element model

The weld is modelled more realistically than the model proposed by Akhlaghi [9] where only chamfering was used without the rounding of the corners. The stresses in the crossbeam are extracted along the path perpendicular to the weld line using the local rectangular coordinate system. It can be predicted that the elements at the corner of the weld will have some bulging effect. However, this effect will not affect the stresses at the reference points. The stress and deformation contour plots of the solid element models are presented in Appendix-I. The meshing of the investigated detail is performed in a structured manner as shown in Figure 4.10. The global mesh size is 50 mm.

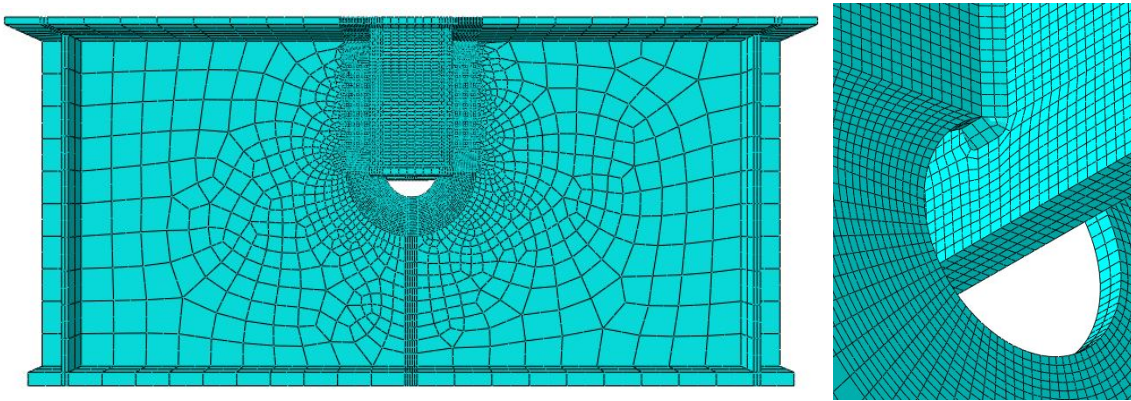


Figure 4.10: Detail with solid elements having a mesh size of 4 mm

Mesh sensitivity study with solid elements: Both linear and quadratic solid elements are used for the mesh sensitivity study. The following mesh sizes of 8 mm, 4 mm and 2 mm are chosen for the mesh sensitivity study. Figure 4.11 shows the stress profiles of linear and quadratic solid elements with different mesh sizes. Appendix-C, shows the detailed mesh sensitivity study for location 'HS1' with solid elements for 400 kN in-plane load. A mesh size of 4 mm is chosen for further analysis with the solid element model. This is because mesh convergence is achieved at an element size of 4 mm.

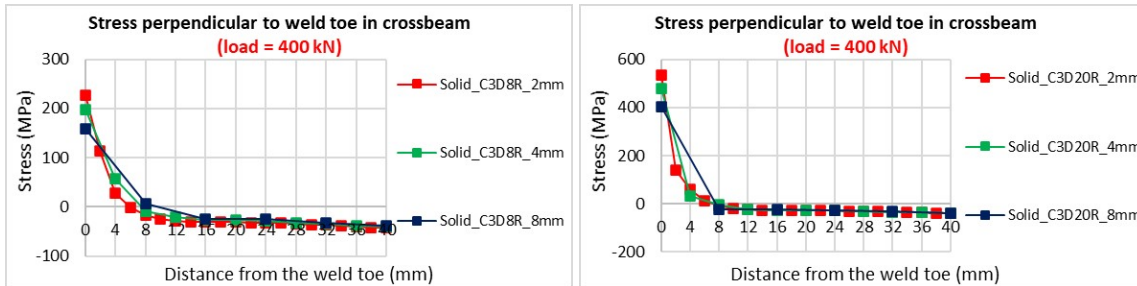


Figure 4.11: Stress distribution perpendicular to weld toe for linear and quadratic solid elements of different mesh sizes

Element type study with the solid element model: From the case study on simple welded details, it is seen that reduced integration gave sufficient accuracy with less computation time. The stress profiles of different solid element types for 4 mm mesh size are shown in Appendix-C for an in-plane load of 400 kN. For this specific detail also, elements with reduced integration gave sufficient accuracy compared to elements with full integration (Table 4.1).

Table 4.1: Comparison of SHSS between different element types with the solid model at HS1

Quadratic Extrapolation – Mesh size 4mm - Load - 400kN				
Element	Element Type	SHSS (MPa)	Experiment SHSS (MPa)	Ratio SHSS (FEM/Experiment)
Solid	C3D8R	209.5	202	1.04
	C3D20R	193.2		0.96
	C3D8	250.1		1.24
	C3D20	233.8		1.16

The solid model with linear elements and reduced integration (C3D8R) overestimated the measured SHSS by 4%. The solid model with quadratic elements and reduced integration (C3D20R) underestimated the measured SHSS by 4%. This difference of +/-4% is considered as acceptable. Linear and quadratic elements with full integration overestimated SHSS values measured from the experiment by 24% and 16% respectively. The stress distribution of different solid element types is shown in Figure 4.12. At a distance of 12 mm away from weld toe, all the curves converged together. Elements with reduced integration, on the other hand gave SHSS values which are closer to the measured SHSS.

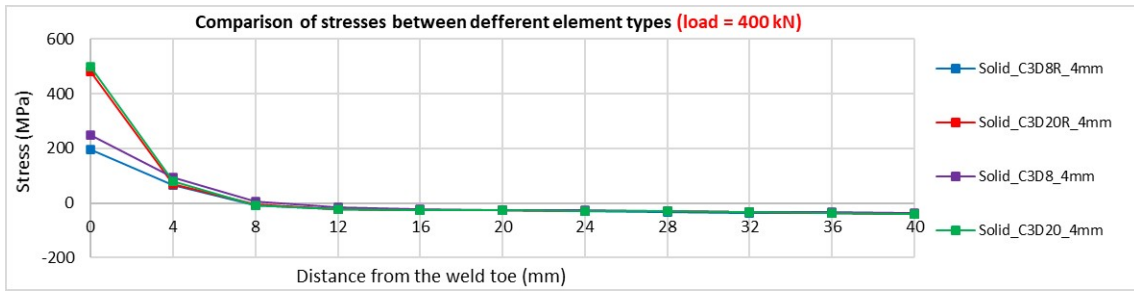


Figure 4.12: Stress distribution perpendicular to weld toe of different element types in solid model (left) and shell model (right)

The contour plots of stress S11 for the solid model with different element types are shown in Figure 4.13. The contour plots clearly show that the elements with full integration showed higher stress values compared to the elements with reduced integration. From the numerical investigation in Chapter-3, it is found that the convergence rate of quadratic solid elements is higher than linear solid elements subject to bending load. Thus, quadratic solid elements with reduced integration is recommended as an appropriate element type for further analysis. Also, it was recommended by Akhlaghi [9] to use quadratic solid elements with a mesh size of 4 mm for the numerical analysis.

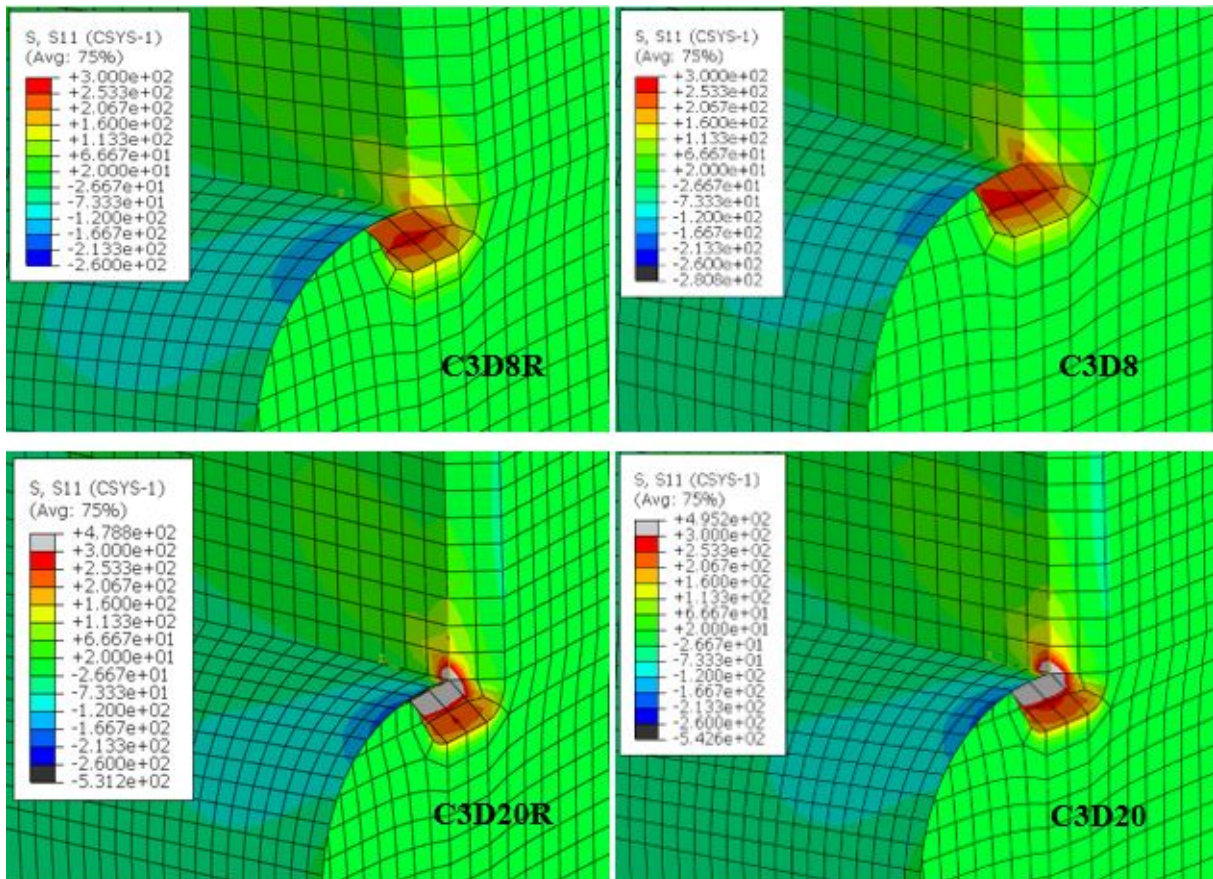


Figure 4.13: Contour plots of stress (S11) for solid models with different element types having same scale

Strain validation of solid model with experimental measurements: The applied load of 200 kN is distributed symmetrically on the two ends of the stiffener in the form of patch loading. The strain values are extracted perpendicular to weld toe along the global x-direction. The global coordinate system is shown in Figure 4.8. The strain validation of the solid model is shown in Figure 4.14. The strain values obtained the solid element model are in line with the strain values measured from the experiment near the weld toe region. There was no measurement data from 0-4 mm near the weld toe.

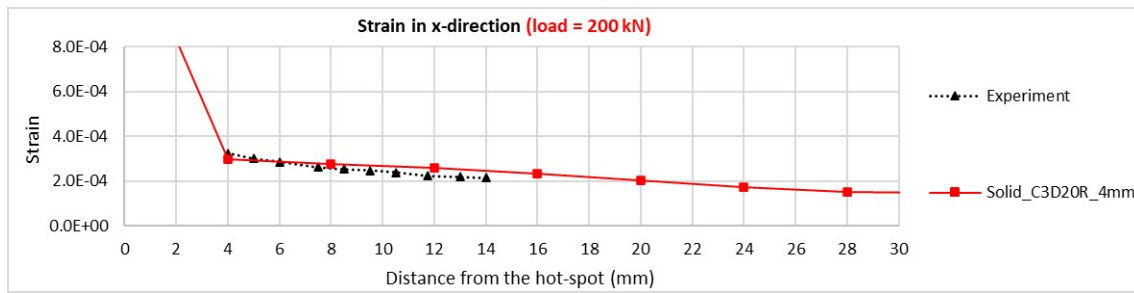


Figure 4.14: Stress validation of the solid models with the experimental measurements at HS1

The percentage differences between the normal strain in x-direction obtained from the solid element model and the measured strains are shown in Appendix-E. The average percentage difference of the stress values from the measured points is within **10%**. The solid element model is considered as a reference model.

4.9. Measurement of SHSS from the experiments

Structural hot spot stresses at HS1 and HS2 are calculated from the quadratic extrapolation of the stresses at 4 mm, 8 mm, and 12 mm from the weld toe as both of them belong to type-“b” hot-spot (Akhlaghi [9]). The values of the SHSS are obtained from the research of Akhlaghi [9] [10]: For a load range of 200 kN, the SHSS measured from the experiment of Akhlaghi for HS1 is 101 MPa [9]. For a load range of 400 kN, the SHSS measured from the experiment of Akhlaghi for HS1 is 202 MPa [9] [10]. For a load range of 350 kN, the SHSS measured from the experiment of Akhlaghi for HS1 is 176.8 MPa [9]. For a load range of 370 kN, the SHSS measured from the experiment of Akhlaghi for HS1 is 186.9 MPa [9].

4.10. Calculation of SHSS from the solid element model

The calculation of SHSS based on FEM according to the IIW recommendations [40] involves determination of stresses from specific points away from the weld toe. From these points, the stress values are extracted and SHSS is determined according to the type of hot-spot defined in Chapter-2. The SHSS is calculated for the numerical model with quadratic solid elements (C3D20R) at hot-spot region HS1 for a load range of 400 kN. The SHSS is calculated using quadratic extrapolation following the IIW guidelines [28] [40]. The stress perpendicular to the weld toe is extracted. For the investigated detail, the hot-spot located at the weld toe of the crossbeam plate is classified as Type-“b” according to the IIW recommendations. Thus, the stresses from the reference points 4 mm, 8 mm and 12 mm is obtained and the SHSS is calculated. The stress distribution perpendicular to weld is shown in Figure 4.15 where the reference points are also shown.

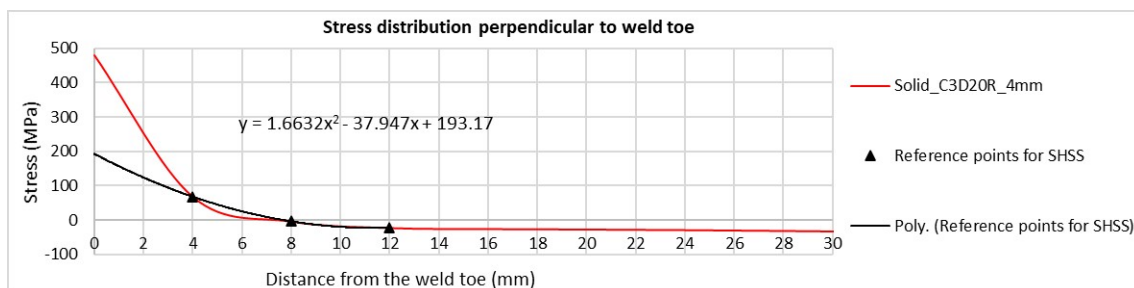


Figure 4.15: Hot-spot stress calculation from the solid finite element model for the detail having type-b hot-spot [40]

From the figure, the SHSS values obtained from the solid element model for the load range of 400 kN is **193.2 MPa** for hot-spot location HS1. The SHSS values from the experiment for the same loading conditions is **202 MPa** (Figure 4.4). The average percentage difference between the SHSS results of FEM and measurements is within +/- **5%**. This difference in percentage is considered as acceptable and thus the solid element model is said to be completely validated with the experimental results.

4.11. Modelling with shell elements

The shell element models are developed using 8 node quadratic elements with reduced integration (S8R). In order to place the nodes exactly at the stress extrapolation points, the shell model is also divided using partitions just like the solid models. The stress profile obtained from a non-structured mesh showed some difference compared to that from a structured mesh. But, this difference is within **5%**. A structured mesh is used for the investigated detail in the shell model as shown in Figure 4.16. The global mesh size is 50 mm. A local mesh refinement is done at the investigated region as shown in the figure. The cope hole is modelled using the same radius as that from the solid model. The contour plots of the shell element models are presented in Appendix-I.

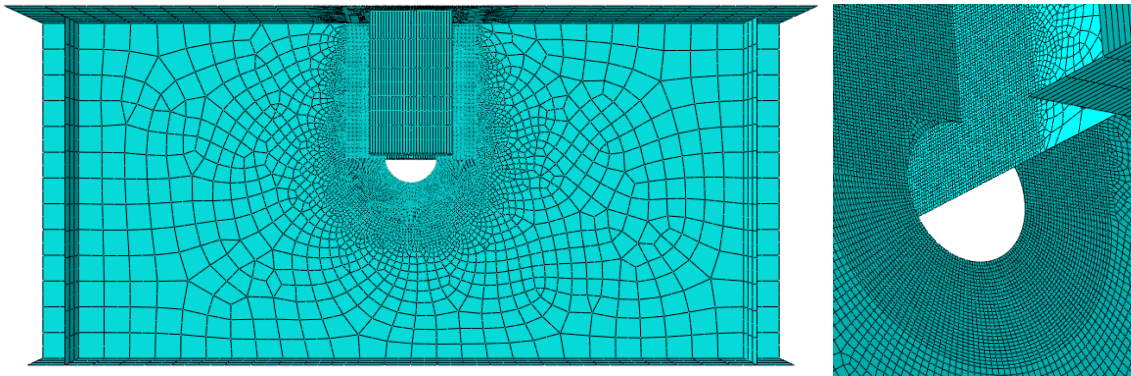


Figure 4.16: Detail with shell elements having a mesh size of 2 mm

In Chapter-3, it was seen that for the single side fillet welded longitudinal plate joint, the shell element model developed using shell offset - bottom surface gave SHSS values which were not in good agreement with the SHSS values obtained by Śledziwski [54]. This was because of eccentricity which results in additional moments in the shell models with bottom surface approach. These moments lead to additional stresses in the model. Thus, the geometry of the crossbeam, stiffener, deck plate and bottom flange of the present detail are constructed using the mid-surface offset approach. This means that the total height of the crossbeam included half of the thickness of the deck plate and half of the thickness of the bottom flange. This is done to make sure that the total height is consistent. There is some overlapping of material at the intersection of every component of this detail.

Figure 4.17 shows how the shell element model is made using the mid-plane modelling approach. The rendered shell view is also shown in the same figure in order to have a clear visualisation of the modelling. The important locations are shown in Figure 4.18.

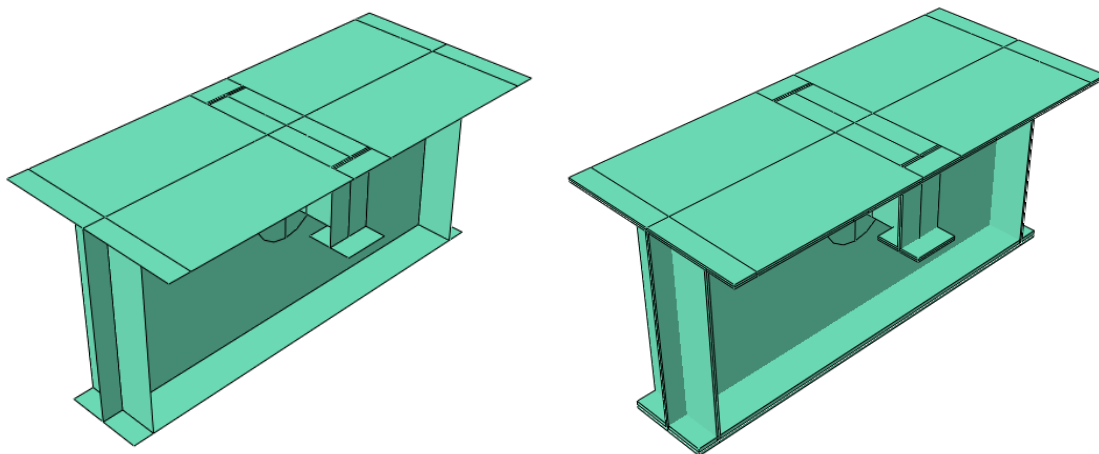


Figure 4.17: Shell element model using mid-plane geometry

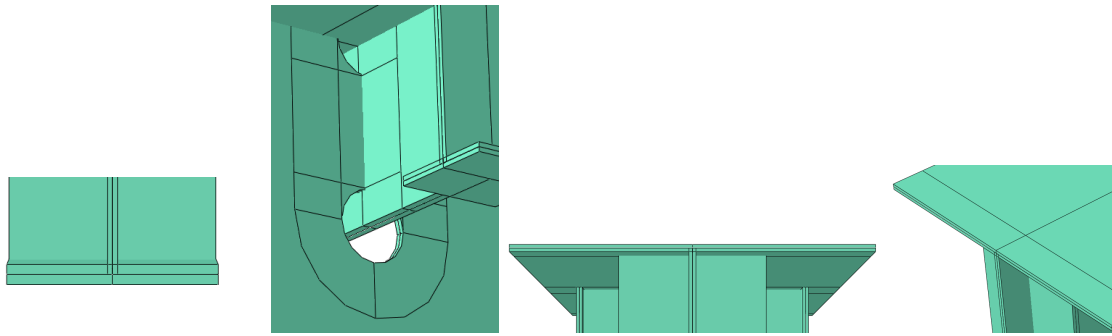


Figure 4.18: Rendering of shell thickness and offset in property module along with locations of interest

Mesh sensitivity study with shell elements: Both linear and quadratic shell elements are used for mesh sensitivity study. The following mesh sizes of 1 mm, 2 mm, 4 mm and 8 mm are chosen for numerical analysis. The same load of 400 kN is applied and a structured mesh is used for all the shell models. Figure 4.19 shows the stress profiles of linear and quadratic shell element models with different mesh sizes. It can be observed that the quadratic shell elements gave a higher stress concentration compared to the linear shell elements of the same element size.

Appendix-C shows the detailed mesh sensitivity study for location HS1 with shell elements. It has been observed that there is a huge stress increase near the weld toe due to singularity in all the models. Both linear and quadratic models are mesh insensitive below a mesh size of 2 mm. At a distance of 20 mm from the weld toe all the curves converge.

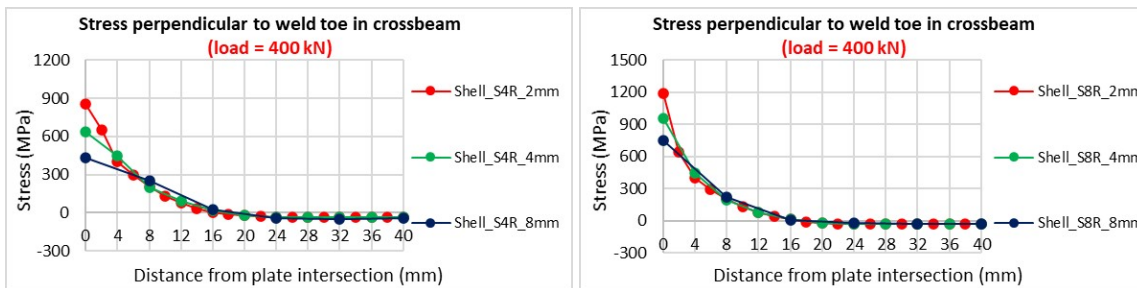


Figure 4.19: Stress distribution perpendicular to weld toe for linear and quadratic shell elements of different mesh sizes

Element type study for the shell element model: The stress profiles of different shell element types for 2 mm mesh are shown in Appendix-C. The SHSS values are calculated using quadratic extrapolation and are shown in Table 4.2. A huge difference in SHSS values is observed between the shell models with different element types. Also, the SHSS obtained from the shell model is in general quite high compared to the SHSS of the solid model. This is also observed from the numerical results of Akhlaghi [10] (Figure 4.4). The percentage difference is almost 2% between the linear and quadratic elements with reduced integration. Full integration linear shell elements gave very high SHSS values.

Table 4.2: Comparison of stresses between different shell models at HS1

Quadratic Extrapolation - Mesh 2mm - Load - 400kN				
Element	Element Type	SHSS (MPa)	Experiment SHSS (MPa)	Ratio SHSS (FEM/Experiment)
Shell	S4R	660.8	202	3.27
	S8R	672.5		3.33
	S4	756.6		3.75

4.12. Comparison of SHSS with numerical results of Akhlaghi (2009)

Akhlaghi [10] in his research, had obtained, the hot-spot stress value from the solid model as 230 MPa and that from the shell model as 873 MPa. The SHSS ratio of FEM to experiment, was 1.14 for solids and 4.32 for shells for a load range 400 kN [10]. This is shown in Table 4.3. The ratio of SHSS of shell to solid obtained from his research was 3.8 [10].

Table 4.3: SHSS values at the location HS1 obtained from the research of Akhlaghi [10]

Quadratic Extrapolation, Location - HS1					
Load range (KN)	Experiment SHSS (MPa)	Element Type	SHSS from FEM (MPa)	SHSS ratio FEM/Experiment	SHSS ratio shell/solid
400	202	Solid (C3D20R)	230	1.14	-
		Shell (S8R)	873	4.32	3.8

After complete analysis in the current study, the SHSS values are evaluated for a load range of 400 kN from the numerical models. The results are compared with the SHSS from the experiment as shown in Table 4.4.

Table 4.4: SHSS values at the location HS1

Quadratic Extrapolation, Location - HS1					
Load range (KN)	Experiment SHSS (MPa)	Element Type	SHSS from FEM (MPa)	SHSS ratio FEM/Experiment	SHSS ratio shell/solid
400	202	Solid (C3D20R)	193.2	0.96	-
		Shell (S8R)	672.5	3.33	3.48

It is found that the ratio of SHSS obtained from the numerical model to measured SHSS is 0.96 for solids and 3.33 for shells for a load range of 400 kN at HS1. The SHSS values calculated from the solid model is about **4%** lower than the experimental values, which is acceptable, considering the effect of mis-alignments and residual stresses in the real specimen. The ratio of SHSS obtained from the shell model to that from the solid model is 3.48.

The main reason for the occurrence of such large stresses in the shell model is because of insufficient stiffness at the weld region when compared to the solid model. In addition, the origin for stress extrapolation for the regular shell model is taken at the plate intersection. But, in the solid model the origin is taken at the weld toe.

4.13. Shell elements including weld geometry

The weld is modelled by a local increase in the thickness of the elements in the weld region. Niemi [39] suggested the use of shell elements with increased thickness at the intersection region of welded joints. Niemi [39] mentioned only the intersection region of the weld without recommending thickness and size that should be used in the modelling. Eriksson [20] had suggested using this technique for modelling of fillet welds in shell element model. It is recommended using two rows of shell elements with increased thickness, for example, elements with increased thickness both in the attached plate and the parent plate for a double-sided fillet weld.

The IIW [40] also provides some guidelines for this method as mentioned in Chapter-2 (Figure 2.36). Since, the weld is modelled, the origin of the stress profile is now at the weld toe which is the same for both the shell and solid models. Thus, both the stress profiles can be plotted on the same graph. It is found that this type of shell model with quadratic elements which included the stiffening effect of the welds had a similar stress gradient with the solid element model. The IIW approach [40] of weld modelling is implemented in this study as can be seen in Figure 4.20.

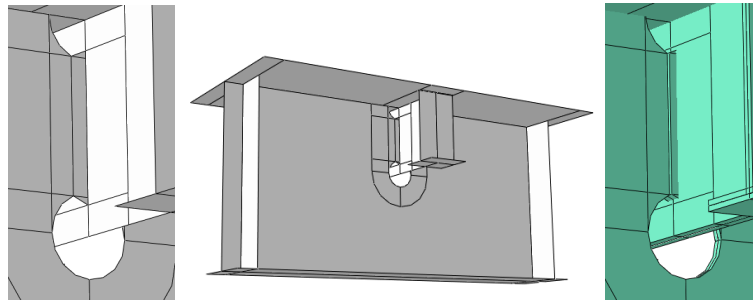


Figure 4.20: Shell element model with weld modelled using local increase of thickness at the weld region

4.14. Numerical models subjected to different load cases

Quadratic solid elements (C3D20R) are used with a mesh size of 4 mm. Quadratic shell elements (S8R) are used with a mesh size of 2 mm. The boundary conditions remained unchanged for all the load cases investigated. In order to have a good comparison between the solid model, the shell model and shell model with welds, the stress gradients are compared. In addition, the maximum principal stress and the absolute maximum principal stress is also used for the comparison study. The following load cases are investigated: load case 1: in-plane bending of crossbeam, load case 2: out-of-plane bending of crossbeam and load case 3: in-plane bending of crossbeam with local load introduction on top of the stiffener.

Load case 1: Pure in-plane bending of crossbeam - For this case, equal loads of 200 kN are applied on either side of the crossbeam at equal distances away from the stiffener in order to capture the pure in-plane behaviour of the crossbeam as shown in Figure 4.21.

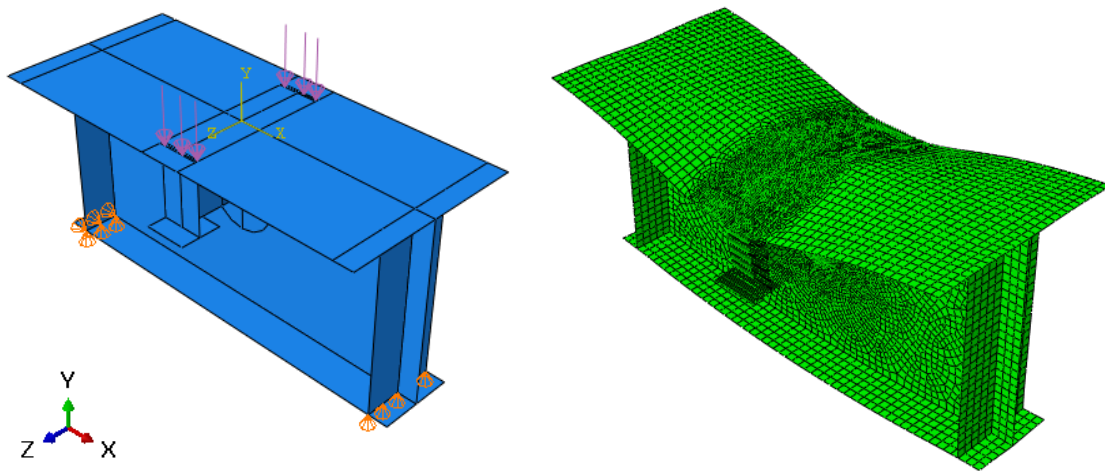


Figure 4.21: In-plane behaviour of the crossbeam: loading and deformed mesh

The stress perpendicular to weld toe and maximum principal stress distribution of the three numerical models are shown in Figure 4.22. The stress values from shell element model with welds is in good agreement with the stress from solid element model. This means that with the weld modelling approach using shell elements, a correct estimation of the in-plane stiffness of the numerical model can be obtained. When weld is not included in shell element models, sharp increase of stress in vicinity of the weld toe is found and high stress concentration is observed. The stress values converge beyond a distance of 16 mm. For this load case, the direction of maximum principal stress is found to be the same as the direction of stress perpendicular to weld toe. Thus, the maximum principal stress is close to the stress perpendicular to weld toe. The stress gradient of the shell model with welds using the IIW [40] approach was similar to the stress gradient from the solid model for all the stress components.

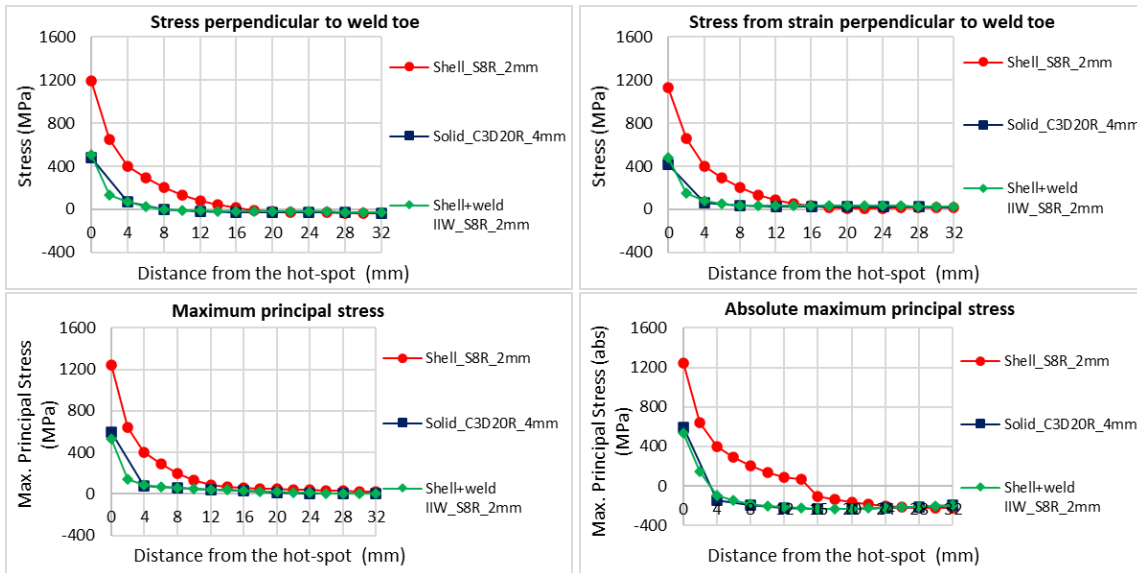


Figure 4.22: Stress profiles of the numerical models in crossbeam for LC-1

Load case 2: Pure out-of-plane bending of crossbeam - In this section the pure out-of-plane deformation behaviour of the crossbeam is studied and the stress profiles of the shell and solid numerical models are investigated in order to check for a difference in behaviour. A load of 10 kN is applied in the upward direction on one load patch and in downward direction in the other. The load patches are directly located on the deck plate at top of the stiffener as shown in Figure 4.23.

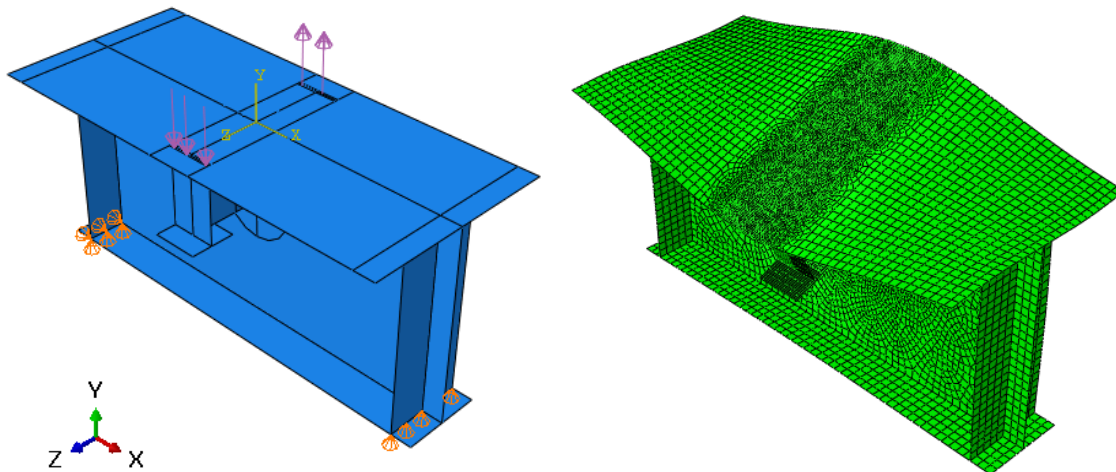


Figure 4.23: Out-of-plane behaviour of the crossbeam: loading and deformed mesh

It is observed that the shell element model is having a more gradual stress gradient compared to the solid element model at HS1. However, it is also observed that the shell+weld IIW model overestimates the stress values compared to the solid model. The stress profiles of the numerical models converged at a distance of 30 mm away from the stress concentration. The shell element model with welds, have a steeper stress gradient and higher stress peak. The trend-line of the stress from the shell+weld IIW model was similar to the trend-line of the solid element model as shown in Figure 4.24. The maximum principal stress is almost zero for all the numerical models. For this load case, the stress gradient of the component perpendicular to weld toe is comparable to the stress gradient of absolute maximum principal stress.

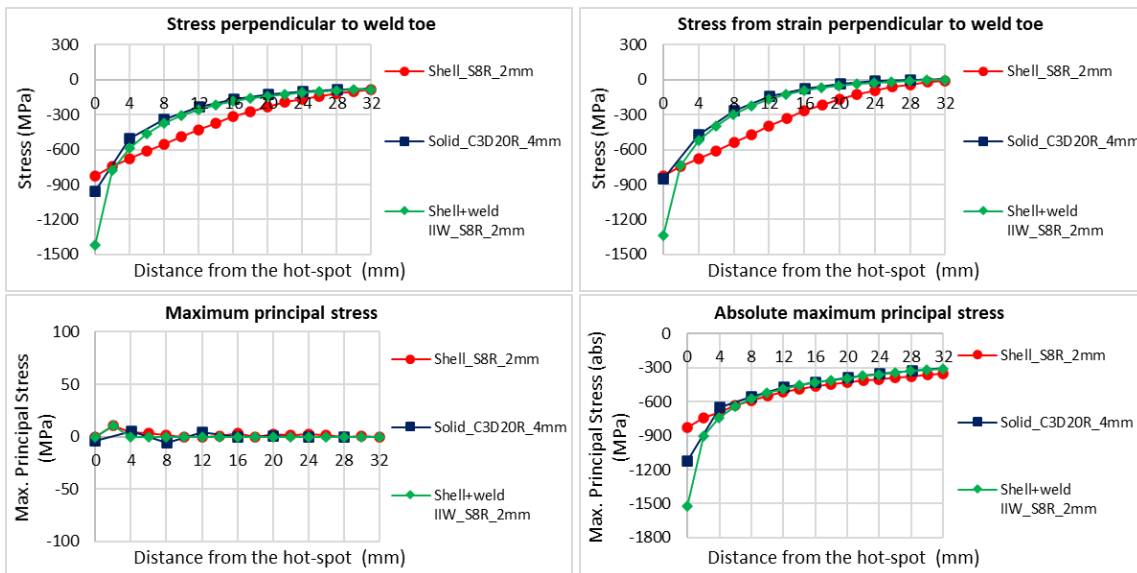


Figure 4.24: Stress profiles of the numerical models in crossbeam for LC-2

Load case 3: Pure in-plane bending of crossbeam with local load introduction on top of the stiffener - A load of 400 kN is applied at the centre of the deck plate as a load patch shown in Figure 4.25. In this section the in-plane of the crossbeam is studied with the effect of local load introduction on top of the stiffener. Here also, the boundary conditions remained unchanged and thus all the numerical models are consistent with respect to the boundary conditions.

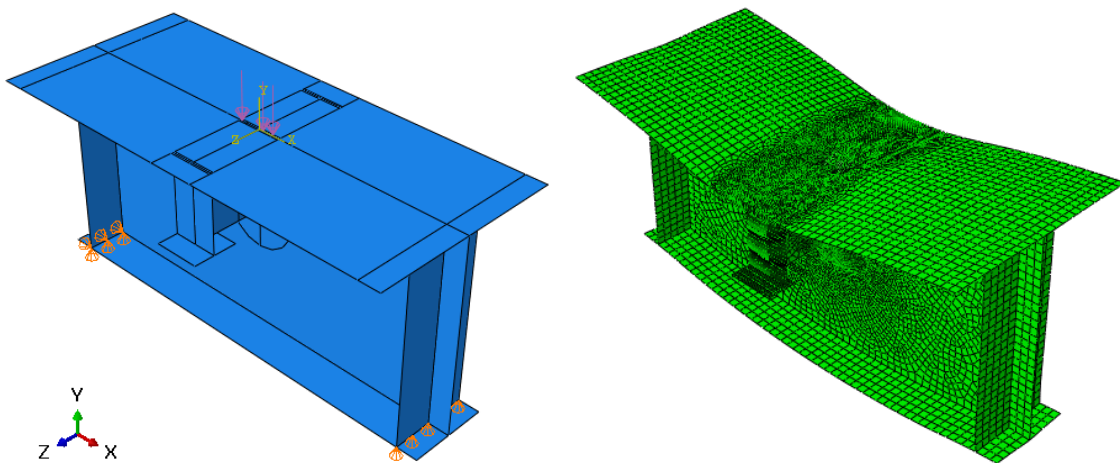


Figure 4.25: In-plane behaviour of the crossbeam with local load introduction on the stiffener: loading and deformed mesh

The stress profiles of the shell and solid numerical models are investigated in order to check for a difference in behaviour. The comparison of stress gradients between the numerical models are shown in Figure 4.26. Just like for LC-1, here also it is observed that the stress values from shell+weld IIW model are in good agreement with that from solid element model. The stress perpendicular to the weld toe converged at a distance of 20 mm away from the weld toe for all the numerical models. The stress gradient of the shell model was more flat when compared to that of the solid model. The stress values are also obtained from the strain perpendicular to weld toe in order to investigate the effect of lateral contraction. It is observed from the stress profiles that this effect is very small.

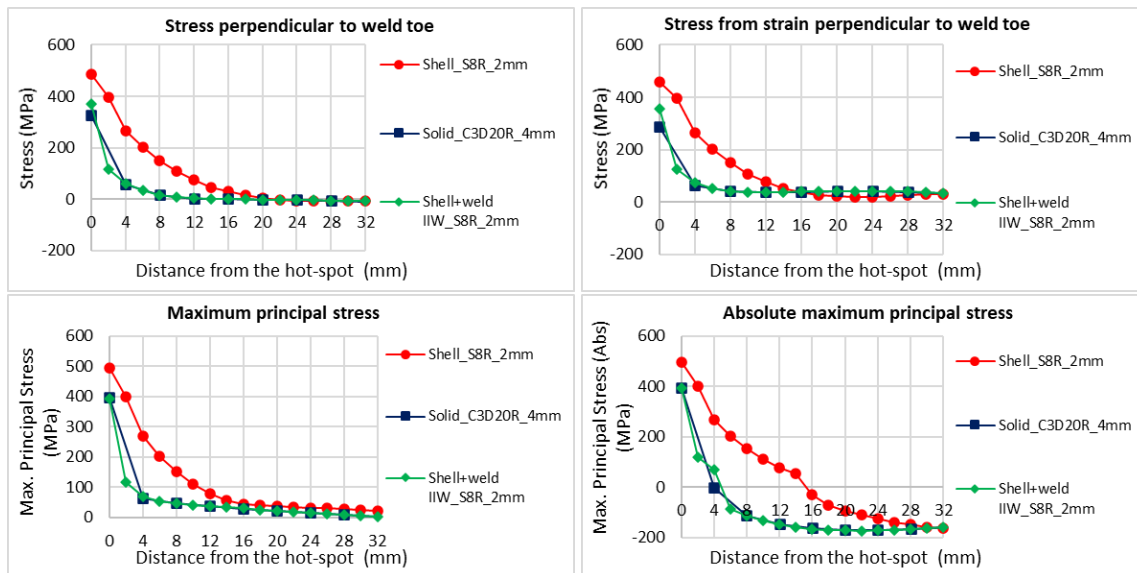


Figure 4.26: Stress profiles of the numerical models in crossbeam for LC-3

From different stress profiles of the numerical models, it is evident that the shell model with welds developed using the IIW approach shows a good match in stress gradient for LC-1 and LC-3. The contour plots of stress and deformation are shown in Appendix-I. The following tables give the summary of the hot-spot stress values from the numerical models. The SHSS is first calculated considering the stress perpendicular to weld toe in Table 4.5.

Table 4.5: Summary of SHSS results for different load cases based on stress perpendicular to weld toe

Load Case	Description	Shell_S8R_2mm	Solid_C3D20R_4mm	Shell+weld_S8R_2mm	Ratio	
					Ratio SHSS shell/solid	Ratio SHSS shell+weld/solid
1	Pure in-plane	672.5	193.2	193.0	3.48	1.00
2	Pure out-of-plane	-815.2	-724.9	-890.9	1.12	1.23
3	In-plane + local	421.7	121.1	138.0	3.48	1.14

The ratio of SHSS between the shell elements to that of the solid elements is also shown in Table 4.5. It is observed that the hot-spot stress ratio improved a lot for LC-1 and LC-3 after modelling welds with shell elements according to IIW [40] approach. For LC-2 (out-of-plane loading), this was not the case. Thus, it was concluded that the weld modelling approach recommended by the IIW [40] only improved the in-plane stiffness. Other weld modelling strategies using the increased thickness method is recommended for accurately modelling the out-of-plane stiffness for such details. The SHSS is also calculated using the maximum principal stress in Table 4.6. The ratio of SHSS between the shell elements to that of the solid elements is also shown.

Table 4.6: Summary of SHSS results for different load cases based on maximum principal stress

Load Case	Description	Shell_S8R_2mm	Solid_C3D20R_4mm	Shell+weld_S8R_2mm	Ratio	
					Ratio SHSS shell/solid	Ratio SHSS shell+weld/solid
1	Pure in-plane	689.0	101.5	130.0	6.79	1.28
2	Pure out-of-plane	-818.6	-772.5	-995.8	1.06	1.29
3	In-plane + local	424.6	84.3	109.0	5.04	1.29

In this case, the direction of the maximum principal stress stress varies with change of load case. Thus, getting consistent SHSS ratio is more difficult when maximum principal stress is used in calculation of hot-spot stress.

5

Parametric analysis of fillet welded transverse and longitudinal cruciform joint

“You never fail until you stop trying.”

Albert Einstein

In this chapter a parametric sensitivity study is first performed on a fillet welded longitudinal and transverse cruciform joint subjected to bending. In addition to the shell and solid models, the shell model incorporating welds using the increased thickness method is investigated. The increase of thickness of the plate along the weld region is done using three different approaches: the Eriksson’s approach [20], the approach given by the IIW recommendations [40] and a combination of these two approaches. The purpose of this study is to obtain consistency in the ratio of calculated SHSS values from shell elements to that from solid elements for this particular detail.

5.1. Motivation

In the following sections, a detailed investigation of hot-spot stress is performed for a fillet welded transverse and longitudinal cruciform joint under bending. In Chapter-3, a fillet welded transverse cruciform joint having the geometry from the study by Karabulut and Lombaert [31] is investigated under a tensile load. It is observed that the SHSS obtained from the solid model gave a good estimation of the SHSS which is experimentally obtained. Thus, in this study, the solid model is considered as a reference for comparison with other numerical models for this specific detail. A parametric study is performed with this type of joint having dimensions of the crossbeam and stiffener plates based on the light and heavy OSD variants.

5.2. Weld modelling with increased thickness method

There are two approaches of modelling the welds with shell elements using the increased thickness method which is discussed in detail in Chapter-2 as shown below:

Weld modelling approach using the increased thickness method as recommended by the IIW guidelines [40] - The first approach for weld modelling with shell elements is performed by locally increasing the thickness at the plate intersection and having downward sloping ends (weld fillet) as per the IIW recommendations (Figure 2.36). In this approach, the thickness of one of the two connected plates is increased at the welded connection. The two governing parameters in this approach are the weld leg length (l) and the thickness of the connected plate (t). The throat thickness of the weld at the joint is (a) and thus the weld leg length ($l = a\sqrt{2}$). Since, the shell model is developed using mid-plane geometry, the height of the weld plate strip is equal to the weld leg length (l) plus half of the thickness of the stiffener ($t_s/2$). The weld is modelled using an inclined plate extended from the crossbeam having a thickness increased by the weld leg length (l). Thus, the increased value of plate thickness = ($t_p + l$), where t_p is the thickness of the crossbeam and l is the weld leg length.

Weld modelling approach using the increased thickness method as recommended by Niemi [39] and Eriksson [20] - The second approach for weld modelling with shell elements (Figure 2.35 [20]) is performed by locally increasing the thickness at the plate intersection without any downward sloping end. Niemi [39] and Eriksson [20] proposed this modelling technique where the stiffness of the weld is simulated without representing the weld fillet (downward sloping ends). The role of the weld is played by the shell elements with an increased thickness along the welded region. In this approach, the thickness of both plates is increased at the welded connection. The two governing parameters in this approach of weld modelling are the weld throat thickness (a) and the thickness of the connected plates (t). The Eriksson's approach [20] is investigated in detail for a simple fillet welded cruciform joint subjected to different load cases in the following sections.

5.3. Numerical models of fillet welded cruciform joint

The numerical models of the transverse and longitudinal fillet welded cruciform joints which are investigated in this study are shown in Figures 5.1 and 5.2 respectively. Three different models are made with the transverse joint and five different models are made with the longitudinal joint. The coordinate system, loading and boundary conditions are taken to be consistent in all the numerical models in order to have a better comparison.

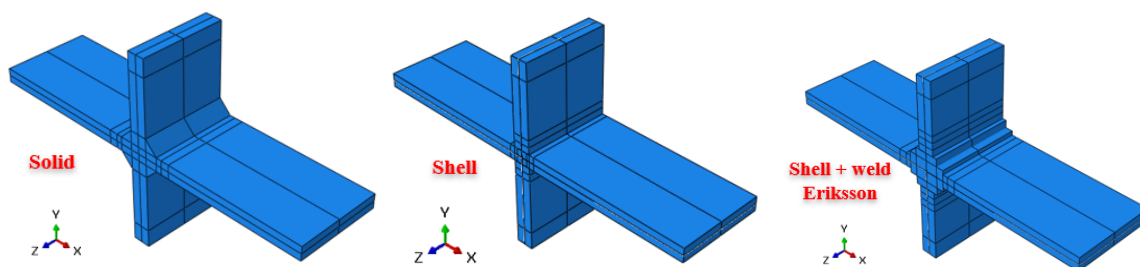


Figure 5.1: Numerical models of transverse cruciform joints

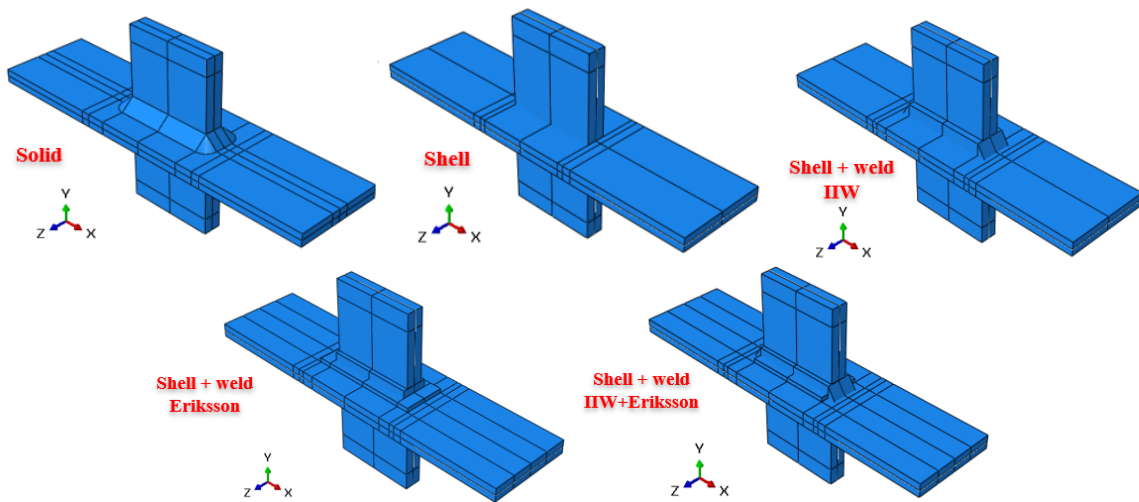


Figure 5.2: Numerical models of longitudinal cruciform joints

For the solid model, the stiffener is modelled as a continuous plate to which two crossbeam plates are welded on top and bottom. The solid models are developed using the crack assign-seam tool, to model the gap in between the connected plate inside the weld. However, it is observed that the difference in stress results obtained from the solid models with and without seam is within 1%. The origin for stress extrapolation is taken at the weld toe for solid model.

For the shell model, the mid-planes of the stiffener and crossbeam is modelled, and the total length of the top and bottom plates included the length of the individual plates plus the thickness of the base plate. The origin for stress extrapolation is taken at the plate intersection for shell model. In addition to the shell and solid models, the weld modelling approach with shell elements has been investigated in detail in the following sections.

A parametric study has been performed on the transverse and longitudinal cruciform joint as shown in Figure 5.3.

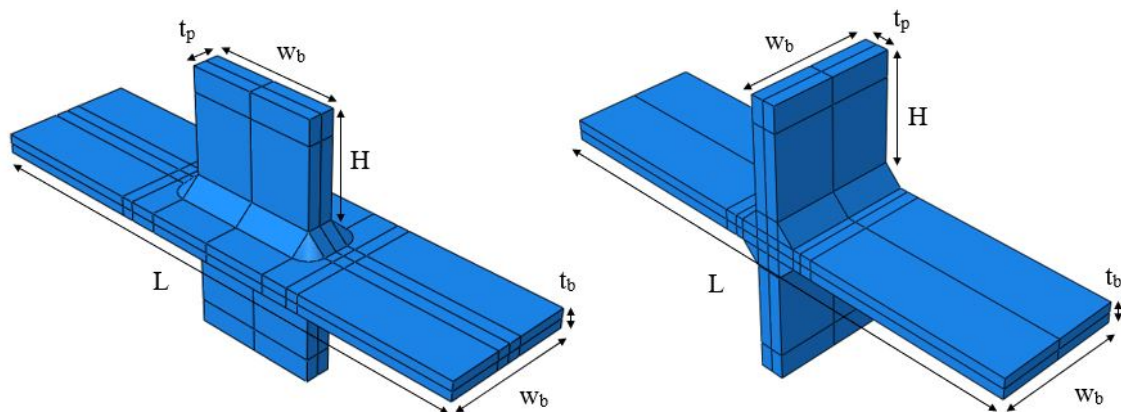


Figure 5.3: Dimension of components for parametric study on cruciform joint: longitudinal (left) and transverse (right)

Both the transverse and longitudinal cruciform joints are subjected to the same reference load cases and load combinations. The dimension of the base plate is based on the dimension of the continuous stiffener of OSD. The dimension of the top and bottom plates are based on the dimension of the crossbeam of OSD. Table 5.1 shows the values of the constants and variables for the parametric study on the cruciform joints. The variables for the numerical models for the parametric study are thickness of base plate (t_b) and thickness of top plate (t_p). All other parameters are kept constant.

Table 5.1: Dimensions of different components of the cruciform joint based on the dimensions of OSD variants

Components	Variant 1 (based on old/light OSD)	Variant 2 (based on new/heavy OSD)
Length of the base plate (L)	200 mm	200 mm
Height of the top and bottom plates (H)	50 mm	50 mm
Thickness of the base plate (t_b)	8 mm	10 mm
Thickness of the top and bottom plates (t_p)	10 mm	16 mm
Width of the base plate (w_b)	50 mm	50 mm
Width of the top and bottom plate (w_b)	50 mm	50 mm
Throat thickness of the weld (a)	5 mm	5 mm

5.4. Parametric study on transverse fillet welded cruciform joint based on the dimensions of OSD

Load case 1 (LC-1): in-plane bending - In order to investigate the effect of pure in-plane bending, the detail is loaded under a uniform pressure applied on bottom surface of bottom plate in the negative y direction. The total force applied is 1kN and it is uniformly distributed as a pressure loading (Figure 5.4). The point of maximum stress concentration is located at the middle of the base plate for this load case.

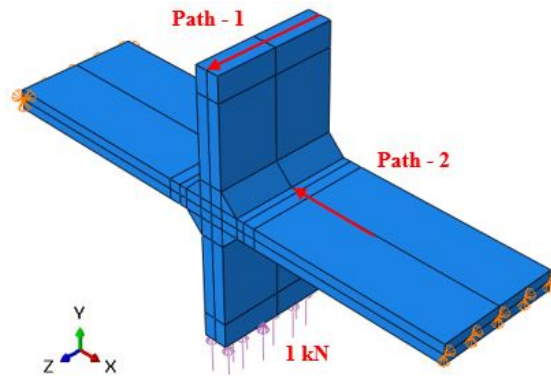


Figure 5.4: Solid model variant 1 under load case-1 (LC-1) for transverse cruciform joint

Figure 5.5 shows the deformation of the model in the y-direction along path-1 for LC-1. The maximum deformation of the shell model is 0.38 mm for variant-1 and 0.2 mm for variant-2. The deformations of the solid model and the shell+weld Eriksson model are almost the same and are equal to 0.29 mm for variant-1 and 0.14 mm for variant-2. From the figures, it can be seen that there is an overlap of deformations between the solid model and shell+weld Eriksson model.

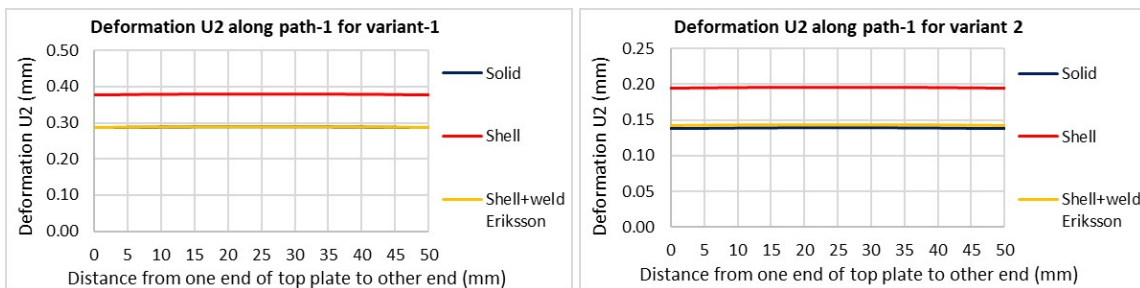


Figure 5.5: Deformation (U2) along path-1 for load case-1 (LC-1) for variant-1 (left) and variant-2 (right)

The stress distribution perpendicular to weld toe along path-2 for both the light and heavy OSD variants for LC-1 is also shown in Figure 5.6. The regular shell model gives a consistent overestimation of stresses in the range of **20-25%** compared to the solid model for both the variants.

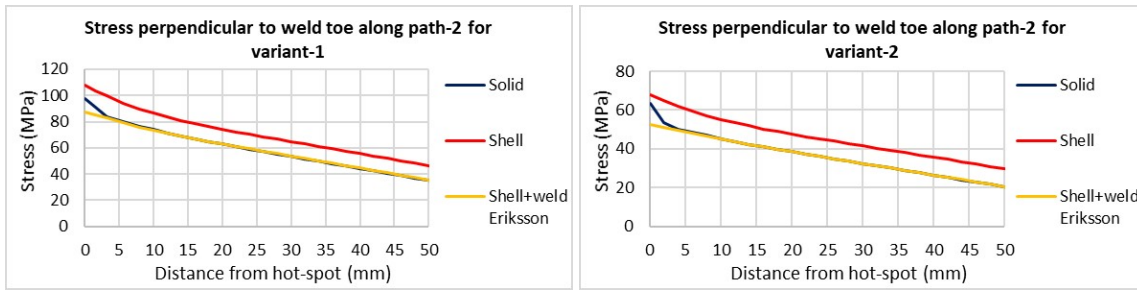


Figure 5.6: Stress distribution perpendicular to weld toe along path-2 for variant-1 (left) and variant-2 (right) under LC-1

Load case 2 (LC-2): in-plane torsion - In order to investigate in-plane torque on the detail, 2×1 kN total force is applied with one on top plate in the negative x direction and the other on bottom plate along positive x direction, according to Figure 5.7. The point of maximum stress concentration is located at the middle of the base plate for this load case.

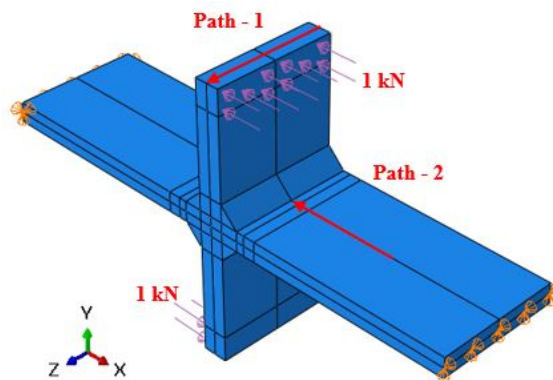


Figure 5.7: Solid model variant 1 under load case-2 (LC-2) for transverse cruciform joint

From Figure 5.8, the maximum deformation of the model in the x-direction for LC-2 of shell model is 0.25 mm for variant 1 and 0.12 mm for variant 2, respectively. The deformation of the solid model is 0.18 mm for variant 1 and 0.085 mm for variant 2. The deformation of the shell+weld Eriksson model is very close to that of the solid model which is 0.19 mm for variant 1 and 0.089 mm for variant 2 respectively.

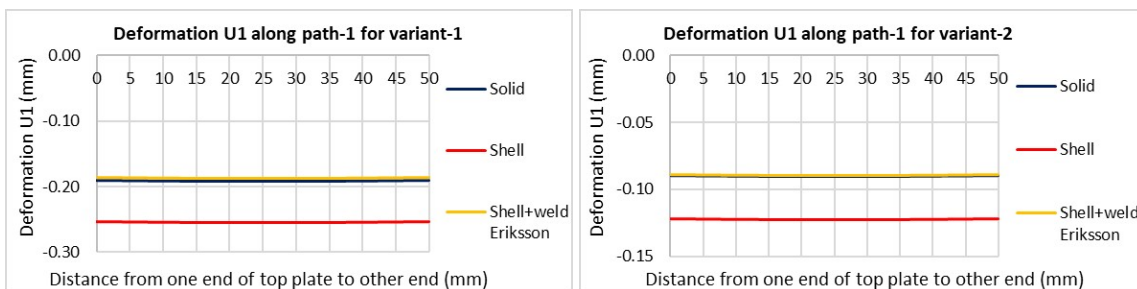


Figure 5.8: Deformation (U2) along path-1 under LC-2 for variant-1 (left) and variant-2 (right)

The stress distribution perpendicular to weld toe along path-2 for both the light and heavy OSD variants in the case of LC-2 is shown in Figure 5.9. It can be observed that, the stress value at 50 mm away from weld toe is almost the same for the solid model and the shell+weld Eriksson model. However, the regular shell model gives a higher stress value at 50 mm away from weld toe. Furthermore, the regular shell model gave a consistent overestimation of stresses in the range of **15-20%** compared to the solid model for both the variants.

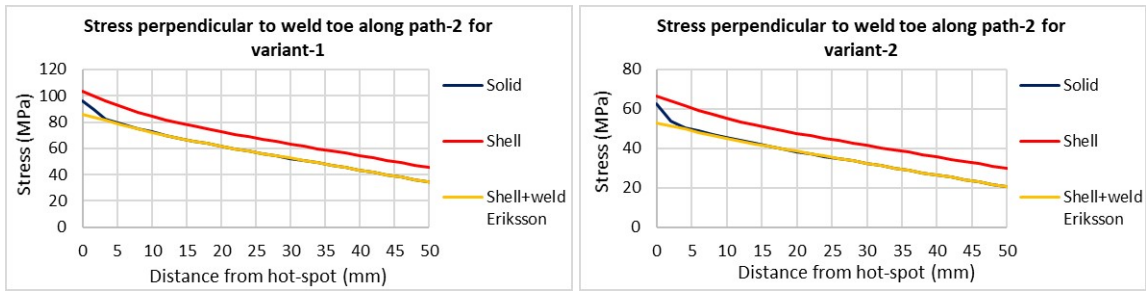


Figure 5.9: Stress distribution perpendicular to weld toe along path-2 for variant-1 (left) and variant-2 (right) and LC-2

Load case 3 (LC-3): out-of-plane torsion - For investigating the out-of-plane torque of the detail, 2×1 kN total force is applied on top plate along positive z direction and on bottom plate along negative z direction (Figure 5.10). The deformations are shown in the following figures (Figures 5.11, 5.12 and 5.13).

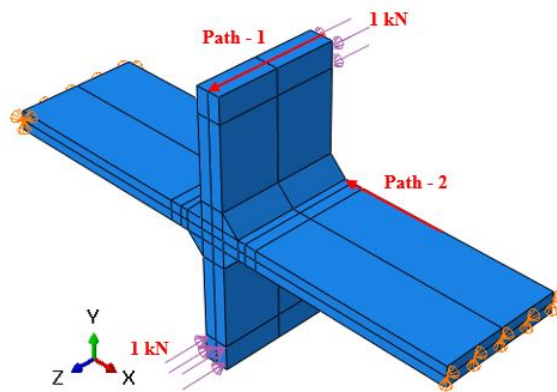


Figure 5.10: Solid model variant 1 under load case-3 (LC-3) for transverse cruciform joint

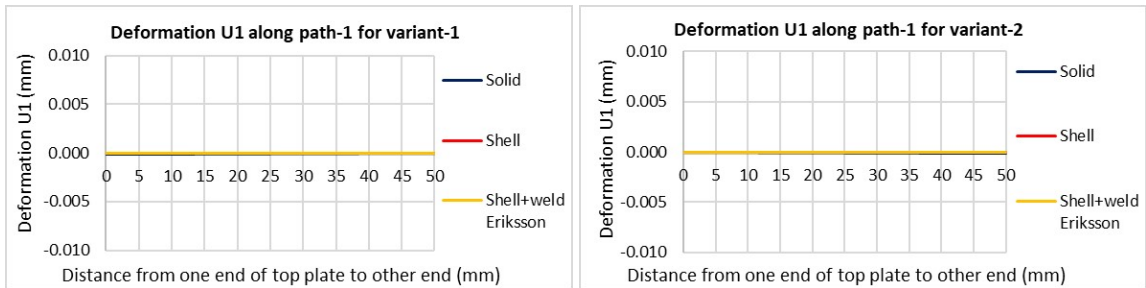


Figure 5.11: Deformation (U1) along path-1 under LC-3 for variant-1 (left) and variant-2 (right)

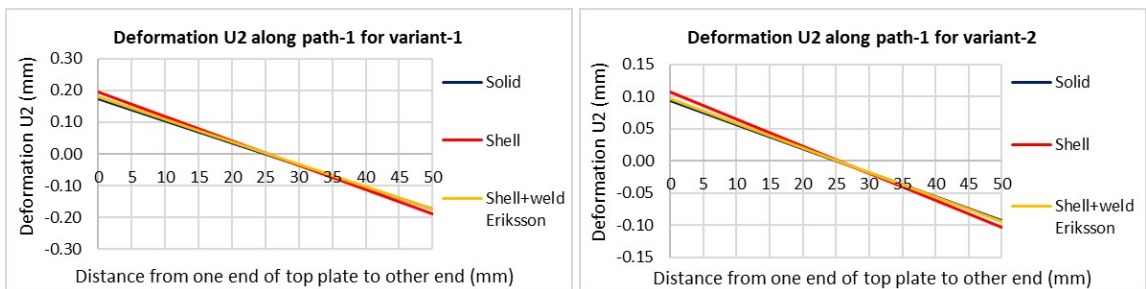


Figure 5.12: Deformation (U2) along path-1 under LC-3 for variant-1 (left) and variant-2 (right)

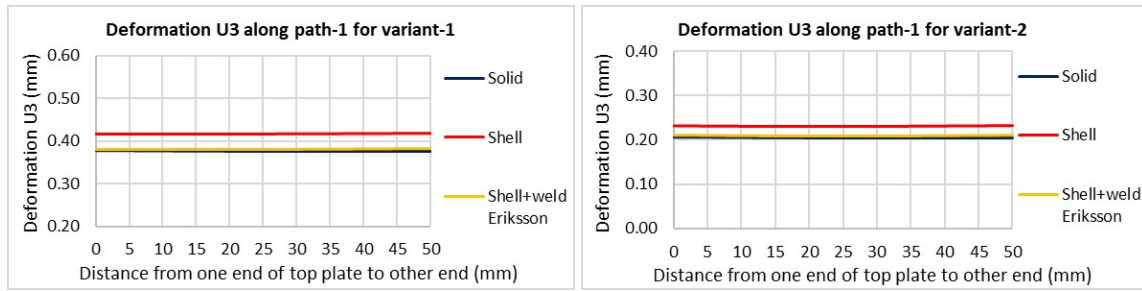


Figure 5.13: Deformation (U3) along path-1 under LC-3 for variant-1 (left) and variant-2 (right)

The point of maximum stress concentration is located at the side of the base plate for this load case. From the above figures, it can be observed that the deformations of the solid model and the shell+weld Eriksson model are almost the same for LC-3. This proves that the out-of-plane torsional stiffness of the solid model can be modelled properly by the shell+weld Eriksson model.

The stress distribution perpendicular to weld toe along path 2 is also shown in Figure 5.14. The shell model with welds result in an underestimation of stresses of the order of **2%** compared to the solid model. Whereas the normal shell model show an overestimation of stresses in range of **20-25%** compared to the solid model. At a distance of 50 mm, the stress values from all the numerical models converge.

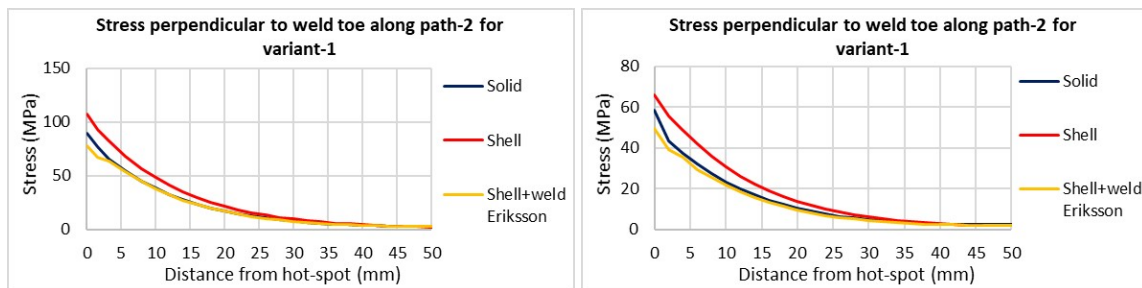


Figure 5.14: Stress distribution perpendicular to weld toe along path-2 for variant-1 (left) and variant-2 (right) under LC-3

The contour plots of deformation of the numerical models in the case of transverse cruciform joint are shown in Appendix-I. The out-of-plane load case (LC-3) has been investigated further in Appendix-J for this detail. Not only the edge path, but also other paths on the base plate have been considered during the comparison study of the stress gradients between the numerical models. Also, a small study is done to find the appropriate boundary conditions for the solid model (Appendix-J). It is found that for the solid models, the mid-line edge support is regarded as an appropriate boundary condition in order to have a good comparison with all the shell element models.

In addition to the three reference load cases, four load combinations are also investigated as shown in Figures 5.15-5.18. For all the load combinations, similar observations are found as from the standard load cases LC-1, LC-2 and LC-3. The regular shell element model gave an overestimation of stresses in the range **15-25%** compared to the solid element model. The stress gradient of the shell+weld Eriksson model is similar to the stress gradient of the solid model. Furthermore, the stress value at a distance of 50 mm away from the weld toe is exactly same for the solid model and the shell+weld Eriksson model. The regular shell element model gave an overestimation of stresses in the range **15-25%** compared to the solid element model. The contour plots of deformation of the numerical models of the transverse cruciform joint for these load cases are shown in Appendix-I.

Table 5.2 shows the SHSS values and the SHSS ratios obtained for all the load cases. After modelling welds using the Eriksson's approach, the SHSS ratios are consistent having a mean of **0.98** and a CV of **0.4%**. This is considered as acceptable.

Load combination-1 (LC1+LC2)

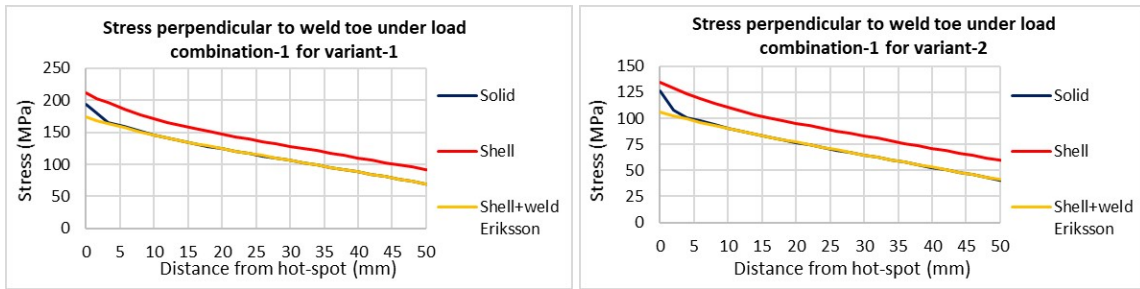


Figure 5.15: Stress perpendicular to weld toe for variant-1 (left) and variant-2 (right) under load combination-1

Load combination-2 (LC1+LC3)

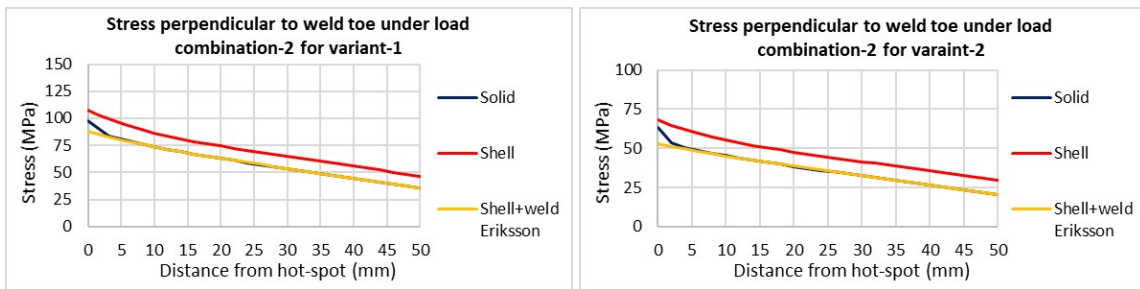


Figure 5.16: Stress perpendicular to weld toe for variant-1 (left) and variant-2 (right) under load combination-2

Load combination-3 (LC2+LC3)

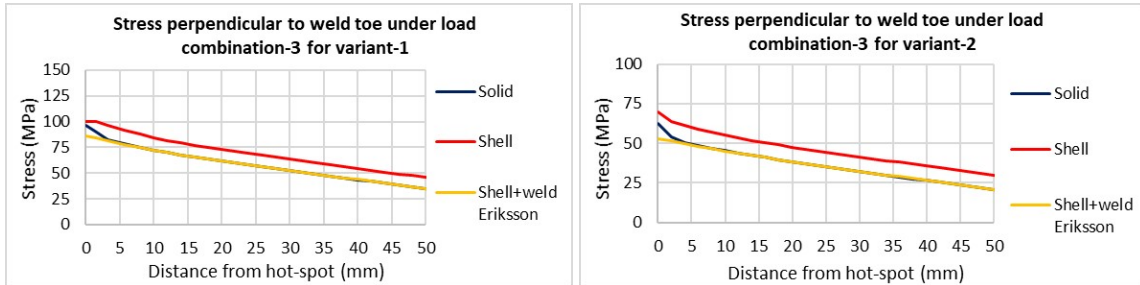


Figure 5.17: Stress perpendicular to weld toe for variant-1 (left) and variant-2 (right) under load combination-3

Load combination-4 (LC1+LC2+LC3)

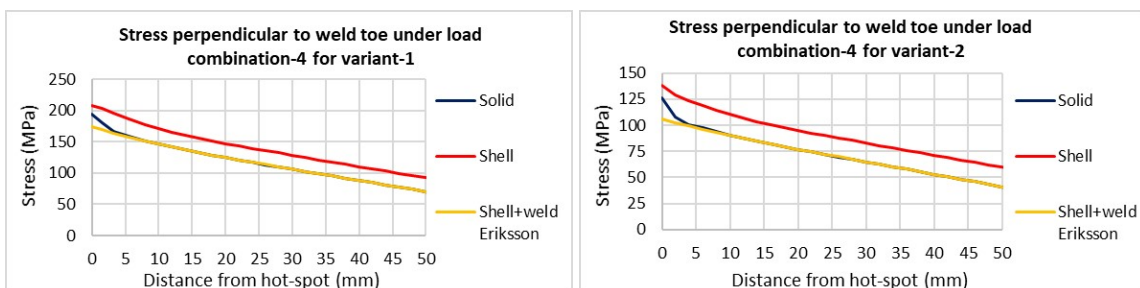


Figure 5.18: Stress perpendicular to weld toe for variant-1 (left) and variant-2 (right) under load combination-4

Table 5.2: SHSS of transverse cruciform joint

Geometry Variant	Load Case	Hot-spot stress (MPa)			Ratio	
		Solid	Shell	Shell+weld Eriksson	SHSS shell/solid	SHSS shell+weld Eriksson/solid
Variant 1 (Light variant OSD)	LC1	88.2	106.0	87.0	1.20	0.99
	LC2	87.0	102.3	85.8	1.17	0.99
	LC1+LC2	175.2	208.2	172.8	1.19	0.99
	LC1+LC3	88.2	105.9	87.0	1.20	0.99
	LC2+LC3	87.0	102.2	85.8	1.17	0.99
	LC1+LC2+LC3	175.2	208.2	172.8	1.19	0.99
Variant 2 (Heavy variant OSD)	LC1	53.7	66.5	52.6	1.24	0.98
	LC2	54.0	65.7	52.8	1.22	0.98
	LC1+LC2	107.6	132.2	105.4	1.23	0.98
	LC1+LC3	53.7	66.5	52.6	1.24	0.98
	LC2+LC3	54.0	65.7	52.8	1.22	0.98
	LC1+LC2+LC3	107.6	132.2	105.4	1.23	0.98

5.5. Parametric study on fillet welded longitudinal cruciform joint based on the dimensions of OSD

Load case 1 (LC-1) - Similar to the transverse cruciform joint, the detail is loaded under a uniform pressure applied on bottom surface of bottom plate in the negative y direction in order to investigate in-plane bending (Figure 5.19).

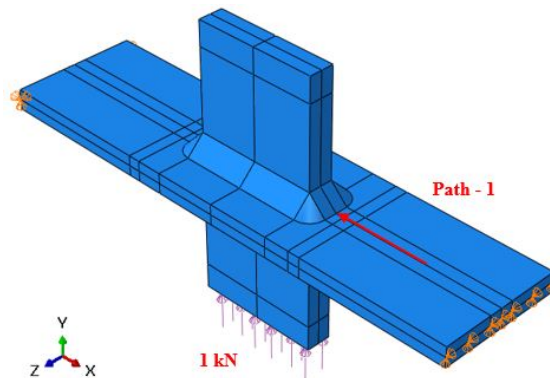


Figure 5.19: Solid model variant 1 under load case-1 (LC-1) for longitudinal cruciform joint

The stress profiles of the solid element model and all the shell element models for both the variants are shown in Figure 5.20.

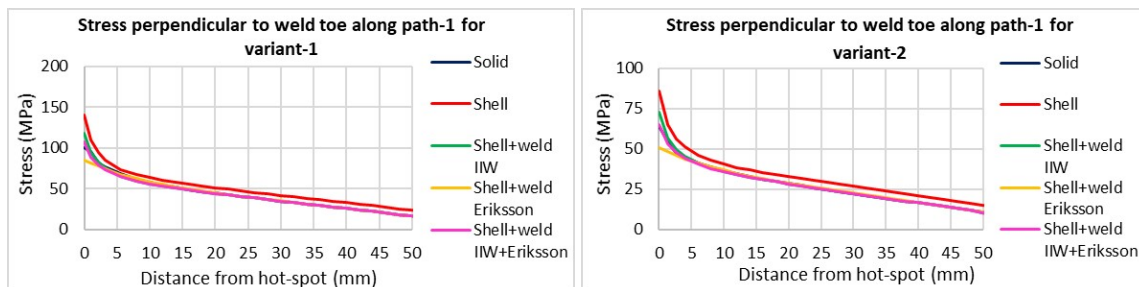


Figure 5.20: Stress perpendicular to weld toe for variant-1 (left) and variant-2 (right) under LC-1

From the figures, it is observed that the regular shell model gave a consistent overestimation of stresses by **13-16%** compared to the solid model for both the variants. After weld modelling with shell elements, the stress gradients improved when compared to the solid model. The stress gradient of the shell models with welds are in good agreement with the stress gradient of solid model. Furthermore, the stress value obtained at a distance of 50 mm away from weld toe from the shell+weld combined model were exactly the same as that obtained from the solid element model.

Load case 2 (LC-2) - Just like for the transverse cruciform joint, 2×1 kN total force is applied with one on top plate in the negative x direction and the other on bottom plate along positive x direction in order to investigate in-plane torsion (Figure 5.21).

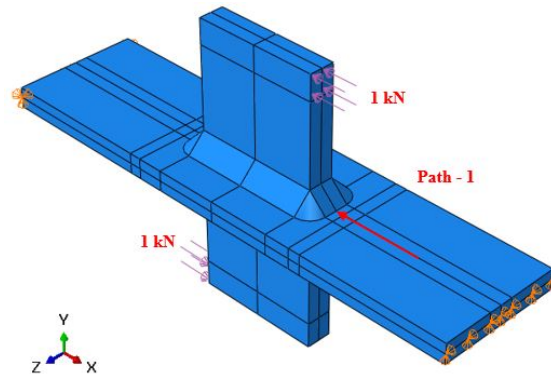


Figure 5.21: Solid model variant 1 under load case-1 (LC-2) for longitudinal cruciform joint

The stress profiles of the solid element model and all the shell element models for both the variants are shown in Figure 5.22.

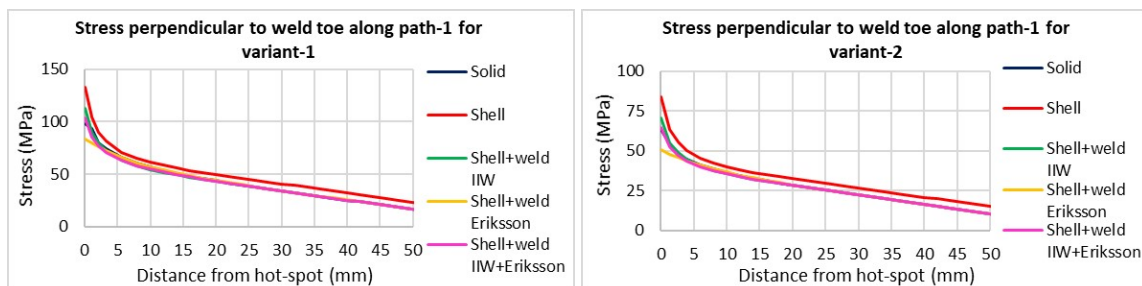


Figure 5.22: Stress perpendicular to weld toe for variant-1 (left) and variant-2 (right) under LC-2

From the above figure, it can clearly be observed that the shell model overestimates the stress values by **11-15%** compared to the solid model. At a distance of 50 mm away from weld toe, the shell model gives a higher value of stress in comparison to the solid model. The shell+weld models gave a good match in stress gradient compared to the solid model for this load case.

Four load combinations are investigated for the longitudinal cruciform joint. The corresponding stress profiles are shown in Figures 5.23-5.26. In all these cases, the shell model overestimates the stress values by **11-16%** when compared compared to the solid model. The stress at a distance of 50 mm away from weld toe is almost same for the solid element model and the all shell+weld models.

Load combination-1 (LC1+LC2)

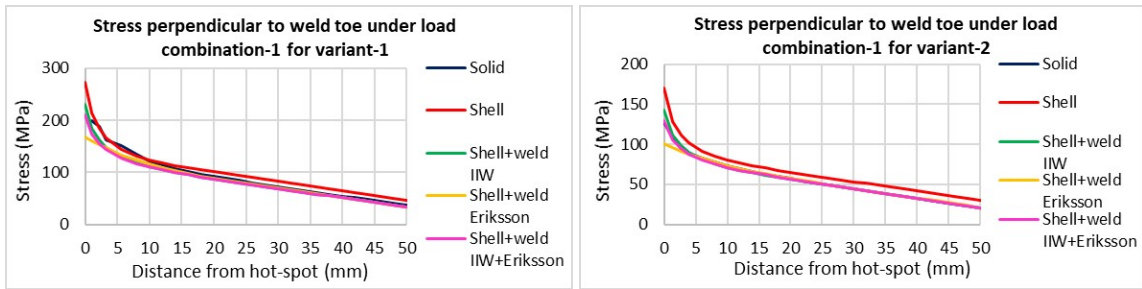


Figure 5.23: Stress perpendicular to weld toe for variant-1 (left) and variant-2 (right) under load combination-1

Load combination-2 (LC1+LC3)

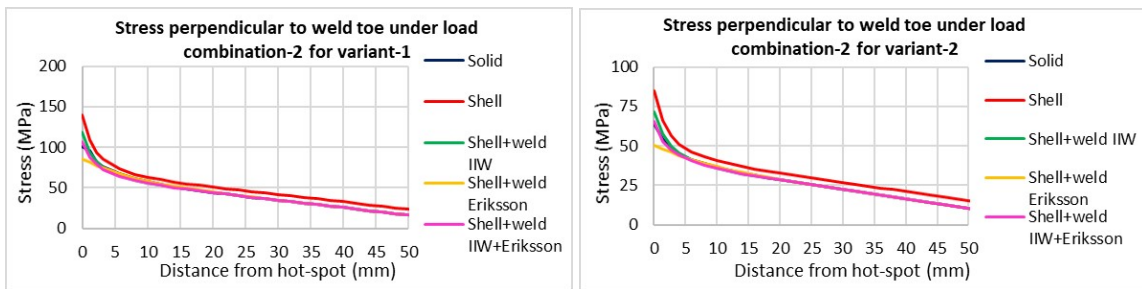


Figure 5.24: Stress perpendicular to weld toe for variant-1 (left) and variant-2 (right) under load combination-2

Load combination-3 (LC2+LC3)

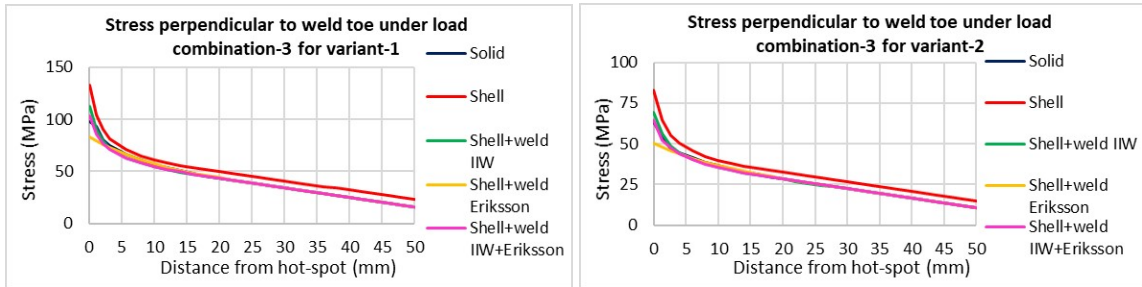


Figure 5.25: Stress perpendicular to weld toe for variant-1 (left) and variant-2 (right) under load combination-3

Load combination-4 (LC1+LC2+LC3)

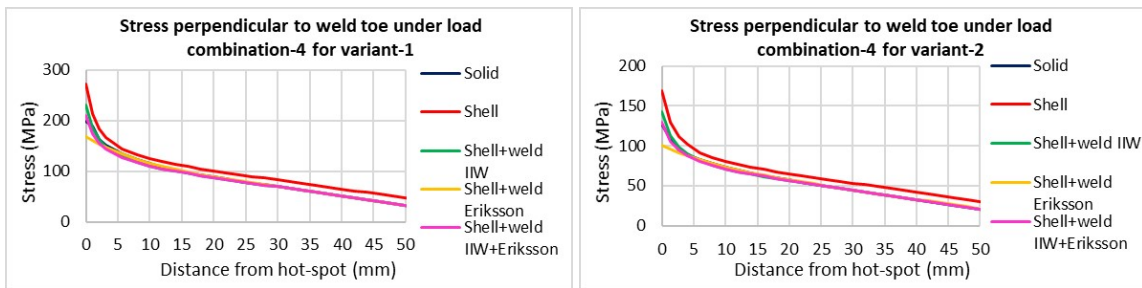


Figure 5.26: Stress perpendicular to weld toe for variant-1 (left) and variant-2 (right) under load combination-4

The contour plots of deformation of the numerical models of the longitudinal cruciform joint for these load cases are shown in Appendix-I. Table 5.3 shows the SHSS values and the SHSS ratios obtained for all the load cases.

Table 5.3: SHSS of longitudinal cruciform joint

Geometry Variant	Load Case	Hot-spot stress (MPa)					Ratio			
		Solid	Shell	Shell+weld IIW	Shell+weld Eriksson	Shell+weld IIW+Eriksson	SHSS shell/solid	SHSS shell+weld IIW/solid	SHSS shell+weld Eriksson/solid	SHSS shell+weld IIW+Eriksson/solid
Variant 1 (Light variant OSD)	LC1	85.8	96.9	85.6	82.4	82.2	1.13	1.00	0.96	0.96
	LC2	83.6	92.7	82.3	80.3	79.9	1.11	0.98	0.96	0.96
	LC1+LC2	169.4	189.6	167.9	162.7	162.1	1.12	0.99	0.96	0.96
	LC1+LC3	85.8	96.9	85.6	82.4	82.2	1.13	1.00	0.96	0.96
	LC2+LC3	83.6	92.7	82.3	80.3	79.9	1.11	0.98	0.96	0.96
	LC1+LC2+LC3	169.4	189.6	167.9	162.7	162.1	1.12	0.99	0.96	0.96
Variant 2 (Heavy variant OSD)	LC1	50.1	58.2	51.7	48.6	49.6	1.16	1.03	0.97	0.99
	LC2	49.8	57.2	50.7	48.6	49.3	1.15	1.02	0.98	0.99
	LC1+LC2	99.9	115.4	102.4	97.2	98.9	1.16	1.03	0.97	0.99
	LC1+LC3	50.1	58.3	51.7	48.6	49.6	1.16	1.03	0.97	0.99
	LC2+LC3	49.8	57.2	50.8	48.6	49.3	1.15	1.02	0.98	0.99
	LC1+LC2+LC3	99.9	115.5	102.4	97.2	98.9	1.16	1.03	0.97	0.99

From Table 5.3, it is clear that the regular shell models cannot be used to calculate the SHSS using surface stress extrapolation. The maximum overestimation in hot-spot stress with regular shell element model is **16%** compared to the solid element model. The stress obtained from the regular shell model at a distance of 50 mm away from weld toe is also significantly higher compared to the solid model. This is considered as unacceptable. After modelling welds with shell elements, the following observations are noted:

- With the IIW approach, the SHSS ratios are consistent having a mean of **1.01** and a CV of **1.9%**.
- With the Eriksson's approach, the SHSS ratios are consistent having a mean of **0.97** and a CV of **0.7%**.
- With the combined approach, the SHSS ratios are also consistent having a mean of **0.97** and a CV of **1.8%**.

Thus, it can be concluded that all the above three methods of weld modelling are good for the case of a simple longitudinal cruciform joint subjected to bending. This is because the mean value of the SHSS ratio is within the range of **0.97-1.01** and the CV is within the range of **0.7%-1.9%**.

6

Parametric analysis of OSD

“Invention is not the product of logical thought, even though the final product is tied to a logical structure.”

Albert Einstein

In this chapter, a preliminary and a detailed parametric investigation is performed on an OSD. The main regions of interest are based on two types of cracks on the open stiffener-to-crossbeam welded joint with (1) crack in crossbeam and (2) crack in longitudinal open stiffener. In the first half of this chapter, a preliminary investigation is performed on the OSD for some reference load cases. A comparison of stress gradients and structural hot-spot stress (SHSS) is done for the numerical models. In the next half of this chapter, the influence lines of SHSS are computed for six different numerical models which are investigated in this study for the light and heavy OSD variants. In addition, the critical points with maximum and minimum SHSS are determined for all the numerical models. The ratio of SHSS of shell model to solid model and the ratio of SHSS of shell model with welds to solid model using different approaches are obtained and summarised in the later sections of this chapter.

6.1. Motivation

A parametric analysis is performed for the OSD consisting of the detail of open stiffener and crossbeam with a cope hole. The general approach followed is to first make a global shell model of the OSD and then develop the local sub-solid model in the region of interest. Since the focus of this thesis is on the cracks in the crossbeam and stiffener, the middle crossbeam and middle stiffener is selected for investigation. This is because, this region is subjected to maximum bending when the load is applied at the centre of the deck-plate. This study is performed with realistic dimensions from the existing and new bridges in The Netherlands as shown in Table 6.1. The starting dimensions of the detail to be investigated is based on the dimensions of the Haringvlietbrug [7] and is obtained from the drawings provided by Rijkswaterstaat. The main purpose of this study is to achieve consistency in the ratio of SHSS from the shell element model to that from the solid element model.

6.2. Geometrical variants for the parameter model

The parametric models are based on realistic dimensions of bridges in The Netherlands. The influence of geometry of bridge components is taken by considering the light and heavy of OSD variants (Table 6.1). The newly designed OSD bridges generally have thicker deck plates compared to the old OSD bridges. The thickness and height of the crossbeam is more for the new OSD bridges than that of the old ones in The Netherlands.

The goal is to investigate two main geometrical variants of the OSD. The first variant with the dimensions of the old and existing bridges in The Netherlands (variant-1). The thickness of the components of this variant are lower compared to that of the newly designed bridges. This variant can be regarded as the light variant. The second variant with the dimensions of newly designed bridges in The Netherlands (variant-2). This variant is regarded as the heavy variant.

Table 6.1: Details of geometry of OSD variants for parametric study

Sl. No.	Component	Variant-1	Variant-2
1	Thickness of deck plate (t_{dp})	10 mm	16 mm
2	Spacing (centre-to-centre distance) between crossbeams	2000 mm	2000 mm
3	Spacing (centre-to-centre distance) between open stiffeners	300 mm	300 mm
4	Length of deck plate (L_{dp})	11500 mm	11500 mm
5	Width of deck plate (W_{dp})	6000 mm	6000 mm
6	Length of crossbeam (L_{cb})	11500 mm	11500 mm
7	Total number of crossbeams to be modelled	3	3
8	Thickness of crossbeam web ($t_{cb,w}$)	10 mm	16 mm
9	Thickness of crossbeam bottom flange ($t_{cb,bf}$)	12 mm	20 mm
10	Width of crossbeam bottom flange ($b_{cb,bf}$)	250 mm	300 mm
11	Height of crossbeam web ($h_{cb,w}$)	650 mm	1000 mm
12	Length of open stiffener (L_s)	6000 mm	6000 mm
13	Total number of open stiffeners to be modelled	38	38
14	Height of open stiffener (h_s)	160 mm	220 mm
15	Thickness of open stiffener (t_s)	8 mm	10 mm
16	Diameter of cope hole ($d_{cope-hole}$)	45 mm	60 mm
17	Shape of cope hole	Circular	Circular

6.3. Material properties and boundary conditions

The following material properties are assumed: $E = 210000$ MPa and $\nu = 0.3$. Since the main beam is not modelled, some assumptions are made for modelling appropriate boundary conditions for the crossbeam in the OSD parameter model. The boundary conditions are chosen with the crossbeam being fully restrained against translation in x, y and z directions as shown in Figure 6.1. The boundary conditions are chosen in order to study the in-plane bending behaviour of the crossbeam.

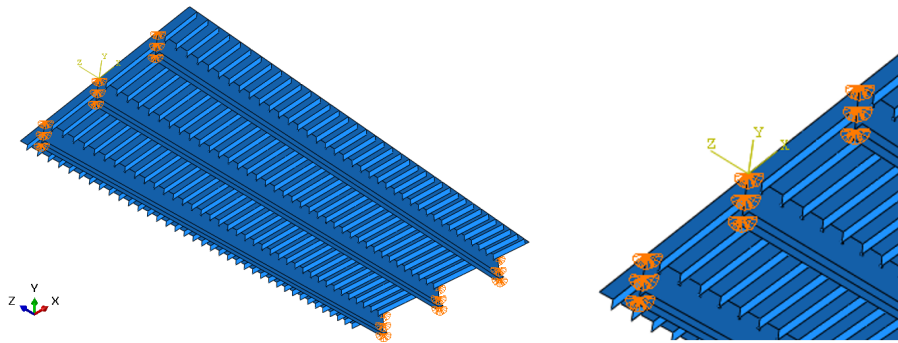


Figure 6.1: Boundary conditions of the OSD parametric model

6.4. Load cases for preliminary parametric study

Before starting the complete parametric analysis, the numerical models based on the OSD variants, are studied for some reference load cases. The loads are applied in the central region of the deck plate. The middle crossbeam and the middle stiffeners are investigated. The crossbeam ends are restrained against translation in x, y and z directions. The load cases 1, 2 and 3 are shown in Figure 6.2. For load case 3, there are two sub-load cases: load applied on the stiffener and load applied between the stiffeners which are also shown in Figure 6.2. A wheel load area of 270 mm x 320 mm (Figure 6.14). All the different load cases are to be investigated in the subsequent sections.

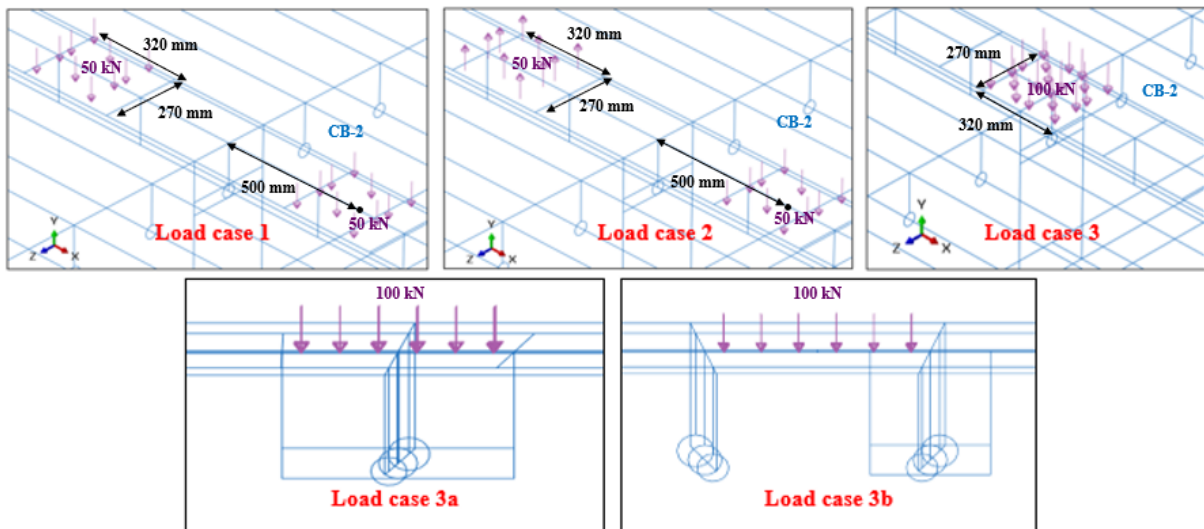


Figure 6.2: Middle crossbeam of the OSD parametric model with the three different load cases

- Load case 1: Pure in-plane behaviour of the crossbeam** - The total load applied for studying this type of behaviour is 100 kN as a tyre loading. Two patch loads (50 kN each of area 270 mm x 320 mm) are applied on the deck plate at equal distances of 500 mm from the centre of the web of CB-2. This is done to investigate pure in-plane behaviour without the effect of local loads on the crossbeam for the shell and solid models. (Figure 6.2).
- Load case 2: Pure out-of-plane behaviour of the crossbeam** -The out-of-plane behaviour is studied by applying two patch loading areas on the deck plate at equal distances of 500 mm from the centre of the web of the middle-crossbeam. However, these patch loads are not the same as for LC-1. Instead, these loads are applied in opposite directions. The effect of pure out-of-plane behaviour of the crossbeam on the shell and solid models is investigated. (Figure 6.2).
- Load case 3: In-plane behaviour of the crossbeam with local load introduction** - In a similar manner as the previous load case, a tyre loading of 100 kN (in the form of one patch area of

270 mm x 320 mm) is applied on the deck-plate right on top of the middle-crossbeam-stiffener connection. The influence of local load introduction with the in-plane behaviour is investigated for shell and solid models. Two sub load cases have been investigated under this category. These sub-load cases are also shown in (Figure 6.2).

1. **Load Case 3a:** Load applied over the deck plate right on top of the stiffener (LC3a)
2. **Load Case 3b:** Load applied over the deck plate in between two stiffeners (LC3b)

6.5. Global shell model

The global shell model of OSD variant-1 is shown in Figures 6.3 and 6.4. The dimensions of OSD are based on the existing bridges in the Netherlands and it has been summarised in Figure 6.1. The shell element model is constructed using mid-surface modelling approach. Generally these elements are used to model the middle planes of plates and the plate thickness is given as a property of the element. This is because, using this approach, it is observed that the stress gradient far away from the plate intersection for shell elements is comparable with the stress gradient from the solid element model as explained in earlier chapters for this particular detail.

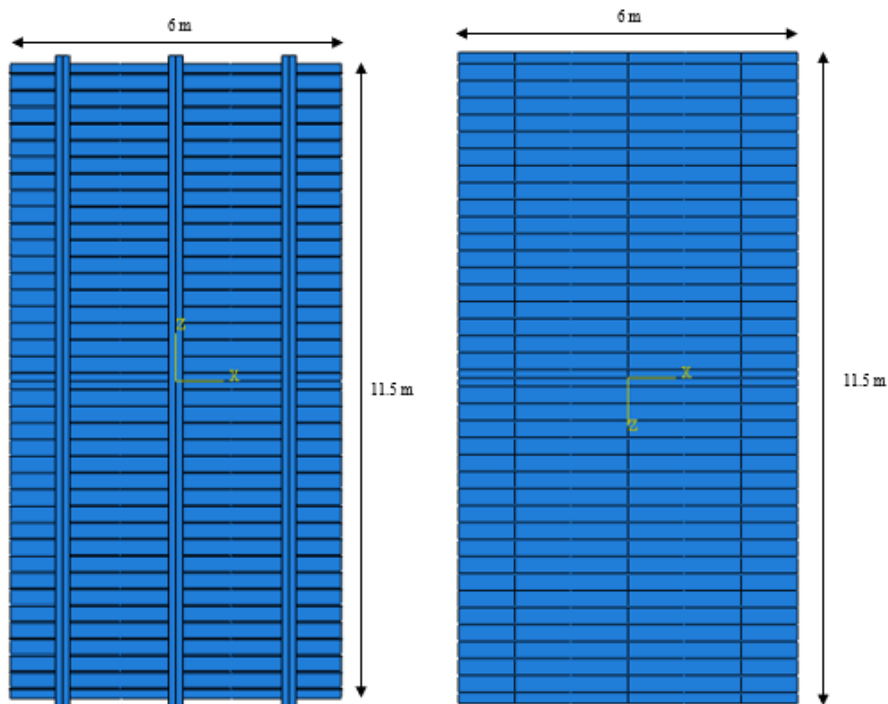


Figure 6.3: Parametric shell model of the OSD variant-1 (based on old/light OSD) - top and bottom view

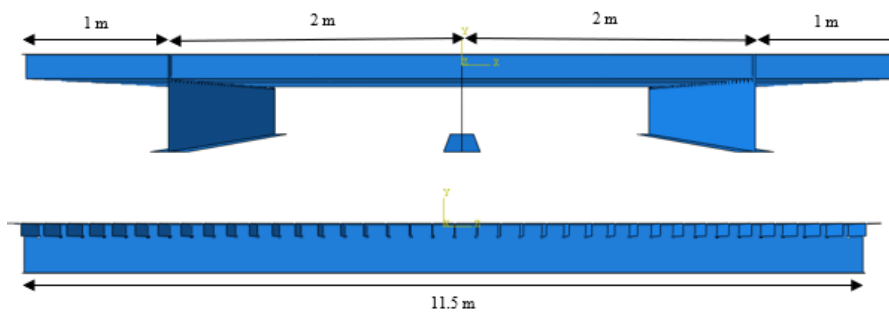


Figure 6.4: Parametric shell model of the OSD variant-1 (based on old/light OSD) - side views

6.6. Sub-solid model

The dimensions of the open stiffener of geometric variant-1 is based on the dimensions of the stiffeners in Haringvlietbrug (160 mm x 8 mm). For the variant-2, the dimensions of the stiffeners are taken a bit higher (220 mm x 10 mm). For the first geometric variant, the sub-model is made with two different sizes in order to check the effect of the interface conditions on the size of the solid sub-model as shown in Figure 6.5.

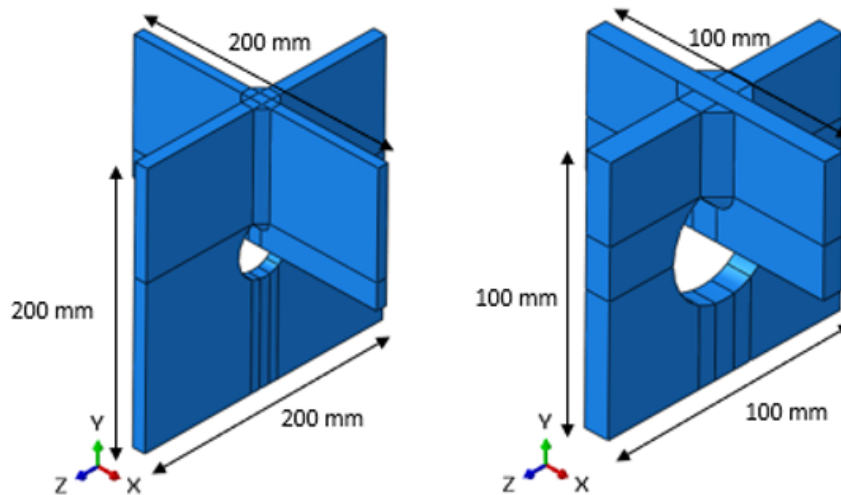


Figure 6.5: Solid sub-models for size effect study (Left: large model, Right small model)

The weld modelling with solid elements is done in a simplified approach using fillet welds. Full penetration of the welds is not considered. A full penetration weld is a type of weld that has completely consumed the root of the joint. The weld is modelled using the solid extrusion and sweep tool in ABAQUS. The corner of the welds is rounded in order to have a more realistic weld geometry. The throat thickness of the weld is 5 mm and thus the weld leg length is 7.07 mm. The stiffener is modelled to be continuous and the small gap between the crossbeam and stiffener plate is modelled using the assign seam tool. This is shown in Figure 6.6. The sub-model is attached to the global shell element model using tie-constraints. The plate edge surface of the solid sub-model is taken as the master surface. The plate mid surface of the shell model is taken as the slave surface.

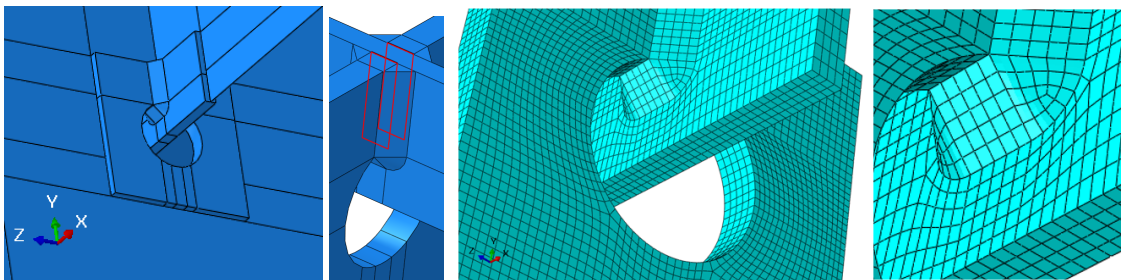


Figure 6.6: OSD parametric sub-solid model of light OSD variant and modelling of welds with solid elements

A fully structured meshing approach is used for the solid element sub-model as shown in Figure 6.6. This is achieved by the help of partitioning tool. An element size of 2 mm is recommended for the solid element sub-model after performing a mesh sensitivity study. C3D20R elements are recommended for the analyses. The mesh near the weld toe is also modelled in a structured way. It can be seen from the figure that all the elements near the weld toe are not straight and there is some bulging of elements. However, all the elements shown in the above figure and also around the cope hole are structured. The details of meshing of the global shell model of the OSD and the local meshing of the numerical models at the point of interest is shown in the next section.

6.7. Global mesh - shell

The global meshing of the OSD is shown in Figure 6.7. The global mesh size is taken as 100 mm. The mesh size below the wheels of the axle (axle type C) are taken as 10 mm.

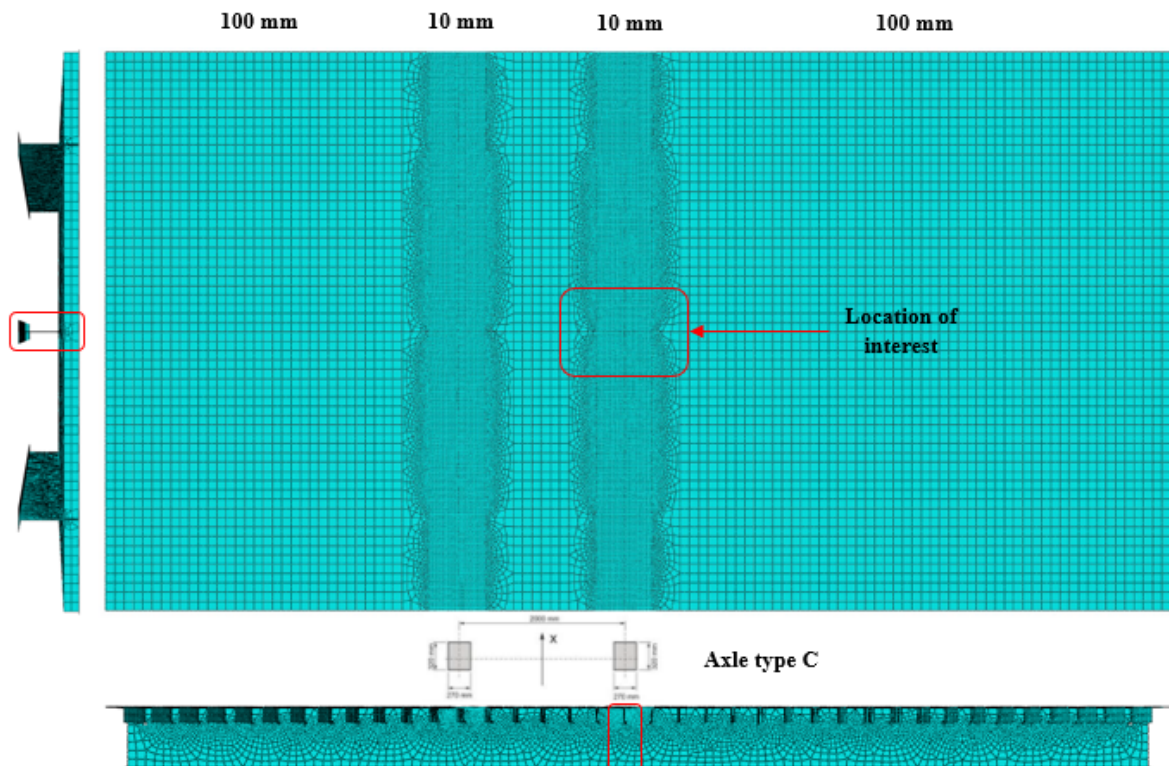


Figure 6.7: Global mesh of the OSD parameter model

6.8. Local mesh - shell and solid

The local meshing of the OSD is shown in Figure 6.8. The local mesh size is taken as 2 mm for all the numerical models after a mesh sensitivity study.

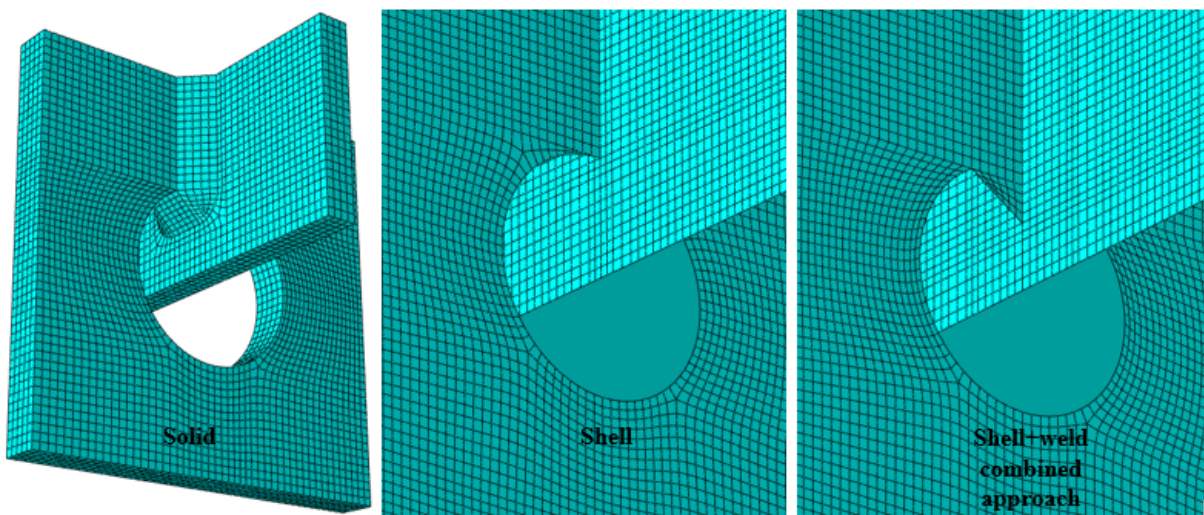


Figure 6.8: Local mesh of the OSD parameter model

Path for stress extraction: The following stress paths have been selected for stress extraction from the numerical models: stress along the crossbeam and stress along the stiffener (horizontal and vertical direction). These two stress paths are shown in Figure 6.9 for both the shell and solid element models. The origin of the stress paths for the shell element model is taken from the plate intersection. Whereas, the origin of the stress paths for the solid element model is taken as the weld toe. For the paths along stiffener, the stresses along the horizontal direction are higher than that along the vertical direction. Thus, stresses along horizontal direction are considered to be governing for the stiffener and is further investigated.

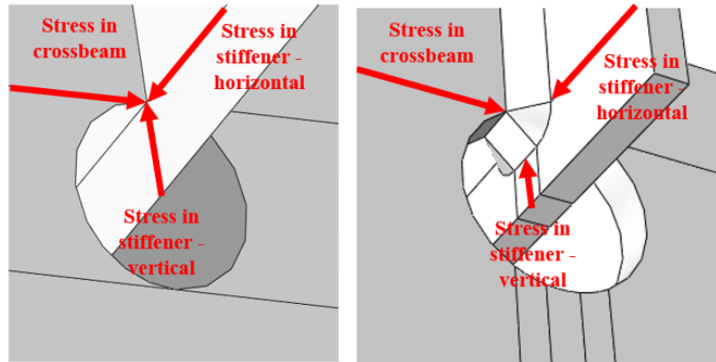


Figure 6.9: The two regions of interest based on cracks in crossbeam and cracks in stiffener

Hot-spot types: For the investigated detail, SHSS located at the weld toe of crossbeam plate is classified as type-“c” and that located at the weld toe of stiffener is classified as type-“a” according to the DNVGL [6] (Figure 6.10). However, for the crack in crossbeam, the SHSS is calculated twice, once by considering it as type-“c” and then by considering it as type-“b” hot-spot for obtaining the influence lines. A stark difference between the three types of hot-spots has been identified from Figure 6.10 and also from Chapter-2. For type-“a” hot-spot, the crack originates from the toe of the edge weld located at top surface of plate. For type-“c” hot-spot, the crack originates from the toe of the side weld located at the side surface of plate. For type-“b” hot-spot, the crack originates from the toe of the edge weld located at the edge of plate.

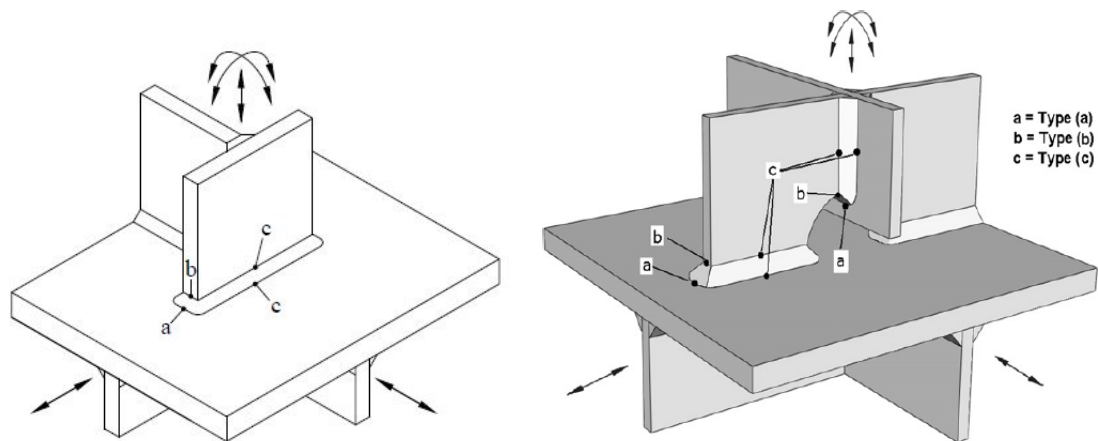


Figure 6.10: Types of hot-spots [6] [13]

The first sub-solid model is made of dimensions $200 \times 200 \times 200$ [mm³]. The second sub-solid model is developed using exactly half the size i.e. $100 \times 100 \times 100$ [mm³]. The stress perpendicular to the weld toe is plotted in the crossbeam and in the stiffener for the load cases: LC-1, LC-2 and LC-3. The SHSS is computed using the stress perpendicular to the weld toe for both the sub-solid models (small and large) as shown in Table 6.2.

It can be seen that the maximum percentage difference in SHSS values due to the size of the solid sub-model is **5%** and the average is **3%**. Since, this difference is quite small, it is decided to use the small solid sub-model $100 \times 100 \times 100$ [mm³] for further analysis, in order to save computation time. From Figures 6.11, 6.12 and 6.13, it can be seen that the difference between the stress gradients of the small and large sub-models are small.

Table 6.2: SHSS determination of the small and large solid sub-model for LC-1 and LC-2

Geometry variant	Location	Load case	Solid_C3D20R_2mm_Small	Solid_C3D20R_2mm_Large	Percentage Difference (%)
			SHSS (MPa)	SHSS (MPa)	
Variant - 1 (light variant OSD)	Crossbeam	LC1 (in-plane)	19.5	19.3	1%
		LC2 (out-of-plane)	-96.7	-93.8	3%
	Stiffener	LC1 (in-plane)	-142.7	-146.8	-3%
		LC2 (out-of-plane)	-5.1	-5.4	-5%
	Average percentage (%)				3%

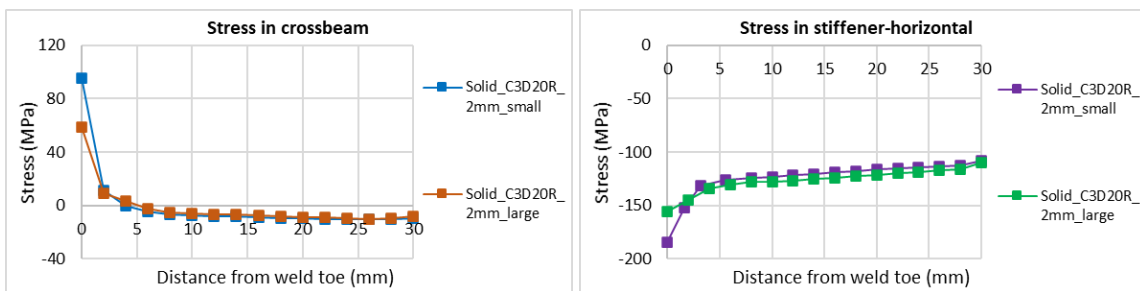


Figure 6.11: Stress distribution perpendicular to the weld toe in crossbeam (left) and stiffener (right) for LC-1

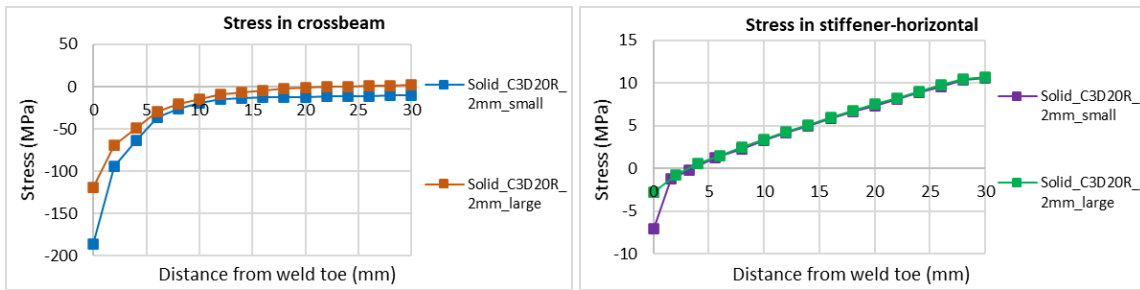


Figure 6.12: Stress distribution perpendicular to the weld toe in crossbeam (left) and stiffener (right) for LC-2

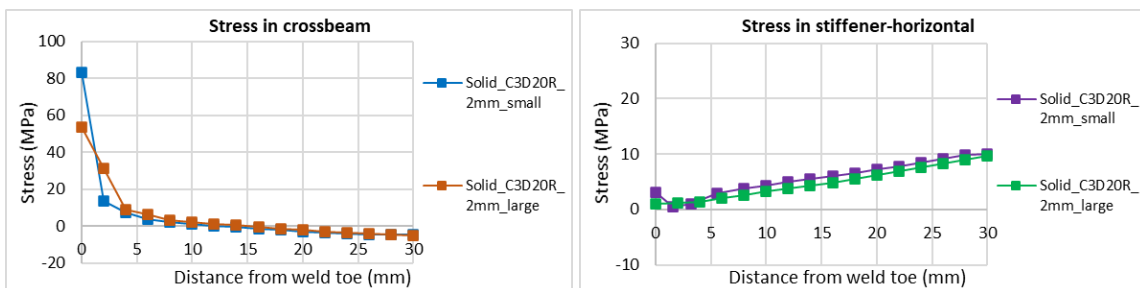


Figure 6.13: Stress distribution perpendicular to the weld toe in crossbeam (left) and stiffener (right) for LC-3a

6.9. Procedure for parametric study including influence lines

An axle load of 100 kN and axle type C is used for the main parametric study using the influence line approach. The axle type C consists of two load patches of dimension 270 mm x 320 mm which are spaced 2 m apart from each other. Both of these load patches are modelled at specific locations of the deck plate and the influence lines are obtained using the DLOAD user subroutine in ABAQUS. Two geometric variants: one based on the dimensions of the old/light OSD (variant-1) and the other based on the dimensions of the new/heavy OSD (variant-2) are considered in the analysis. The details of the axle types for fatigue load model 4 are shown in Figure 6.14 [4].

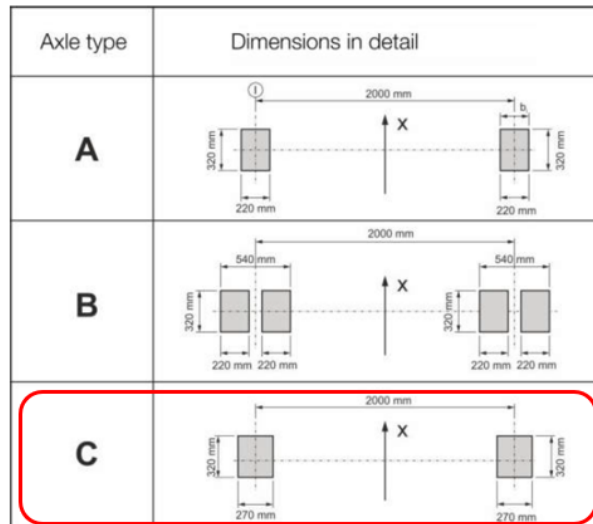


Figure 6.14: Different axle types for FLM4 [4]

User subroutine DLOAD: The subroutine DLOAD is used when a load is a complex function of time and/or position. It can be used to define the variation of the distributed load magnitude as a function of position, time, element number and load integration point number. The user has to define only the variable F in the subroutine. The following variables are passed into the subroutine:

1. KSTEP: Step number
2. KINC: Increment number
3. TIME(1): Current value of step time
4. TIME(2): Current value of total time
5. NOEL: Element number
6. NPT: Load integration point number within element or on element's surface depending on load type
7. LAYER: Layer number
8. KSPT: Section point number
9. COORDS: An array containing the coordinates of the load integration point
10. JLTYP: Identifies the load type for which this call to DLOAD is being made
11. SNAME: Surface name for a surface-based load definition

The interface of the DLOAD subroutine is shown in Figure 6.15.

```

SUBROUTINE DLOAD(F, KSTEP, KINC, TIME, NOEL, NPT,
1 LAYER, KSPT, COORDS, JLTYP, SNAME)
C
C   INCLUDE 'ABA_PARAM.INC'
C
C   DIMENSION TIME(2), COORDS(3)
C   CHARACTER*80 SNAME

user coding to define F

RETURN
END

```

Figure 6.15: DLOAD sub-routine interface

Coordinate system for DLOAD sub-routine: A local coordinate system (redraw it to make it clear) is made at the edge of deck plate which is completely aligned with the global coordinate system (Figure 6.16). The x-direction is selected as transverse direction and z-direction is selected as longitudinal direction.

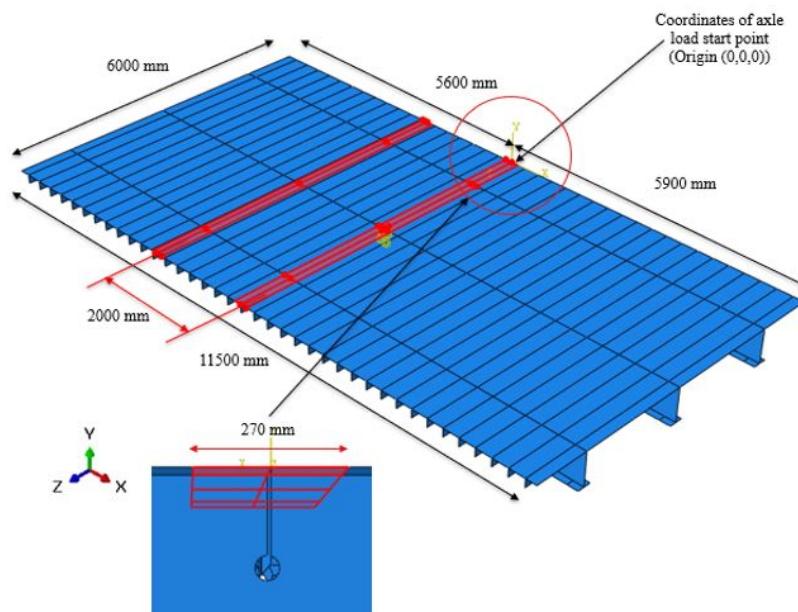


Figure 6.16: Coordinate system for the parametric study

Axle load path 1 (Load applied on top of stiffener): One of the wheel loads is placed on top of the stiffener located on the middle section of the deck plate. The axle load is moved along the longitudinal (z) direction at increments of 200 mm using the DLOAD subroutine in ABAQUS. The hot-spot stress is calculated for every load step and the influence line is drawn. From the influence line, the positions of the maximum and minimum hot-spot stress is determined.

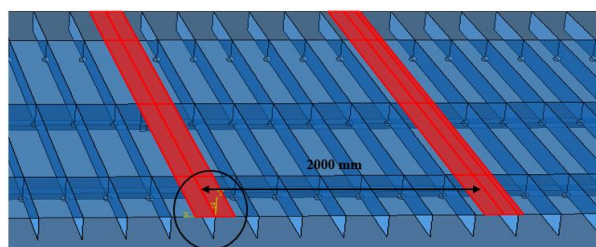


Figure 6.17: Axle load path 1 - Wheel load patch on top of one of the middle stiffeners

Axle load path 2 (Load applied in between two stiffeners): The wheel load patch is shifted by 150 mm in the transverse (x) direction, in order to have the load patch placed directly in between the two stiffeners located on the middle section of the deck plate. In the same manner as the previous case, axle load is moved along the longitudinal (x) direction at increments of 200 mm using the DLOAD subroutine in ABAQUS. The hot-spot stress is calculated for every load step and the influence line is drawn. From the influence line, the positions of the maximum and minimum hot-spot stress is determined.

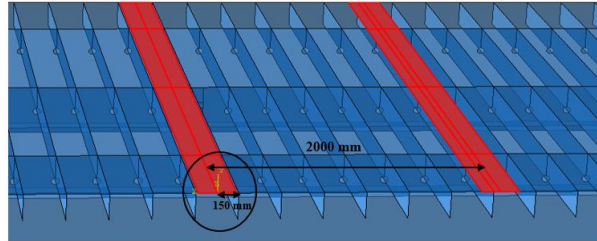


Figure 6.18: Axle load path 2 (Load applied in between two stiffeners)

Axle load path 3 (Load applied in between path 1 and 2): For this load path, the wheel load is placed in between axle load path 1 and axle load path 2. In a similar way, the SHSS is calculated and the positions of the maximum and minimum hot-spot stress is determined. All the three transverse axle load paths are placed at a spacing of 75 mm away from each other.

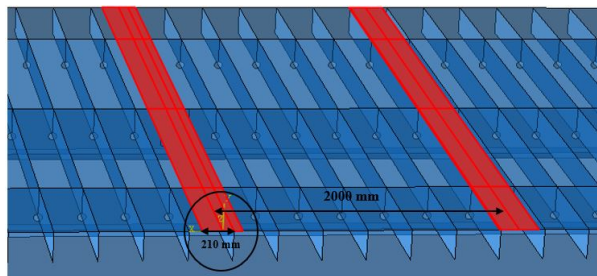


Figure 6.19: Axle load path 3 (Load applied in between path 1 and 2)

After determining the locations of the maximum and minimum hot-spot stress from the influence lines, the axle loads are applied manually on top of the critical locations. A recalculation of the hot-spot stress is performed on the investigated detail for these critical locations. This is because manual placing of the axle loads give better accuracy compared to the DLOAD subroutine in ABAQUS. Both the light and heavy OSD variants are considered in the analysis. For the detail which is investigated, the stress perpendicular to the weld toe is chosen for the determination of hot-spot stress with shell and solid elements. However, the hot-spot stress values are also determined using the maximum principal stress and is shown in Appendix-H.

6.10. Weld modelling with shell elements for the OSD

The recommendations from Chapter-5 for weld modelling with shell elements are followed for the detail in OSD.

- **Weld modelling approach using increased thickness method as recommended by IIW [28]:** The first approach for weld modelling with shell elements is performed by locally increasing the thickness at the plate intersection and having downward sloping ends (weld fillet) as per the IIW recommendations [28]. This method has been discussed in detail in Chapter-2. In this approach, the thickness of one of the two connected plates is increased at the welded connection. The two governing parameters in this approach are the weld leg length (l) and the thickness of the connected plate (t). The investigated detail after applying this weld modelling strategy with shell elements is shown in Figure 6.20. The throat thickness of the weld at the joint is (a) and thus the weld leg length (l) = $a\sqrt{2}$. Since, the shell model is developed using mid-plane geometry, the

height of the weld plate strip is equal to the weld leg length (l) plus half of the thickness of the stiffener ($t_s/2$). The weld is modelled using an inclined plate extended from the crossbeam having a thickness increased by the weld leg length (l). Thus, the increased value of plate thickness = ($t_p + l$), where t_p is the thickness of the crossbeam and l is the weld leg length. The origin of stress extraction of the shell model without welds is chosen from the intersection of mid-planes of the plates as recommended by IIW guidelines. The origin of stress extraction of the solid model is taken at the weld toe. Due to the inclusion of welds, the starting point or origin of stress extraction (weld toe), are now the same for both the solid element model and the shell model with welds. This resulted in a better comparison between the numerical models.

- **Weld modelling approach using increased thickness method as recommended by Niemi [39] and Eriksson [20]:** The second approach (Figure 6.20 [20]) for weld modelling with shell elements is performed by locally increasing the thickness at the plate intersection without any downward sloping end. Niemi [39] and Eriksson [20] proposed this modelling technique where the stiffness of the weld is simulated without representing the weld fillet (downward sloping ends). The role of the weld is played by the shell elements having an incremented thickness along the welded region. In this approach, the thickness of both plates is increased at the welded connection. The two governing parameters in this approach of weld modelling are the weld throat thickness (a) and the thickness of the connected plates (t). The investigated detail after applying this weld modelling strategy with shell elements is shown in Figure 6.20.
- In addition to the above two approaches of weld modelling with shell elements using increased thickness method, a combination of the two approaches is also investigated. This combined approach is also shown in Figure 6.20. Another new approach of weld modelling with shell elements having increased thickness has been investigated for the OSD as an additional study in Appendix-K.

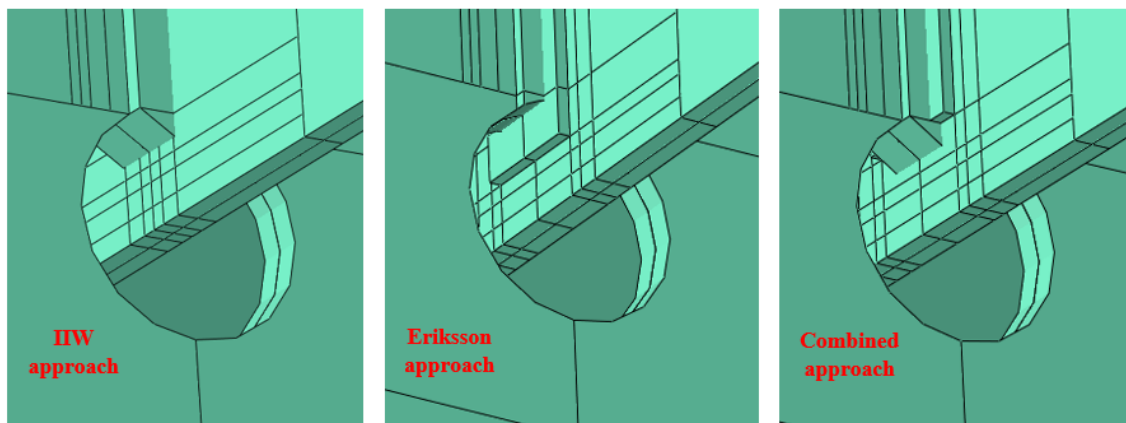


Figure 6.20: Rendered shell models with welds modelled using the increased thickness method for the OSD

6.11. Mesh sensitivity study of the OSD variants

The mesh sensitivity study of OSD is performed with both shell and solid elements, the details of which are given in Appendix-D.

Shell elements: A mesh sensitivity study with shell elements is performed to find the most suitable mesh size for analysis. This mesh size is selected based on a local mesh refinement at the region of interest followed by using elements of decreasing order of sizes: 8 mm, 4 mm, 2 mm and 1 mm, respectively. Quadratic shell elements with reduced integration (S8R) are used in the numerical analysis. The details of the load case for studying this behaviour of the crossbeam is given in earlier sections. The figures in Appendix-D, show the mesh sensitivity study of the two regions of interest with shell elements for both the geometrical variants. The stress profiles using quadratic shell elements converge below a mesh size of 2 mm for both along the stiffener and along the crossbeam directions. Convergence

is observed in the stress profiles at all regions except at the plate intersection due to singularity. After investigating a range of mesh sizes with shell elements, from coarse to fine, it is decided to use an element size of 2 mm for determination of SHSS for all the above mentioned load cases.

Solid elements: In the same way as for shell elements, a mesh sensitivity analysis is also performed using solid elements to find an appropriate element size for analysis. The element size is selected based on a local mesh refinement at the region of interest followed by using elements of decreasing order of sizes: 8 mm, 4 mm, 2 mm and 1 mm, respectively. Quadratic solid elements having 20 nodes with reduced integration (C3D20R) are used in the numerical analysis. The figures in Appendix-D, show the mesh sensitivity study of the two regions of interest with solid elements for the geometrical variants. From the figures it can be observed that the stress profiles using quadratic solid elements converge below a mesh size of 2 mm for both along the stiffener and along the crossbeam directions. After investigating a range of mesh sizes for solid elements, from coarse to fine, it is decided to use an element size of 2 mm for determination of SHSS for all the load cases.

6.12. Multi-axial stress state in fatigue assessment

The structural hot-spot stress (SHSS) method can be applied for the following two cases: (i) when the nominal stress is not clearly defined, (ii) when the connection differs from the detail categories provided by the design codes for fatigue calculations based on nominal stress. Multi-axial fatigue occurs when two or more stress components act in a detail. The stress components may be dependent or independent of each other depending on geometry and loading. The problems encountered when using the hot-spot method for multi-axial loaded specimens arise from the way of determining the stresses at weld toe from finite element models. When the stress state is bi-axial, the actual stress might be up-to **10%** higher than that obtained from the uni-axial stress condition.

Different authors of the IIW guidelines propose different ways of calculation of the SHSS in uni-axial and multi-axial stress state. A. Hobbacher [28] recommends using maximum principal stress for calculating the SHSS in uni-axial stress condition. According to A. Hobbacher [40], if the principal stress acts predominantly perpendicular to the weld toe or within an angle less than $\pm 60^\circ$ from the line perpendicular to the weld, then the SHSS value is taken to be equal to the maximum principal stress for a bi-axial stress state at the plate surface. This is explained in Figure 6.21 [40]. If the direction of the maximum principal stress is outside the above range which is more than 60° , the SHSS value is taken as the stress component normal to weld toe or the minimum principal stress whichever shows the largest range. When the directions of principal stress changes during a load cycle, the partial fatigue load factor (γ_{Ff}) should be increased [40]

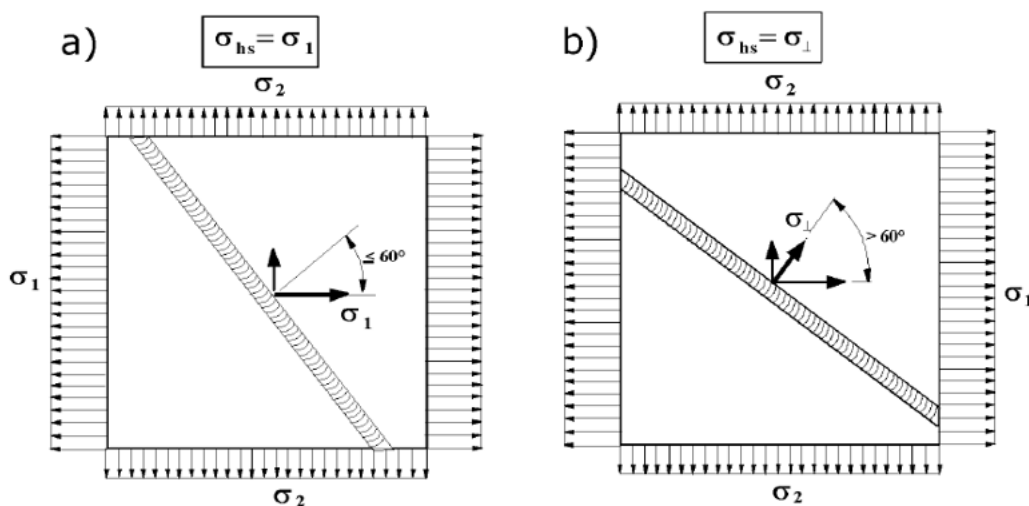


Figure 6.21: Definition of the stress component used as SHSS when both principal stresses are tensile (bi-axial) [40]

On the contrary, E. Niemi [38] suggested that the stress perpendicular to weld toe is more suitable for determination of the SHSS in welded details based on the type of loading for multi-axial stress state. Fatigue design data have been generally obtained under unidirectional axial or bending loads. However, it is common for details in real structures to experience more complex loading conditions, notably by bi-axial or by combined loading for example bending and torsion.

For the two reference load cases LC-1 (in-plane loading) and LC-2 (out-of-plane loading), the angle of the maximum principal stress with the line perpendicular to the weld toe is found manually from the solid models. This is shown in Figure 6.22 and 6.23.

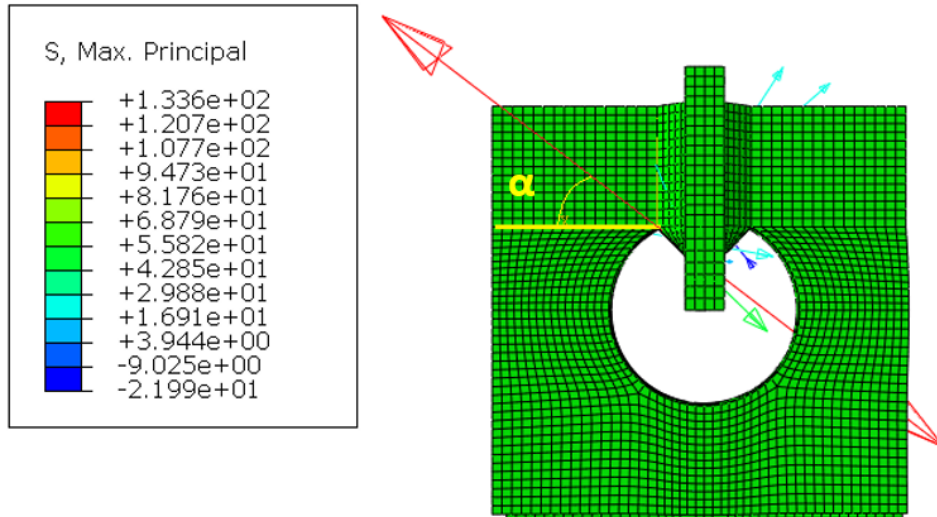


Figure 6.22: Direction of maximum principal stress w.r.t the line perpendicular to weld toe in crossbeam for LC-1

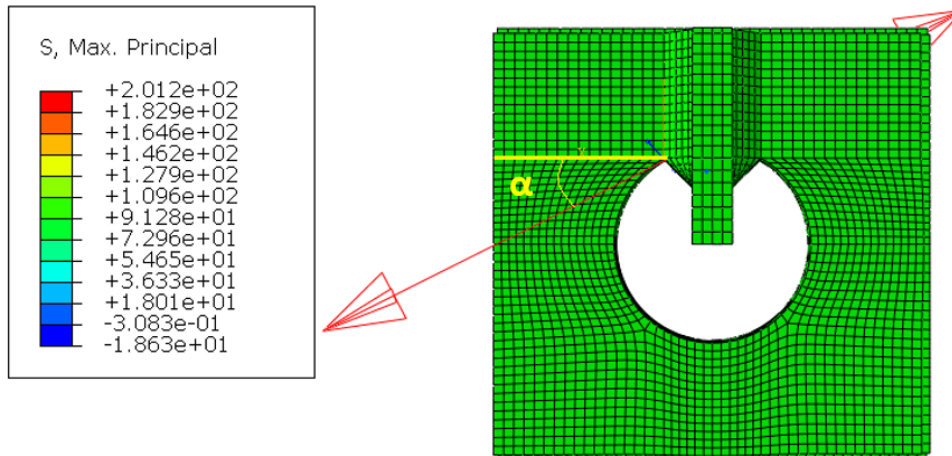


Figure 6.23: Direction of maximum principal stress w.r.t the line perpendicular to weld toe in crossbeam for LC-2

The principal direction is at an angle α from the line perpendicular to the weld toe. The value of angle α is 40° (approximately) for LC-1 and 30° (approximately) for LC-2. Thus, it is found that the direction of the principal stress is depending on the load case and the angle varied for different load cases. Different approaches are found from different guidelines. For example, in EN 1993-1-9 [2] there are S-N curves which should be used for hot-spot stresses. All these S-N curves assume stress perpendicular to weld.

6.13. Numerical analysis of OSD

In a similar procedure as for the simple details from Chapter-3, a global shell model is developed as the first variant for the parametric study. This is based on the dimensions of the light variant OSD. After that, a sub-model is made using solid elements at the connection of the stiffener and crossbeam with the presence of a cope hole. Two types of cracks are investigated in the detail: cracks in crossbeam and cracks in longitudinal stiffener. Similar procedure is then applied for the heavy OSD variant.

In the first step, the stresses at a distance far away from the load positions in the global shell model is investigated in order to see if the global geometry is an appropriate representation of an actual bridge. In the next step, a preliminary parametric study is performed on the OSD. The geometric variants are investigated for four standard load cases as shown in Figure 6.2. After a mesh sensitivity study, an appropriate mesh size is selected for the shell and solid element models which is 2 mm. C3D20R elements are recommended for the solid element sub-model and S8R elements are recommended for the global shell model. The stress profiles of the stress perpendicular to the weld toe is plotted for all the load cases. In the final step, a detailed parametric study is performed where the hot-spot stress influence lines are plotted for three transverse axle load positions on OSD. The critical locations are determined from the influence lines. The stress profiles of the stress perpendicular to the weld toe is shown for all the critical locations. In both studies, the structural hot-spot stress is calculated based on the stress perpendicular to weld toe. The SHSS is also calculated using the maximum principal stress in Appendix-H, where the stress distribution is also shown .

6.13.1. Nominal stress determination using three axle loads (six load patches)

The nominal stress is defined as the far-field stress as stated in Chapter-2. For the determination of nominal stress, the OSD variant-1 and OSD variant-2 from Table 6.1 are subjected to loading from truck type-3 (FLM-4), according to the Eurocode 1 (EN 1991-2) [4] as shown in Figure 6.24. The rear axles of the truck type-3 are used in the study. Three axle loads of 90 kN each and axle type C are chosen to have a realistic load on the deck plate. For getting an idea about the nominal stress, the stress at a distance of 1 m away from the wheel load are shown for both the light and heavy geometric variants of OSD in Figure 6.24.

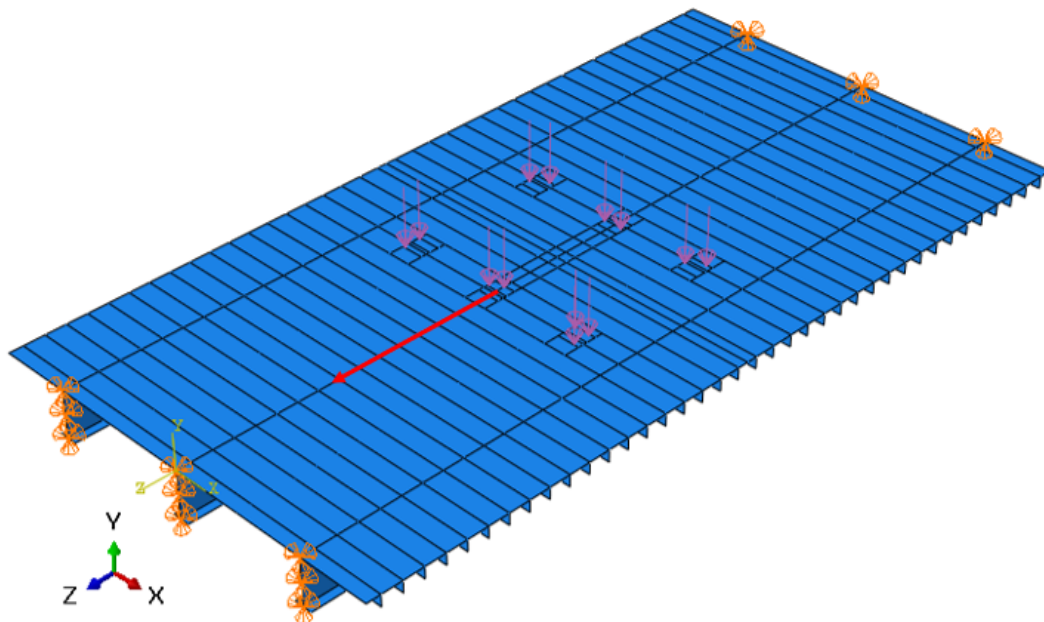


Figure 6.24: The three axles of type C having an axle load of 90 kN each

The stress profiles are also shown in Figure 6.25 and the deformations are shown in Figure 6.26. Table 6.3 shows the stress at the top and bottom of crossbeam at a distance of 1 m away from the wheel load location. The maximum vertical deformation is also shown in Table 6.3.

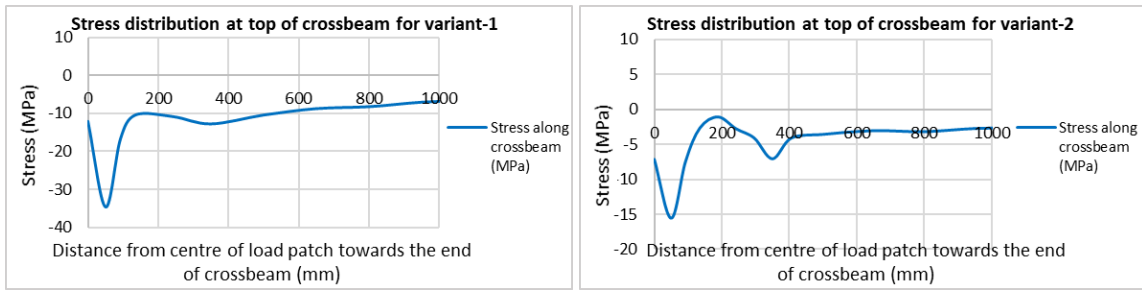


Figure 6.25: Stress distribution at top of crossbeam (deck plate)

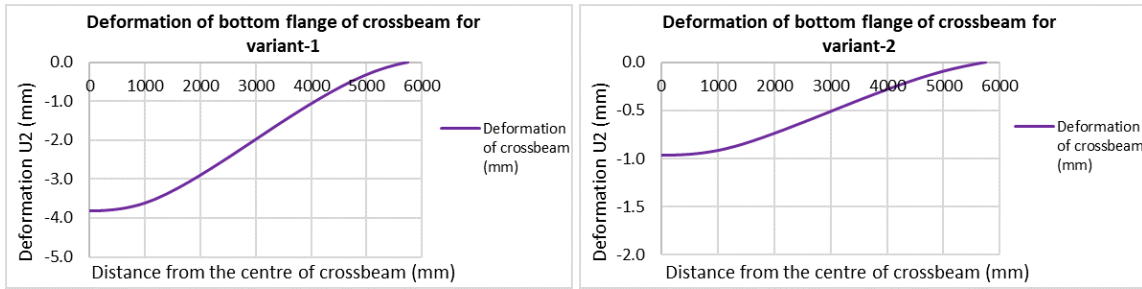


Figure 6.26: Deformation of bottom flange of crossbeam

Table 6.3: Summary of nominal stress results for both the light and heavy OSD variants

Load : 3 axle loads of 90 kN each			
Geometry Variants	Stress at 1 m from wheel load at top of crossbeam (deck plate) (MPa)	Stress at 1 m from wheel load at bottom of crossbeam (bottom flange) (MPa)	Deformation (mm)
Variant 1 (light OSD variant)	-8	45	3.8
Variant 2 (heavy OSD variant)	-3	14	1.0

It can be assumed that the stress at 1 m away from the load location is the nominal stress. The heavy variant of OSD showed lower value of nominal stress (14 MPa) compared to the light variant of OSD (45 MPa) at the bottom flange of the crossbeam. This is because the depth of crossbeam for the old geometric variant is 650 mm and that of the new geometric variant is 1000 mm. Another reason for the decrease in nominal stress in the new variant is that the plate thickness of components of the new variant are more than that of the old variant (according to Figure 6.1). From the stress values at 1 m away from the bottom of the wheel load, it is concluded that the dimensions of the light and heavy OSD variants are such that it gave logical values of stress far away from the investigated detail.

6.13.2. Preliminary parametric study on OSD

Load case 1: Pure in-plane bending of the crossbeam - The stress distribution perpendicular to the weld toe is investigated under LC-1 for all the numerical models of both the OSD variants. Figure 6.27 shows the stress distribution in the crossbeam and stiffeners for the numerical models subjected to load case LC-1. The stress gradient in the crossbeam for shell model with welds is found to be similar to that of the solid model. The nominal stress values are almost same for the shell and solid models in the horizontal stiffener direction.

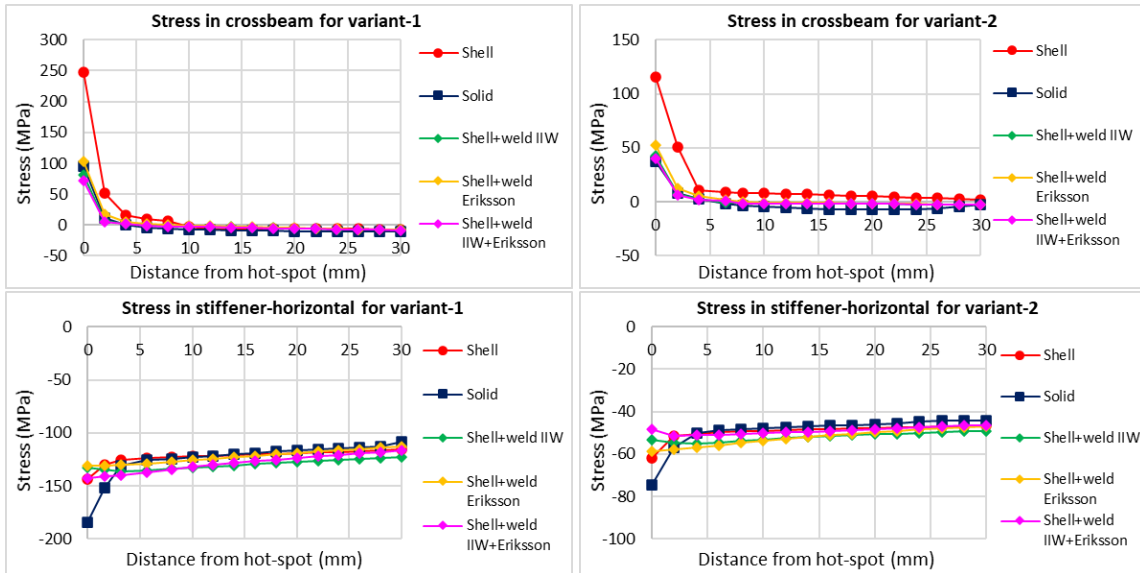


Figure 6.27: Stress distribution perpendicular to weld toe under LC-1

Load case 2: Pure out-of-plane bending of the crossbeam - Here again, the stress distribution perpendicular to the weld toe is investigated under LC-2 for all the numerical models for both the OSD variants. The appropriate mesh size of 2 mm is selected after a mesh sensitivity study, for both the shell and solid element models. Figure 6.28 shows the stress distribution in the crossbeam and stiffener for the numerical models subjected to load case LC-2.

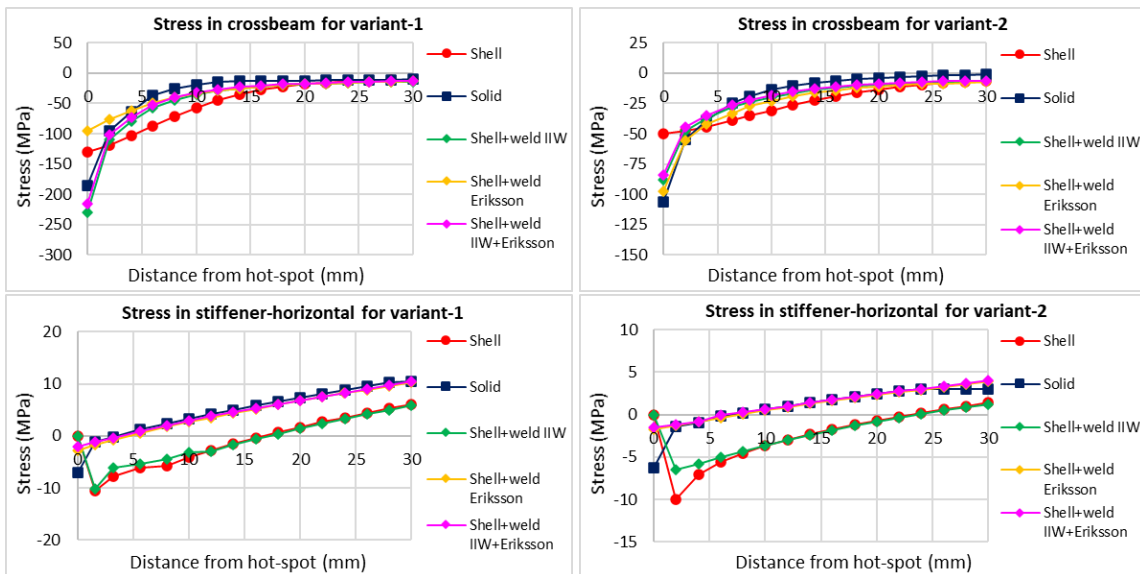


Figure 6.28: Stress distribution perpendicular to weld toe under LC-2

Load case 3: Pure in-plane bending of the crossbeam with local load introduction - The stress perpendicular to the weld toe is investigated for load cases LC-3a and LC-3b (as shown in Figure 1). The appropriate mesh size is selected after a mesh sensitivity study, for both the shell and solid element models. Figures 6.29 and 6.30 shows the stress distribution of the numerical models for load cases: LC-3a and LC-3b.

Load directly on top of the stiffener (LC3a): It is observed that just like for load case LC-1, the stress gradient of shell model with welds is same as that of the solid model in the crossbeam.

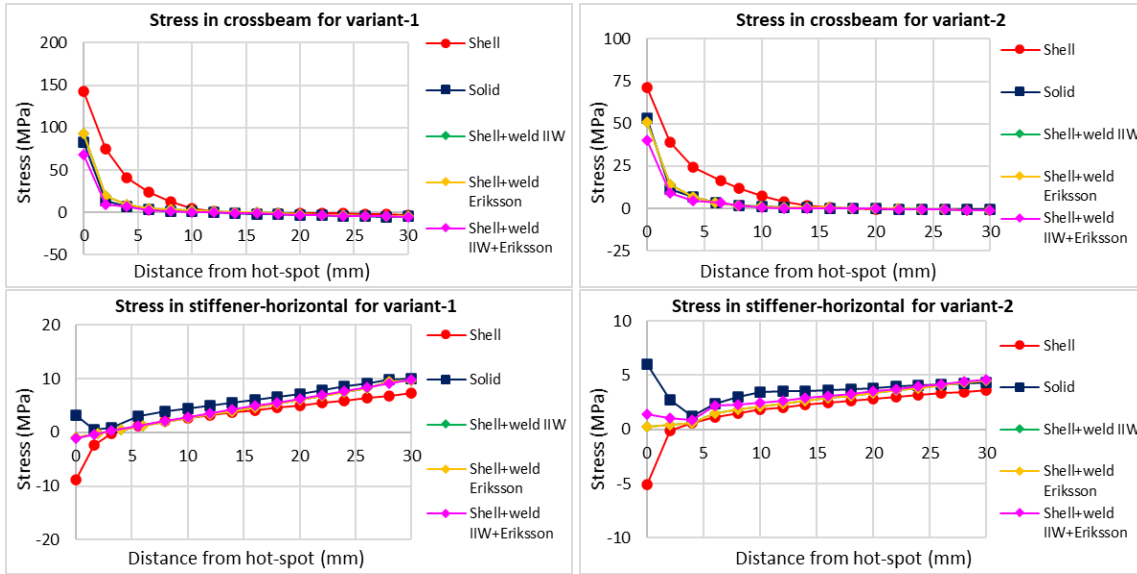


Figure 6.29: Stress distribution perpendicular to weld toe under LC-3a

Load in between the stiffeners (LC3b): It is observed that in this load case also the stress gradient of shell model with welds is same as that of the solid model for the crossbeam (just like LC-1 and LC-3a).

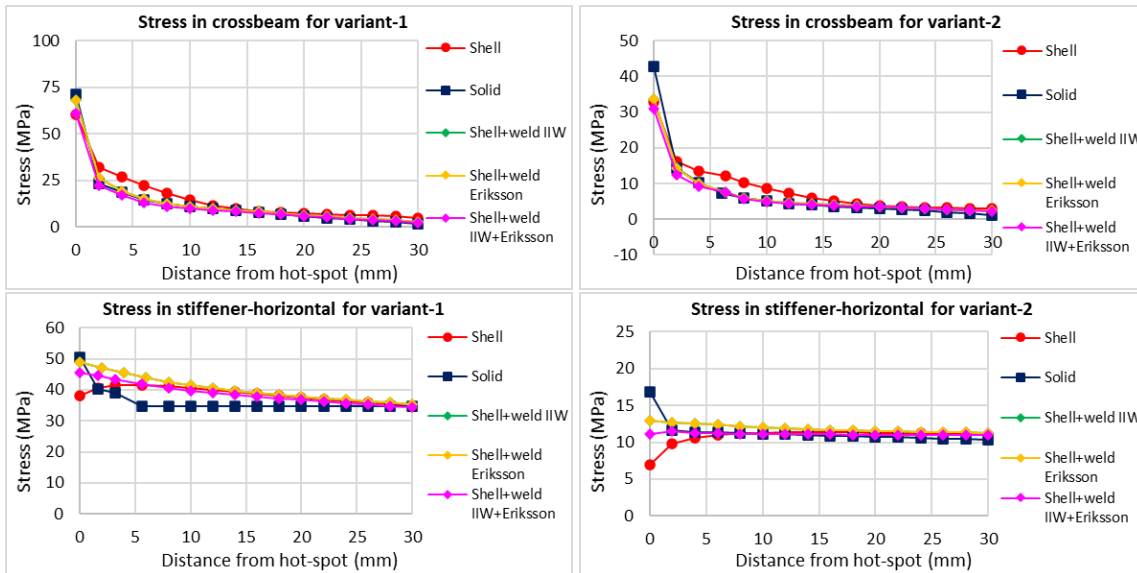


Figure 6.30: Stress distribution perpendicular to weld toe under LC-3b

The structural hot-spot stress (SHSS) values are calculated for all the above load cases and for the five different numerical models of the light and heavy variant (variant 1 and 2). The stress perpendicular to the weld toe is used in the computation of SHSS. The ratio of the SHSS of shell to that of solid is also

calculated. However, this ratio is not consistent for the different load cases. Moreover, modelling the welds with shell elements also changed the ratio of SHSS for different load cases. The SHSS results are summarised in Table 6.4.

Table 6.4: Summary of SHSS results of a preliminary parametric investigation with four load cases

Geometry variant	Location	Load case	Solid	Shell	Shell+weld IIW	Shell+weld Eriksson	Shell+weld IIW+Eriksson	Ratio			
			SHSS (MPa)	SHSS (MPa)	SHSS (MPa)	SHSS (MPa)	SHSS (MPa)	Ratio SHSS shell/solid	Ratio SHSS shell+weld IIW/solid	Ratio SHSS shell+weld Eriksson/solid	Ratio SHSS shell+weld IIW+Eriksson/solid
Variant - 1 (light variant OSD)	Crossbeam	LC1	5.2	27.1	5.6	8.0	5.3	5.25	1.09	1.54	1.03
		LC2	-93.7	-134.7	-109.0	-80.2	-100.8	1.44	1.16	0.86	1.08
		LC3a	11.9	65.6	9.6	13.4	11.1	5.51	0.80	1.13	0.94
	Stiffener - horizontal	LC3b	23.6	34.8	23.4	24.7	21.6	1.48	0.99	1.05	0.91
		LC1	-135.6	-127.9	-137.4	-132.1	-143.2	0.94	1.01	0.97	1.06
		LC2	-1.9	-9.0	-7.1	-2.5	-1.9	4.82	3.83	1.32	1.02
		LC3a	-1.0	-1.6	-4.7	-0.5	-1.0	1.65	4.76	0.49	1.04
		LC3b	41.9	41.8	41.1	47.4	45.3	1.00	0.98	1.13	1.08
		LC1	2.0	11.0	0.4	3.5	2.3	5.39	0.20	1.73	1.11
Variant - 2 (heavy variant OSD)	Crossbeam	LC2	-36.6	-51.9	-39.0	-46.9	-36.6	1.42	1.07	1.28	1.00
		LC3a	5.5	26.8	4.3	5.7	5.9	4.85	0.78	1.04	1.08
		LC3b	9.9	16.8	9.8	9.9	10.1	1.69	0.99	0.99	1.02
	Stiffener - horizontal	LC1	-51.9	-51.7	-56.3	-58.9	-51.8	1.00	1.09	1.14	1.00
		LC2	-2.0	-9.3	-7.3	-1.7	-1.9	4.53	3.55	0.82	0.92
		LC3a	-0.2	-0.2	-0.4	-0.4	-0.2	0.84	2.10	2.02	0.97
		LC3b	11.6	10.1	9.9	12.9	11.4	0.87	0.86	1.11	0.98

From the table, it can be seen that the SHSS ratio of shell/solid has a big range of **1.42-5.51** for the crossbeam and **0.84-4.82** for the stiffener. This amount of deviation in both variants for standard load cases is not acceptable. The maximum difference in hot-spot stress between shell and solid model in crossbeam is 53.7 MPa. This is observed for LC-3a in variant-1 where the SHSS of solid model is 11.9 MPa. The maximum difference in hot-spot stress between shell and solid model in stiffener is 7.7 MPa. This is observed for LC-1 in variant-1 where the SHSS of the solid model is -135.6 MPa. These differences are huge and cannot be accepted. Thus, the regular shell model cannot be used to determine SHSS for the investigated detail. After using the combined weld modelling approach, the SHSS ratio is within a range of **0.91-1.08** for the crossbeam and **0.92-1.08** for the stiffener. Also, the differences between the SHSS of solid model and the shell+weld model using the combined approach is less and is thus considered acceptable. The SHSS values of the heavy OSD variant are lower than that of the light OSD variant for all the investigated load cases. This is due to the effect of thickness of the heavy variant which reduces the stress concentrations (Figure 6.1). Initially a large difference is observed between the SHSS of shell and solid. After modelling welds with shell elements, the difference in SHSS reduced. For the crack in crossbeam, the shell+weld combined IIW+Eriksson model gives a mean value of SHSS ratio is **1.02** and the CV is **6.8%**. For the crack in stiffener, the shell+weld combined IIW+Eriksson model gives a mean value of SHSS ratio is **1.01** and the CV is **5.1%**.

Study on through thickness in crossbeam: The main difference between type-“c” and type-“b” hot-spot types lies in the stress distribution through the thickness of the plate with anticipated cracking. While the stress in type-“c” hot-spots varies substantially through the thickness of the cracked plate, it is more uniform in type-“b” hot-spots. The selected paths for stress extraction is shown in (Figure 6.32).

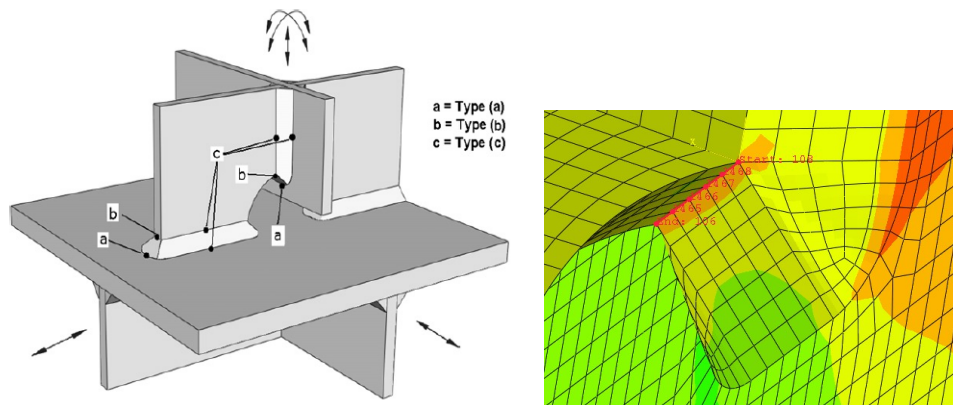


Figure 6.31: Study on through thickness in crossbeam

The stresses are extracted through the thickness of the crossbeam as shown in Figure 6.31 for the critical points of maximum hot-spot stress for the 3 transverse axle load positions. From the above figures, it is concluded that since the stress distribution through the thickness is non-uniform, the recommended hot-spot type for the crossbeam would be type-”c”. However, the SHSS calculation for influence lines is done using both hot-spot types type-”b” and type-”c” for the sake of comparison.

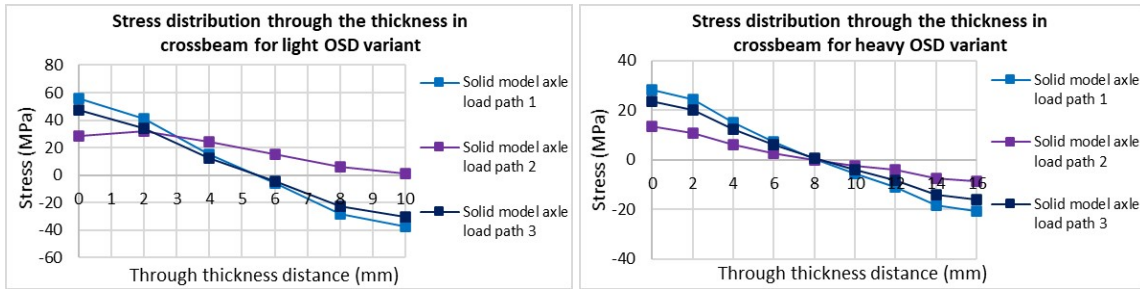


Figure 6.32: Stress distribution through the thickness of crossbeam for both OSD variants

Study on different paths in crossbeam above the cope hole: Two different paths one at 10 mm and other at 20 mm above the cope hole are selected for the reference load LC-1 (Figure 6.33) in variant-1.

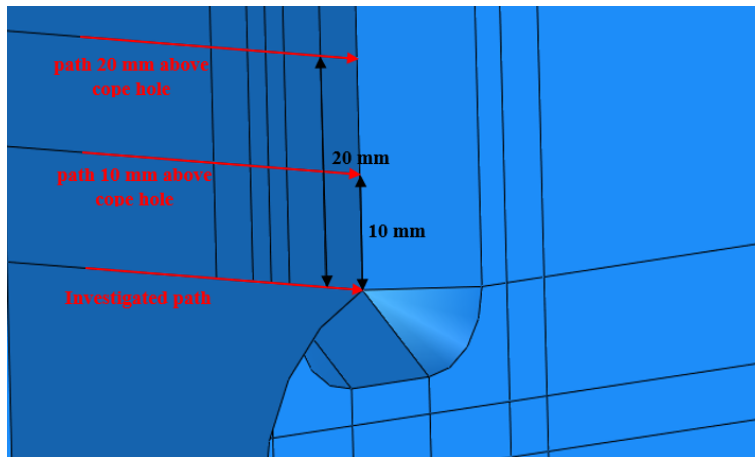


Figure 6.33: Study on different paths in crossbeam above cope hole for LC-1

Stresses from two additional paths were studied in order to make sure that the critical location is at the investigated path. The critical location may not always be at the investigated path. The stress distribution perpendicular to the weld toe for all the numerical models is plotted for the crossbeam as shown in Figure 6.34.

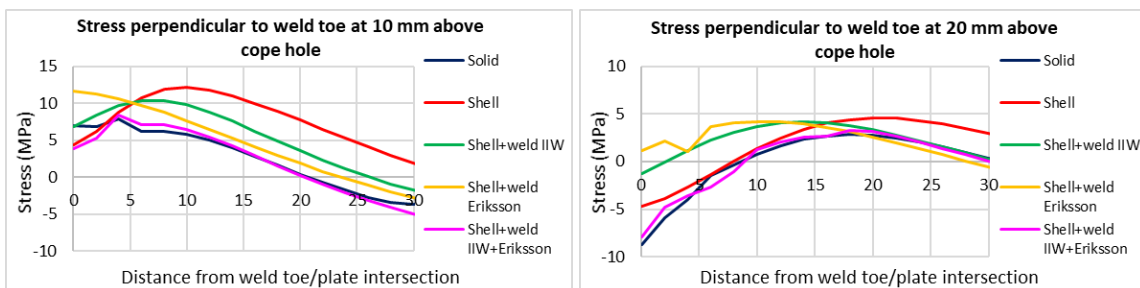


Figure 6.34: Stress distribution perpendicular to weld toe under LC-1 (in-plane loading)

6.13.3. Main parametric study (Influence lines of SHSS for light OSD variant)

In this section, the SHSS influence lines are plotted, and the critical points are determined for the 3 transverse axle load paths as mentioned in Figures 6.17, 6.18 and 6.19. These three load paths have a spacing of 75 mm from each other in the transverse (x) direction. The origin of the influence lines is taken at the second crossbeam. The right side of the influence line from origin is taken as positive part and the left side is taken as negative part of the influence line diagram. The hot-spot stress influence lines for both the crossbeam and the stiffener are plotted over the deck plate starting from the first crossbeam ($z = -2000$ mm) to the third crossbeam ($z = +2000$ mm).

Axle load path 1 (Load applied on top of stiffener): Figure 6.35 and Figure 6.36 show the SHSS influence lines of variant 1 and for axle load path 1 in crossbeam where the hot-spot stress is calculated using type-“c” and type-“b” calculation procedure as mentioned in section 6. The SHSS of all the six different models are shown.

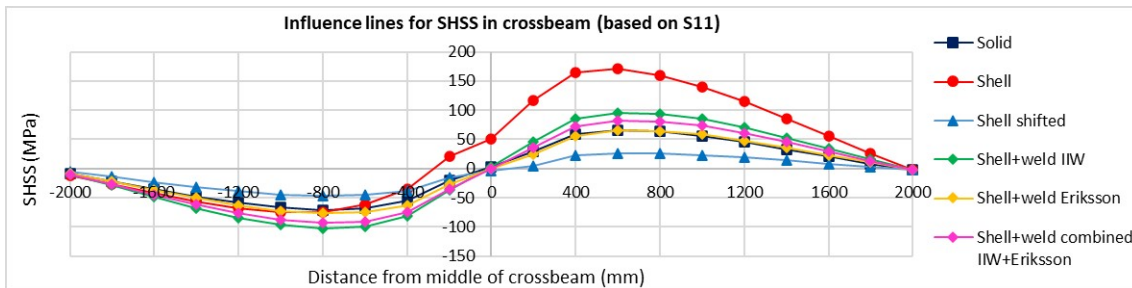


Figure 6.35: SHSS influence lines of crossbeam for variant 1 (old OSD) and axle load path 1 based on type-c calculation

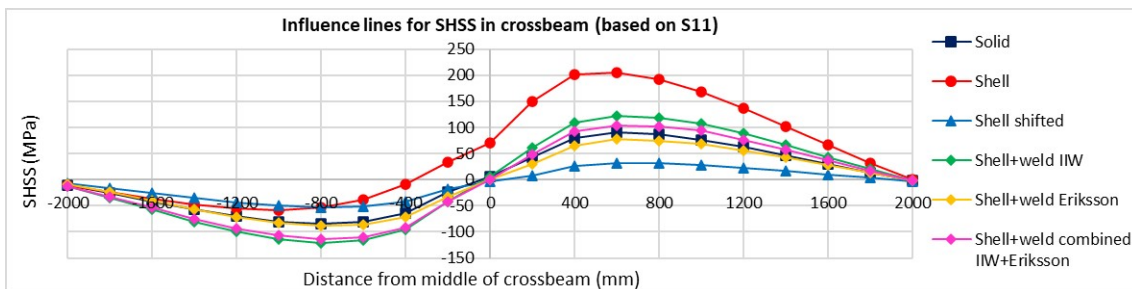


Figure 6.36: SHSS influence lines of crossbeam for variant 1 (old OSD) and axle load path 1 based on type-b calculation

The SHSS influence lines from the above figures clearly show that the classification of hot-spot type is very important for a detail under investigation. The hot-spot stress obtained from type-“b” calculation are higher than that obtained from type-“c” calculation.

From the SHSS influence lines of **crossbeam**, it is observed that there is a huge difference in SHSS between the shell and solid models (Figure 6.35 and Figure 6.36). This gap is reduced when the welds are modelled using the Eriksson’s approach [20] by increasing the thickness of the shell elements at the weld region. The maximum and minimum value of hot-spot stress from the solid model influence line is observed at $z = +600$ mm and $z = -800$ mm respectively from the middle crossbeam (Table 6.5).

For the **stiffener**, the investigated hot-spot is of type-“a”. Thus, the influence lines for stress in the horizontal direction along the stiffener is selected for determination of the critical locations of the OSD. Figure 6.37 shows the SHSS influence lines of variant 1 and for axle load path 1 for stiffener. The maximum and minimum value of hot-spot stress from the solid model influence line is observed at $z = 0$ mm and $z = -800$ mm respectively from the middle crossbeam (Table 6.5).

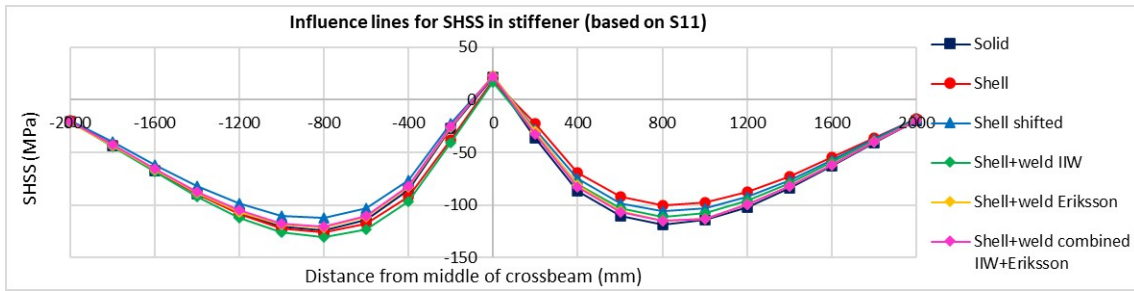


Figure 6.37: SHSS influence lines of stiffener for variant 1 (old OSD) and axle load path 1 based on type-a calculation

Axle load path 2 (Load applied in between two stiffeners): Just like for axle load path 1, Figure 6.38 and 6.39 show the SHSS influence lines of variant 1 and for axle load path 2 for crossbeam.

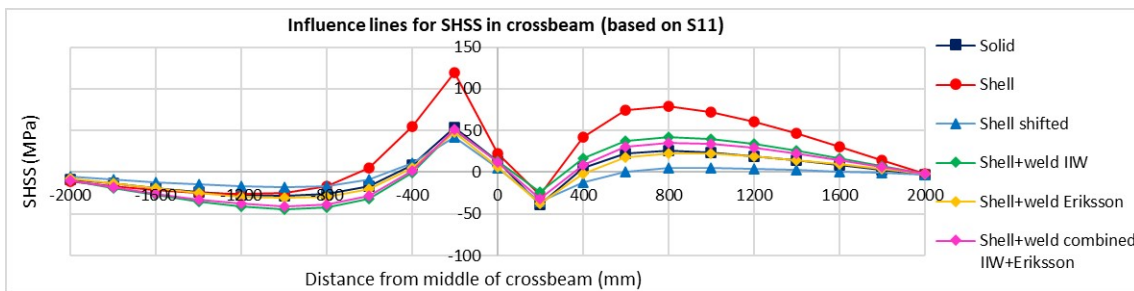


Figure 6.38: SHSS influence lines of crossbeam for variant 1 (old OSD) and axle load path 2 based on type-c calculation

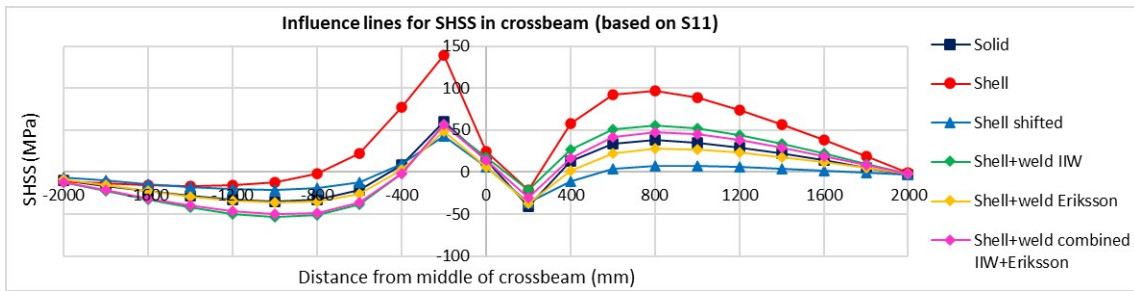


Figure 6.39: SHSS influence lines of crossbeam for variant 1 (old OSD) and axle load path 2 based on type-b calculation

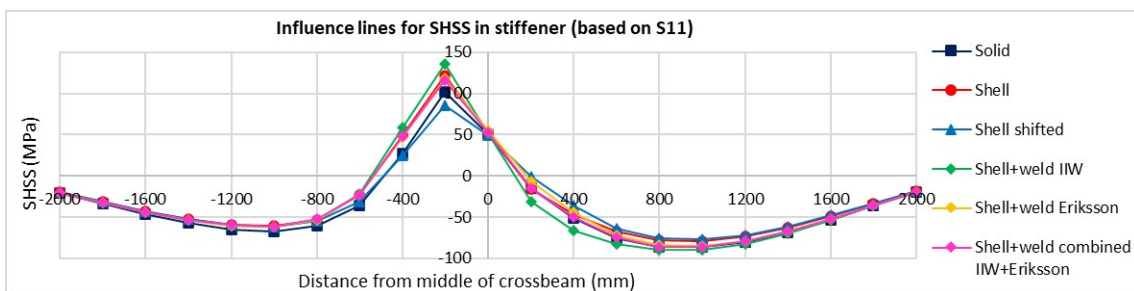


Figure 6.40: SHSS influence lines of stiffener for variant 1 (old OSD) and axle load path 2 based on type-a calculation

Figure 6.40 shows the SHSS influence lines of variant 1 and for axle load path 2 for stiffener. In this case, it can be seen that at the critical locations, the shell model with and without welds give SHSS values which are close to the SHSS obtained from the solid model.

Axle load path 3 (Load applied in between path 1 and 2)): Similar to axle load path 1 and 2, Figure 6.41 and 6.42 shows the SHSS influence lines of variant 1 and for axle load path 3 for crossbeam.

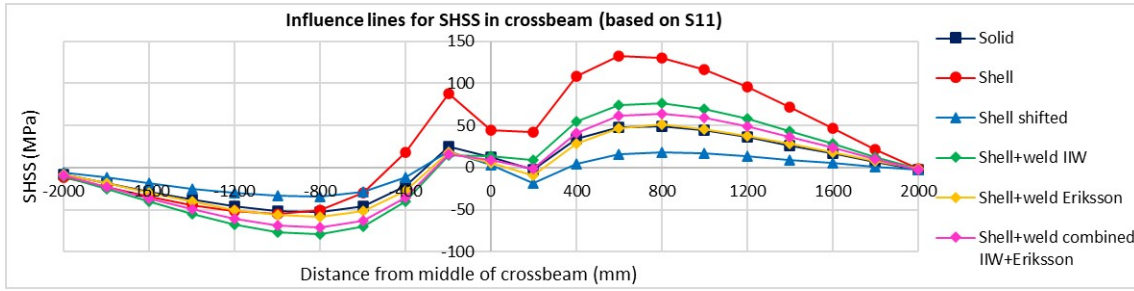


Figure 6.41: SHSS influence lines of crossbeam for variant 1 (old OSD) and axle load path 3 based on type-c calculation

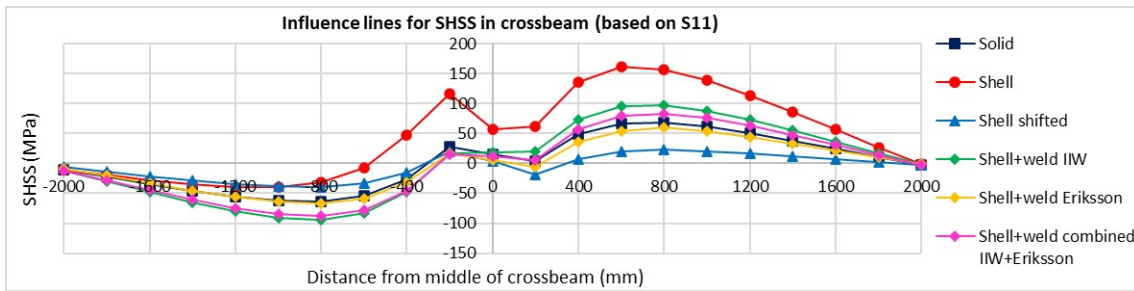


Figure 6.42: SHSS influence lines of crossbeam for variant 1 (old OSD) and axle load path 3 based on type-b calculation

Figure 6.43 shows the SHSS influence lines of variant 1 and for axle load path 3 for stiffener. In this case also, it can be seen that at the critical locations, the shell model with and without welds give SHSS values which are close to the SHSS obtained from the solid model.

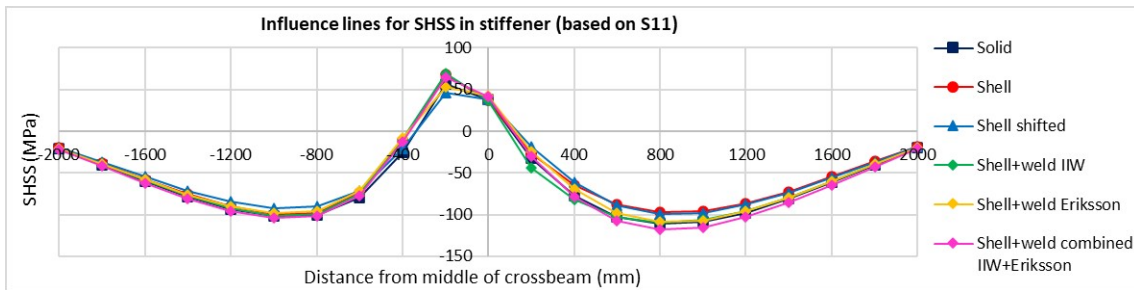


Figure 6.43: SHSS influence lines of stiffener for variant 1 (old OSD) and axle load path 3 based on type-a calculation

The Eriksson’s method [20] of weld modelling gave good results when compared to the SHSS obtained from the solid model for the light OSD variant. However, there is a small underestimation of SHSS at the critical locations. The IIW approach [40] of weld modelling on the other hand gave overestimated SHSS values in comparison to the solid element model at the critical locations. The combined method of weld modelling by Eriksson and IIW showed good results in comparison to both the above mentioned methods. From the SHSS influence line study on the light OSD variant, 6 critical points can be identified as shown in Table 6.5. These critical locations have been further investigated in the subsequent sections.

6.13.4. Main parametric study (Influence lines of SHSS for heavy OSD variant)

Similar to the light OSD variant, the SHSS influence lines are plotted, and the critical points are determined for the new OSD variant having the same 3 transverse axle load paths as mentioned in Figure 6.17, 6.18 and Figure 6.19.

Axle load path 1 (Load applied on top of stiffener): Figure 6.44 and 6.45 show the SHSS influence lines of variant 2 and for axle load path 1 for crossbeam where the hot-spot stress is calculated using type-“c” and type-“b” calculation procedure as mentioned in section 6. The SHSS of all the six different models are shown.

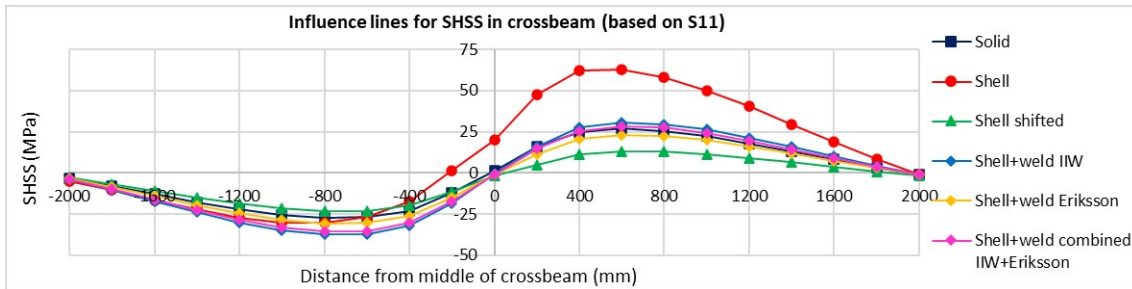


Figure 6.44: SHSS influence lines of crossbeam for variant 2 (new OSD) and axle load path 1 based on type-c calculation

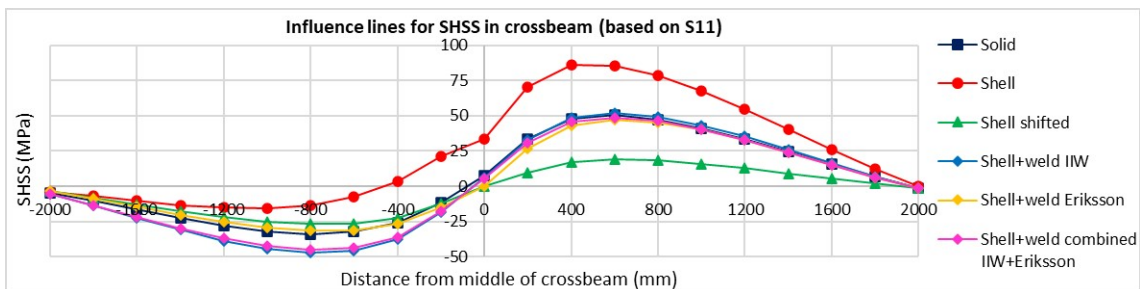


Figure 6.45: SHSS influence lines of crossbeam for variant 2 (new OSD) and axle load path 1 based on type-b calculation

The SHSS influence lines in stiffener for variant 2 in axle load path 1 is shown in Figure 6.46 where the hot-spot stress is calculated using type-a calculation procedure.

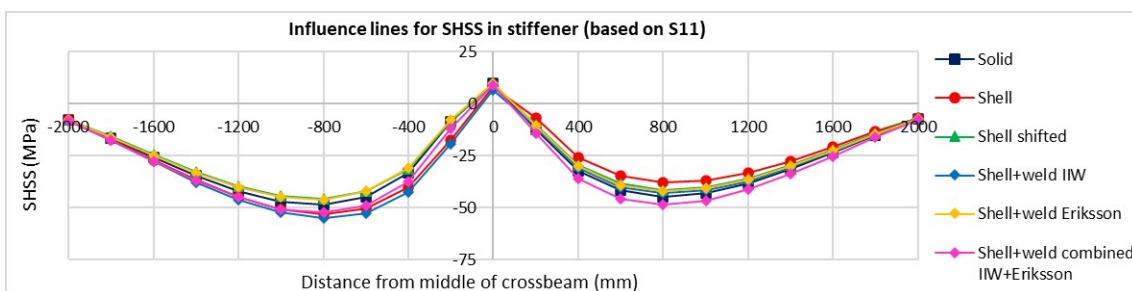


Figure 6.46: SHSS influence lines of stiffener for variant 2 (new OSD) and axle load path 1 based on type-a calculation

Axle load path 2 (Load applied in between two stiffeners): Just like for axle load path 1, Figure 25 shows the SHSS influence lines of variant 2 and for axle load path 2 for crossbeam. The hot-spot stress is calculated using type-c and type-b calculation procedure. It is observed that the shell model with welds modelled using the Eriksson’s approach gave good results for hot-spot stress in crossbeam compared to the solid model.

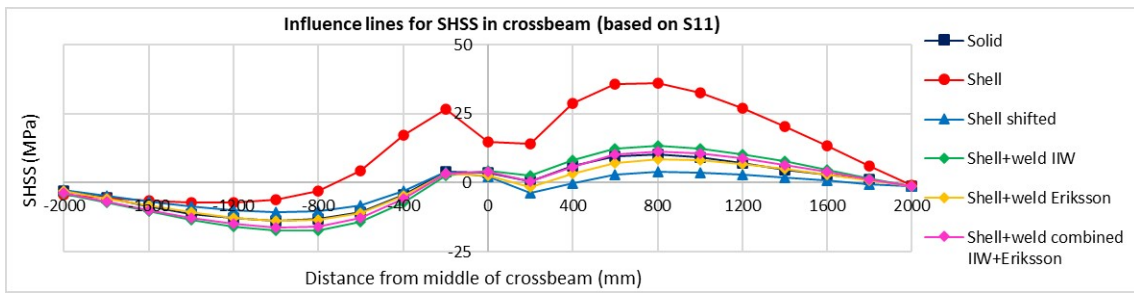


Figure 6.47: SHSS influence lines of crossbeam for variant 2 (new OSD) and axle load path 2 based on type-c calculation

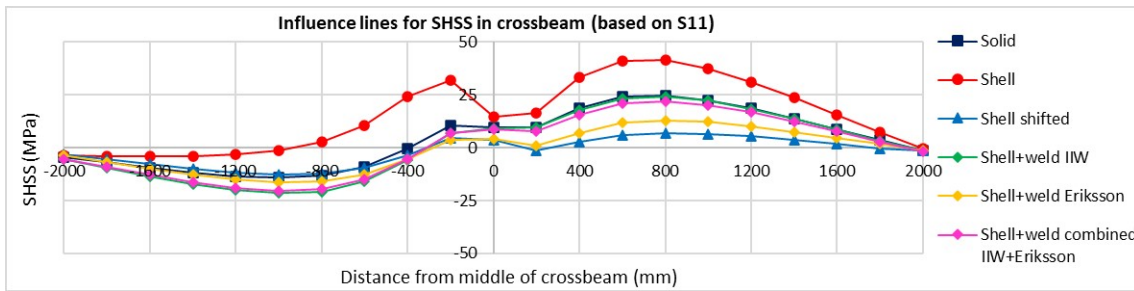


Figure 6.48: SHSS influence lines of crossbeam for variant 2 (new OSD) and axle load path 2 based on type-b calculation

The SHSS influence lines in stiffener for variant 2 in axle load path 2 is shown in Figure 6.49 where the hot-spot stress is calculated using type-a calculation procedure.

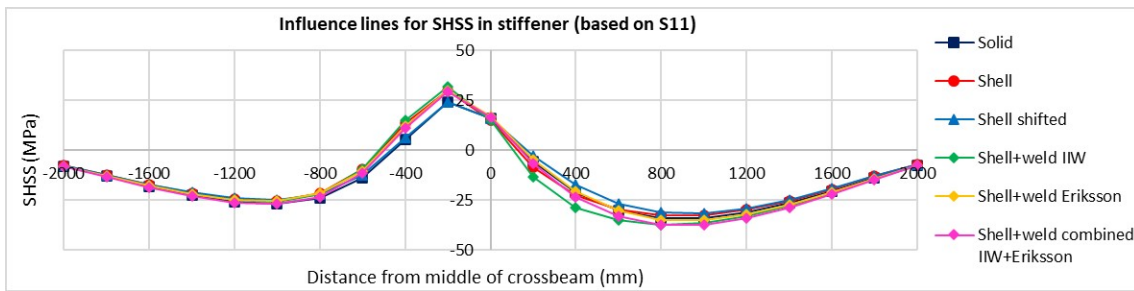


Figure 6.49: SHSS influence lines of stiffener for variant 2 (new OSD) and axle load path 2 based on type-a calculation

Axle load path 3 (Load applied in between path 1 and 2): Similar to axle load path 1 and 2, Figure 6.50 shows the SHSS influence lines of variant 2 and for axle load path 3 for crossbeam where the hot-spot stress is calculated using type-c and type-b calculation procedure. The SHSS influence lines in stiffener for variant 2 in axle load path 3 is shown in Figure 6.52 where the hot-spot stress is calculated using type-a calculation procedure.

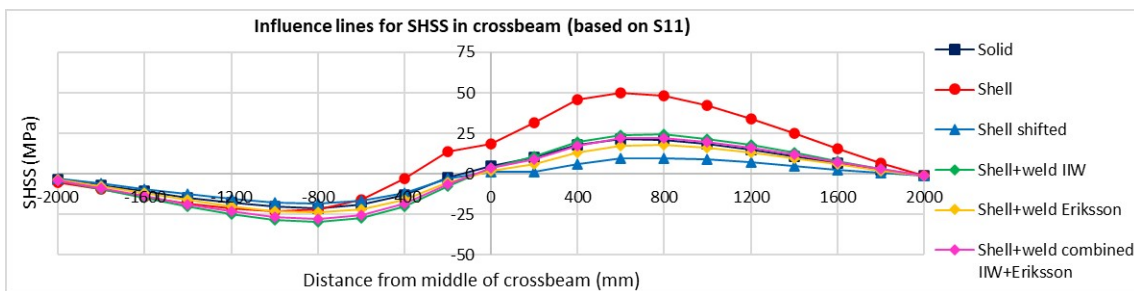


Figure 6.50: SHSS influence lines of crossbeam for variant 2 (new OSD) and axle load path 3 based on type-c calculation

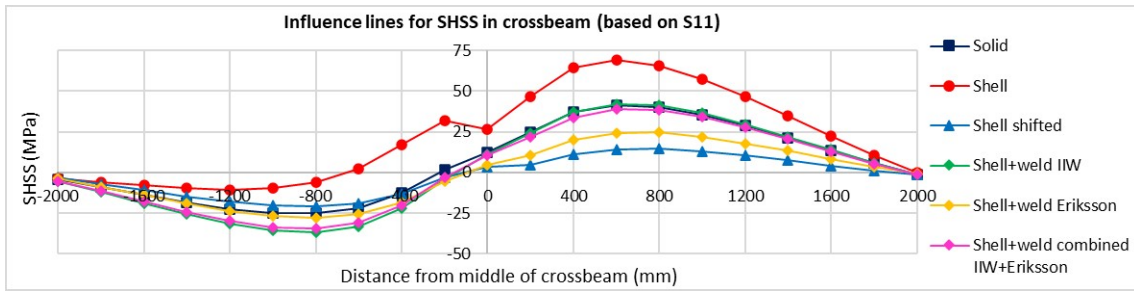


Figure 6.51: SHSS influence lines of crossbeam for variant 2 (new OSD) and axle load path 3 based on type-b calculation

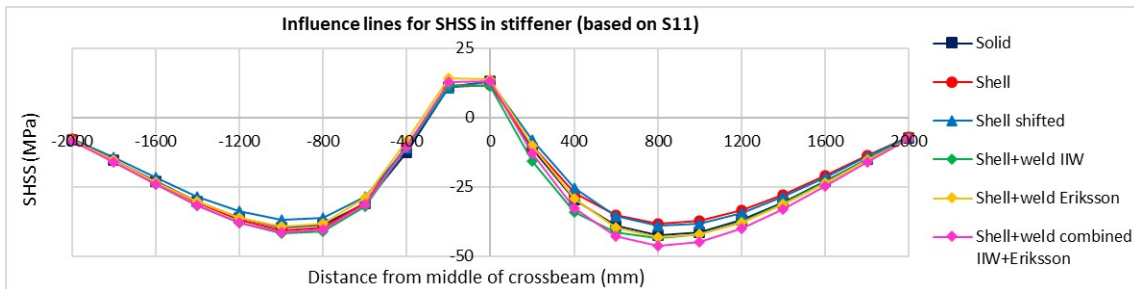


Figure 6.52: SHSS influence lines of stiffener for variant 2 (new OSD) and axle load path 3 based on type-a calculation

6.14. Determination of critical points based on axle load paths 1, 2 and 3

The critical points are determined from the influence lines for three transverse axle load paths 1, 2 and 3 which are equally spaced at 75 mm from each other. The longitudinal distance of these critical points are calculated from the middle crossbeam. From Tables 6.5 and 6.6, twelve different critical points can be identified for both the light and heavy variants of the OSD. For all these critical points, the stress distribution perpendicular to weld toe and the maximum principal stress are shown in the following sections.

Table 6.5: Critical points for the 3 transverse axle load paths for variant 1 (old OSD)

Component of OSD (old)	Crossbeam		Stiffener	
	Maximum SHSS location	Minimum SHSS location	Maximum SHSS location	Minimum SHSS location
	Distance from the middle crossbeam (mm)			
Axle load path 1	600	-800	0	-800
Axle load path 2	-200	200	-200	900
Axle load path 3	700	-900	-100	900

Table 6.6: Critical points for the 3 transverse axle load paths for variant 2 (new OSD)

Component of OSD (new)	Crossbeam		Stiffener	
	Maximum SHSS location	Minimum SHSS location	Maximum SHSS location	Minimum SHSS location
	Distance from the middle crossbeam (mm)			
Axle load path 1	600	-800	0	-800
Axle load path 2	800	-1000	-200	900
Axle load path 3	700	-900	-100	900

6.14.1. Critical points for light OSD variant based on S11

Axle load path 1 – Load on top of stiffener:

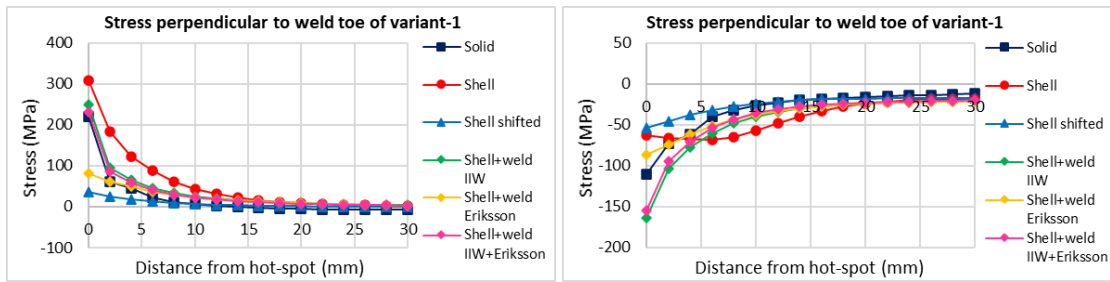


Figure 6.53: Stress perpendicular to weld toe for maximum SHSS (left) and minimum SHSS (right) in crossbeam for axle load path 1 of variant 1

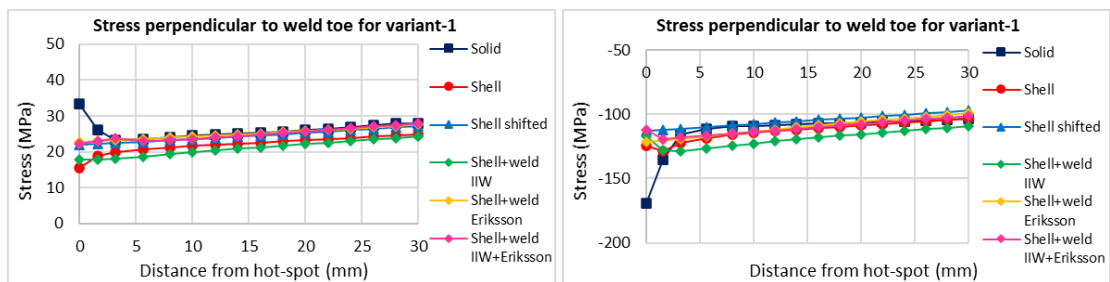


Figure 6.54: Stress perpendicular to weld toe for maximum SHSS (left) and minimum SHSS (right) in stiffener for axle load path 1 of variant 1

Axle load path 2 – Load between stiffeners:

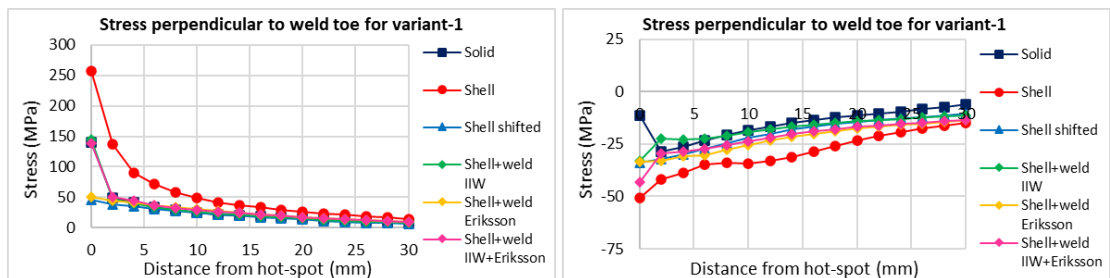


Figure 6.55: Stress perpendicular to weld toe for maximum SHSS (left) and minimum SHSS (right) in crossbeam for axle load path 2 of variant 1

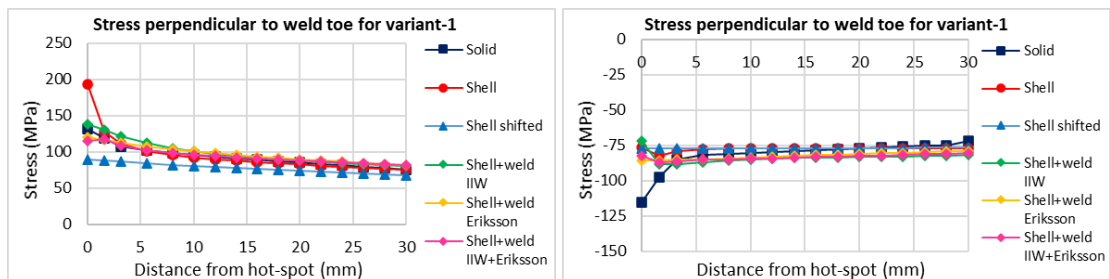


Figure 6.56: Stress perpendicular to weld toe for maximum SHSS (left) and minimum SHSS (right) in stiffener for axle load path 2 of variant 1

Axle load path 3 – Load between axle load paths 1 and 2:

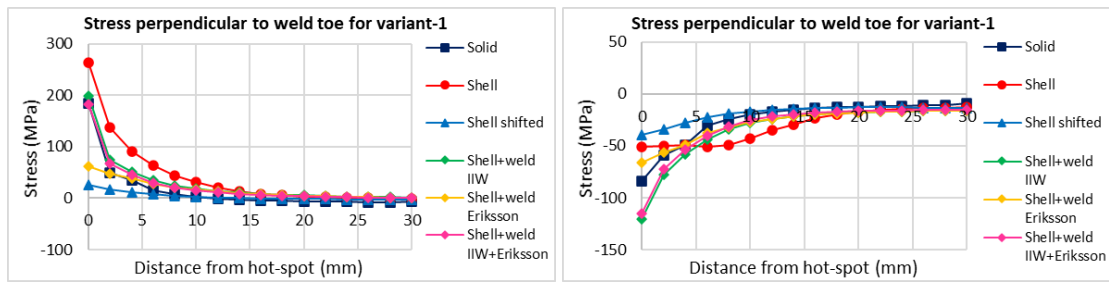


Figure 6.57: Stress perpendicular to weld toe for maximum SHSS (left) and minimum SHSS (right) in crossbeam for axle load path 3 of variant 1

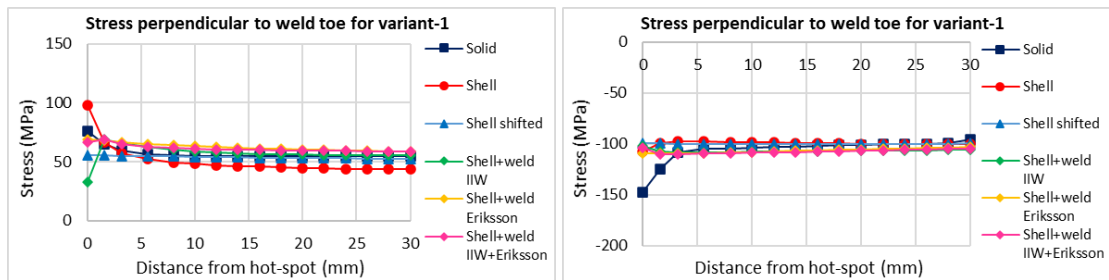


Figure 6.58: Stress perpendicular to weld toe for maximum SHSS (left) and minimum SHSS (right) in stiffener for axle load path 3 of variant 1

6.14.2. Critical points for heavy OSD variant based on S11

Axle load path 1 – Load on top of stiffener:

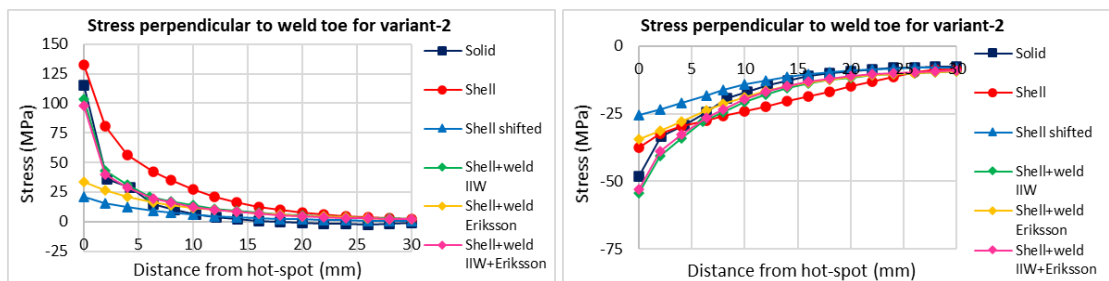


Figure 6.59: Stress perpendicular to weld toe for maximum SHSS (left) and minimum SHSS (right) in crossbeam for axle load path 1 of variant 2

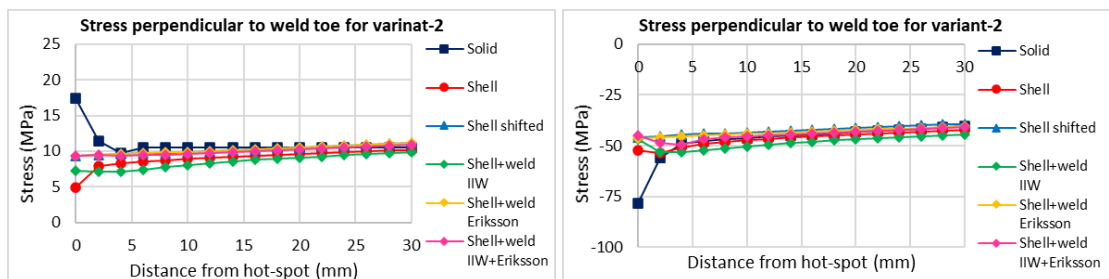


Figure 6.60: Stress perpendicular to weld toe for maximum SHSS (left) and minimum SHSS (right) in stiffener for axle load path 1 of variant 2

Axle load path 2 – Load between stiffeners:

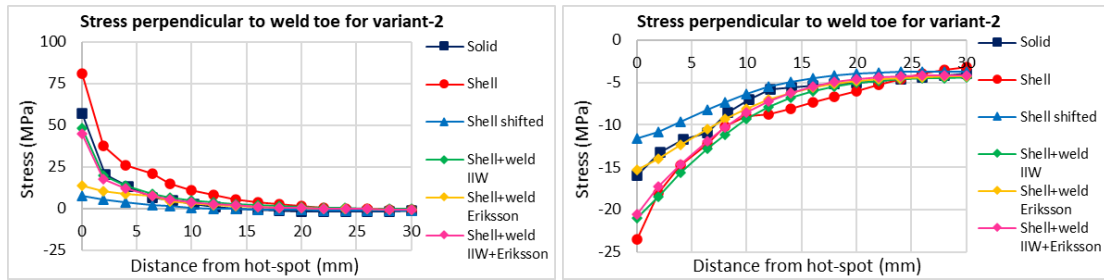


Figure 6.61: Stress perpendicular to weld toe for maximum SHSS (left) and minimum SHSS (right) in crossbeam for axle load path 2 of variant 2

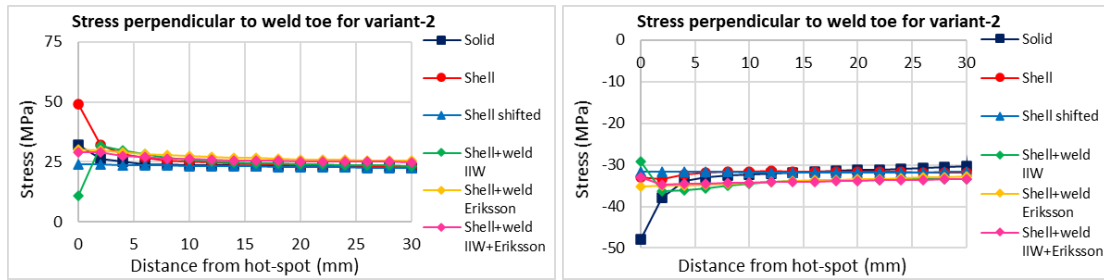


Figure 6.62: Stress perpendicular to weld toe for maximum SHSS (left) and minimum SHSS (right) in stiffener for axle load path 2 of variant 2

Axle load path 3 – Load between axle load paths 1 and 2:

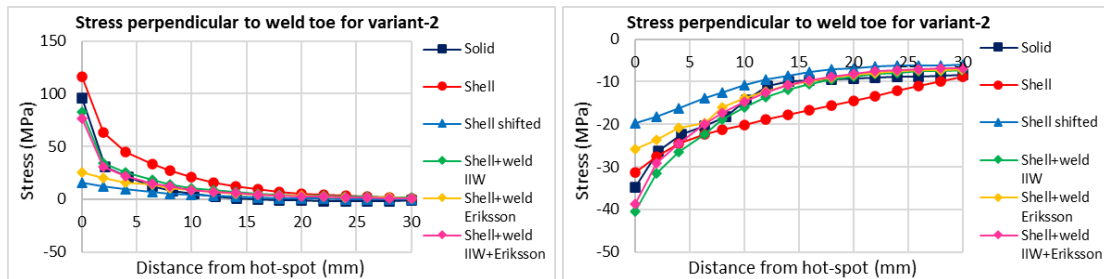


Figure 6.63: Stress perpendicular to weld toe for maximum SHSS (left) and minimum SHSS (right) in crossbeam for axle load path 3 of variant 2

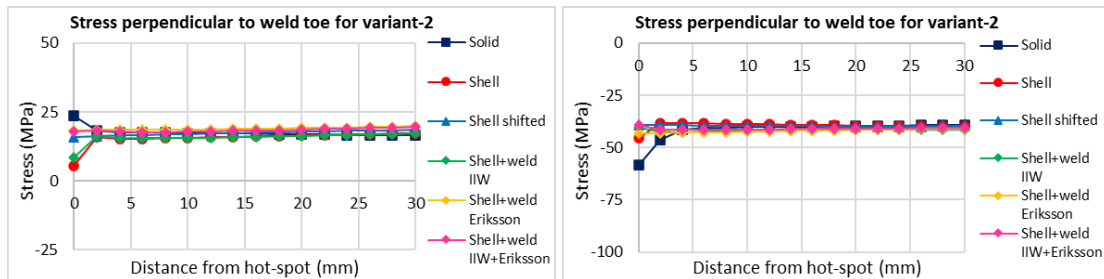


Figure 6.64: Stress perpendicular to weld toe for maximum SHSS (left) and minimum SHSS (right) in stiffener for axle load path 3 of variant 2

The stress perpendicular to weld toe (S11) is used for the calculation of hot-spot stress for the critical points. From Figures 6.53 - 6.64, it can be observed that the shell+weld combined model is the best in comparison to the other weld modelling approaches. The stress gradients obtained from the shell+weld combined model is similar to the stress gradient obtained from the solid element model. For the crossbeam, it is observed that the stress gradient of the regular shell model is steeper than that of the solid model. For the stiffener, the stress gradients of both the regular shell and solid models are flat. A comparison of stress gradients and stress value at 30 mm away from weld toe is made for the numerical models. After comparing all the weld modelling approaches with shell elements, it is found that the combined weld modelling approach is the best one in comparison to the solid model. In Appendix-I, the same procedure is applied but with maximum principal stress. Table 6.7 and 6.8 shows the ratio of SHSS for light and heavy variant OSD respectively.

Table 6.7: SHSS values and ratios for light variant OSD based on stress perpendicular to weld toe

Variant 1 (Light variant OSD)	Axle Load Path 1				Axle Load Path 2				Axle Load Path 3			
	Crossbeam		Stiffener		Crossbeam		Stiffener		Crossbeam		Stiffener	
	Maxima	Minima	Maxima	Minima	Maxima	Minima	Maxima	Minima	Maxima	Minima	Maxima	Minima
Numerical Model	SHSS (MPa)	SHSS (MPa)	SHSS (MPa)	SHSS (MPa)	SHSS (MPa)	SHSS (MPa)	SHSS (MPa)	SHSS (MPa)	SHSS (MPa)	SHSS (MPa)	SHSS (MPa)	SHSS (MPa)
Solid	72.32	-86.02	22.78	-120.44	53.03	-31.56	114.54	-87.53	58.01	-68.54	62.23	-111.44
Shell	174.34	-73.93	19.12	-126.45	119.04	-42.16	122.00	-79.90	130.54	-53.90	62.72	-97.47
Shell shifted	25.58	-47.09	21.97	-112.79	41.08	-35.14	89.20	-77.21	18.97	-34.61	55.40	-99.74
Shell+weld IIW	92.44	-102.26	17.05	-131.05	48.62	-25.38	133.31	-89.90	73.27	-78.82	69.64	-109.44
Shell+weld Eriksson	65.95	-77.49	22.70	-121.71	49.12	-34.71	118.61	-85.97	54.08	-63.42	68.66	-110.13
Shell+weld IIW+Eriksson	83.51	-94.66	24.10	-120.33	54.62	-31.74	116.11	-87.09	65.07	-71.85	67.21	-110.54
Ratio												
SHSS shell/solid	2.41	0.86	0.84	1.05	2.24	1.34	1.07	0.91	2.25	0.79	1.01	0.87
SHSS shell shifted/solid	0.35	0.55	0.96	0.94	0.77	1.11	0.78	0.88	0.33	0.50	0.89	0.90
SHSS shell+weld (IIW)/solid	1.28	1.19	0.75	1.09	0.92	0.80	1.16	1.03	1.26	1.15	1.12	0.98
SHSS shell+weld (Eriksson)/solid	0.91	0.90	1.00	1.01	0.93	1.10	1.04	0.98	0.93	0.93	1.10	0.99
SHSS shell+weld (IIW+Eriksson)/solid	1.15	1.10	1.06	1.00	1.03	1.01	1.01	0.99	1.12	1.05	1.08	0.99

Table 6.8: SHSS values and ratios for heavy variant OSD based on stress perpendicular to weld toe

Variant 2 (Heavy variant OSD)	Axle Load Path 1				Axle Load Path 2				Axle Load Path 3			
	Crossbeam		Stiffener		Crossbeam		Stiffener		Crossbeam		Stiffener	
	Maxima	Minima	Maxima	Minima	Maxima	Minima	Maxima	Minima	Maxima	Minima	Maxima	Minima
Numerical Model	SHSS (MPa)	SHSS (MPa)	SHSS (MPa)	SHSS (MPa)	SHSS (MPa)	SHSS (MPa)	SHSS (MPa)	SHSS (MPa)	SHSS (MPa)	SHSS (MPa)	SHSS (MPa)	SHSS (MPa)
Solid	24.76	-33.32	9.15	-51.19	11.59	-14.75	26.06	-34.78	20.57	-27.40	17.88	-42.52
Shell	62.80	-33.69	7.80	-52.99	32.27	-15.50	30.30	-32.82	49.84	-26.10	15.13	-38.17
Shell shifted	13.22	-23.31	9.31	-45.61	3.97	-10.68	23.98	-31.58	9.84	-18.03	16.08	-39.22
Shell+weld IIW	30.55	-37.39	6.55	-55.07	13.36	-17.41	32.16	-37.23	26.35	-30.45	15.90	-43.19
Shell+weld Eriksson	23.07	-30.77	9.32	-46.13	11.94	-13.87	29.98	-35.29	20.71	-26.46	18.40	-43.31
Shell+weld IIW+Eriksson	28.26	-35.61	9.21	-52.18	11.68	-16.23	28.67	-34.82	21.82	-26.99	17.82	-41.52
Ratio												
SHSS shell/solid	2.54	1.01	0.85	1.04	2.78	1.05	1.16	0.94	2.42	0.95	0.85	0.90
SHSS shell shifted/solid	0.53	0.70	1.02	0.89	0.34	0.72	0.92	0.91	0.48	0.66	0.90	0.92
SHSS shell+weld (IIW)/solid	1.23	1.12	0.72	1.08	1.15	1.18	1.23	1.07	1.28	1.11	0.89	1.02
SHSS shell+weld (Eriksson)/solid	0.93	0.92	1.02	0.90	1.03	0.94	1.15	1.01	1.01	0.97	1.03	1.02
SHSS shell+weld (IIW+Eriksson)/solid	1.14	1.07	1.01	1.02	1.01	1.10	1.10	1.00	1.06	0.99	1.00	0.98

From the above tables, it is clearly observed that the regular shell model is not suitable for hot-spot stress determination for both the crack in crossbeam and the crack in stiffener. This is because it gives either extremely overestimated or extremely underestimated SHSS results compared to the solid element model. After application of a shift of weld leg length plus half the thickness of the attached plate, the hot-spot stress did not improve with respect to the solid element model. Only after application of weld modelling with shell elements, the hot-spot stress ratio improved. The consistency in the ratio of hot-spot stress is explained in detail in the following sections.

It is also observed that there is a difference in hot-spot stress value calculated using maximum principal stress (Appendix-I) and that calculated using stress perpendicular to weld toe. This is because, the direction of the maximum principal stress varied for different critical load locations. The maximum and minimum values of hot-spot stress obtained from shell+weld combined model, for both stiffener and crossbeam are considered as acceptable when compared to the solid model.

Figures 6.65 and 6.66 shows a histogram where all the different strategies to model shell elements are mentioned. This is done in order to have a visual representation of the improvement in the hot-spot stress ratio with different weld modelling approaches with shell elements. There are three transverse

axle load positions and for each load position there are four critical points (maximum SHSS and minimum SHSS of crossbeam and stiffener). Thus, in total there are 12 critical points in the OSD. These 12 critical points are shown in the histogram.

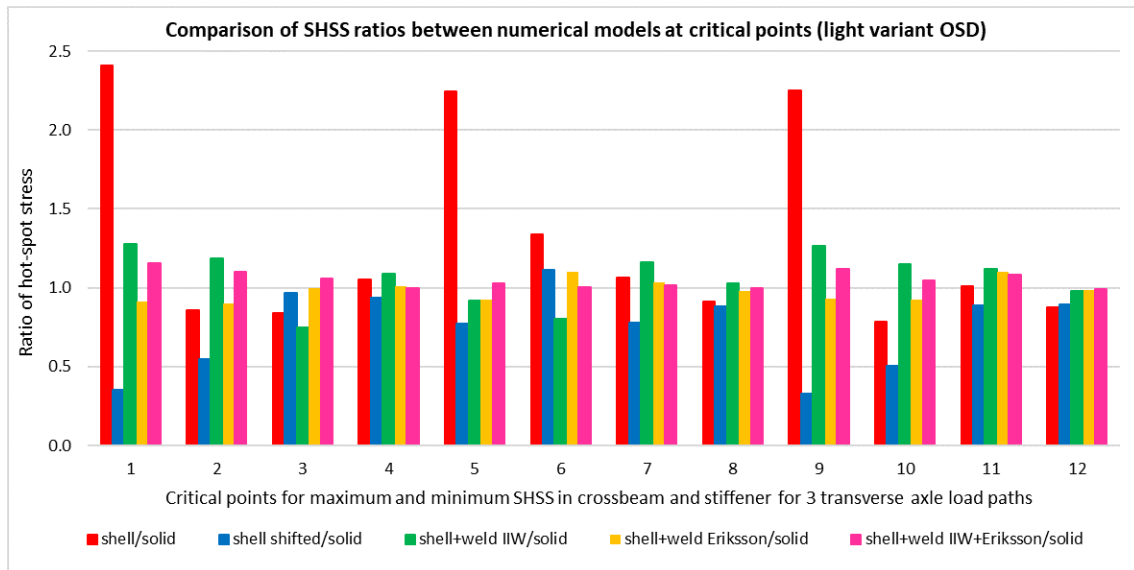


Figure 6.65: Histogram of SHSS ratio for different numerical models of light variant OSD based on stress perpendicular to weld toe

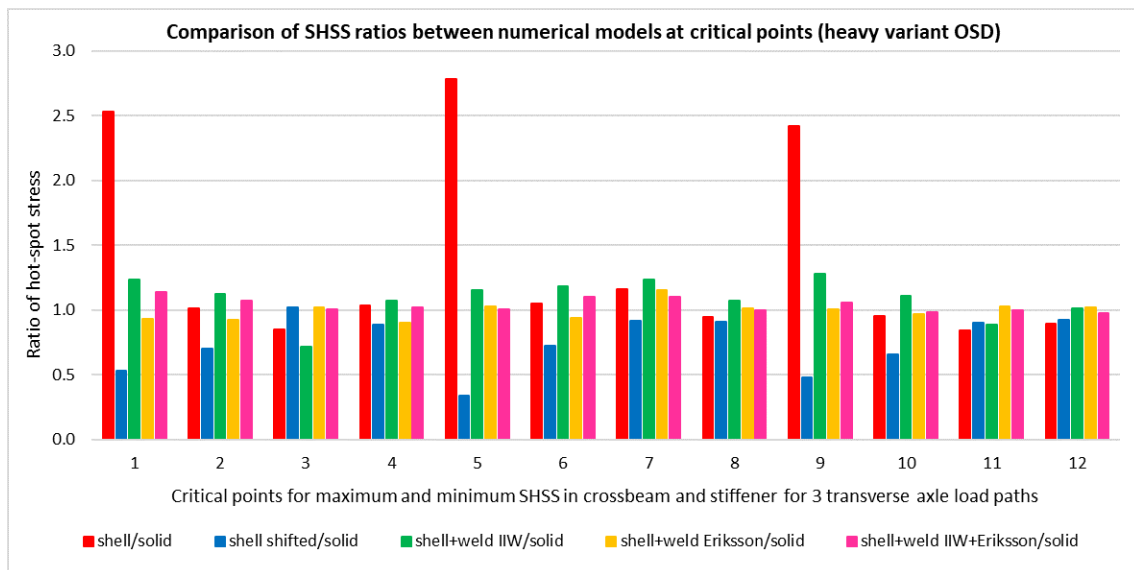


Figure 6.66: Histogram of SHSS ratio for different numerical models of heavy variant OSD based on stress perpendicular to weld toe

From Figures 6.65 and 6.66, the bars represent the ratio of hot-spot stress obtained from a particular modelling strategy to that from the solid model. It is clear, that the normal shell model does not give proper hot-spot stress results compared to the solid model. After application of a shift of the weld leg length plus half the thickness of plate, the results still did not improve compared to the solid model. It is seen from both the histograms that the pink bars are very close to unity which represent the combined approach of IIW and Eriksson. The deformed mesh and contour plots of stress and deformation are shown in Appendix-H for all the numerical models of the OSD. Here also, the limits of the scale of the contour plots have been taken to be the same for a better comparison between the numerical models.

6.15. Calculation of statistical parameters

Coefficient of variation: In statistics, the coefficient of variation (CV), also known as relative standard deviation (RSD), is a standardized measure of dispersion of a probability distribution or frequency distribution. It is defined as the ratio of the standard deviation σ to the mean μ . The following equations are used for the calculation of the statistical parameters.

$$\mu = \frac{\sum x}{n}$$

$$\sigma = \sqrt{\frac{\sum (x - \mu)^2}{n - 1}}$$

$$C_v = \frac{\sigma}{\mu}$$

Table 6.9 and 6.10 shows the coefficient of variation of SHSS ratios on crossbeam for the light and heavy OSD variants. Similarly, Table 6.11 and 6.12 shows the coefficient of variation of SHSS ratios on stiffener for the light and heavy OSD variants. It can be observed that the CV reduces to approximately **5.4%** for crossbeam and to **4.0%** for stiffener after using the combined approach of weld modelling with shell elements. Also, the mean value of SHSS ratio data-set is found to be close to 1 in both stiffener and crossbeam after weld modelling.

Table 6.9: Coefficient of variation for SHSS ratios in crossbeam for light OSD variant

Variant-1 (Light OSD)						
Axle load	Component	Ratio SHSS shell/solid	Ratio SHSS shell shifted/solid	Ratio SHSS shell+weld (IIW)/solid	Ratio SHSS shell+weld (Eriksson)/solid	Ratio SHSS shell+weld (IIW+Eriksson)/solid
Axle load path-1	Crossbeam (max)	2.41	0.35	1.28	0.91	1.15
	Crossbeam (min)	0.86	0.55	1.19	0.90	1.10
Axle load path-2	Crossbeam (max)	2.24	0.77	0.92	0.93	1.03
	Crossbeam (min)	1.34	1.11	0.80	1.10	1.01
Axle load path-3	Crossbeam (max)	2.25	0.33	1.26	0.93	1.12
	Crossbeam (min)	0.79	0.50	1.15	0.93	1.05
Statistical parameters	Mean (μ)	1.65	0.60	1.10	0.95	1.08
	SD (σ)	0.74	0.30	0.19	0.07	0.06
	CV	0.45	0.49	0.18	0.08	0.05
	CV (%)	45.1%	49.2%	17.7%	7.9%	5.4%

Table 6.10: Coefficient of variation for SHSS ratios in crossbeam for heavy OSD variant

Variant-2 (heavy variant OSD)						
Axle load	Component	Ratio SHSS shell/solid	Ratio SHSS shell shifted/solid	Ratio SHSS shell+weld (IIW)/solid	Ratio SHSS shell+weld (Eriksson)/solid	Ratio SHSS shell+weld (IIW+Eriksson)/solid
Axle load path-1	Crossbeam (max)	2.54	0.53	1.23	0.93	1.14
	Crossbeam (min)	1.01	0.70	1.12	0.92	1.07
Axle load path-2	Crossbeam (max)	2.78	0.34	1.15	1.03	1.01
	Crossbeam (min)	1.05	0.72	1.18	0.94	1.10
Axle load path-3	Crossbeam (max)	2.42	0.48	1.28	1.01	1.06
	Crossbeam (min)	0.95	0.66	1.11	0.97	0.99
Statistical parameters	Mean (μ)	1.79	0.57	1.18	0.97	1.06
	SD (σ)	0.87	0.15	0.07	0.04	0.06
	CV	0.49	0.26	0.06	0.05	0.05
	CV (%)	48.6%	25.9%	5.6%	4.5%	5.4%

Table 6.11: Coefficient of variation for SHSS ratios in stiffener for light OSD variant

Variant-1 (light variant OSD)						
Axle load	Component	Ratio SHSS shell/solid	Ratio SHSS shell shifted/solid	Ratio SHSS shell+weld (IIW)/solid	Ratio SHSS shell+weld (Eriksson)/solid	Ratio SHSS shell+weld (IIW+Eriksson)/solid
Axle load path-1	Stiffener (max)	0.84	0.96	0.75	1.00	1.06
	Stiffener (min)	1.05	0.94	1.09	1.01	1.00
Axle load path-2	Stiffener (max)	1.07	0.78	1.16	1.04	1.01
	Stiffener (min)	0.91	0.88	1.03	0.98	0.99
Axle load path-3	Stiffener (max)	1.01	0.89	1.12	1.10	1.08
	Stiffener (min)	0.87	0.90	0.98	0.99	0.99
Statistical parameters	Mean (μ)	0.96	0.89	1.02	1.02	1.02
	SD (σ)	0.10	0.06	0.15	0.05	0.04
	CV	0.10	0.07	0.15	0.04	0.04
	CV (%)	9.9%	7.1%	14.5%	4.4%	3.6%

Table 6.12: Coefficient of variation for SHSS ratios in stiffener for heavy OSD variant

Variant-2 (heavy variant OSD)						
Axle load	Component	Ratio SHSS shell/solid	Ratio SHSS shell shifted/solid	Ratio SHSS shell+weld (IIW)/solid	Ratio SHSS shell+weld (Eriksson)/solid	Ratio SHSS shell+weld (IIW+Eriksson)/solid
Axle load path-1	Stiffener (max)	0.85	1.02	0.72	1.02	1.01
	Stiffener (min)	1.04	0.89	1.08	0.90	1.02
Axle load path-2	Stiffener (max)	1.16	0.92	1.23	1.15	1.10
	Stiffener (min)	0.94	0.91	1.07	1.01	1.00
Axle load path-3	Stiffener (max)	0.85	0.90	0.89	1.03	1.00
	Stiffener (min)	0.90	0.92	1.02	1.02	0.98
Statistical parameters	Mean (μ)	0.96	0.93	1.00	1.02	1.02
	SD (σ)	0.12	0.05	0.18	0.08	0.04
	CV	0.13	0.05	0.18	0.08	0.04
	CV (%)	12.8%	5.0%	17.8%	7.7%	4.3%

Figure 6.67 shows the scattering of SHSS ratios in the form of a coefficient of variation (CV) histogram. The SHSS ratio of shell/solid and of shell shifted/solid showed a huge variation for the crossbeam. However, for the stiffener, the shell+weld model developed using the IIW approach showed the maximum amount of variation.

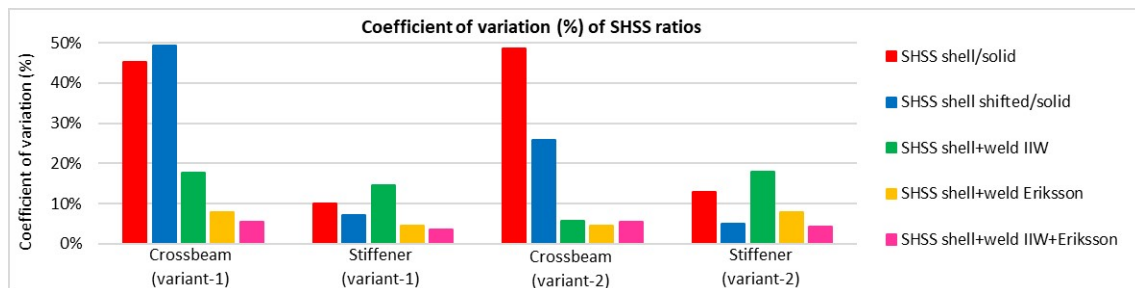


Figure 6.67: Coefficient of variation for SHSS ratios

From the coefficient of variation (CV) histogram of the current study, it can be seen that there is a sufficient improvement of the difference of SHSS ratio after weld modelling with shell elements using the combined approach. The critical points obtained from the influence line study from three transverse axle load positions are also assessed for SHSS obtained from maximum principal stress in Appendix-H as an additional study. However, it is observed that the angle of the maximum principal stress varied for every load position. Thus, it is recommended to use the stress perpendicular to weld toe for finding the SHSS of such details in OSDs.

7

Results and Discussion

“Everything should be made as simple as possible, but not simpler. If you can’t explain it simply, you don’t understand it well enough.”

Albert Einstein

In this chapter, all the analyses results of the current study have been explained in a sequential manner. A similar study is performed on the connection of longitudinal closed stiffener to crossbeam in an OSD by Dennis van der Ende (Master thesis; MSc candidate, TU Delft) [19]. The results obtained from the analyses on closed stiffener-to-crossbeam connection has also been stated in this chapter.

7.1. Results and discussion

In **Chapter-3**, two different types of welded connections are validated and analysed. The first detail is a single side fillet welded longitudinal plate joint (Śledziwski [54]). In this detail, the stress concentration is observed at the base plate surface near the edge of the longitudinal attachment. The second detail is a double side fillet welded transverse cruciform joint (Karabulut and Lombaert [31]). In, this detail, the stress concentration is observed at the base plate surface near the middle of the transverse plate. Thus, the hot-spot is of type-“a” for both the details. A brief discussion on the results obtained from the analyses of these two details is mentioned as follows:

- **Single side fillet welded longitudinal plate joint (detail type a):** This detail is subjected to two types of load cases, uniform tension and bending. At first, the solid element model is validated with the numerical results of Śledziwski [54] for tension load case. Then the regular shell element model and the shell model with welds simulated using the IIW [40] approach are developed. For detail type a, both the linear and quadratic extrapolation methods gave SHSS values which were quite close to each other with a difference within **4%** for the solid model and within **5%** for the shell model for both the load cases. In the next step, a parametric study is performed where the thickness of the two connected plates are varied. From the parametric study for tension load case (Table 3.11), it is found that there is a difference in the ratio of SHSS shell/solid in the range of **0.96-1.13**. This difference however, did not reduce when the shell elements are modeled with welds using the increased thickness method according to the IIW [28] for this load case. From the parametric study for bending (Table 3.18), it is found that there is again a considerable amount of variation in the ratio of SHSS shell/solid in the range of **0.91-1.15**. However, this variation is reduced to some extent from a coefficient of variation (CV) of **7.0%** to **4.6%** by modelling the welds with shell elements using increased thickness at the welded region according to IIW [28].
- **Double side fillet welded transverse cruciform joint (detail type b):** This detail is subjected to pure tension. Initially, the solid element model is developed and validated with experimental results of Karabulut and Lombaert [31] (Table 3.20). The SHSS results from the solid model with linear extrapolation is **4.2%** lower than the measured SHSS of 87.6 MPa. The SHSS results from the solid model with quadratic extrapolation is **1.6%** lower than the measured SHSS. This difference in results is considered as acceptable and thus the solid model gave good results of SHSS. The SHSS results from the shell model with linear extrapolation is **10.7%** lower than the measured SHSS. The SHSS results from the shell model with quadratic extrapolation is **11.3%** lower than the measured SHSS. This difference in results cannot be acceptable as the underestimation is large with shell elements. Furthermore, the SHSS values from the shell element model are consistently lower compared to the solid element model for all element types and mesh sizes. This is because there is no stress concentration in the shell element model under tension. Therefore, it can be concluded that the shell elements cannot be used to find SHSS for these types of joints loaded in pure tension. Even after application of weld modelling with shell elements, there will be no improvement in the SHSS for such details loaded under pure tension. Thus, it is recommended to use the nominal stress method for analysing such details with shell elements.

Chapter-4 consists of numerical modelling and validation of a complex fillet welded connection between deck-plate, open stiffener and crossbeam with a cope hole. It is observed that the average percentage difference between the strain results from the solid model and the experimental strain measurements is about **9%** for the hot-spot region HS1 under a load range of 200 kN (Appendix-H). It is also observed that the average percentage difference between the strain results from the shell model with welds according to IIW approach [28] [40] and the experimental strain measurements is about **15%** under the hot-spot region 'HS1' for a load range of 200 kN (Appendix-H). It is thought that the difference in numerical strains between the solid element model and the experimental measurement data might occur due to the presence of misalignment in geometry in the actual test specimen. In the numerical model, the weld is modelled using ideal geometry having constant throat thickness. Another reason might be due to inaccurate placing of strain gauges at the locations close to weld toe. This might lead to a different measured strain value.

The SHSS obtained from the quadratic solid model is **4%** lower than the experimental SHSS which is thus viewed as a good result as it is within **+/-5%**. The SHSS obtained from the shell element model

is significantly higher than the SHSS obtained from the solid element model by a factor of **3.48**. (Table 4.4). From the research of Akhlaghi [10], this ratio of SHSS of shell to that of solid is **3.80** (Table 4.3). This difference occurred as the solid element model in the present research is developed more realistically compared to that developed in the research of Akhlaghi [10].

A parametric study is performed on this complex fillet welded detail with three load cases: LC-1: in-plane bending of crossbeam, LC-2: out-of-plane bending of crossbeam and LC-3: in-plane bending of crossbeam with local load introduction on top of the stiffener. The analysis is performed and SHSS is determined for three different numerical models: solid element model, shell element model and shell element model with welds modelled using the IIW approach [40]. It is found that weld modelling with shell elements with increased thickness at the weld location (using IIW approach [28]) results in a reduction in the SHSS value compared to the original shell element model. The main reason behind this is due to the addition of extra stiffness at the weld location. This reduction of ratio of SHSS of shell to solid is from **3.48** to **1.00** for LC-1 and from **3.48** to **1.14** for LC-3 as shown in Table 4.5.

For LC-2, the shell modelling with welds does not prove to be very effective as the original shell model without welds has better results. The origin of stress extraction is taken at the weld toe for the solid model and the intersection of mid-planes of the plates for the shell model. The stress gradient of the crossbeam at the investigated detail for the shell element model with welds is better compared to the normal shell models for the in-plane behaviour of the crossbeam (Figure 4.22 and 4.26). For the out-of-plane behaviour of the crossbeam, there is a high peak in stress value which is observed in the shell model with welds Figure 4.24. It is also observed that the stress values at a distance 30 mm away from the weld toe are same for all the numerical models and for all the load cases.

In **Chapter-5**, two types of fillet welded cruciform joints loaded in bending, are analysed for hot-spot stress with shell and solid elements. A parametric analysis is performed on two geometrical variants of the cruciform joint. The first one having the same thickness of crossbeam and stiffener plates as that from the light variant OSD. The second one having the same thickness of crossbeam and stiffener plates as that from the heavy variant OSD. These two types of fillet welded details are mentioned below:

- **Transverse fillet welded cruciform joint:** For the transverse fillet welded cruciform joint, the solid element model is first developed with a support at the middle line of the two end surfaces. Then the shell element model is developed using the middle surface offset approach. A comparison between the regular shell and solid element model gives an overestimation of SHSS ratio, with a big scatter in the range of **1.17-1.24** (Table 5.2). This scatter is reduced to **0.98-0.99**, after modelling the welds with shell elements using the Eriksson's approach [20]. Not only the SHSS but also the stress values at 50 mm away from the weld toe of solid model are close to the corresponding values from the shell+weld Eriksson model. Similar behaviour is observed for both the geometrical variants of the detail.
- **Longitudinal fillet welded cruciform joint** - For the longitudinal fillet welded cruciform joint, SHSS is calculated from the shell model with welds using all the three approaches: Eriksson's approach [20], IIW approach [28] and the combined IIW and Eriksson's approach. In a similar manner, the solid and shell element model is developed with appropriate boundary conditions. A comparison between the regular shell and solid element model gave an overestimation of SHSS ratio, with a big scatter in the range of **1.11-1.16** (Table 5.3). Again, a similar behaviour is observed for both the geometrical variants of the detail.
 - The scatter of SHSS ratio is reduced to a range of **0.98-1.03**, after modelling welds with shell elements using IIW approach [40]. The mean value is **1.01** and CV is **1.9%**.
 - The scatter of SHSS ratio is reduced to a range of **0.96-0.98**, after modelling welds with shell elements using Eriksson's approach [20]. The mean value is **0.97** and CV is **0.7%**.
 - The scatter of SHSS ratio is reduced to a range of **0.96-0.99**, after modelling welds with shell elements using combined approach. The mean value is **0.97** and CV is **1.8%**.

Thus, SHSS values obtained after each of the weld modelling approaches, are close to the corresponding SHSS values calculated from the solid model within **+/-5%** for both the representative bending

load cases and also for the load combinations. It is concluded that for such details, the shell model with welds gives a good prediction of the behaviour of stresses and deformation compared to the solid model for both representative bending load cases as well as load combinations. The deformation for both in-plane and out-of plane loading, is consistent after modelling of welds with shell elements.

Chapter-6 encapsulates a preliminary and a detailed parametric study on the OSD. Both of these studies have been described as follows:

- **Preliminary parametric study:** This study is performed based on some representative load cases using solid elements and shell elements with and without weld as described in section 6.13.2: LC-1 (in-plane bending), LC-2 (out-of-plane bending), LC-3a (in-plane bending with load application on top of stiffener) and LC-3b (in-plane bending with load application in between stiffeners). The SHSS ratio is within a range of **0.91-1.08** for the crossbeam and **0.92-1.08** for the stiffener as seen from Table 6.4 after using the combined weld modelling approach. The coefficient of variation in SHSS ratio for crossbeam is **6.8%** and that for stiffener is around **5.1%**. The stress gradient of the shell model with welds using the combined approach are also in good agreement with that of the solid models for all the load cases.
- **Detailed parametric study:** This study is performed based on the influence lines for determination of critical points on the OSD. From the histograms Figures 6.65 and 6.66, it can be clearly seen that the regular shell model is not feasible for determination of SHSS for this detail. After application of a shift of weld leg length plus half the plate thickness in the shell model, the SHSS ratio is extremely underestimated. Several weld modelling techniques with shell elements have been investigated for the 12 critical locations of the OSD. Using the combined weld modelling technique with shell elements (IIW [28] and Eriksson[20]), a consistent ratio of SHSS is obtained. The stress gradient of the shell model with the combined weld modelling approach is closer to that of the solid model within a range of **5-10%** for the crossbeam and **1-5%** for the stiffener. The focus of this study is on the following two crack locations on OSD:

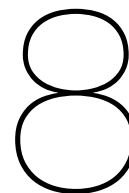
1. Crack in connection between open stiffener to crossbeam - current study

- **Crack in crossbeam near the cope hole parallel to the weld:** For the crack in crossbeam the regular shell model is not suitable for calculation of hot-spot stress from structural intersection point. Huge variation is observed in the ratio of SHSS obtained from the regular shell and solid elements. After weld modelling with shell elements using the combined approach, the mean value of the SHSS ratio data-set is **1.07** and the CV is **5.4%** for the crossbeam.
- **Crack in web of open stiffener parallel to the weld toe:** For the crack in stiffener also the weld modelling is performed using the combined approach which resulted in a mean value of SHSS ratio data-set of **1.02**. The CV of the SHSS ratio is **4%** for the stiffener.

2. Crack in connection between closed stiffener to crossbeam - (Dennis van der Ende [19])

In this study, the same combined approach of weld modelling with shell elements was recommended. A comparison study of the SHSS ratio was also made between the shell+weld combined model and the solid element model.

- **Crack in crossbeam near the soft toe parallel to the weld:** The crack in crossbeam for closed stiffener OSDs is investigated by Dennis van der Ende (Master thesis; MSc candidate, TU Delft) [19]. This crack in the crossbeam started at some distance away from the soft toe, parallel to the weld toe. Weld modelling using the combined approach is investigated and the SHSS ratios are obtained. The SHSS ratio between solid and shell model is found to be **0.79** using the combined weld modelling approach. The CV for the light variant is found to be **10.1%** and for the heavy OSD variant is **6.1%**.
- **Crack in closed stiffener web starting at the lower end of the weld toe:** The crack in stiffener for closed stiffener OSDs is also investigated by Dennis van der Ende (Master thesis; MSc candidate, TU Delft) [19]. The SHSS ratio between solid and shell model is found to be **1.04** using the combined weld modelling approach. The CV for the light variant is found to be **0.8%** and for the heavy OSD variant is **2.2%**.



Conclusions and Recommendations

“Curiosity has its own reason for existence. One cannot help but be in awe when he contemplates the mysteries of eternity, of life, of the marvelous structure of reality. It is enough if one tries merely to comprehend a little of this mystery each day.”

Albert Einstein

In this chapter the conclusions are presented. The end of this chapter will sum up the answers to the research questions in Chapter-1 followed by recommendations for further research.

8.1. Conclusions

In this report, SHSS results on various simple and complex fillet welded details are investigated with shell and solid finite elements. Different weld modelling approaches of the increased thickness method with shell elements have been explored. An answer is found on the following research question:

What is the most consistent method for finding the stress range for fatigue assessment using shell elements compared to the hot-spot stress range using solid elements in modelling the connection between the open stiffener and crossbeam with a cope hole in OSD bridges?

The following conclusions are drawn from this research:

1. From the initial study on a single side fillet welded longitudinal plate joint (detail type a), it can be concluded that with regular shell elements a consistent ratio of SHSS shell/solid cannot be obtained. There is a scatter in the ratio of SHSS between shell and solid elements in the range of **0.96-1.13** for tension and **0.91-1.15** for bending. This scatter is dependent on type of loading and thickness of connected plates. For this detail under bending, the coefficient of variation (CV) of the SHSS ratio reduced from **7.0%** to **4.6%** with a mean value close to 1, after using the weld modelling approach according to IIW [28]. Thus, it can be concluded that the weld modelling approach with shell elements following the IIW recommendations [40] improves the in-plane bending behaviour of detail type a. From the analysis of the transverse cruciform joint under tension (detail type b), it is observed that for such details, the shell models and the shell models with welds cannot be used to calculate the hot-spot stress. This is because, there is no stress concentration at the connection between the plates. Thus, nominal stress approach is recommended for shell models of detail type b.
2. The weld modelling approach of IIW [28] is then extended to the complex fillet welded detail of deck-plate, crossbeam and stiffener with the presence of a cope hole. From the in-plane load cases (LC-1 and LC-3), it can be concluded that the stress profile and the stress gradient of the shell model with welds is similar to that of the solid model. Not only the SHSS value but also the stress at a distance of 30 mm away from weld toe showed a good match between the solid and shell model with welds. Similar behaviour is however, not observed for the out-of-plane load case (LC-2). This is because, the weld modelling approach using shell elements from IIW [28], only improved the in-plane stiffness of the joint and not the out-of-plane stiffness.
3. A parametric study on transverse and longitudinal cruciform joints with different load cases is performed on two geometrical variants. From this analysis, it is found that the combined approach of weld modelling using both the recommendations of IIW and Eriksson together gave a good match of SHSS and deformations when they are compared with the solid model. The stress values from solid model at a distance of 50 mm away from weld toe is also very well captured by the shell model with welds. This is observed for all the standard load cases as well as for combinations of those load cases. Thus, the combined approach of weld modelling using the recommendations of IIW and Eriksson, improved both the in-plane and out-of-plane stiffness for this detail.
4. The parametric study on OSD is divided into two parts: a preliminary parametric study and a detailed parametric study.
 - The influence of the effect of loading and geometry on the SHSS of OSD is studied by performing a preliminary parametric study with heavy and light OSD variants. For the crack in the crossbeam of OSD, it is recommended to define it as a “type-c” hot-spot instead of “type-b” since the stress distribution through the thickness is non-uniform. From this study, it is found that after weld modelling with shell elements using the combined approach of IIW and Eriksson, less scatter is observed in the SHSS ratios. The mean value of SHSS ratio for crossbeam is **1.02** and for stiffener is **1.01** for the reference load cases of the preliminary parametric study. The coefficient of variation (CV) of the crossbeam is **6.8%** and that of the stiffener is around **5.1%**.

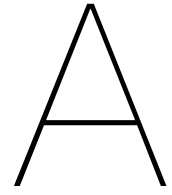
- From the detailed parametric investigation, it is found that SHSS obtained from the light OSD variant is larger compared to the heavy OSD variant by a factor of approximately 3 for both crossbeam and stiffener. The mean value of the SHSS ratio data-set is **1.07** for crossbeam and **1.02** for the stiffener. The coefficient of variation (CV) of the SHSS ratio is **5.4%** for the crossbeam and **4%** for the stiffener. From the stress profiles of the critical points, it is observed that stress gradient of the shell model with the combined weld modelling approach is closer to that of the solid model.

For the details having cope holes in OSD, the normal shell elements are not suitable for fatigue assessment from hot-spot stress method using surface extrapolation. This is due to the insufficient stiffness at the weld region and this can be solved by modelling welds with shell elements to incorporate the additional weld stiffness. The solid elements provided enough accuracy in the determination of hot-spot stress for both simple details, complex details and for the OSD. It is thus concluded that the combined weld modelling technique with shell elements could be used for accurate fatigue life assessment of the investigated detail using hot-spot stress method, where the measure of accuracy is with respect to solid elements.

8.2. Recommendations

Based on the results presented in this report, some aspects which require more detailed investigation have appeared. Those recommendations for further research have been presented in this section.

- Further research is required on calculation of SHSS in case of multi-axial stress state in welded details. In order to correctly use the hot-spot stress to predict multi-axial fatigue strength, it should be resolved into two stress components: one perpendicular to weld toe and the other one parallel to the weld toe. This is because, from this research, it is observed that for bi-axial stress state, some differences occur between the stress perpendicular to weld toe, the maximum principal stress and the minimum principal stress components.
- A detailed investigation of different types of cope holes is required. In this thesis, circular shaped cope holes have been studied. It is recommended to also perform a similar investigation for other shapes and geometries of cope holes to check if the combined weld modelling approach with shell elements give similar improvements in stress results.
- More research on different methods of finding the hot-spot stress apart from surface stress extrapolation is necessary. This thesis is primarily focused on surface stress extrapolation as the procedure could be easily used for validation of numerical models with experimental measurements. However, other methods of determining hot-spot stress should be studied for such details in order to have a comparison with surface stress extrapolation method. These methods include through thickness linearization, Dong method [17][18], the approach proposed by Xiao and Yamada [48] and the one point hot-spot method.
- Some more study on the new approach of weld modelling with shell elements having increased thickness at the weld region is required. This new approach has been preliminarily investigated for the critical locations of OSD in Appendix-K. However, a more detailed investigation is necessary especially for the out-of-plane bending on the OSD.
- Further research on other weld modelling strategies with shell elements is important in order to have greater accuracy for determination of SHSS in comparison to solid elements. This is important as it will result in a lot of saving in computational time and reduce the modelling effort which is always present with solid elements.
- The results of this research show that the combined weld modelling technique with shell elements using the IIW and the Eriksson's method reduce the scatter of the hot-spot stress ratio shell/solid for the investigated detail. In order to check whether this reduction of scatter is also valid for other fatigue details of the OSD, further research is recommended using the combined weld modelling approach with shell elements.



Deformed mesh for shell and solid element models

This chapter displays the deformed meshes of the shell and solid element models for different load cases. A structured mesh was used at the location of interest. Care was taken to limit the amount of distorted elements to a minimum as they tend to have an influence on the stress results.

A.1. Deformed mesh for shell models for different load cases

The deformed mesh and vertical deformation of OSD is shown in Figures A.1-A.4. The scale of deformation is taken as 1:200 and the limits of the deformation contours were taken to be same for both the load cases.

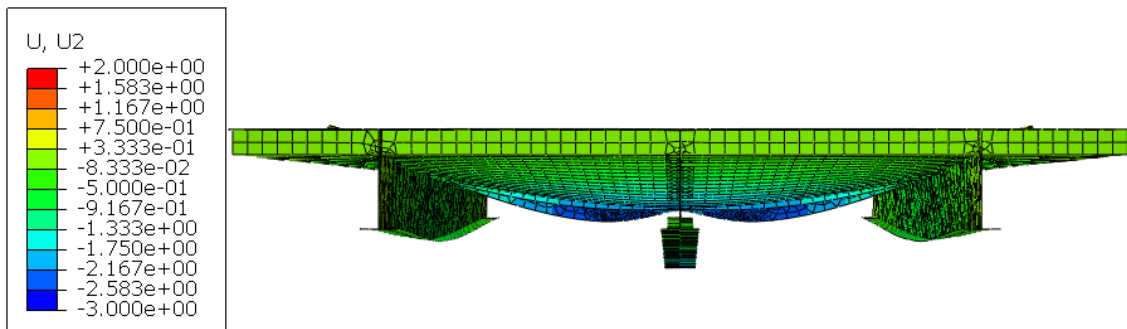


Figure A.1: Deformed mesh of OSD under LC-1 (in-plane loading) for global shell model

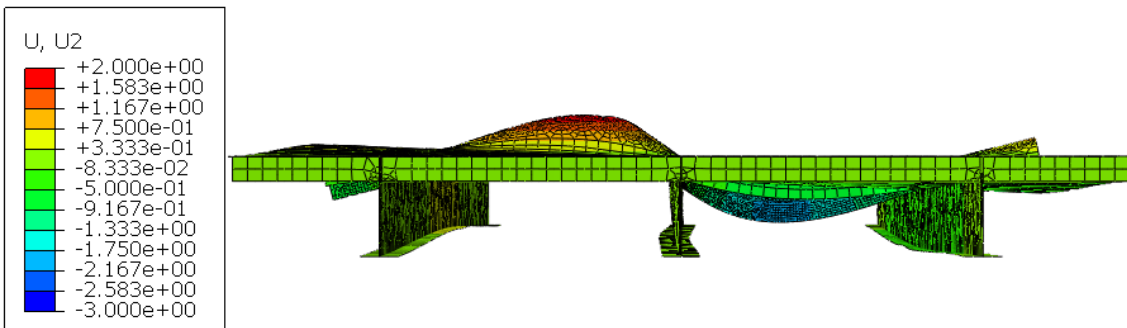


Figure A.2: Deformed mesh of OSD under LC-2 (out-of-plane loading) for global shell model

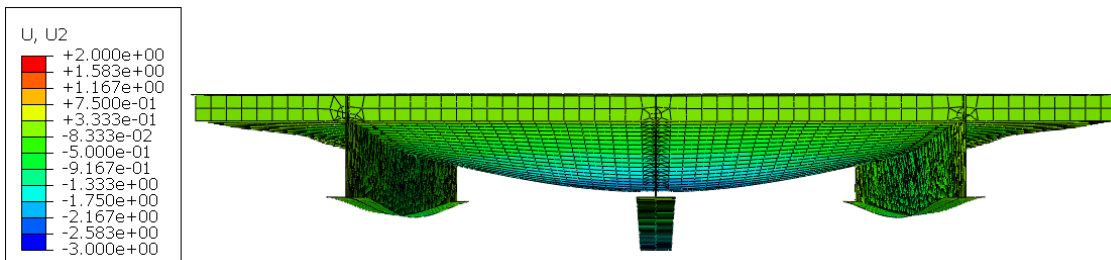


Figure A.3: Deformed mesh of OSD under LC-3a (in-plane loading with local load introduction: load on top of stiffener) for global shell model

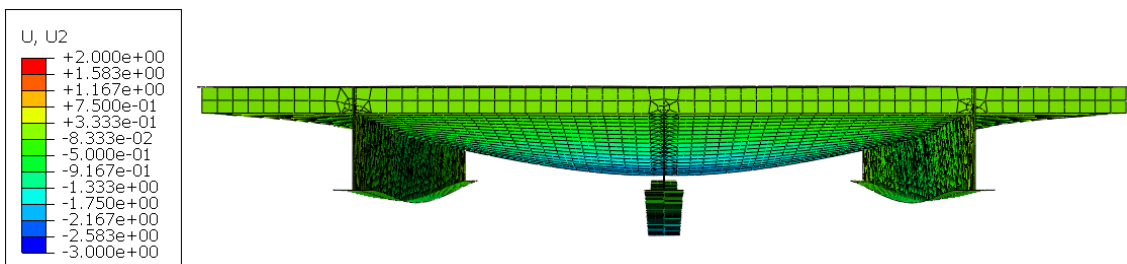


Figure A.4: Deformed mesh of OSD under LC-3b (in-plane loading with local load introduction: load in between two stiffeners) for global shell model

A.2. Deformed mesh for solid models for different load cases

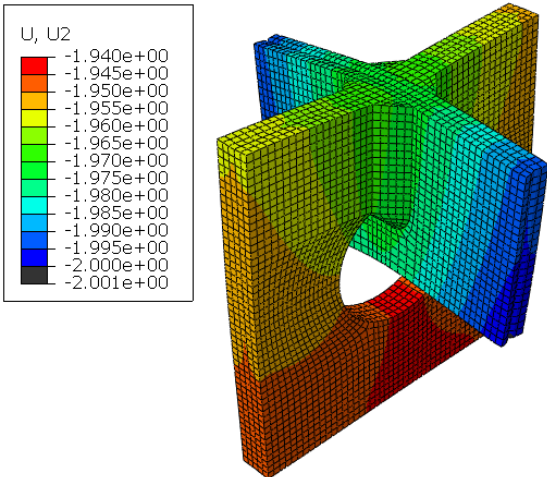


Figure A.5: Deformed mesh of OSD under LC-1 for solid model

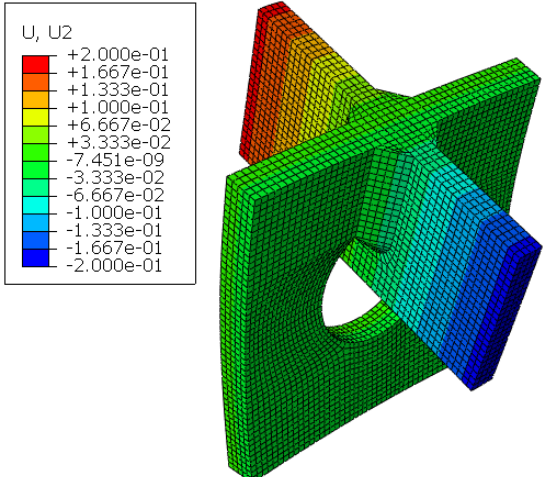


Figure A.6: Deformed mesh of OSD under LC-2 for solid model

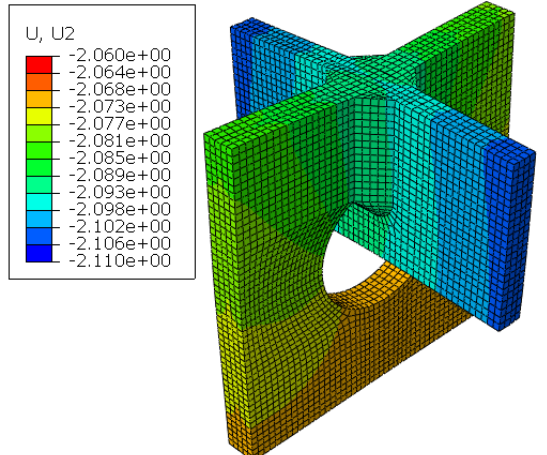
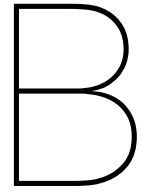


Figure A.7: Deformed mesh of OSD under LC-3a for solid model



Mesh and element sensitivity study for simple fillet welded details

This chapter encapsulates the mesh and element sensitivity study for simple fillet welded details.

B.1. Fillet welded T-joint

Mesh sensitivity with reduced integration for tension

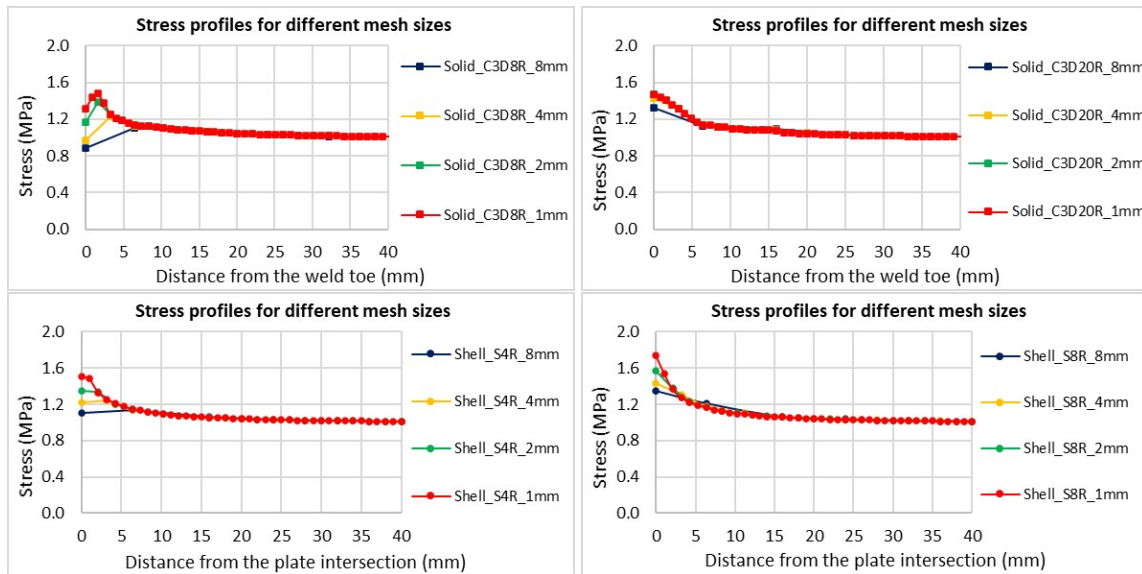


Figure B.1: Mesh sensitivity with reduced integration for tension

Mesh sensitivity with full integration for tension

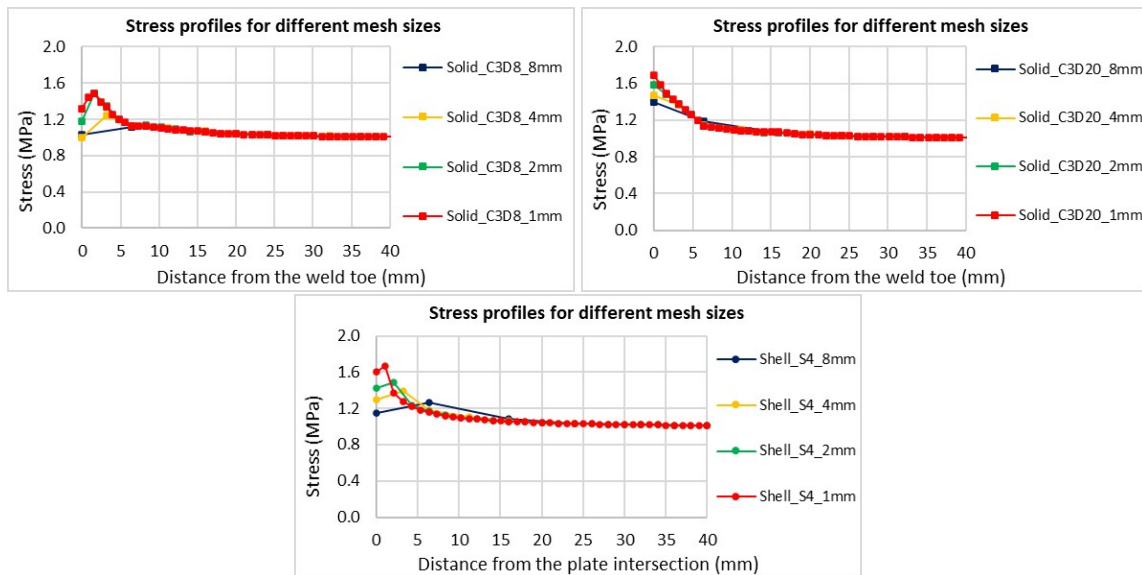


Figure B.2: Mesh sensitivity with full integration for tension

Mesh sensitivity with reduced integration for bending

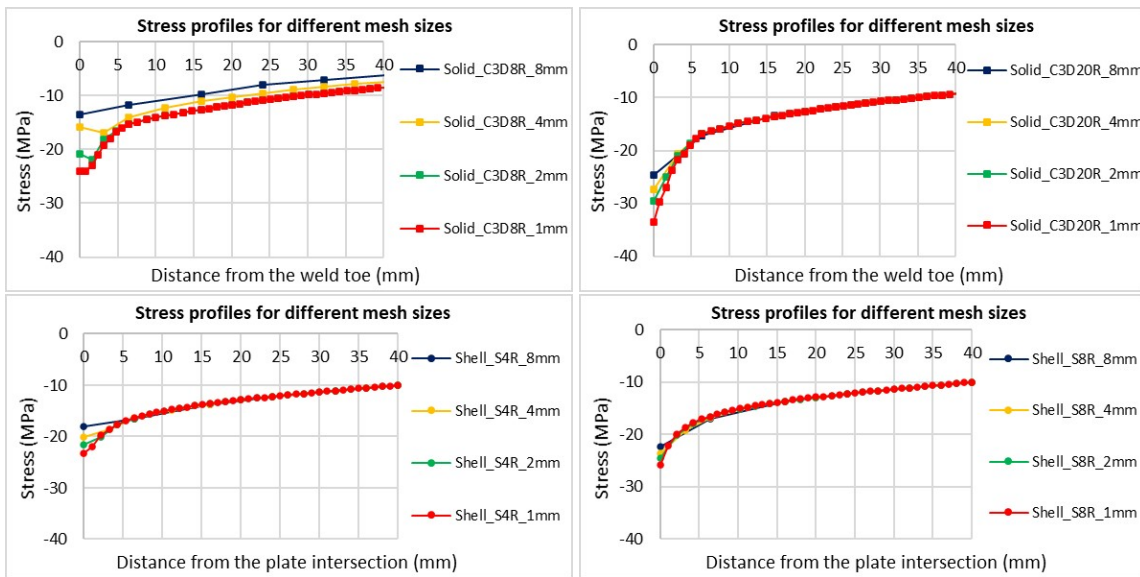


Figure B.3: Mesh sensitivity with reduced integration for bending

Mesh sensitivity with full integration for bending

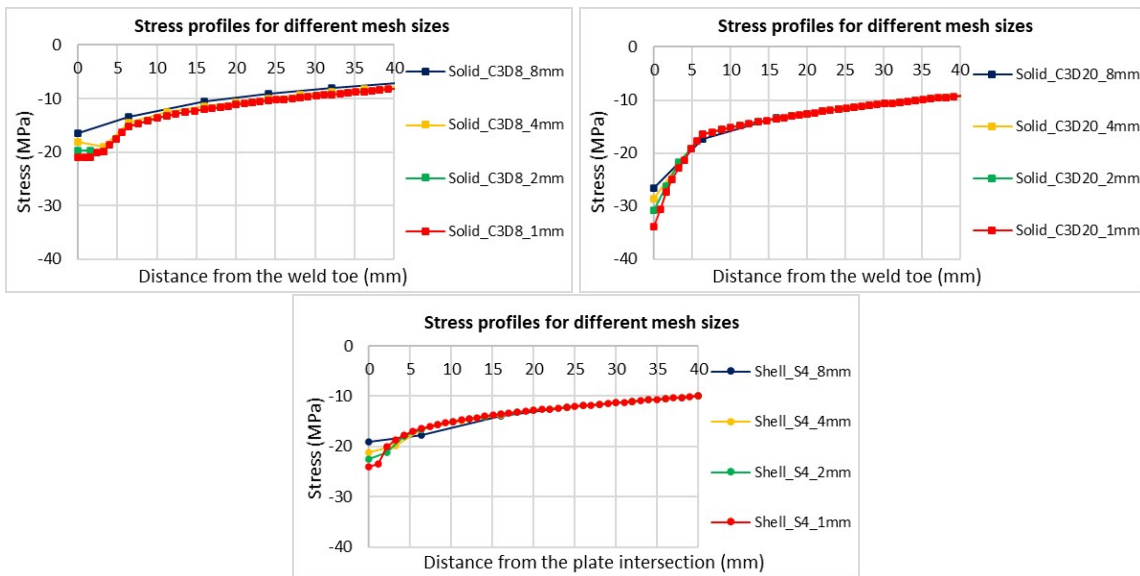


Figure B.4: Mesh sensitivity with full integration for bending

Element type investigation of same mesh size for tension

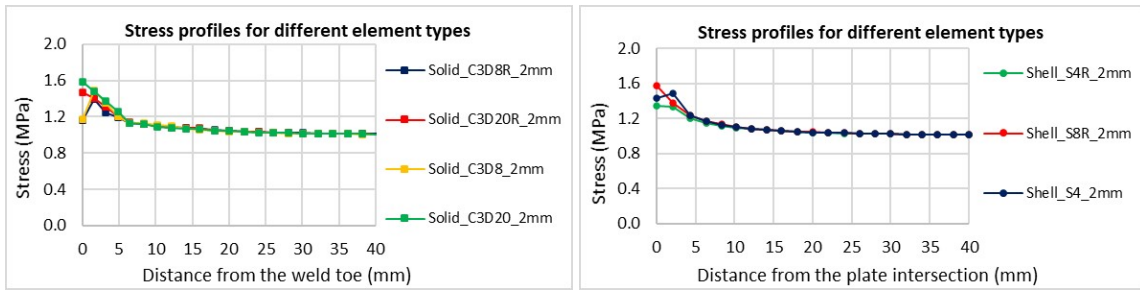


Figure B.5: Element type study with same mesh size of 2 mm for tension

Element type investigation of different mesh sizes for tension

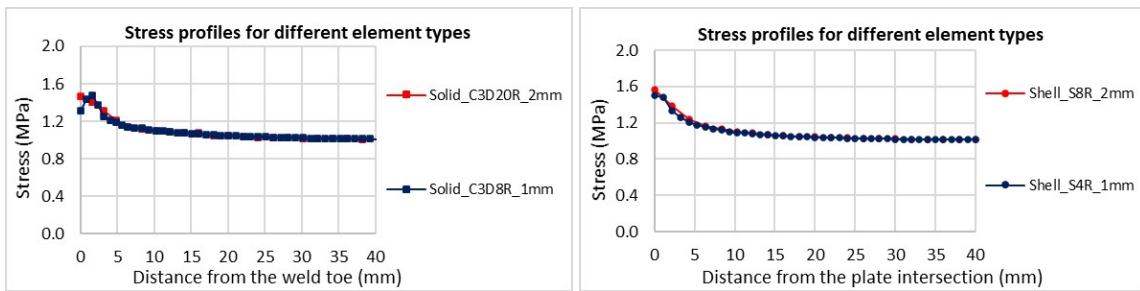


Figure B.6: Element type study with different mesh sizes of 1 mm and 2 mm for tension

Element type investigation of same mesh size for bending

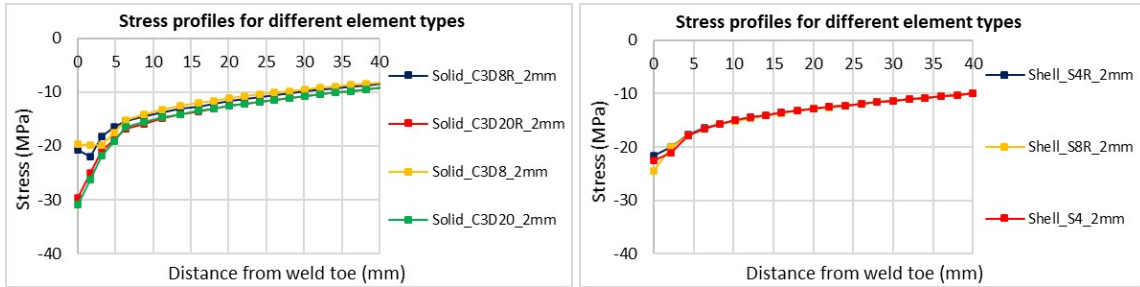


Figure B.7: Element type study with same mesh size of 2 mm for bending

Element type investigation of different mesh size for bending

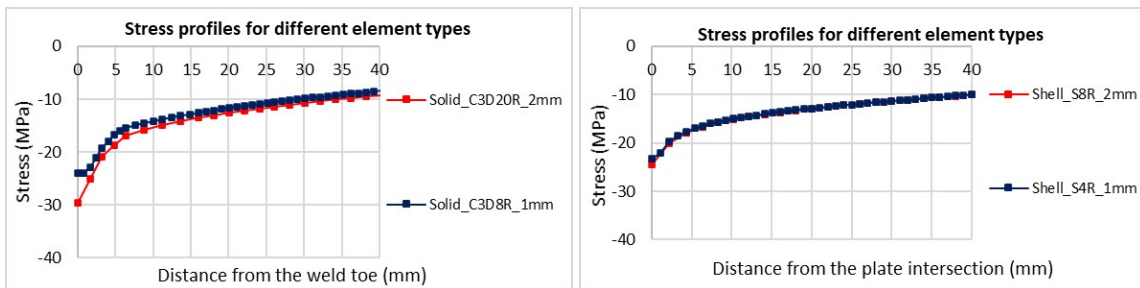


Figure B.8: Element type study with same mesh size of 2 mm for bending

B.2. Fillet welded cruciform joint

Mesh sensitivity with reduced integration for tension

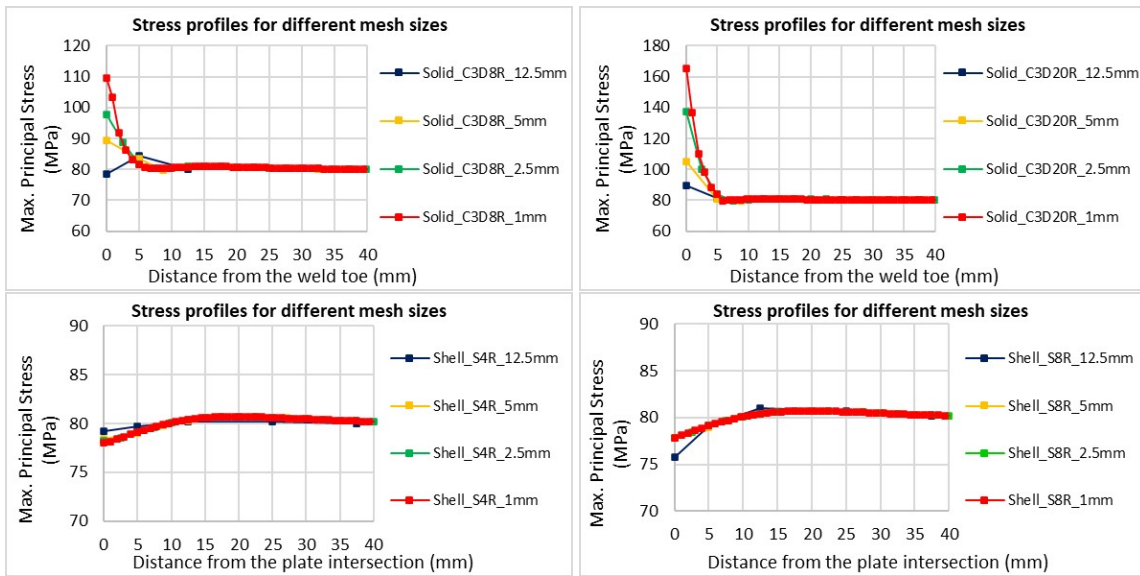


Figure B.9: Mesh sensitivity with reduced integration for tension

Element type investigation for same mesh size

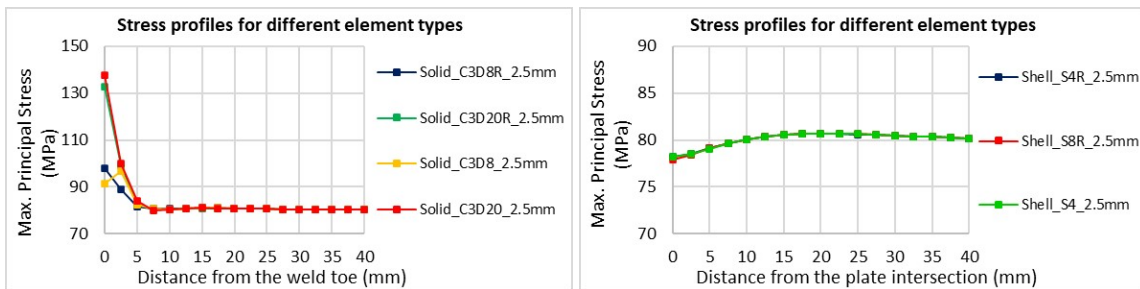
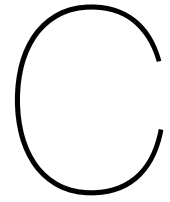


Figure B.10: Element type investigation for tension



Mesh and element sensitivity study for complex fillet welded details

This chapter encapsulates the mesh and element sensitivity study for complex fillet welded details.

C.1. Detail of open-stiffener to crossbeam connection with a cope hole

Mesh sensitivity with the solid model

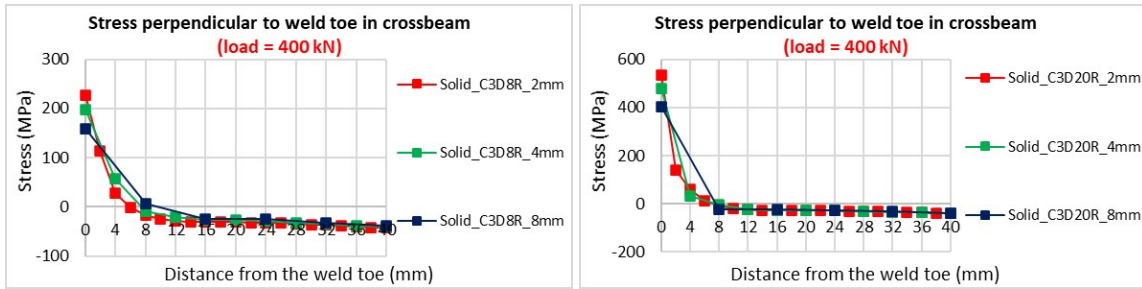


Figure C.1: Stress distribution perpendicular to weld toe for linear and quadratic solid elements of different mesh sizes

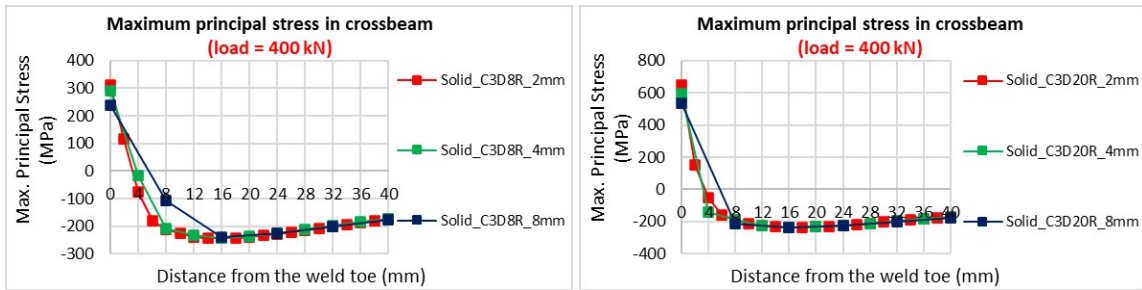


Figure C.2: Maximum principal stress distribution for linear and quadratic solid elements of different mesh sizes

Mesh sensitivity with the shell model

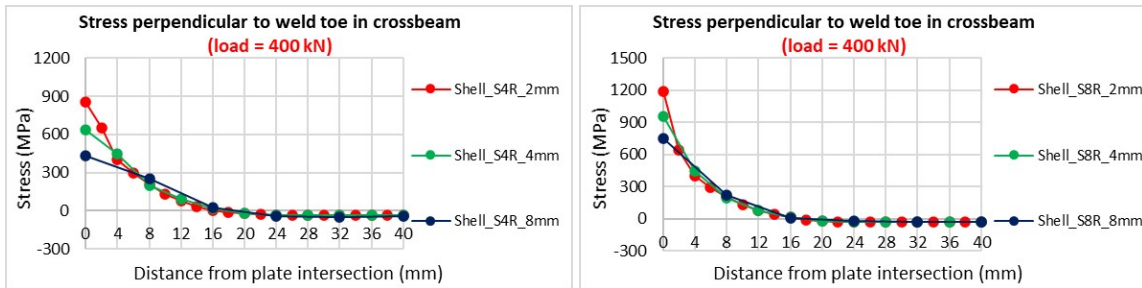


Figure C.3: Stress distribution perpendicular to weld toe for linear and quadratic shell elements of different mesh sizes

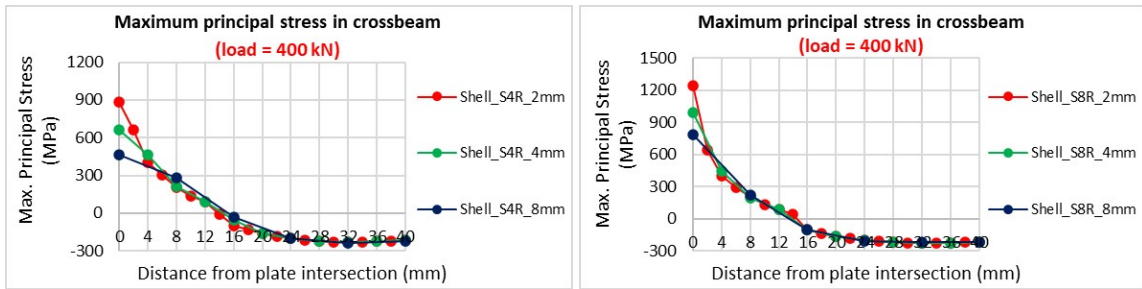


Figure C.4: Maximum principal stress distribution for linear and quadratic shell elements of different mesh sizes

Mesh sensitivity with the shell model with welds according to IIW

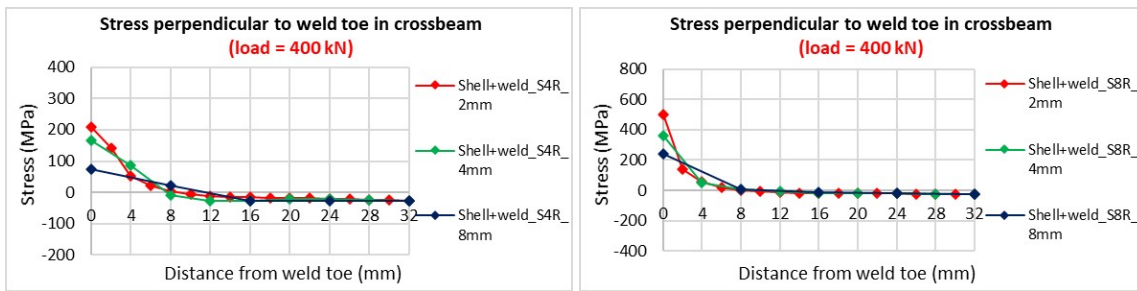


Figure C.5: Stress distribution perpendicular to weld toe for linear and quadratic shell elements with welds having different mesh sizes

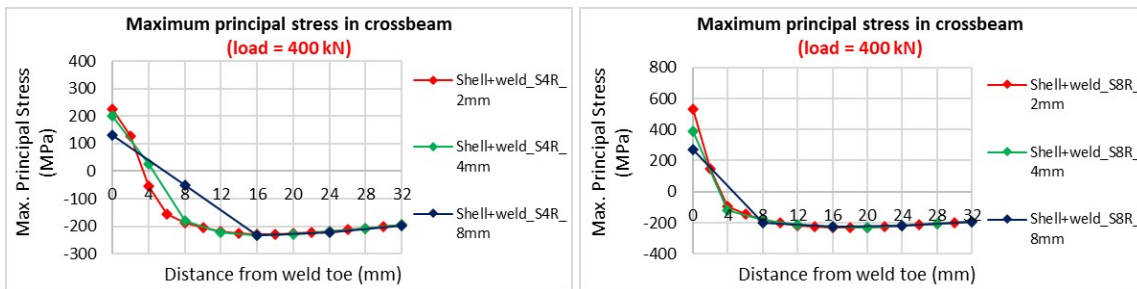


Figure C.6: Maximum principal stress distribution for linear and quadratic shell elements with welds having different mesh sizes

Element type study with the numerical models

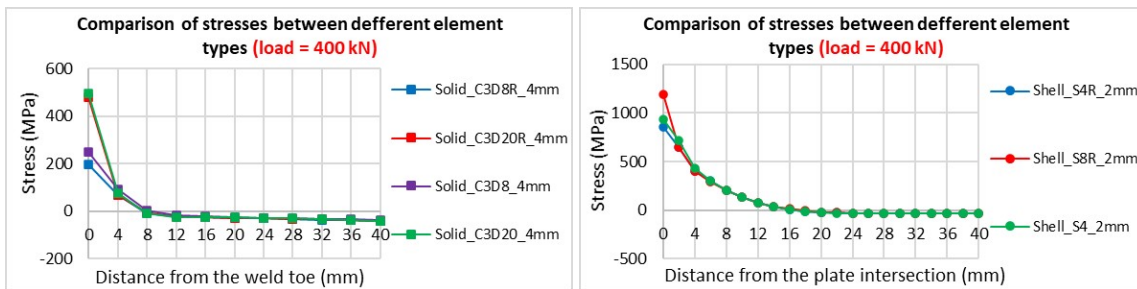


Figure C.7: Stress distribution perpendicular to weld toe of different element types in solid model (left) and shell model (right)

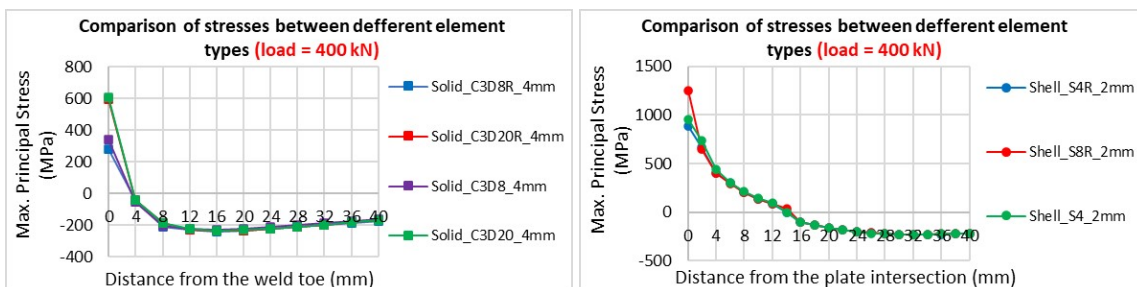
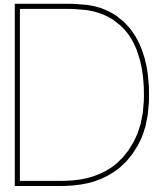


Figure C.8: Maximum principal stress of different element types in solid model (left) and shell model (right)



Mesh and element sensitivity study of the OSD

This chapter encapsulates the mesh and element sensitivity study for an orthotropic steel deck (OSD).

D.1. Mesh sensitivity study on geometry variant-1 (based on old/light OSD)

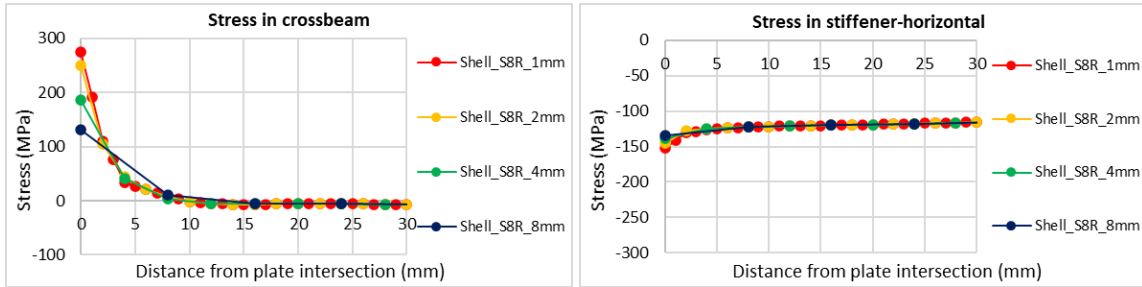


Figure D.1: Mesh sensitivity study with shell elements for geometry variant-1 (old/light OSD) under LC-1

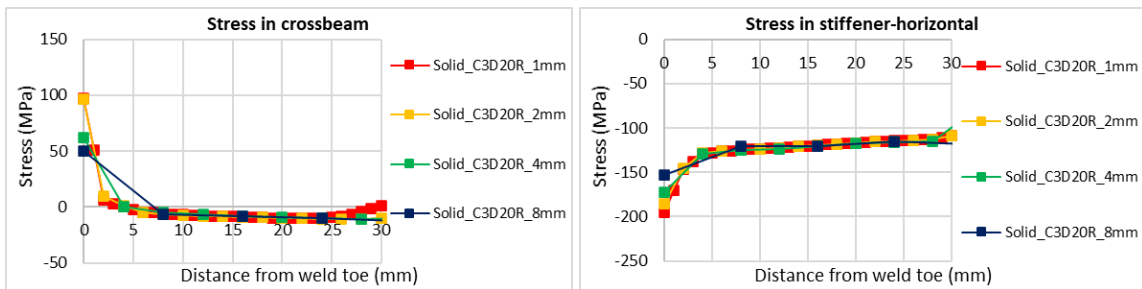


Figure D.2: Mesh sensitivity study with solid elements for geometry variant-1 (old/light OSD) under LC-1

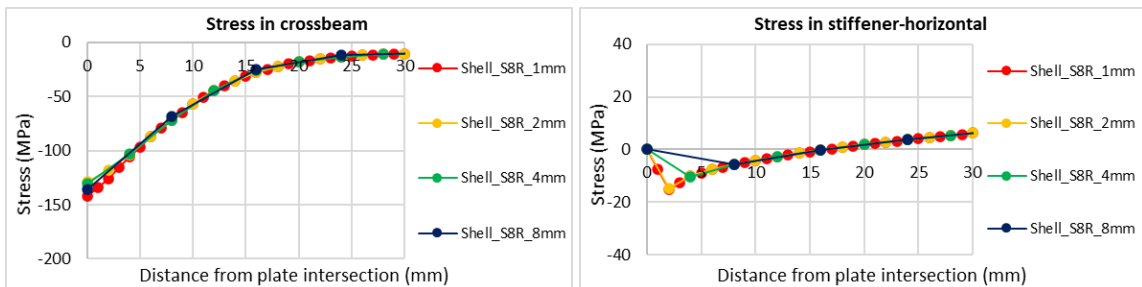


Figure D.3: Mesh sensitivity study with shell elements for geometry variant-1 (old/light OSD) under LC-2

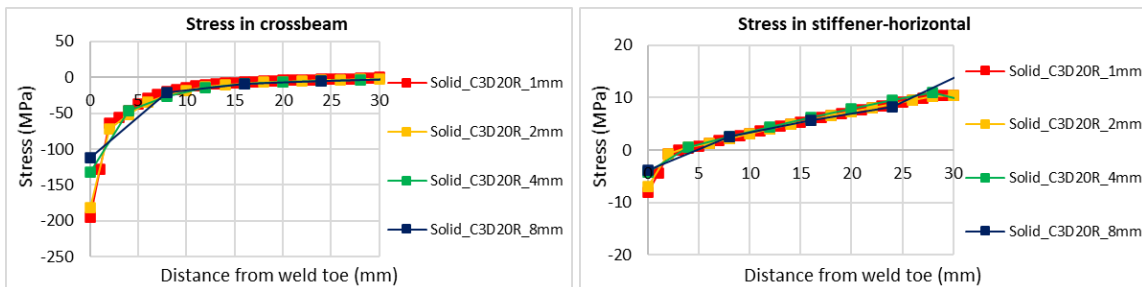


Figure D.4: Mesh sensitivity study with solid elements for geometry variant-1 (old/light OSD) under LC-2

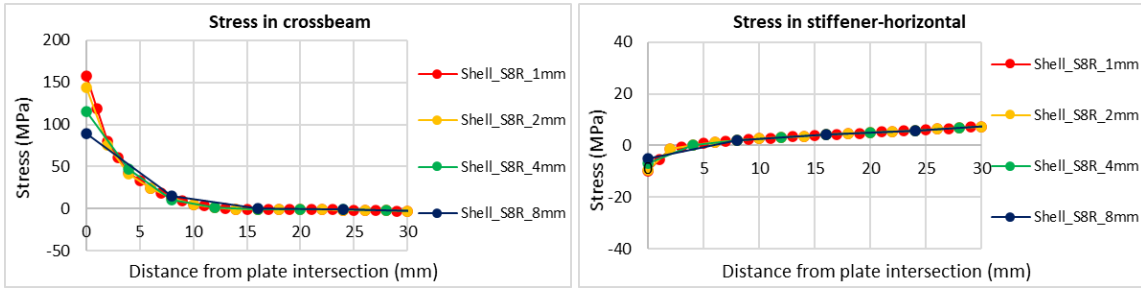


Figure D.5: Mesh sensitivity study with shell elements for geometry variant-1 (old/light OSD) under LC-3a

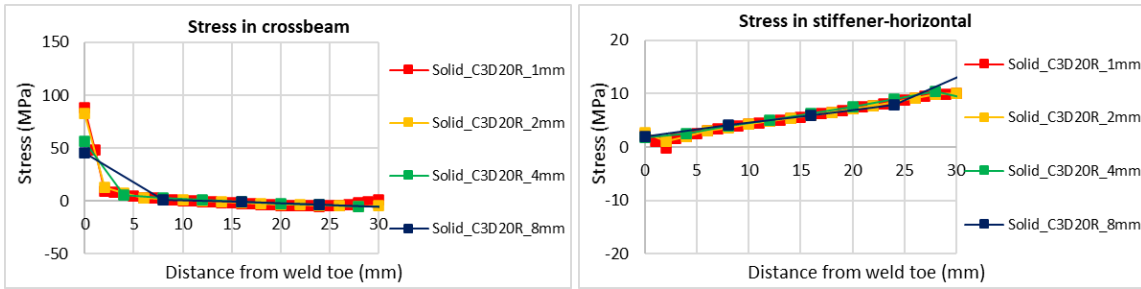


Figure D.6: Mesh sensitivity study with solid elements for geometry variant-1 (old/light OSD) under LC-3a

D.2. Mesh sensitivity study on geometry variant-2 (based on new/heavy OSD)

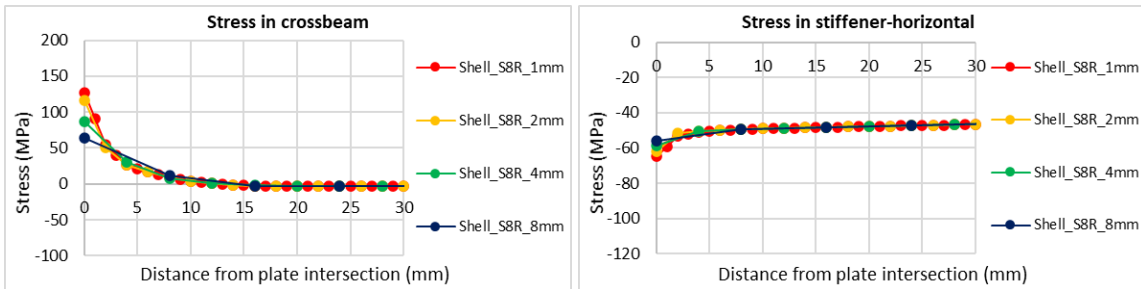


Figure D.7: Mesh sensitivity study with shell elements for geometry variant-2 (new/heavy OSD) under LC-1

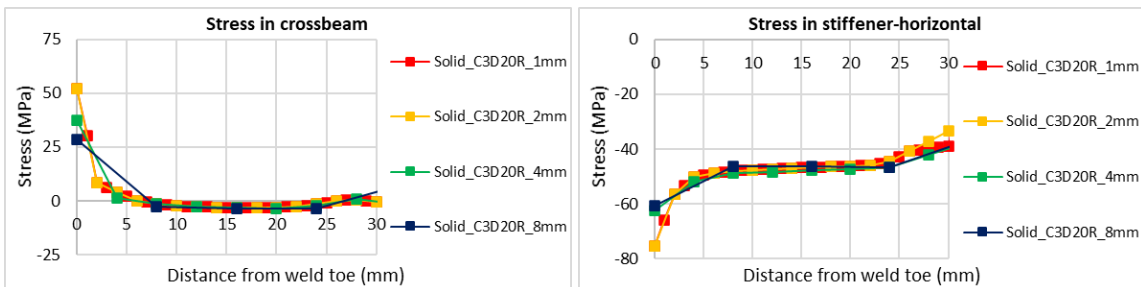


Figure D.8: Mesh sensitivity study with solid elements for geometry variant-2 (new/heavy OSD) under LC-1

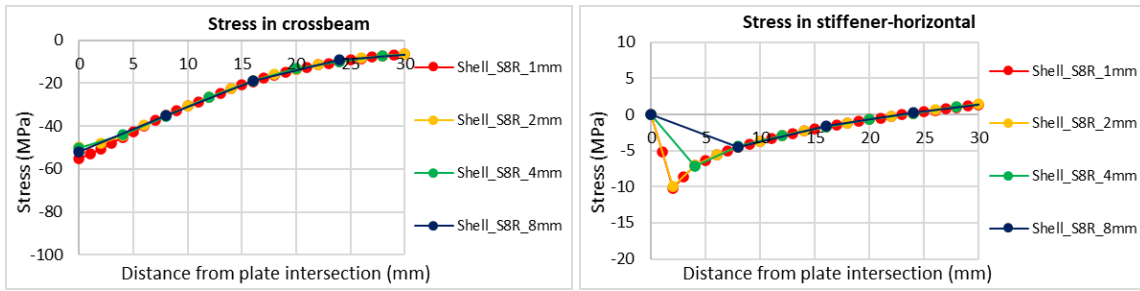


Figure D.9: Mesh sensitivity study with shell elements for geometry variant-2 (new/heavy OSD) under LC-2

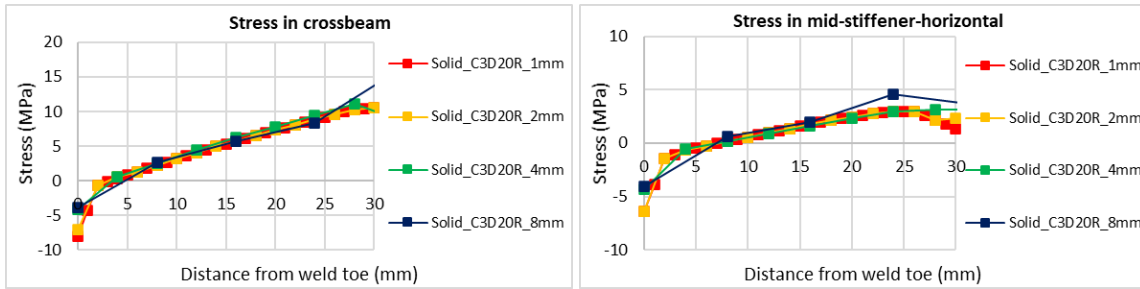


Figure D.10: Mesh sensitivity study with solid elements for geometry variant-2 (new/heavy OSD) under LC-2

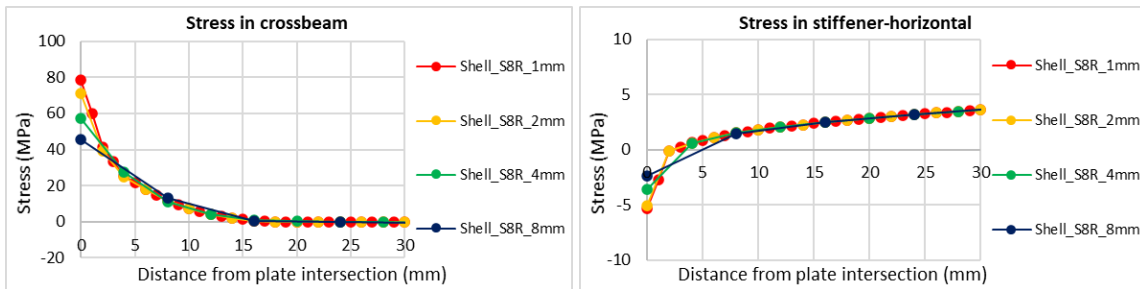


Figure D.11: Mesh sensitivity study with shell elements for geometry variant-2 (new/heavy OSD) under LC-3a

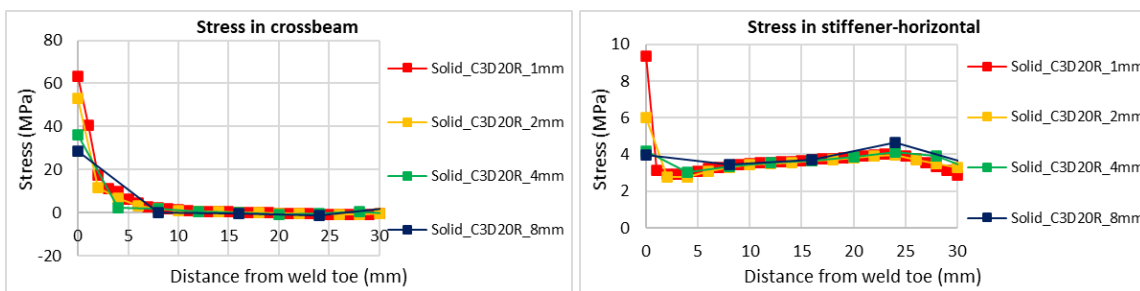
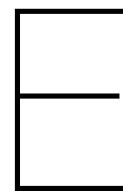


Figure D.12: Mesh sensitivity study with solid elements for geometry variant-2 (new/heavy OSD) under LC-3a



Validation of numerical models

The validation of the complex fillet welded connection of deck-plate, crossbeam and open stiffener with the experimental strain measurements has been presented in this chapter.

E.1. Strain validation of detail of open stiffener-crossbeam with a cope hole

Solid element model: It is observed that the average percentage difference between the strain results from the solid model and the experimental strain measurements is about 9% for the hot-spot region HS1 under a load range of 200 kN. The strain results of the quadratic solid element model are shown below. The stress values are also computed from the strains.

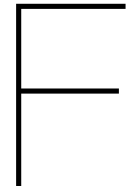
Table E.1: Percentage difference in measure strains between the solid model and experimental measurements at HS1

Strain measurement points - Distance from weld toe (mm)	Test specimen		Solid_C3D20R_4mm		Percentage Difference (%)
	Measured strains along x-direction	Measured stress from strains along x-direction (MPa)	Strain along x-direction	Measured stress from strains along x-direction (MPa)	
4.00	3.2E-04	68.0	3.0E-04	62.2	8%
5.00	3.0E-04	63.0	2.9E-04	61.2	3%
6.00	2.9E-04	60.0	2.9E-04	60.1	0%
7.50	2.6E-04	55.0	2.8E-04	58.5	-6%
8.50	2.5E-04	53.0	2.7E-04	57.4	-8%
9.50	2.5E-04	52.0	2.7E-04	56.4	-9%
10.50	2.4E-04	50.0	2.6E-04	55.4	-11%
11.75	2.2E-04	47.0	2.6E-04	54.2	-15%
13.00	2.2E-04	46.0	2.5E-04	52.7	-14%
14.00	2.1E-04	45.0	2.4E-04	51.4	-14%
				Average	9%

Shell element model with welds using the IIW approach: It is observed that the average percentage difference between the strain results from the shell model with welds according to IIW approach [28] [40] and the experimental strain measurements is about 15% under the hot-spot region HS1 for a load range of 200 kN. The strain results of the quadratic solid element model are shown below. The stress values are also computed from the strains.

Table E.2: Percentage difference in measure strains between the shell model with welds and experimental measurements at HS1

Strain measurement points - Distance from weld toe (mm)	Test specimen		Shell+weld_S8R_2mm		Percentage Difference (%)
	Measured strains along x-direction	Measured stress from strains along x-direction (MPa)	Strain along x-direction	Measured stress from strains along x-direction (MPa)	
4.00	3.2E-04	68.0	3.8E-04	80.2	-18%
5.00	3.0E-04	63.0	3.2E-04	67.1	-6%
6.00	2.9E-04	60.0	2.6E-04	53.9	10%
7.50	2.6E-04	55.0	2.3E-04	47.3	14%
8.50	2.5E-04	53.0	2.1E-04	44.1	17%
9.50	2.5E-04	52.0	2.0E-04	42.1	19%
10.50	2.4E-04	50.0	1.9E-04	40.8	18%
11.75	2.2E-04	47.0	1.9E-04	40.1	15%
13.00	2.2E-04	46.0	1.8E-04	38.6	16%
14.00	2.1E-04	45.0	1.8E-04	37.3	17%
				Average	15%

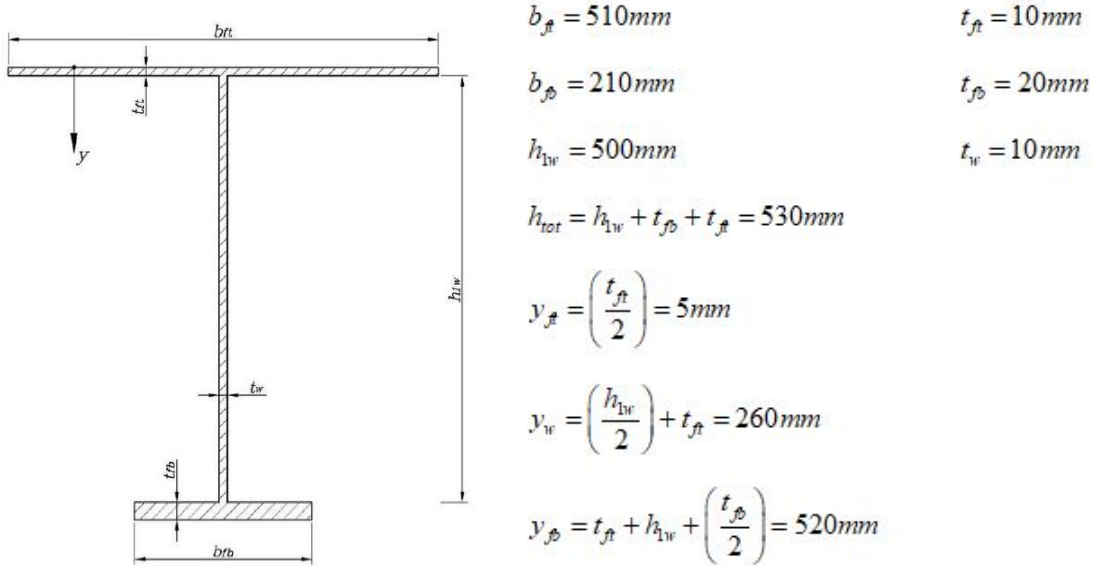


Verification of finite element models

This chapter consists of some preliminary hand calculations for the complex welded detail of deck-plate, crossbeam and open stiffener which is required for the verification of the finite element models.

F.1. Calculation of stresses and beam deflections for verification of FE model of the complex welded detail

Dimensions of the cross section: The dimensions of the test specimen are shown below.



Properties of the cross section

$$A_{beam} = b_{ft}t_{ft} + h_{1w}t_w + b_{fb}t_{fb} = 1.43 \times 10^4 mm^2$$

$$y_{CG} = \left(\frac{b_{ft}t_{ft}y_{ft} + h_{1w}t_w y_w + b_{fb}t_{fb}y_{fb}}{A_{beam}} \right) = 245.42mm$$

$$I_1 = \frac{1}{12} b_{ft}t_{ft}^3 + b_{ft}t_{ft}(y_{CG} - y_{ft})^2 = 2.948 \times 10^8 mm^4$$

$$I_2 = \frac{1}{12} t_w h_{1w}^3 + h_{1w}t_w (y_{CG} - y_w)^2 = 1.052 \times 10^8 mm^4$$

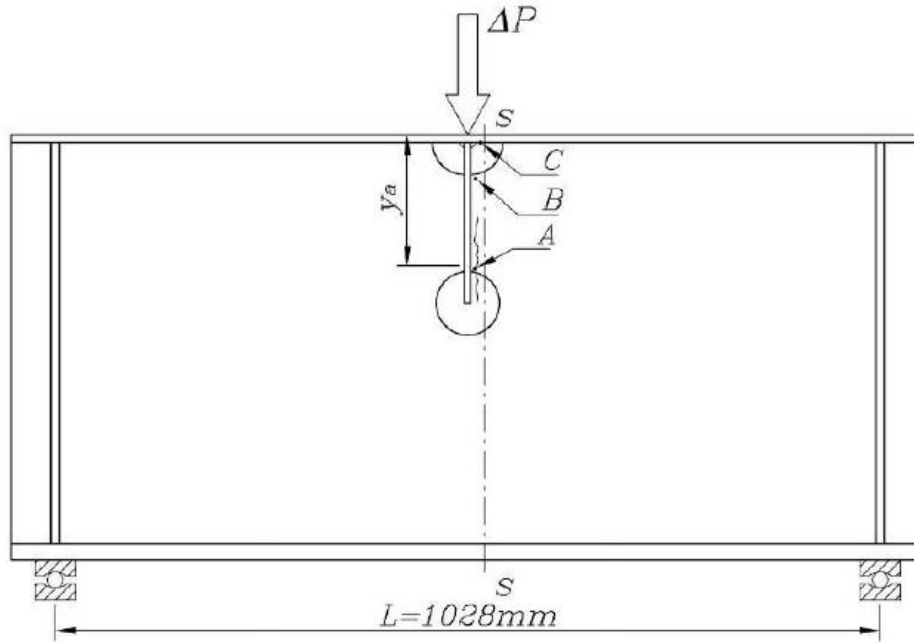
$$I_3 = \frac{1}{12} b_{fb}t_{fb}^3 + b_{fb}t_{fb}(y_{CG} - y_{fb})^2 = 3.168 \times 10^8 mm^4$$

$$I_{beam} = I_1 + I_2 + I_3 = 7.169 \times 10^8 mm^4$$

$$c_{bot} = h_{tot} - y_{CG} = 284.58$$

$$W_{XX} = \left(\frac{I_{beam}}{c_{bot}} \right) = 2.519 \times 10^6 mm^3$$

$$A_{web} = h_{1w}t_w = 5 \times 10^3 mm^2$$



Shear force and moment in the section S-S

$$\Delta P = \begin{pmatrix} 200 \\ 400 \end{pmatrix} \text{kN}$$

$$L_{beam} = 1028\text{mm}$$

$$\Delta V_s = \frac{\Delta P}{2} = \begin{pmatrix} 100 \\ 200 \end{pmatrix} \text{kN}$$

$$\Delta M_s = \Delta P \left(\frac{L_{beam}}{4} \right) = \begin{pmatrix} 51.4 \\ 102.8 \end{pmatrix} \text{kNm}$$

Maximum bending stress in the bottom flange in section S-S

$$\Delta P = \begin{pmatrix} 200 \\ 400 \end{pmatrix} \text{kN}$$

$$L_{beam} = 1028\text{mm}$$

$$\Delta M_s = \Delta P \left(\frac{L_{beam}}{4} \right) = \begin{pmatrix} 51.4 \\ 102.8 \end{pmatrix} \text{kNm}$$

$$\Delta \sigma = \left(\frac{\Delta M_s}{W_{xx}} \right) = \begin{pmatrix} 20.405 \\ 40.810 \end{pmatrix} \text{MPa}$$

Maximum nominal bending stress in the deck plate in section S-S

$$\Delta P = \begin{pmatrix} 200 \\ 400 \end{pmatrix} kN$$

$$L_{beam} = 1028 mm$$

$$\Delta M_S = \Delta P \left(\frac{L_{beam}}{4} \right) = \begin{pmatrix} 51.4 \\ 102.8 \end{pmatrix} kNm$$

$$\Delta \sigma_{Deck} = \left(\frac{\Delta M_S}{\left(\frac{I_{beam}}{y_{CG}} \right)} \right) = \begin{pmatrix} 17.597 \\ 35.194 \end{pmatrix} MPa$$

Maximum deflection at the mid-span

$$E_{steel} = 210 GPa$$

$$\nu_{steel} = 0.3$$

$$G_{steel} = \left(\frac{E_{steel}}{2(1 + \nu_{steel})} \right) = 80.769 GPa$$

$$\delta_{s,flexure} = \left(\frac{\Delta P L_{beam}^3}{48 E_{steel} I_{beam}} \right) = \begin{pmatrix} 0.03 \\ 0.06 \end{pmatrix} mm$$

$$k = \left(\frac{A_{web}}{A_{beam}} \right) = 0.35$$

$$\delta_{s,shear} = \left(\frac{\Delta P L_{beam}}{4 k G_{steel} A_{beam}} \right) = \begin{pmatrix} 0.127 \\ 0.255 \end{pmatrix} mm$$

$$\delta_s = \delta_{s,flexure} + \delta_{s,shear} = \begin{pmatrix} 0.03 \\ 0.06 \end{pmatrix} + \begin{pmatrix} 0.127 \\ 0.255 \end{pmatrix} = \begin{pmatrix} 0.157 \\ 0.315 \end{pmatrix} mm$$

F.2. Verification of finite element model

Table F.1 shows the maximum deflection at the mid-span and the sum of support reactions for the numerical models of the complex welded detail under a load range of 400 kN in-plane loading.

Table F.1: Verification of maximum deformation and equilibrium check for an applied load of 400 kN

Model	Mesh type	Mesh size (mm)	Element type	$\delta_{\text{max_mid_span}}$ (mm)	% difference from hand calculation	Sum of support reactions (kN)
Shell	Coarse	4	S8R	0.320	1.6%	400.000
Shell	Fine	1	S8R	0.310	-1.6%	400.000
Solid	Coarse	4	C3D20R	0.300	-4.8%	399.996
Solid	Fine	1	C3D20R	0.305	-3.2%	399.996



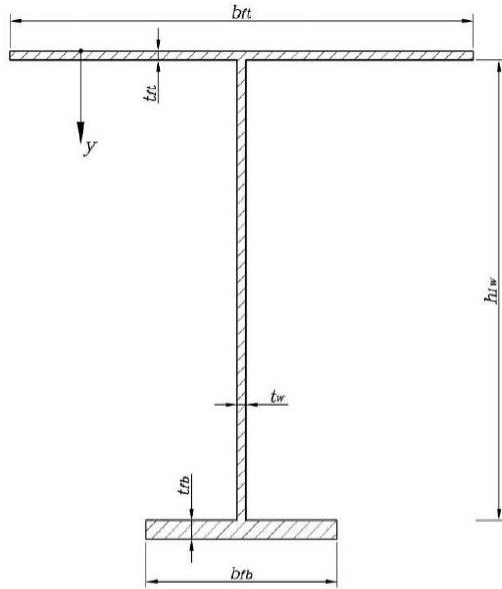
Calculations for nominal stress method

This chapter presents the fatigue damage calculation for the complex welded detail of deck-plate, cross-beam and open stiffener, using the Palmgren Miner's rule as had been discussed in Chapter-2 using the nominal stress method.

G.1. Fatigue life assessment based on nominal stress method for complex welded joint

The calculation is based on chapter 9 of Eurocode 3. The detail category investigated is 56 based on Table 8.9 (orthotropic decks with open stringers) of the Eurocode [2].

Dimensions of the cross-section



$$b_{ft} = 510 \text{ mm}$$

$$t_{fb} = 20 \text{ mm}$$

$$b_{fb} = 210 \text{ mm}$$

$$t_{ft} = 10 \text{ mm}$$

$$h_{1w} = 500 \text{ mm}$$

$$t_w = 10 \text{ mm}$$

$$y_{ft} = \left(\frac{t_{ft}}{2} \right) = 5 \text{ mm}$$

$$y_w = \left(\frac{h_{1w}}{2} \right) + t_{ft} = 260 \text{ mm}$$

$$y_{fb} = t_{ft} + h_{1w} + \left(\frac{t_{fb}}{2} \right) = 520 \text{ mm}$$

Properties of the cross-section

$$A_{beam} = b_{ft} t_{ft} + h_{1w} t_w + b_{fb} t_{fb} = 1.43 \times 10^4 \text{ mm}^2$$

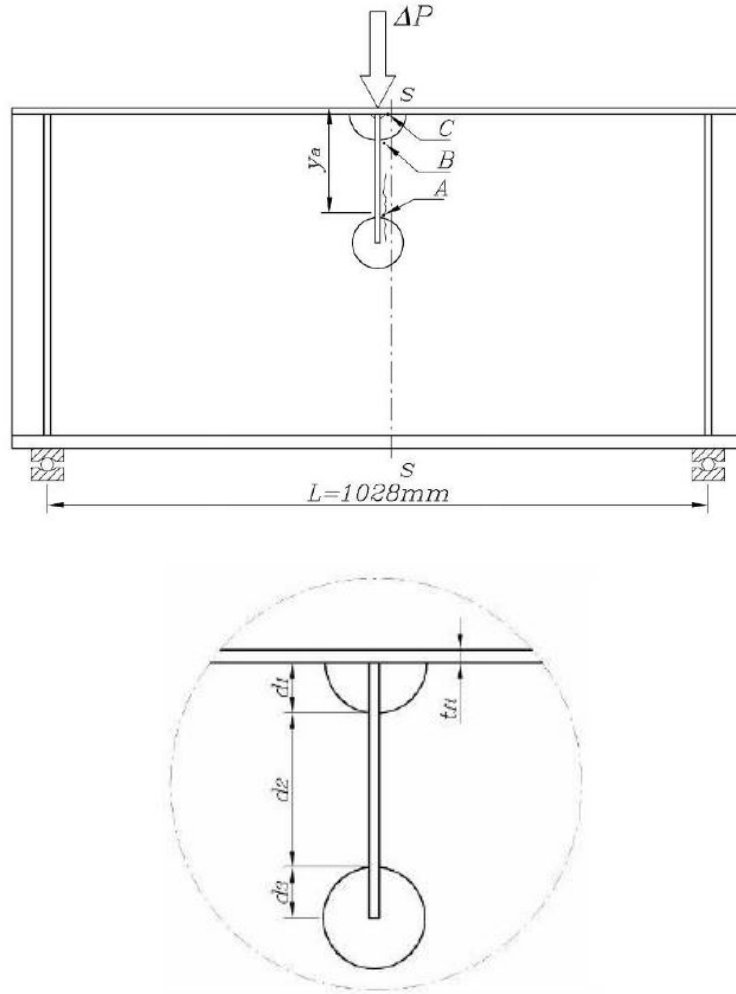
$$y_{CG} = \left(\frac{b_{ft} t_{ft} y_{ft} + h_{1w} t_w y_w + b_{fb} t_{fb} y_{fb}}{A_{beam}} \right) = 245.42 \text{ mm}$$

$$I_1 = \frac{1}{12} b_{ft} t_{ft}^3 + b_{ft} t_{ft} (y_{CG} - y_{ft})^2 = 2.948 \times 10^8 \text{ mm}^4$$

$$I_2 = \frac{1}{12} t_w h_{1w}^3 + h_{1w} t_w (y_{CG} - y_w)^2 = 1.052 \times 10^8 \text{ mm}^4$$

$$I_3 = \frac{1}{12} b_{fb} t_{fb}^3 + b_{fb} t_{fb} (y_{CG} - y_{fb})^2 = 3.168 \times 10^8 \text{ mm}^4$$

$$I = I_1 + I_2 + I_3 = 7.169 \times 10^8 \text{ mm}^4$$



$$d_1 = 40 \text{ mm}$$

$$d_2 = 120 \text{ mm}$$

$$d_3 = 40 \text{ mm}$$

$$y_A = d_1 + d_2 + t_{fl} = 170 \text{ mm} \quad (\text{Location of the cracking point 'A' is section S-S})$$

$$y_B = d_1 + t_{fl} = 50 \text{ mm} \quad (\text{Location of the cracking point 'B' is section S-S})$$

$$y_C = t_{fl} = 10 \text{ mm} \quad (\text{Location of the cracking point 'C' is section S-S})$$

$$A_{net,S} = A_{beam} - (d_1 + 2d_3)t_w = 1.31 \times 10^4 \text{ mm}^2$$

$$y_{CG,red} = \left(\frac{b_{fl} t_{fl} y_{fl} + h_{tw} t_w y_w - d_1 t_w \left(t_{fl} + \frac{d_1}{2} \right) - 2d_3 t_w (t_{fl} + d_1 + d_2 + d_3) + b_{fl} t_{fl} y_{fl}}{A_{net,S}} \right) = 254.16 \text{ mm}$$

$$I_{1,SS} = \frac{1}{12} b_{\beta} t_{\beta}^3 + b_{\beta} t_{\beta} (y_{CG,red} - y_{\beta})^2 = 3.167 \times 10^8 \text{ mm}^4$$

$$I_{2,SS} = \frac{1}{12} t_w h_{1w}^3 + h_{1w} t_w (y_{CG,red} - y_w)^2 = 1.043 \times 10^8 \text{ mm}^4$$

$$I_{3,SS} = \frac{1}{12} b_{\beta} t_{\beta}^3 + b_{\beta} t_{\beta} (y_{CG,red} - y_{\beta})^2 = 2.970 \times 10^8 \text{ mm}^4$$

$$I_{4,SS} = - \left[\frac{1}{12} t_w d_1^3 + d_1 t_w \left(t_{\beta} + \frac{d_1}{2} - y_{CG,red} \right)^2 \right] = -2.015 \times 10^7 \text{ mm}^4$$

$$I_{5,SS} = - \left[\frac{1}{12} t_w (2d_3)^3 + 2d_3 t_w \left(t_{\beta} + d_1 + d_2 + d_3 - y_{CG,red} \right)^2 \right] = -1.987 \times 10^7 \text{ mm}^4$$

$$I_{net,s} = I_{1,SS} + I_{2,SS} + I_{3,SS} + I_{4,SS} + I_{5,SS} = 6.958 \times 10^8 \text{ mm}^4$$

$$W_{net,S,A} = \frac{I_{net,s}}{y_{CG,red} - y_A} = 8.268 \times 10^6 \text{ mm}^3$$

$$W_{net,S,B} = \frac{I_{net,s}}{y_{CG,red} - y_B} = 3.408 \times 10^6 \text{ mm}^3$$

$$W_{net,S,C} = \frac{I_{net,s}}{y_{CG,red} - y_C} = 2.850 \times 10^6 \text{ mm}^3$$

$$A_{w,net,s} = (h_{1w} - d_1 - 2d_3) t_w = 3.8 \times 10^3 \text{ mm}^2$$

Shear force and bending moment in section S-S

$$\Delta P = \begin{pmatrix} 200 \\ 400 \end{pmatrix} \text{ kN}$$

$$L_{beam} = 1028 \text{ mm}$$

$$\Delta V_s = \frac{\Delta P}{2} = \begin{pmatrix} 100 \\ 200 \end{pmatrix} \text{ kN}$$

$$\Delta M_s = \Delta P \left(\frac{L_{beam}}{4} \right) = \begin{pmatrix} 51.4 \\ 102.8 \end{pmatrix} \text{ kNm}$$

Fatigue classes for the assessment points in section S-S: The point A and B belong to Fatigue Class 56 (Table 8.9, second detail category) and point C belong to Fatigue Class 80 (Table 8.4, first detail category) [2].

Calculation of fatigue damage in point 'A'

$$\Delta\sigma_A = \left(\frac{\Delta M_S}{W_{net.S.A}} \right) = \left(\frac{6.217}{12.434} \right) MPa$$

$$\Delta\tau_A = \left(\frac{\Delta V_S}{A_{v.net.S}} \right) = \left(\frac{26.316}{52.632} \right) MPa$$

$$\Delta\sigma_{eq.A} = \frac{1}{2} \left(\Delta\sigma_A + \sqrt{\Delta\sigma_A^2 + 4\Delta\tau_A^2} \right) = \left(\frac{29.607}{59.214} \right) MPa$$

The total damage has to be less than 100% ($D \leq 1$)

The partial factors are set to be one to calculate the real fatigue life without any safety margin

$$\gamma_{Mf} = 1 \quad \gamma_{Ff} = 1$$

$$\Delta\sigma_{C.A} = 56 MPa$$

$$\Delta\sigma_{D.A} = \left(\frac{2}{5} \right)^{1/3} \Delta\sigma_{C.A} = 41.261 MPa$$

$$\Delta\sigma_{L.A} = \left(\frac{5}{100} \right)^{1/5} \Delta\sigma_{D.A} = 22.664 MPa$$

$$N_{A1} = \infty \quad \text{if} \quad \gamma_{Ff} \Delta\sigma_{eq.A1} < \frac{\Delta\sigma_{L.A}}{\gamma_{Mf}}$$

$$N_{A1} = 5 \times 10^6 \left(\frac{\left(\frac{\Delta\sigma_{D.A}}{\gamma_{Mf}} \right)}{\gamma_{Ff} \Delta\sigma_{eq.A1}} \right)^3 \quad \text{if} \quad \gamma_{Ff} \Delta\sigma_{eq.A1} \geq \frac{\Delta\sigma_{D.A}}{\gamma_{Mf}}$$

$$N_{A1} = 5 \times 10^6 \left(\frac{\left(\frac{\Delta\sigma_{D.A}}{\gamma_{Mf}} \right)}{\gamma_{Ff} \Delta\sigma_{eq.A1}} \right)^5 \quad \text{if} \quad \frac{\Delta\sigma_{L.A}}{\gamma_{Mf}} \leq \gamma_{Ff} \Delta\sigma_{eq.A1} \leq \frac{\Delta\sigma_{D.A}}{\gamma_{Mf}}$$

$$N_A = \left(\frac{2.628 \times 10^7}{1.692 \times 10^6} \right)$$

$$n = \left(\frac{5 \times 10^6}{3.8 \times 10^5} \right)$$

$$\Delta D_A = \left(\frac{n_i}{N_{A1}} \right) = \left(\frac{0.190}{0.225} \right)$$

$$\sum \Delta D_A = 0.415$$

Calculation of fatigue damage in point 'B'

$$\Delta\sigma_B = \left(\frac{\Delta M_S}{W_{net.S.B}} \right) = \left(\frac{15.081}{30.163} \right) MPa$$

$$\Delta\tau_B = \left(\frac{\Delta V_S}{A_{net.S}} \right) = \left(\frac{26.316}{52.632} \right) MPa$$

$$\Delta\sigma_{eq.B} = \frac{1}{2} \left(\Delta\sigma_B + \sqrt{\Delta\sigma_B^2 + 4\Delta\tau_B^2} \right) = \left(\frac{34.916}{69.831} \right) MPa$$

The total damage has to be less than 100% ($D \leq 1$)

The partial factors are set to be one to calculate the real fatigue life without any safety margin

$$\gamma_{Mf} = 1 \quad \gamma_{Ff} = 1$$

$$\Delta\sigma_{C.B} = 56 MPa$$

$$\Delta\sigma_{D.B} = \left(\frac{2}{5} \right)^{1/5} \Delta\sigma_{C.B} = 41.261 MPa$$

$$\Delta\sigma_{L.B} = \left(\frac{5}{100} \right)^{1/5} \Delta\sigma_{D.B} = 22.664 MPa$$

$$N_{B,1} = \infty \quad \text{if} \quad \gamma_{Ff} \Delta\sigma_{eq,B,1} < \frac{\Delta\sigma_{L,B}}{\gamma_{Mf}}$$

$$N_{B,1} = 5 \times 10^6 \left(\frac{\left(\frac{\Delta\sigma_{D,B}}{\gamma_{Mf}} \right)}{\gamma_{Ff} \Delta\sigma_{eq,B,1}} \right)^3 \quad \text{if} \quad \gamma_{Ff} \Delta\sigma_{eq,B,1} \geq \frac{\Delta\sigma_{D,B}}{\gamma_{Mf}}$$

$$N_{B,1} = 5 \times 10^6 \left(\frac{\left(\frac{\Delta\sigma_{D,B}}{\gamma_{Mf}} \right)}{\gamma_{Ff} \Delta\sigma_{eq,B,1}} \right)^5 \quad \text{if} \quad \frac{\Delta\sigma_{L,B}}{\gamma_{Mf}} \leq \gamma_{Ff} \Delta\sigma_{eq,B,1} \leq \frac{\Delta\sigma_{D,B}}{\gamma_{Mf}}$$

$$N_B = \left(\frac{1.152 \times 10^7}{1.031 \times 10^6} \right)$$

$$n = \left(\frac{5 \times 10^6}{3.8 \times 10^5} \right)$$

$$\Delta D_B = \left(\frac{n_i}{N_{B,1}} \right) = \left(\frac{0.434}{0.368} \right)$$

$$\sum \Delta D_B = 0.802$$

Calculation of fatigue damage in point 'C'

Only direct stress acts on the detail

$$\Delta\sigma_C = \left(\frac{\Delta M_s}{W_{net.S.C.}} \right) = \left(\frac{18.036}{36.073} \right) MPa$$

$$\Delta\sigma_{C.C.} = 80 MPa$$

$$\Delta\sigma_{D.C.} = \left(\frac{2}{5} \right)^{1/3} \Delta\sigma_{C.C.} = 58.95 MPa$$

$$\Delta\sigma_{L.C.} = \left(\frac{5}{100} \right)^{1/3} \Delta\sigma_{D.C.} = 32.38 MPa$$

The total damage has to be less than 100% ($D \leq 1$)

The partial factors are set to be one to calculate the real fatigue life without any safety margin

$$\gamma_{Mf} = 1 \quad \gamma_{Ff} = 1$$

$$N_{C.I} = \infty \quad \text{if} \quad \gamma_{Ff} \Delta\sigma_{C.I} < \frac{\Delta\sigma_{L.C.}}{\gamma_{Mf}}$$

$$N_{C.I} = 5 \times 10^6 \left(\frac{\left(\frac{\Delta\sigma_{D.C.}}{\gamma_{Mf}} \right)}{\gamma_{Ff} \Delta\sigma_{C.I}} \right)^3 \quad \text{if} \quad \gamma_{Ff} \Delta\sigma_{C.I} \geq \frac{\Delta\sigma_{D.C.}}{\gamma_{Mf}}$$

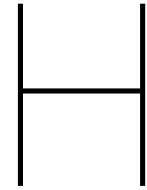
$$N_{C.I} = 5 \times 10^6 \left(\frac{\left(\frac{\Delta\sigma_{D.C.}}{\gamma_{Mf}} \right)}{\gamma_{Ff} \Delta\sigma_{C.I}} \right)^5 \quad \text{if} \quad \frac{\Delta\sigma_{L.C.}}{\gamma_{Mf}} \leq \gamma_{Ff} \Delta\sigma_{C.I} \leq \frac{\Delta\sigma_{D.C.}}{\gamma_{Mf}}$$

$$N_C = \left(\begin{array}{c} \infty \\ 5.83 \times 10^7 \end{array} \right)$$

$$n = \left(\begin{array}{c} 5 \times 10^6 \\ 3.8 \times 10^5 \end{array} \right)$$

$$\Delta D_C = \left(\frac{n_i}{N_{R,i}} \right) = \left(\begin{array}{c} 0 \\ 0.0065 \end{array} \right)$$

$$\sum \Delta D_C = 0.0065$$



SHSS based on maximum principal stress for OSD

In this chapter, the SHSS values are computed based on the maximum principal stress for the orthotropic steel deck (OSD). At first the reference load cases are investigated according to the preliminary parameter study. At a later stage, the critical points based on SHSS influence lines of three transverse axle load positions are studied.

H.1. Study on reference load cases LC1, LC2, LC3a and LC3b

Load case 1: Pure in-plane behaviour of the crossbeam

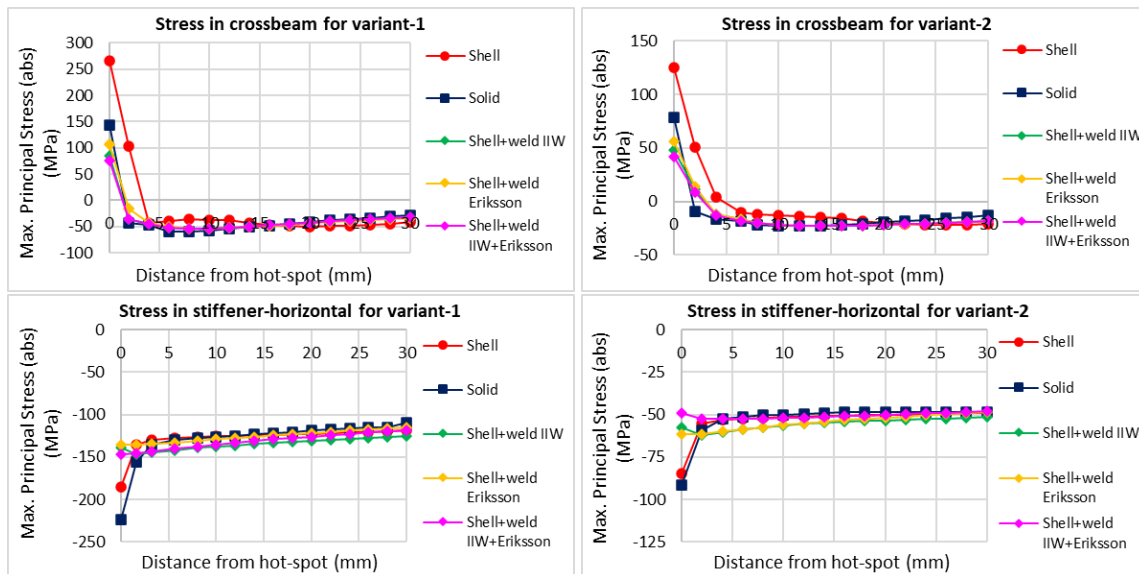


Figure H.1: Maximum principal stress under LC-1

Load case 2: Pure out-of-plane behaviour of the crossbeam

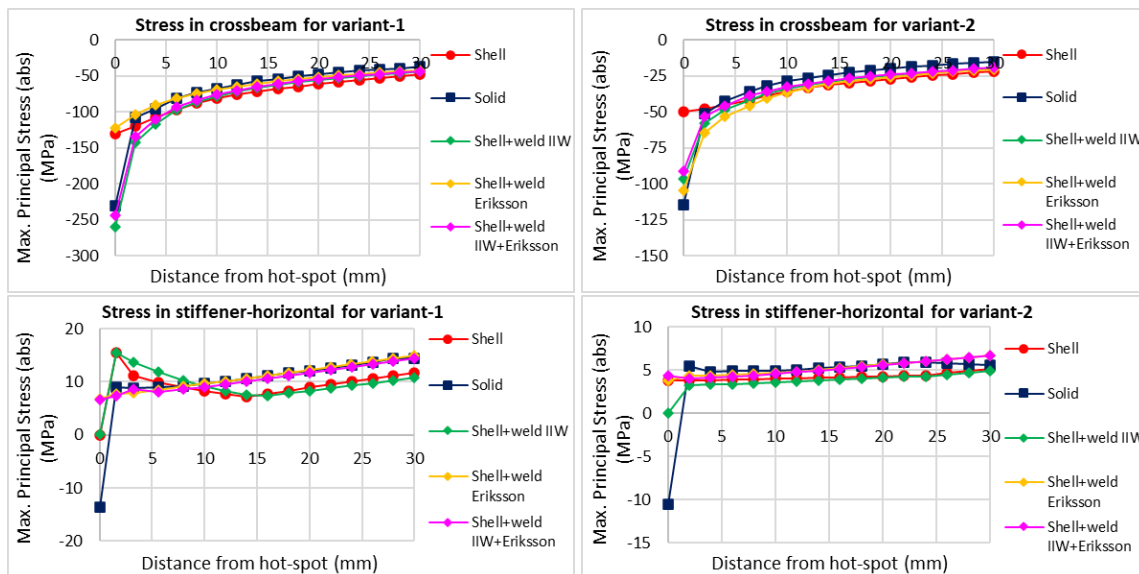


Figure H.2: Maximum principal stress under LC-2

Load case 3: Pure in-plane behaviour of the crossbeam with local load introduction

Load directly on top of the stiffener (LC3a):

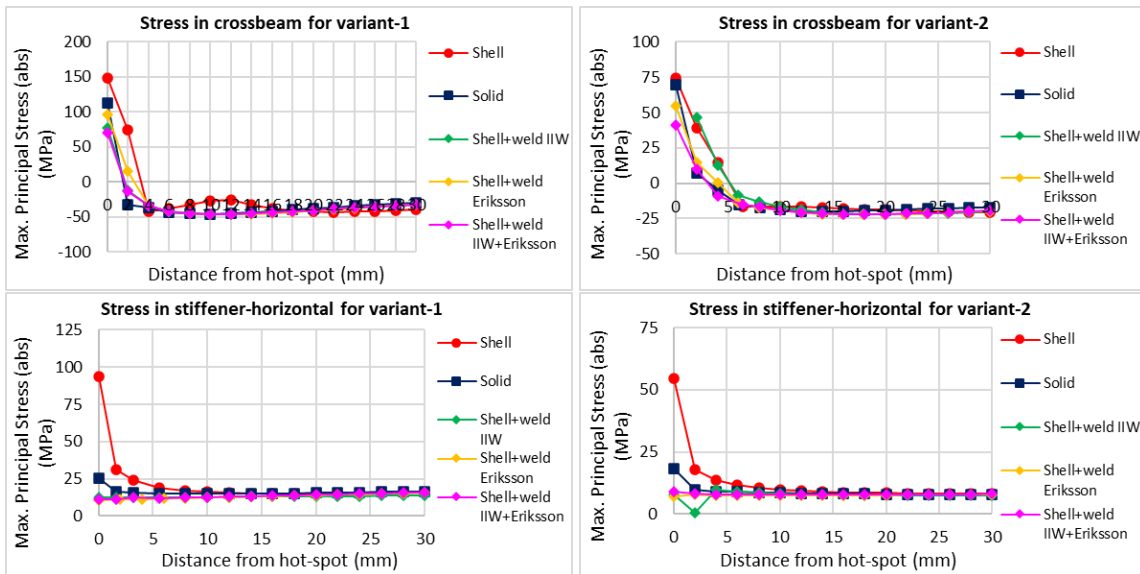


Figure H.3: Maximum principal stress under LC-3a

Load in between the stiffeners (LC3b):

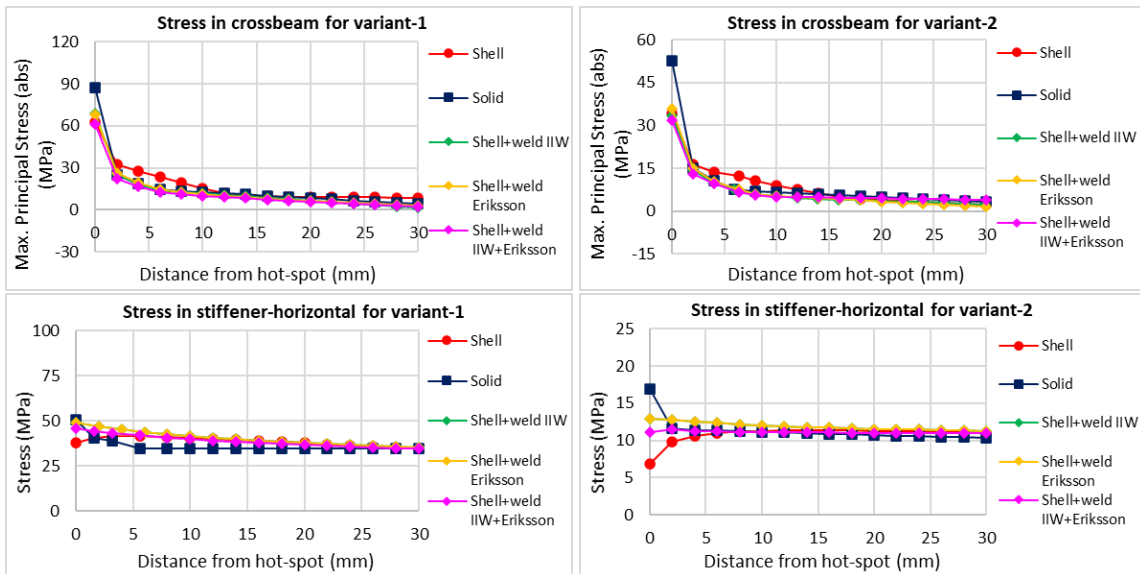


Figure H.4: Maximum principal stress under LC-3b

The SHSS values computed based on maximum principal stress are summarised in Table H.1.

Table H.1: Summary of SHSS results of preliminary parametric investigation for four load cases based on maximum principal stress

Geometry variant	Location	Load case	Solid	Shell	Shell+weld IIW	Shell+weld Eriksson	Shell+weld IIW+Eriksson	Ratio			
			SHSS (MPa)	SHSS (MPa)	SHSS (MPa)	SHSS (MPa)	SHSS (MPa)	Ratio SHSS shell/solid	Ratio SHSS shell+weld IIW/solid	Ratio SHSS shell+weld Eriksson/solid	Ratio SHSS shell+weld IIW+Eriksson/solid
Variant 1 (light variant OSD)	Crossbeam	LC1	-39.4	-47.9	-40.2	-36.7	-40.4	1.22	1.02	0.93	1.03
		LC2	-114.1	-126.3	-142.7	-105.5	-134.3	1.11	1.25	0.92	1.18
		LC3a	-29.9	-51.1	-25.9	-24.9	-26.5	1.71	0.87	0.83	0.89
		LC3b	22.8	35.7	22.7	40.5	37.2	1.57	1.00	1.78	1.63
	Stiffener - horizontal	LC1	-140.0	-132.1	-147.5	-137.1	-147.9	0.94	1.05	0.98	1.06
		LC2	8.6	12.6	15.8	7.1	8.6	1.46	1.83	0.82	0.99
		LC3a	15.6	28.4	12.2	10.9	13.0	1.83	0.78	0.70	0.83
		LC3b	39.3	42.6	42.0	48.5	46.5	1.08	1.07	1.23	1.18
		LC3c	11.7	11.8	11.7	14.1	13.0	1.01	1.00	1.21	1.12
Variant 2 (heavy variant OSD)	Crossbeam	LC1	-16.7	-7.0	-12.9	-12.4	-14.6	0.42	0.78	0.75	0.88
		LC2	-44.4	-49.7	-51.3	-57.0	-46.7	1.12	1.15	1.28	1.05
		LC3a	-12.4	-15.1	-7.5	-7.8	-10.9	1.23	0.61	0.63	0.88
		LC3b	8.7	17.4	17.9	9.8	7.9	2.01	2.07	1.14	0.91
	Stiffener - horizontal	LC1	-54.6	-54.4	-62.6	-62.4	-53.1	1.00	1.15	1.14	0.97
		LC2	4.8	3.7	3.1	4.1	3.8	0.78	0.66	0.86	0.80
		LC3a	9.3	13.6	10.2	7.2	7.8	1.47	1.10	0.78	0.84
		LC3b	11.7	11.8	11.7	14.1	13.0	1.01	1.00	1.21	1.12
		LC3c	11.7	11.8	11.7	14.1	13.0	1.01	1.00	1.21	1.12

H.2. Critical points for light OSD variant based on maximum principal stress

Axle load path 1 – Load on top of stiffener:

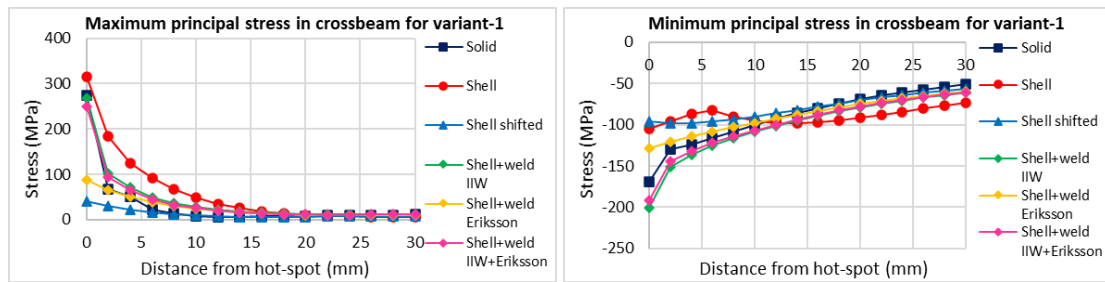


Figure H.5: Principal stress for maximum SHSS (left) and minimum SHSS (right) in crossbeam for axle load path 1 of variant 1

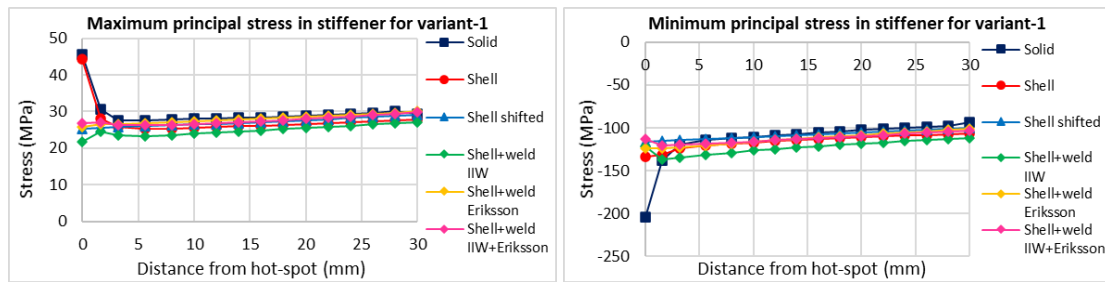


Figure H.6: Principal stress for maximum SHSS (left) and minimum SHSS (right) in stiffener for axle load path 1 of variant 1

Axle load path 2 – Load between stiffeners:

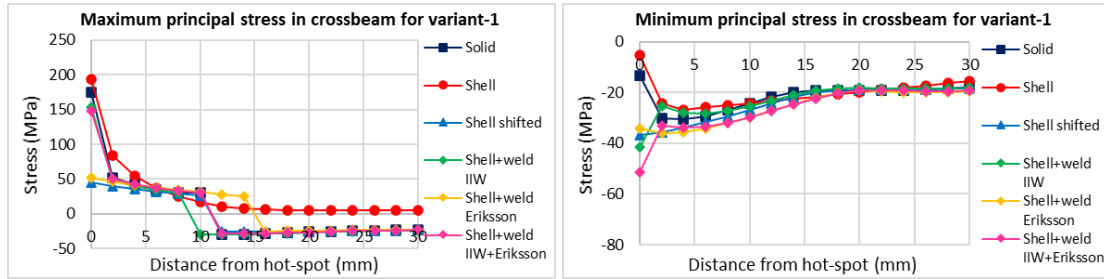


Figure H.7: Principal stress for maximum SHSS (left) and minimum SHSS (right) in crossbeam for axle load path 2 of variant 1

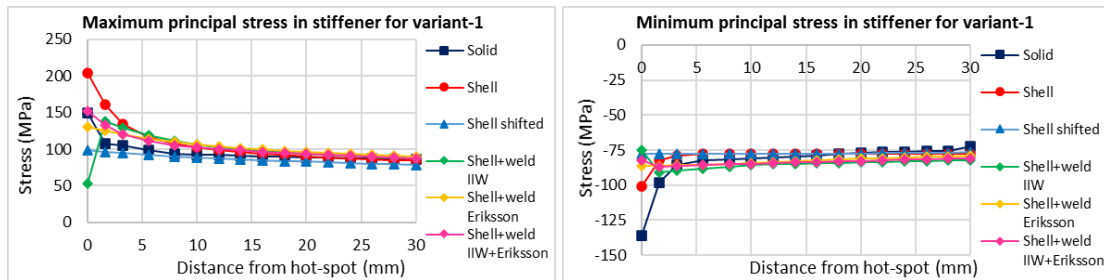


Figure H.8: Principal stress for maximum SHSS (left) and minimum SHSS (right) in stiffener for axle load path 2 of variant 1

Axle load path 3 – Load between axle load paths 1 and 2:

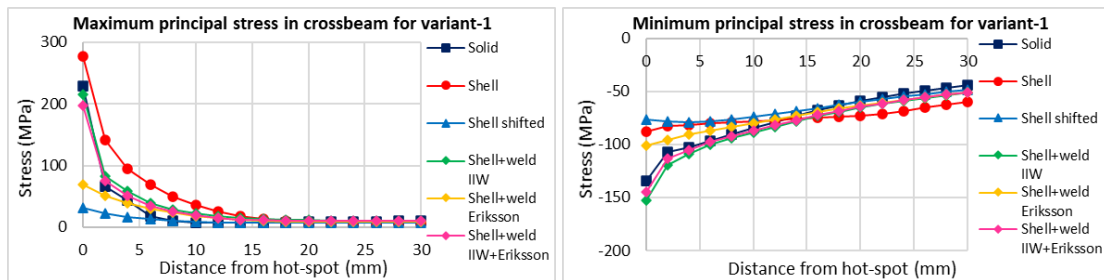


Figure H.9: Principal stress for maximum SHSS (left) and minimum SHSS (right) in crossbeam for axle load path 3 of variant 1

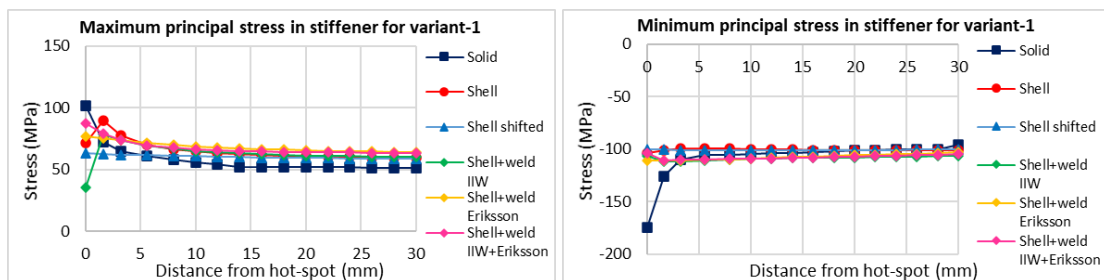


Figure H.10: Principal stress for maximum SHSS (left) and minimum SHSS (right) in stiffener for axle load path 3 of variant 1

H.3. Critical points for heavy OSD variant based on maximum principal stress

Axle load path 1 – Load on top of stiffener:

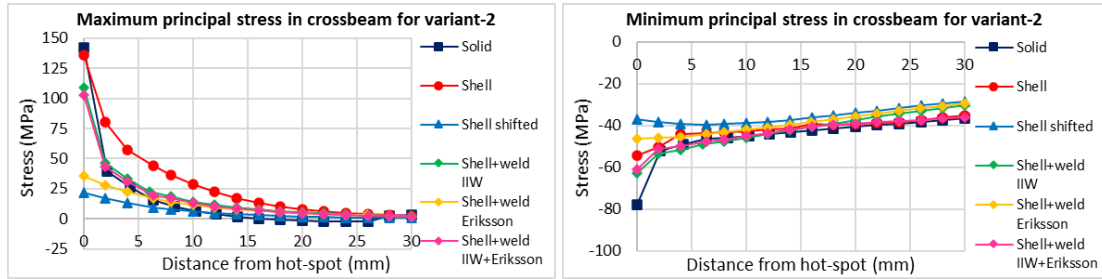


Figure H.11: Principal stress for maximum SHSS (left) and minimum SHSS (right) in crossbeam for axle load path 1 of variant 2

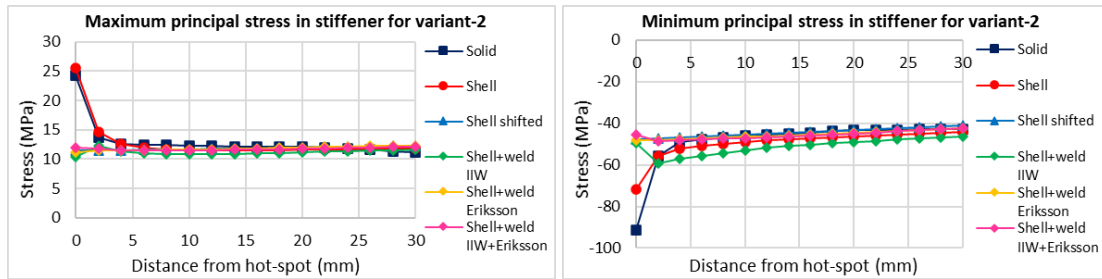


Figure H.12: Principal stress for maximum SHSS (left) and minimum SHSS (right) in stiffener for axle load path 1 of variant 2

Axle load path 2 – Load between stiffeners:

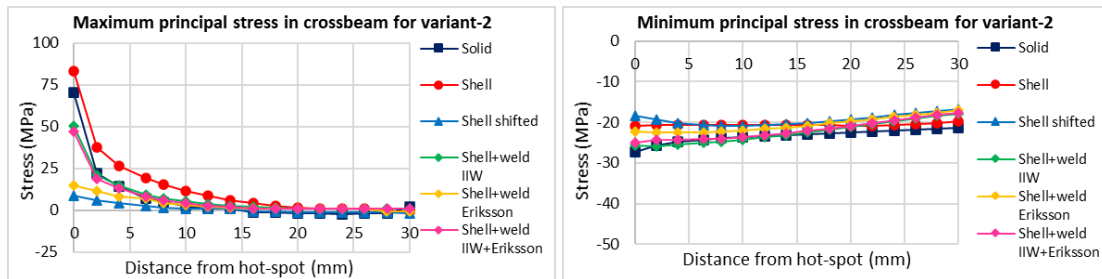


Figure H.13: Principal stress for maximum SHSS (left) and minimum SHSS (right) in crossbeam for axle load path 2 of variant 2

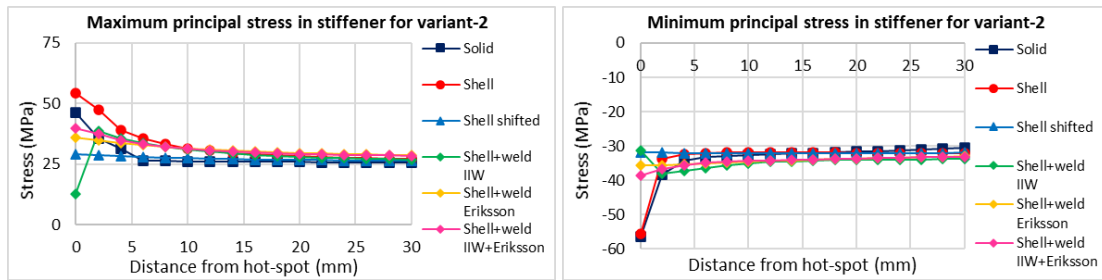


Figure H.14: Principal stress for maximum SHSS (left) and minimum SHSS (right) in stiffener for axle load path 2 of variant 2

Axle load path 3 – Load between axle load paths 1 and 2:

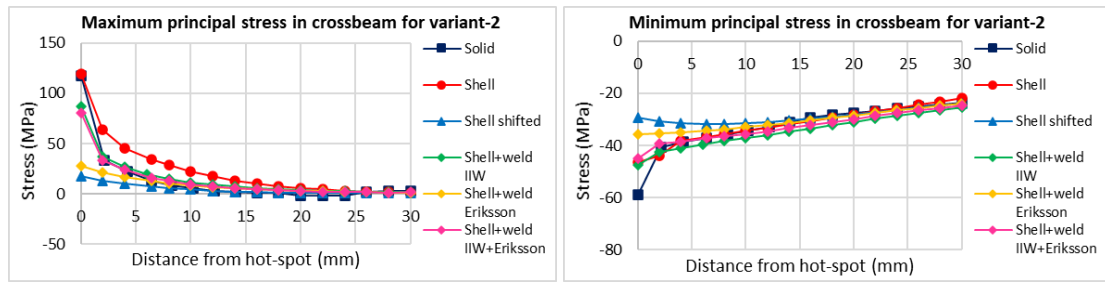


Figure H.15: Principal stress for maximum SHSS (left) and minimum SHSS (right) in crossbeam for axle load path 3 of variant 2

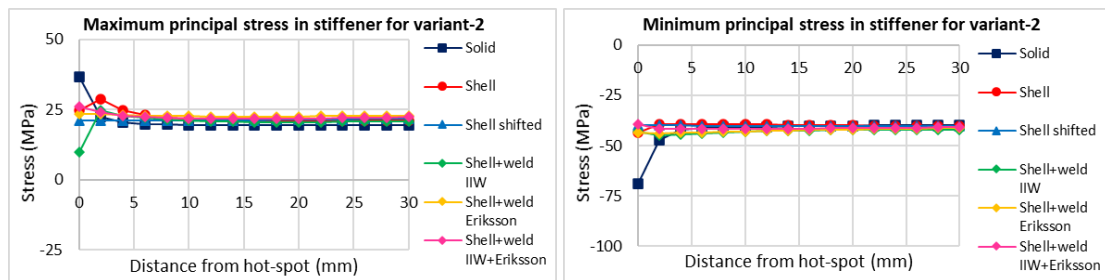


Figure H.16: Principal stress for maximum SHSS (left) and minimum SHSS (right) in stiffener for axle load path 3 of variant 2

Table H.2: SHSS ratios of light OSD variant based on maximum principal stress

Variant 1 (Light variant OSD)	Axle Load Path 1				Axle Load Path 2				Axle Load Path 3			
	Crossbeam		Stiffener		Crossbeam		Stiffener		Crossbeam		Stiffener	
	Maxima	Minima	Maxima	Minima	Maxima	Minima	Maxima	Minima	Maxima	Minima	Maxima	Minima
Numerical Model	SHSS (MPa)	SHSS (MPa)	SHSS (MPa)	SHSS (MPa)	SHSS (MPa)	SHSS (MPa)	SHSS (MPa)	SHSS (MPa)	SHSS (MPa)	SHSS (MPa)	SHSS (MPa)	SHSS (MPa)
Solid	79.88	-140.62	27.39	-123.84	51.34	-34.60	112.15	-88.33	68.48	-115.53	69.02	-112.64
Shell	174.79	-81.32	26.24	-128.29	79.09	-28.50	152.15	-79.96	134.86	-83.69	85.17	-99.32
Shell shifted	29.87	-103.70	25.33	-115.72	41.82	-38.87	97.71	-77.58	21.98	-82.36	62.67	-100.48
Shell+weld IIW	101.29	-155.62	23.27	-139.07	86.91	-29.43	140.59	-91.92	82.00	-122.92	78.14	-112.77
Shell+weld Eriksson	67.28	-124.63	26.20	-125.38	48.94	-39.71	126.98	-86.79	52.31	-98.19	75.98	-111.63
Shell+weld IIW+Eriksson	92.63	-149.36	26.38	-121.34	51.18	-36.60	130.63	-87.04	73.25	-117.22	77.78	-110.58
Ratio												
SHSS shell/solid	2.19	0.58	0.96	1.04	1.54	0.82	1.36	0.91	1.97	0.72	1.23	0.88
SHSS shell shifted/solid	0.37	0.74	0.92	0.93	0.81	1.12	0.87	0.88	0.32	0.71	0.91	0.89
SHSS shell+weld (IIW)/solid	1.27	1.11	0.85	1.12	1.69	0.85	1.25	1.04	1.20	1.06	1.13	1.00
SHSS shell+weld (Eriksson)/solid	0.84	0.89	0.96	1.01	0.95	1.15	1.13	0.98	0.76	0.85	1.10	0.99
SHSS shell+weld (IIW+Eriksson)/solid	1.16	1.06	0.96	0.98	1.00	1.06	1.16	0.99	1.07	1.01	1.13	0.98

Table H.3: SHSS ratios of heavy OSD variant based on maximum principal stress

Variant 2 (Heavy variant OSD)	Axle Load Path 1				Axle Load Path 2				Axle Load Path 3			
	Crossbeam		Stiffener		Crossbeam		Stiffener		Crossbeam		Stiffener	
	Maxima	Minima	Maxima	Minima	Maxima	Minima	Maxima	Minima	Maxima	Minima	Maxima	Minima
Numerical Model	SHSS (MPa)	SHSS (MPa)	SHSS (MPa)	SHSS (MPa)	SHSS (MPa)	SHSS (MPa)	SHSS (MPa)	SHSS (MPa)	SHSS (MPa)	SHSS (MPa)	SHSS (MPa)	SHSS (MPa)
Solid	25.77	-49.33	12.75	-51.05	12.44	-25.29	34.70	-35.22	21.07	-42.42	21.03	-43.14
Shell	64.34	-46.78	13.28	-54.22	29.56	-20.78	44.35	-32.97	50.93	-41.10	26.59	-39.23
Shell shifted	14.01	-41.64	11.45	-47.46	4.55	-21.05	28.77	-31.92	10.90	-33.13	20.90	-39.80
Shell+weld IIW	32.67	-54.64	11.55	-60.02	14.47	-26.91	38.85	-38.50	28.62	-43.64	24.08	-45.42
Shell+weld Eriksson	23.96	-47.95	11.36	-48.24	10.66	-23.47	35.16	-35.78	18.36	-36.86	23.38	-44.11
Shell+weld IIW+Eriksson	28.61	-52.74	11.61	-48.97	12.65	-25.57	37.49	-36.28	23.72	-40.57	23.57	-41.66
Ratio												
SHSS shell/solid	2.50	0.95	1.04	1.06	2.38	0.82	1.28	0.94	2.42	0.97	1.26	0.91
SHSS shell shifted/solid	0.54	0.84	0.90	0.93	0.37	0.83	0.83	0.91	0.52	0.78	0.99	0.92
SHSS shell+weld (IIW)/solid	1.27	1.11	0.91	1.18	1.16	1.06	1.12	1.09	1.36	1.03	1.15	1.05
SHSS shell+weld (Eriksson)/solid	0.93	0.97	0.89	0.94	0.86	0.93	1.01	1.02	0.87	0.87	1.11	1.02
SHSS shell+weld (IIW+Eriksson)/solid	1.11	1.07	0.91	0.96	1.02	1.01	1.08	1.03	1.13	0.96	1.12	0.97

Figures H.17 and H.18 shows histograms of SHSS ratios based on maximum principal stress. The CV (%) is also obtain for these SHSS ratios (Figure H.19). It is found that the CV of SHSS ratio data-

set is around **5.3-6.2%** for the crossbeam and **7.9-8.5%** for the stiffener after application of the weld modelling technique with shell elements using the combined IIW and Eriksson’s method.

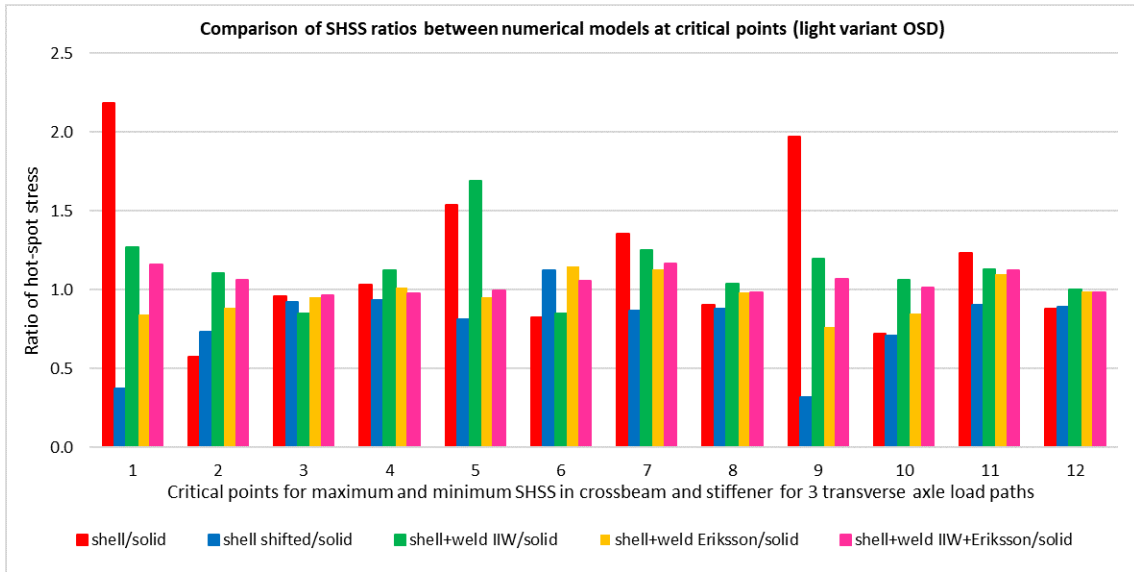


Figure H.17: Histogram of SHSS ratio for different numerical models of light variant OSD based on maximum principal stress

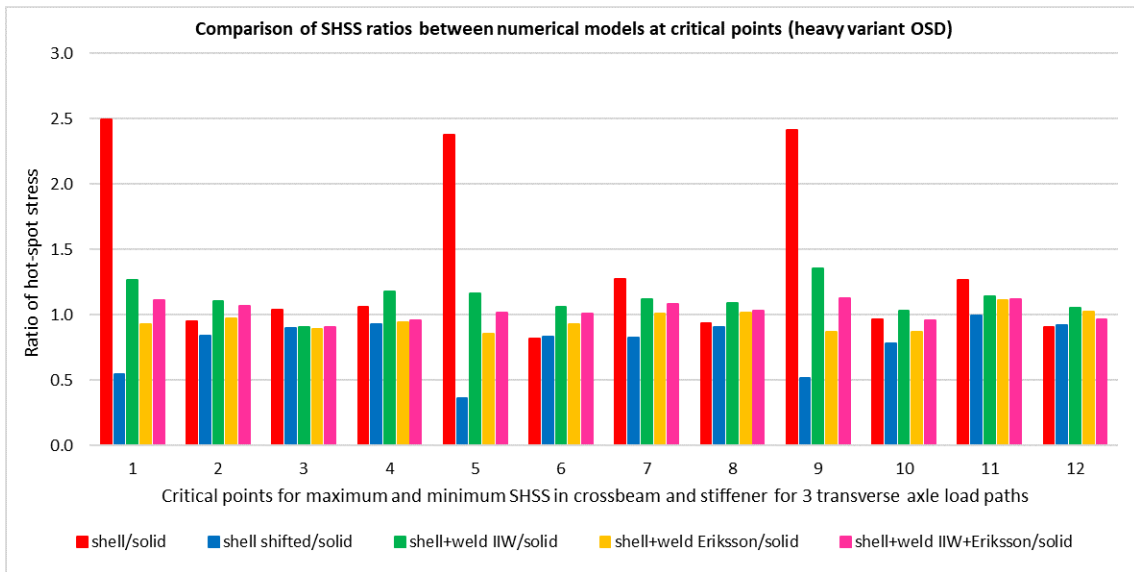


Figure H.18: Histogram of SHSS ratio for different numerical models of heavy variant OSD based on maximum principal stress

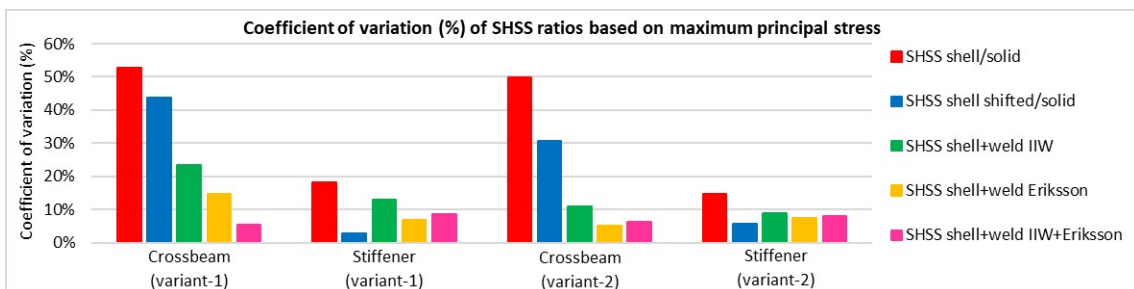


Figure H.19: Coefficient of variation of SHSS ratios based on maximum principal stress



Contour plots

This chapter shows the contour plots of stresses and deformations for all the different numerical models analysed in this thesis.

I.1. Fillet welded T-joint loaded in tension

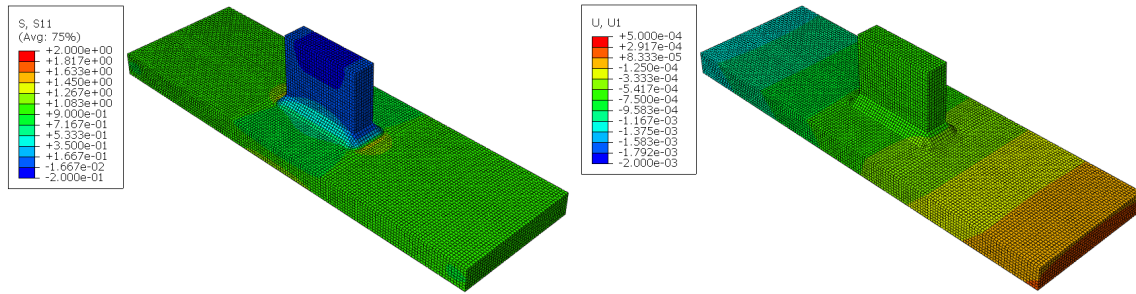


Figure I.1: Stress and deformation contour plot of T-joint with solid elements in tension

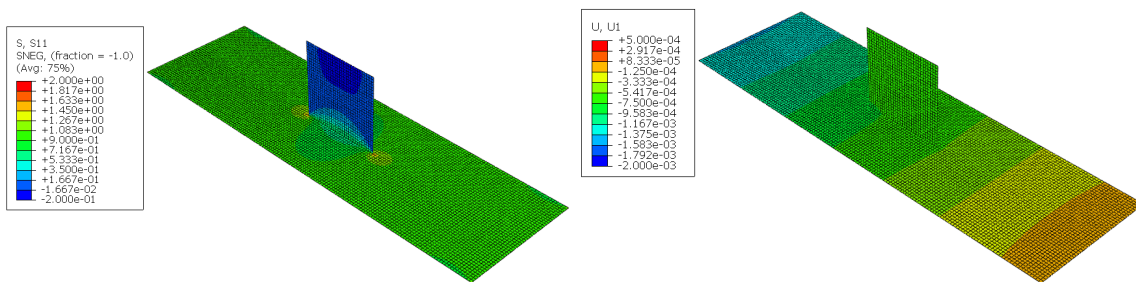


Figure I.2: Stress and deformation contour plot of T-joint with shell elements in tension

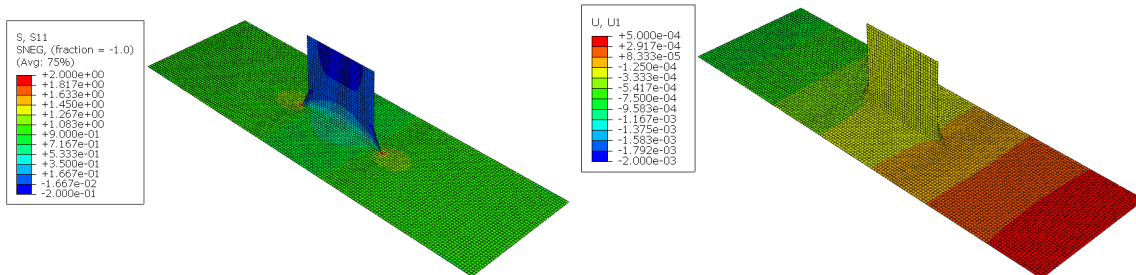


Figure I.3: Stress and deformation contour plot of T-joint with shell elements including welds in tension

I.2. Fillet welded T-joint loaded in bending

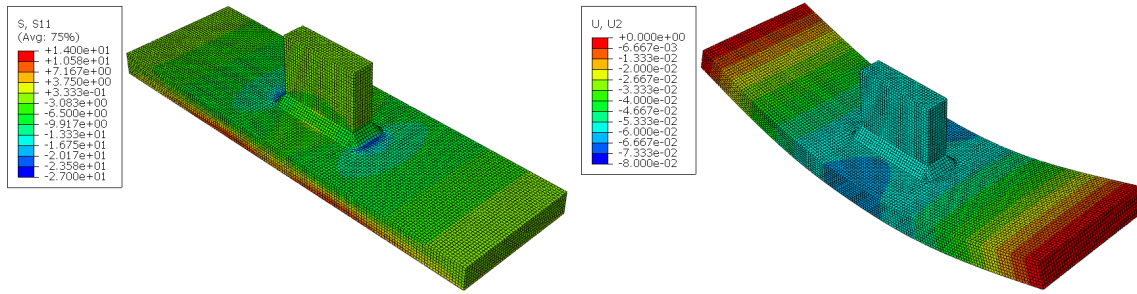


Figure I.4: Stress and deformation contour plot of T-joint with solid elements in bending

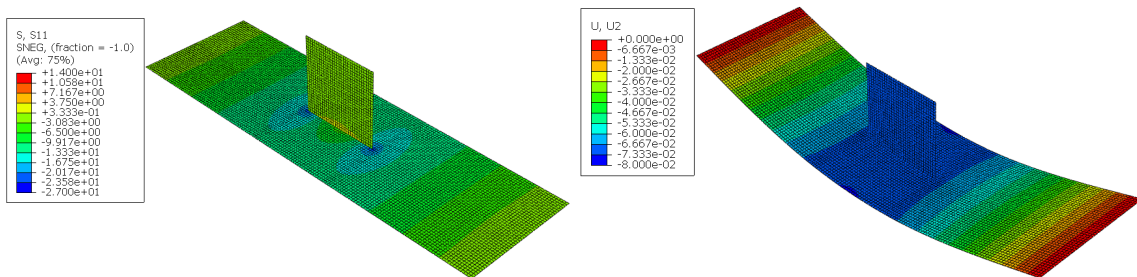


Figure I.5: Stress and deformation contour plot of T-joint with shell elements in bending

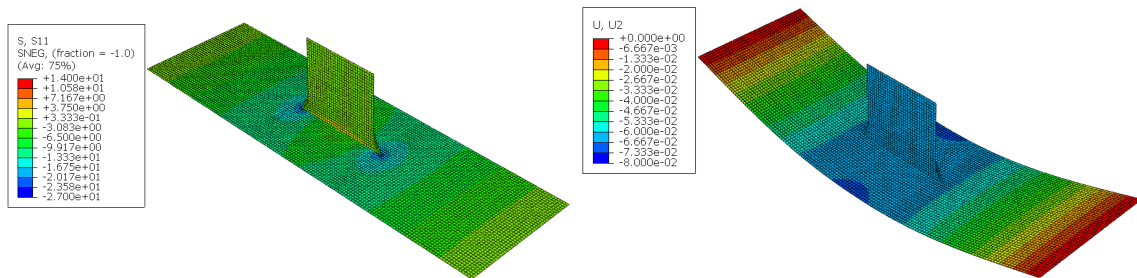


Figure I.6: Stress and deformation contour plot of T-joint with shell elements including welds in bending

I.3. Fillet welded cruciform joint loaded in tension

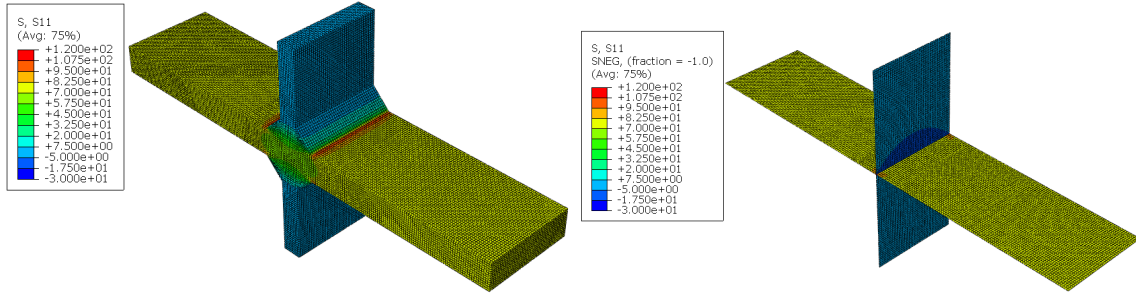


Figure I.7: Stress perpendicular to weld toe plot of cruciform joint with solid and shell elements in tension

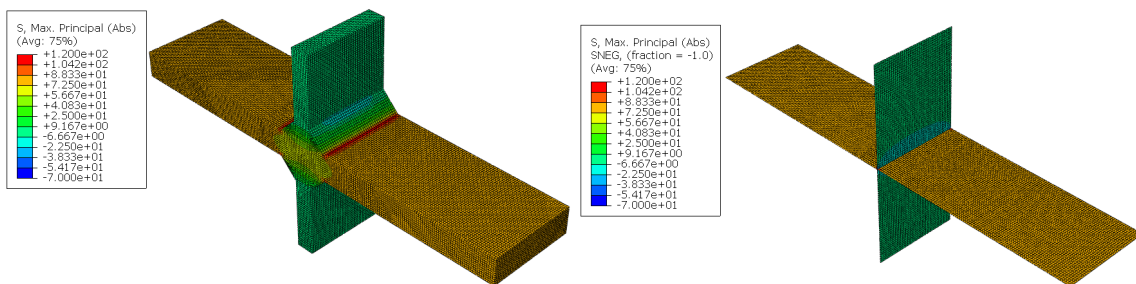


Figure I.8: Absolute maximum principal stress contour plot of cruciform joint with solid and shell elements in tension

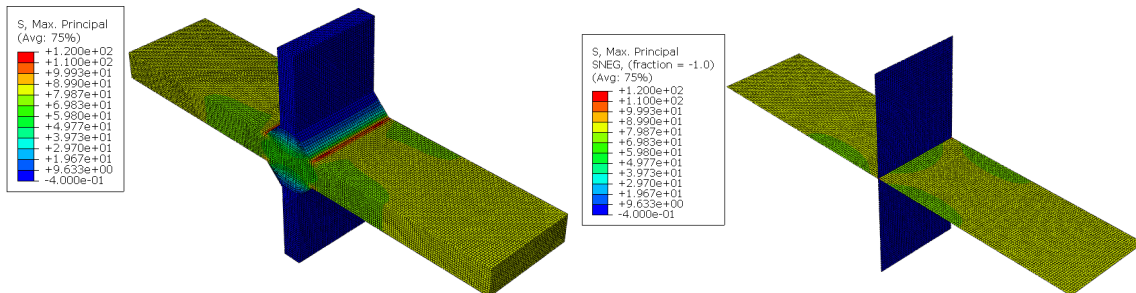


Figure I.9: Maximum principal stress contour plot of cruciform joint with solid and shell elements in tension

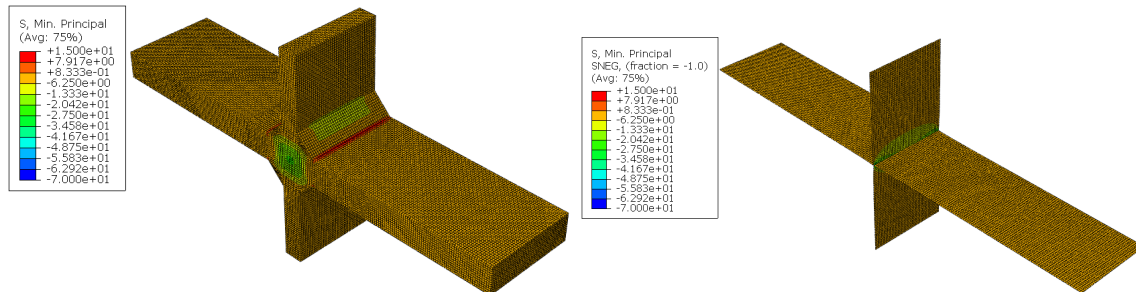


Figure I.10: Minimum principal stress contour plot of cruciform joint with solid and shell elements in tension

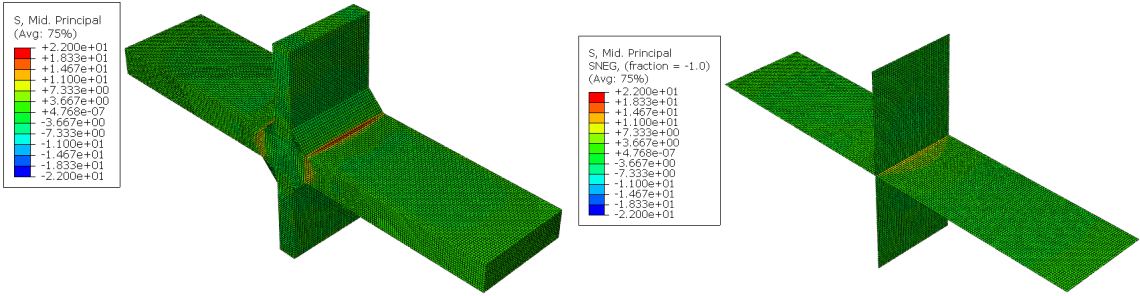


Figure I.11: Mid principal stress contour plot of cruciform joint with solid and shell elements in tension

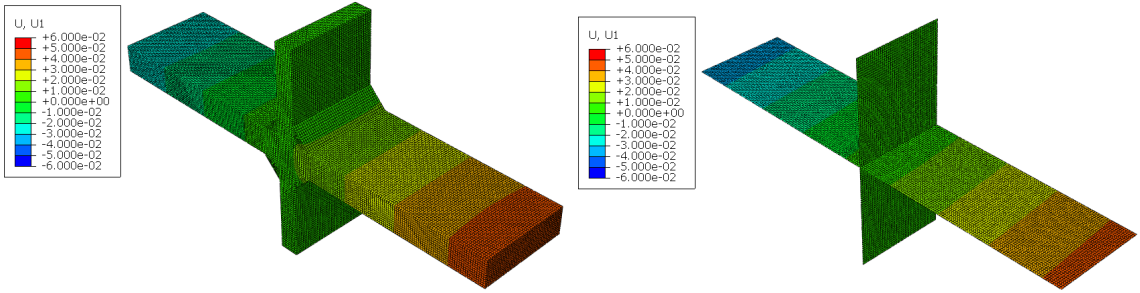


Figure I.12: Deformation (U1) contour of cruciform joint with solid and shell elements in tension

I.4. Detail with deck plate, crossbeam and open-stiffener with a cope-hole

I.4.1. Stress contour plots of the numerical models

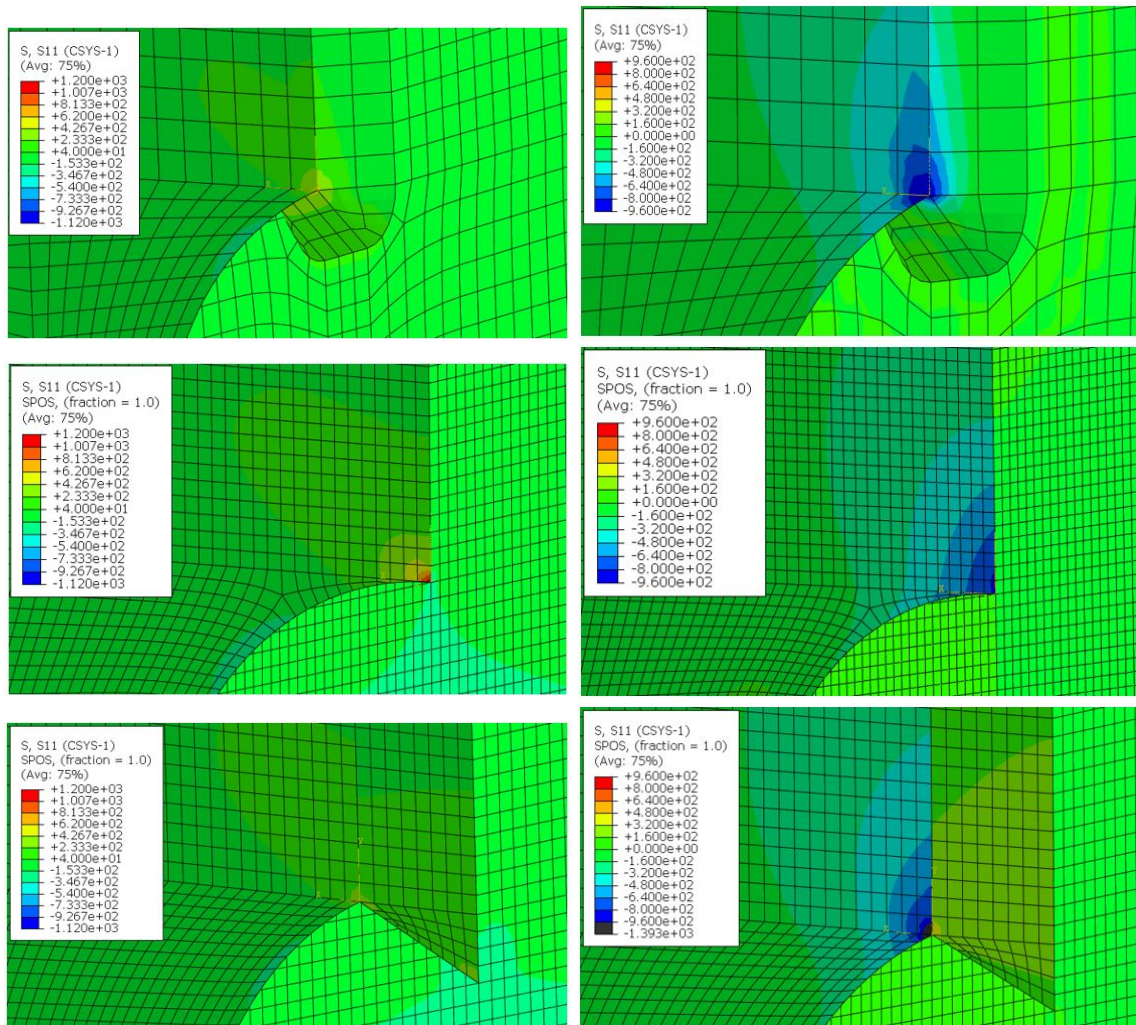


Figure I.13: Stress contour plot of the numerical models for LC1 (left) and LC2 (right)

I.4.2. Deformation contour plots of the numerical models

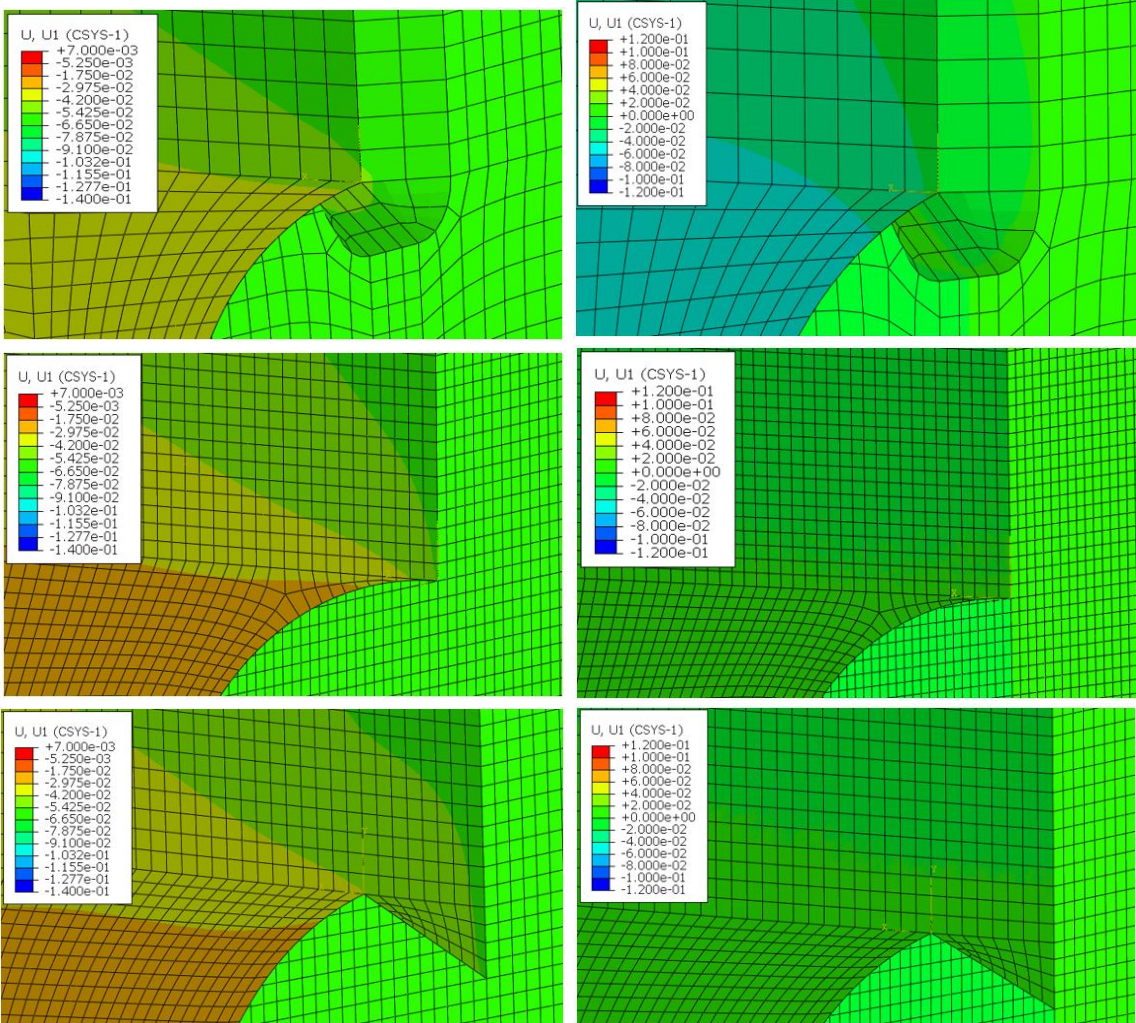


Figure I.14: Deformation contour plot (U1) of the numerical models for LC1 (left) and LC2 (right)

I.5. Fillet welded transverse and longitudinal cruciform joint

I.5.1. Transverse cruciform joint

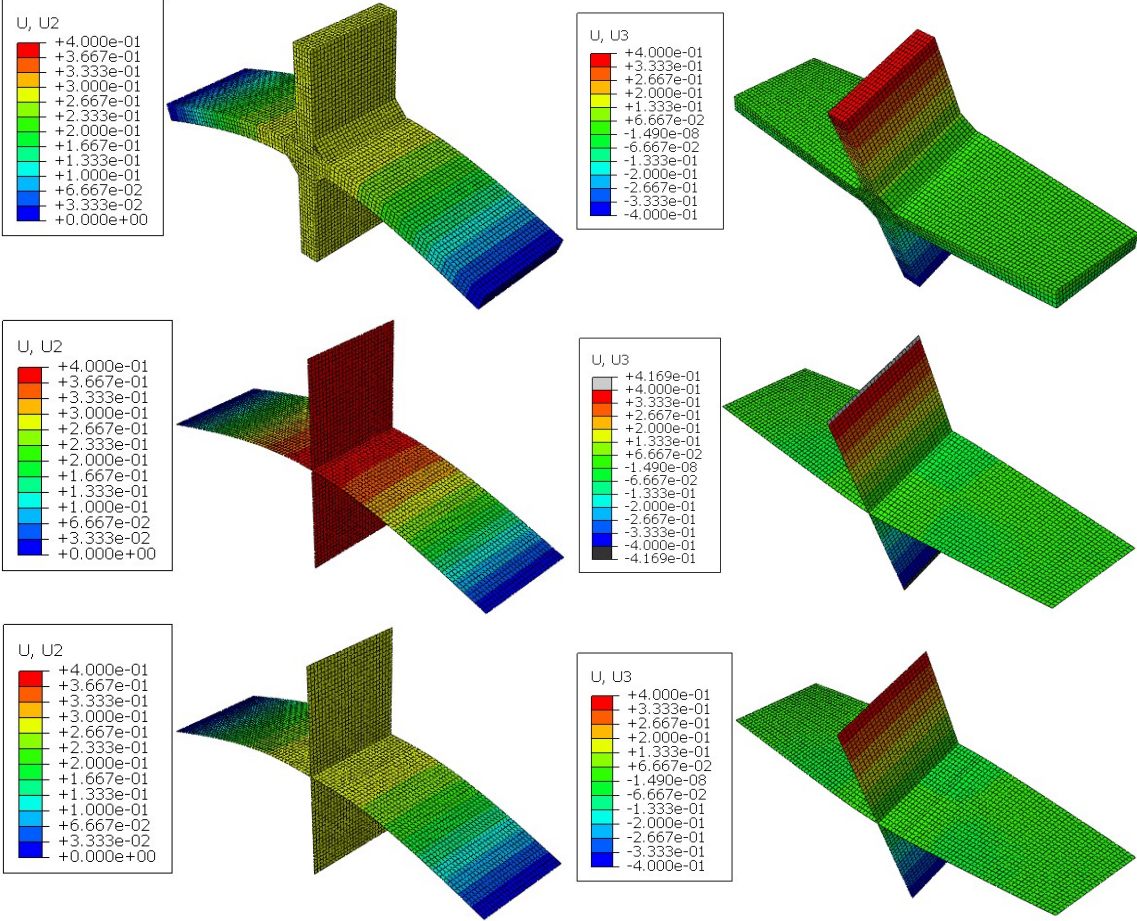


Figure I.15: Contour plots of deformation under LC-1 (left) and LC-3 (right) for transverse cruciform joint variant-1

I.5.2. Longitudinal cruciform joint

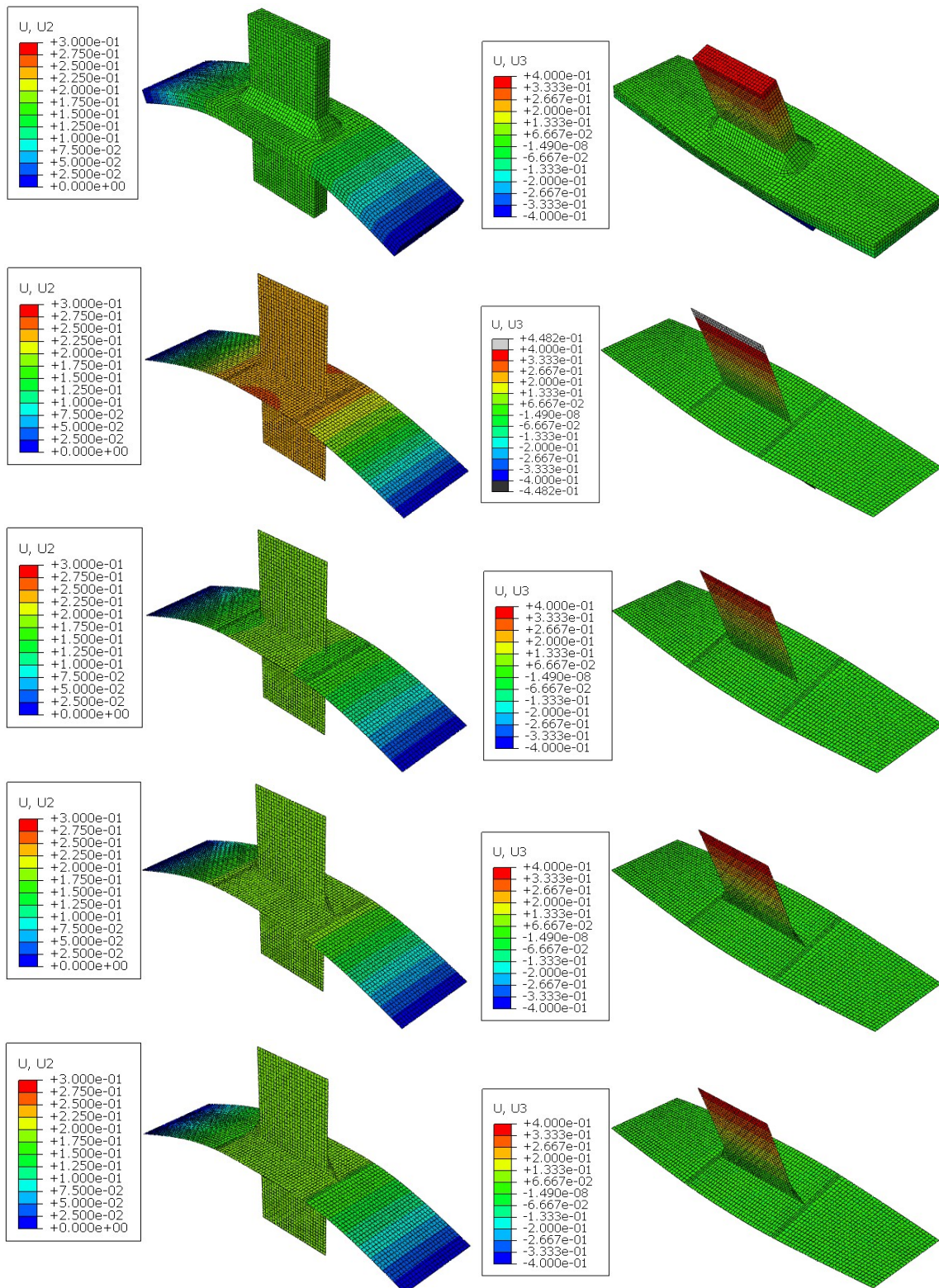


Figure I.16: Contour plots of deformation under LC-1 (left) and LC-2 (right) for longitudinal cruciform joint variant-1

I.6. Orthotropic steel deck parameter model variant - 1 (based on old OSD)

I.6.1. Deformed mesh of shell and solid models

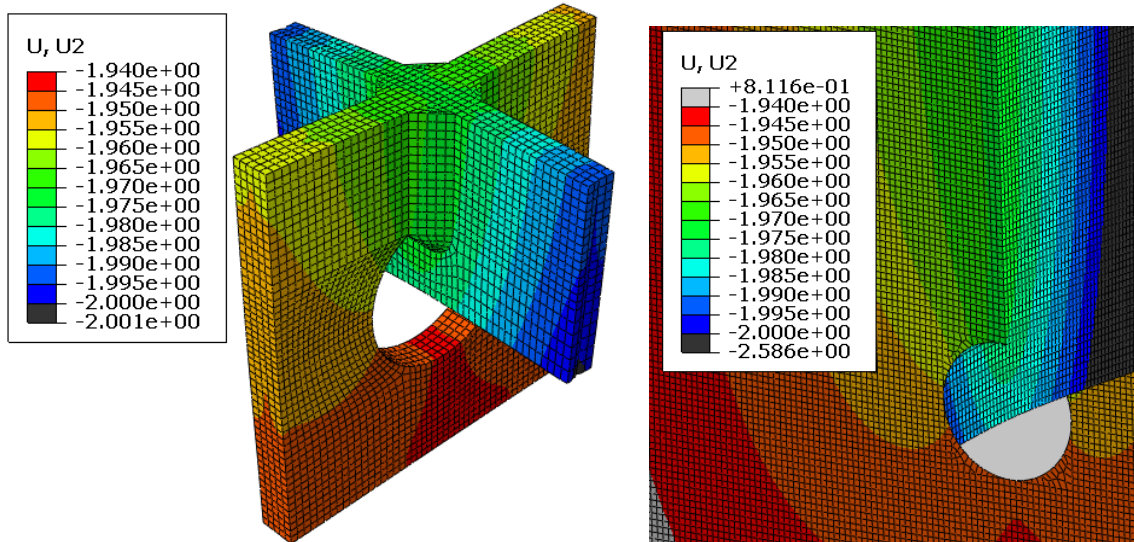


Figure I.17: Deformed mesh of shell and solid model for load case LC-1 (in-plane loading) in global coordinate system

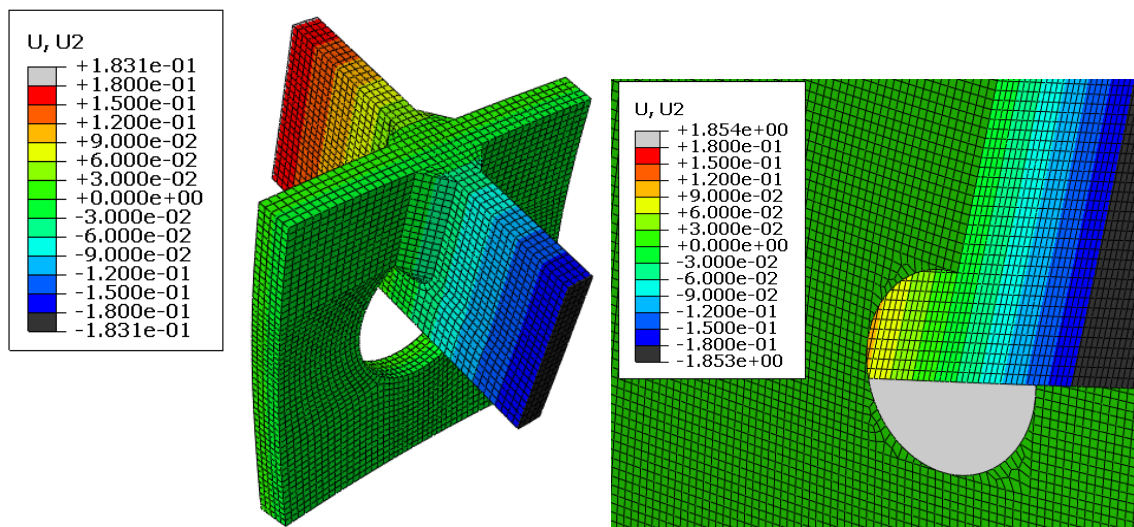


Figure I.18: Deformed mesh of shell and solid model for load case LC-2 (out-of-plane loading) in global coordinate system

I.6.2. Stress contour plots of shell and solid elements

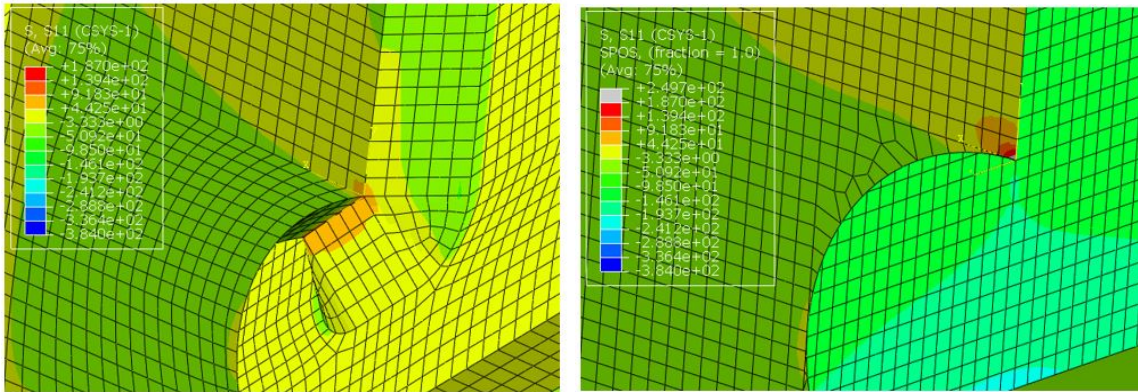


Figure I.19: Contour plot of stress perpendicular to weld toe for LC-1 (in-plane loading)

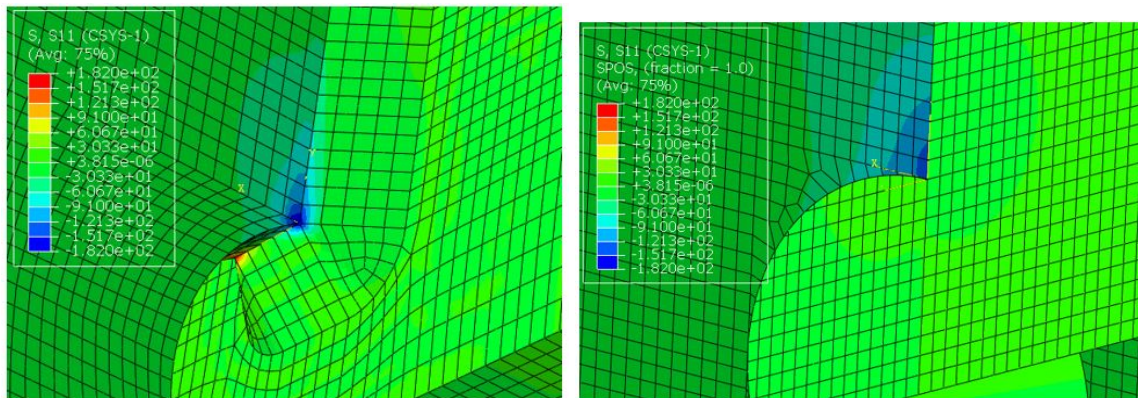


Figure I.20: Contour plot of stress perpendicular to weld toe for LC-2 (out-of-plane loading)

I.6.3. Deformation contour plots of shell and solid elements

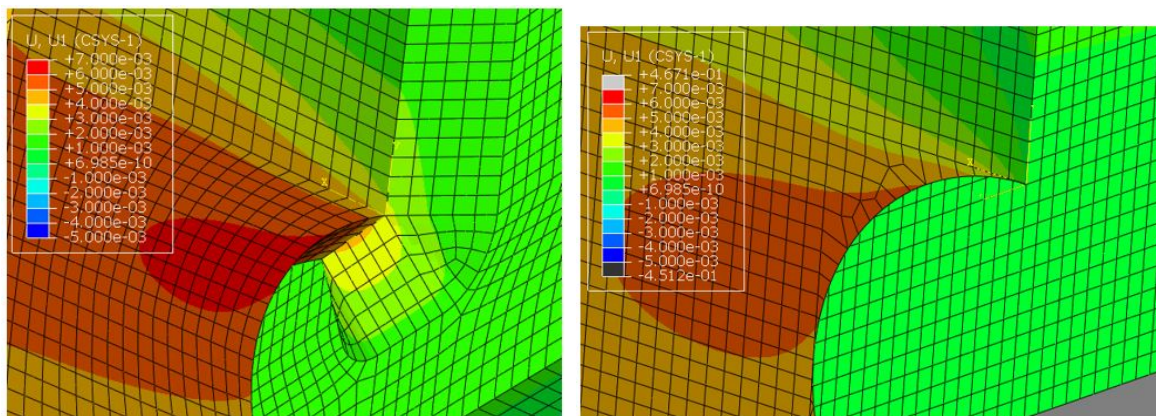


Figure I.21: Contour plot of U1 for LC-1 (in-plane loading)

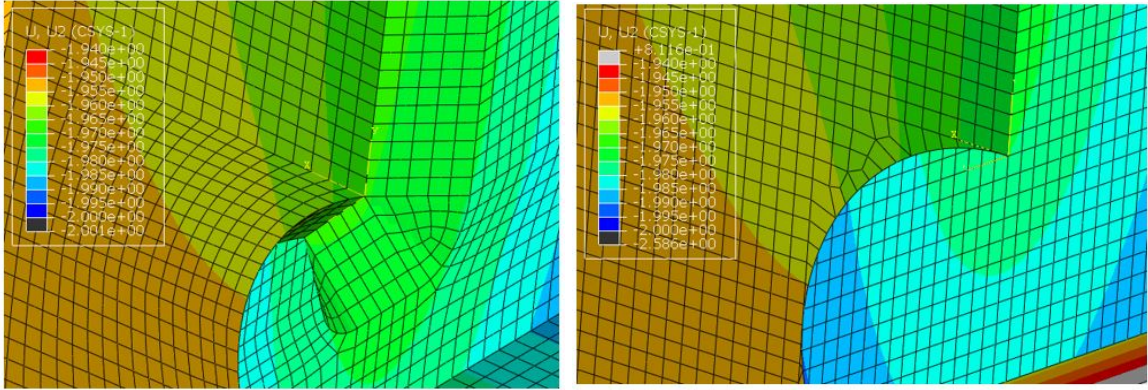


Figure I.22: Contour plot of U2 for LC-1 (in-plane loading)

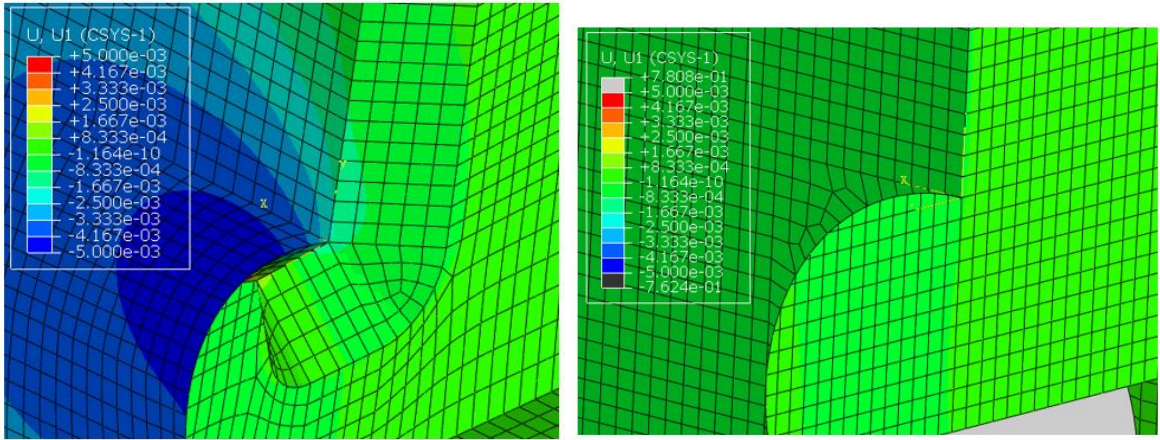


Figure I.23: Contour plot of U1 for LC-2 (out-of-plane loading)

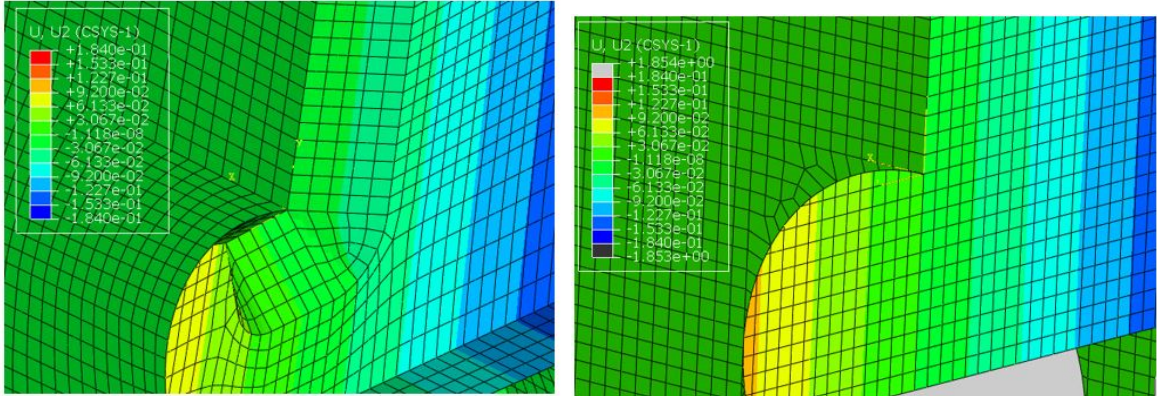


Figure I.24: Contour plot of U2 for LC-2 (out-of-plane loading)



Further investigation of out-of-plane bending

In this chapter, the out-of-plane load case has been further investigated for both simple fillet welded cruciform joint and OSD. In addition to this, a study on boundary conditions is performed with the solid element model of the simple fillet welded detail detail.

J.1. Double side fillet welded transverse cruciform joint

In this section, in addition to the edge path, four different paths perpendicular to weld line, having a spacing of 6 mm are investigated for all the numerical models subject to out-of-plane loading around z following the global coordinate system. This is shown in Figure J.1.

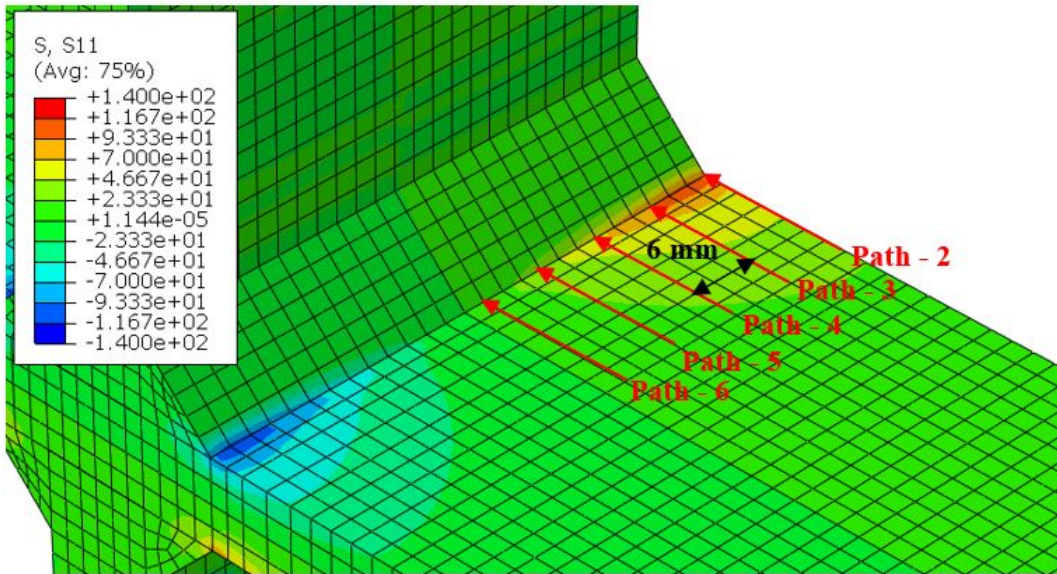


Figure J.1: Different paths perpendicular to weld line for load case 3 (LC-3)

A separate study is performed with the boundary conditions of the solid model. The following boundary conditions are investigated with the solid model (Figure J.2).

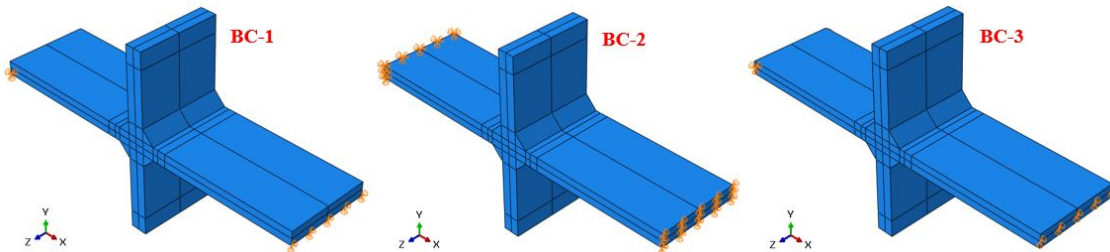


Figure J.2: Boundary condition study with the solid element model (geometry based on light variant OSD)

The stress results are compared with the stress values obtained from the shell model and the shell model with welds using the Eriksson's approach [20]. In both the shell models, the boundary conditions are applied at the mid-surface of the model as shown in Figure J.3.

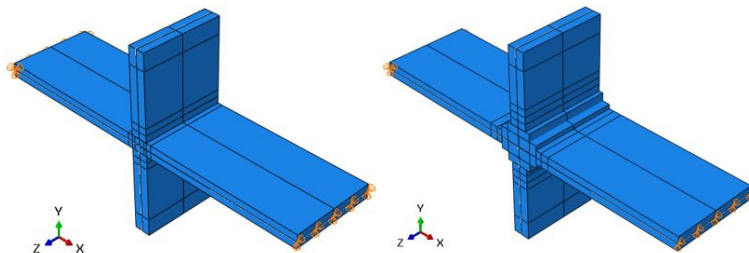


Figure J.3: Boundary condition study with the shell element model (geometry based on light variant OSD)

The following Figures 35 – 39, shows the stress distribution perpendicular to weld toe for the numerical models for the different paths (path-2 (edge) – path-6) (Figure J.4)

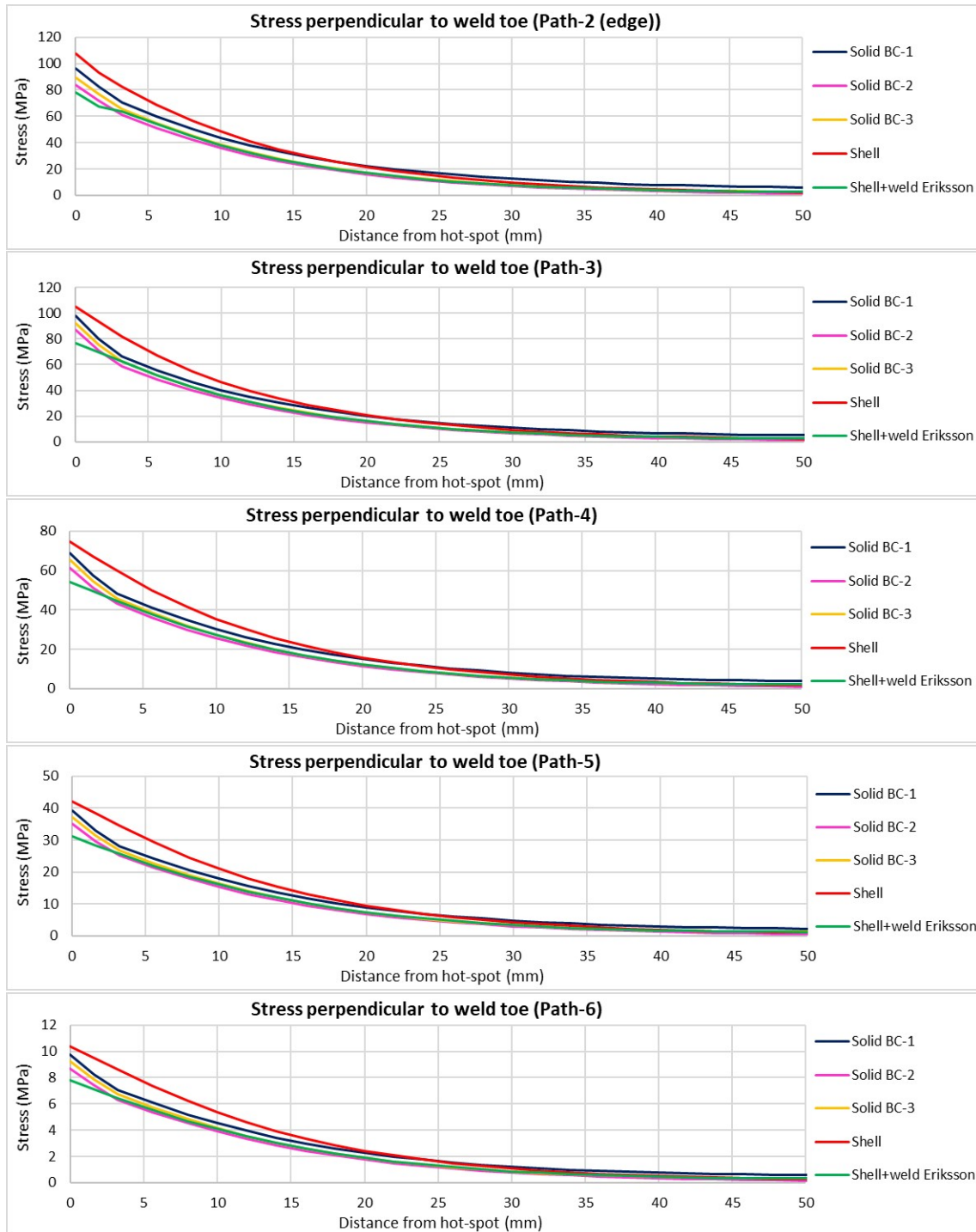


Figure J.4: Stress perpendicular to weld toe for different paths of light variant OSD under LC-3

It is observed that the shell model with welds using the Eriksson’s approach [20] gave a slight underestimation of stress compared to the solid model with BC-1 and BC-3. However, it is also seen that the shell model with welds slightly overestimated the stress compared to the solid model with BC-2. This is further explained after calculation of the hot-spot stress values for the numerical models as shown in Table J.1 for all the 3 boundary conditions of the solid model. In all the solid models, the

surface stresses are extracted from the top surface of the plate as shown in Figure J.1.

Table J.1: Summary of SHSS values for different paths and different boundary conditions of solid model

Geometry Variant	Load Case	Path	SHSS (MPa)					Ratio BC-1		Ratio BC-2		Ratio BC-3	
			Solid BC-1	Solid BC-2	Solid BC-3	Shell	Shell+weld Eriksson	SHSS shell/solid (BC-1)	SHSS shell+weld/solid (BC-1)	SHSS shell/solid (BC-2)	SHSS shell+weld/solid (BC-2)	SHSS shell/solid (BC-3)	SHSS shell+weld/solid (BC-3)
Variant-1	LC-3	Path-2	84.3	74.2	79.4	99.7	75.9	1.18	0.90	1.34	1.02	1.26	0.96
		Path-3	79.4	71.1	75.9	99.5	75.7	1.25	0.95	1.40	1.06	1.31	1.00
		Path-4	57.5	51.8	55.2	72.2	53.2	1.25	0.92	1.39	1.03	1.31	0.96
		Path-5	33.2	30.0	31.9	41.3	30.4	1.24	0.91	1.38	1.01	1.29	0.95
		Path-6	8.3	7.5	8.0	10.3	7.6	1.24	0.91	1.37	1.01	1.29	0.95
		Path-2	49.9	43.6	46.7	60.5	44.4	1.21	0.89	1.39	1.02	1.30	0.95
Variant-2	LC-3	Path-3	47.4	42.3	45.2	62.5	43.4	1.32	0.92	1.48	1.03	1.38	0.96
		Path-4	34.9	31.4	33.5	46.4	31.4	1.33	0.90	1.48	1.00	1.39	0.94
		Path-5	20.3	18.3	19.5	26.8	18.6	1.32	0.92	1.47	1.02	1.38	0.96
		Path-6	5.1	4.6	4.9	6.7	4.6	1.32	0.90	1.46	0.99	1.37	0.93

It is evident from Table J.1 and all the above figures that the average ratio of SHSS of shell model with welds to solid model is slightly overestimated (+2%) with BC-2 and slightly underestimated (-5%) with BC-3. Both these values are considered to be acceptable as they are within +/-5%. In order to have a better judgement of the behaviour of the shell model with welds using the Eriksson’s approach, the stress values at a distance of 50 mm away from weld toe are compared with that of the solid model as shown in Table J.2.

Table J.2: Summary of stress values at 50 mm away from weld toe for different paths and different boundary conditions of solid model

Geometry Variant	Load Case	Path	Stress at 50 mm away from weld toe (MPa)					Ratio BC-1		Ratio BC-2		Ratio BC-3	
			Solid BC-1	Solid BC-2	Solid BC-3	Shell	Shell+weld Eriksson	Stress at 50 mm shell/solid (BC-1)	Stress at 50 mm shell+weld/solid (BC-1)	Stress at 50 mm shell/solid (BC-2)	Stress at 50 mm shell+weld/solid (BC-2)	Stress at 50 mm shell/solid (BC-3)	Stress at 50 mm shell+weld/solid (BC-3)
Variant-1	LC-3	Path-2	6.1	1.4	2.8	2.4	2.7	0.39	0.45	1.69	1.96	0.84	0.97
		Path-3	5.2	1.3	2.7	2.3	2.6	0.44	0.51	1.72	1.98	0.85	0.98
		Path-4	3.8	1.0	2.1	1.7	2.0	0.45	0.53	1.74	2.03	0.83	0.97
		Path-5	2.3	0.6	1.3	1.0	1.2	0.46	0.54	1.75	2.08	0.82	0.97
		Path-6	0.6	0.2	0.3	0.3	0.3	0.46	0.55	1.76	2.09	0.81	0.96
		Path-2	4.4	0.8	2.4	2.1	2.3	0.47	0.51	2.55	2.77	0.85	0.93
Variant-2	LC-3	Path-3	3.9	0.8	2.3	2.0	2.2	0.52	0.57	2.58	2.80	0.87	0.94
		Path-4	2.9	0.6	1.8	1.6	1.7	0.54	0.59	2.63	2.87	0.86	0.94
		Path-5	1.7	0.4	1.1	0.9	1.0	0.53	0.60	2.57	2.94	0.81	0.93
		Path-6	0.4	0.1	0.3	0.2	0.3	0.52	0.61	2.54	2.96	0.79	0.92

From Table J.2 and all the above figures, the average ratio of stress at 50 mm of shell model with welds to solid model is slightly underestimated (-5%) with BC-3. This is considered as acceptable as it is within +/-5% for BC-3. The stress values (at 50 mm) from the solid model having BC-1 are more than that from shell model with welds and the stress values from the solid model having BC-2 are less than that from shell model with welds for all the 5 different paths. The stress values (at 50 mm) from solid model having BC-3 is comparable to that of the shell model with welds. Thus, for the solid models, BC-3 is regarded as an appropriate boundary condition in order to have a good comparison with all the other numerical models.

J.2. OSD

For the out-of-plane load case in OSD as shown in Chapter-6 (Figure 6.2), the combined weld modelling strategy with shell elements using the combination of IIW [28] and Eriksson’s method [20] is further investigated with three combinations (Figure J.5).

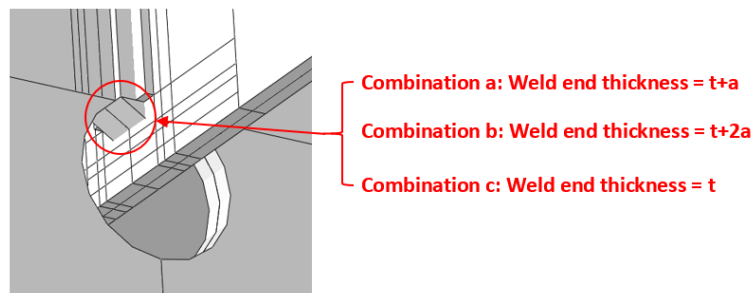


Figure J.5: Combination of weld modelling with shell elements having different thickness of weld tip

For the first combination, the Eriksson’s method [20] is followed. For the second combination, the thickness of the triangular plate is increased by twice the throat thickness. For the third combination, there is no increase of plate thickness. This is shown in Figure J.5. The thickness of the triangular part of the weld with shell elements is varied in order to check the difference in stress gradients compared to that of the solid model which is shown in Figure J.6 and J.7 for the crossbeam and stiffener respectively.

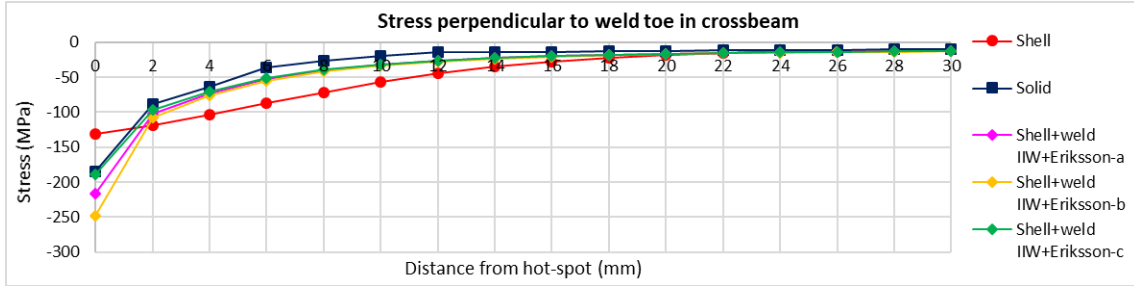


Figure J.6: Stress profiles of numerical models for crossbeam under out-of-plane loading

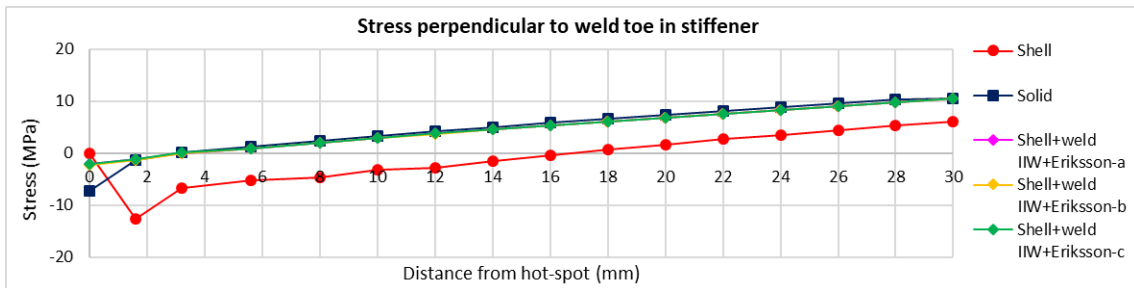
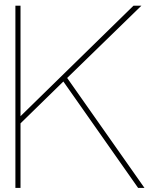


Figure J.7: Stress profiles of numerical models for stiffener under out-of-plane loading

From the stress profiles it can be seen that the stress values far away from the weld toe (for example at 30 mm) are similar for the solid model and the shell model after weld modelling approach. The influence of the change of thickness of the triangular part of the shell element is negligible for the stiffener Figure J.7. The SHSS values and the corresponding SHSS ratios of the three combinations are summarised in Table J.3. From the table, the ratio of SHSS clearly indicated that the combined weld modelling approach is sensitive to the thickness of the triangular weld end with shell elements.

Table J.3: SHSS ratio for different numerical models subject to out-of-plane load case

Numerical Model	Crossbeam		Stiffener	
	SHSS (MPa)	SHSS ratio	SHSS (MPa)	SHSS ratio
Solid	-93.68	-	-1.93	-
Shell	-134.72	1.44	-9.08	4.70
Shell+weld IIW+Eriksson-a	-100.82	1.08	-1.88	0.97
Shell+weld IIW+Eriksson-b	-105.97	1.13	-1.91	0.99
Shell+weld IIW+Eriksson-c	-96.29	1.03	-1.80	0.93



Other weld modelling approaches with shell elements

In this chapter, a new approach of weld modelling approach with shell elements has been presented. This approach also involves increase of thickness of shell elements at the weld region.

K.1. New approach of weld modelling with shell elements

This approach is similar to the Eriksson’s method [20] of weld modelling with shell elements. The only difference is that the increase of thickness of one plate at the weld region also depend on the thickness of the other plate and vice versa. The modelling approach is shown in Figure K.1, for a fillet welded transverse cruciform joint where the second plate is continuous. The coefficients k_1 and k_2 are dependent on the type of joint. For example, for a single side fillet welded transverse plate joint (T-joint), $k_1=1$ and $k_2=0.5$. For a double side fillet welded transverse plate joint (cruciform joint), $k_1=1$ and $k_2=1$.

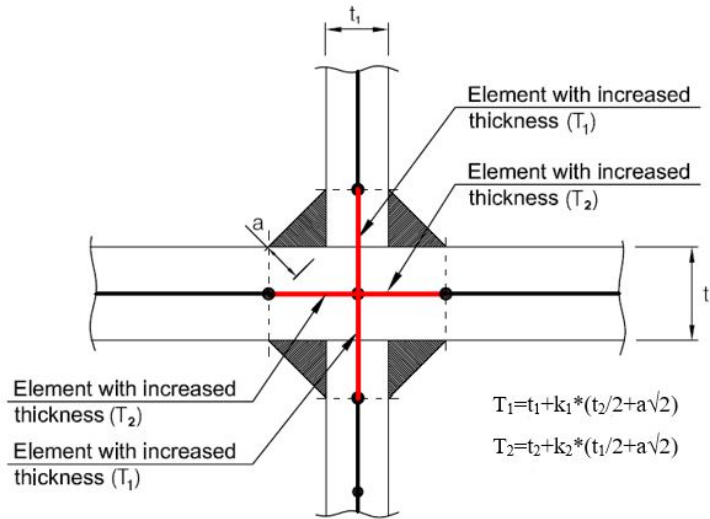


Figure K.1: New approach of weld modelling using shell elements with increased thickness at weld region

Light OSD variant: The stress profiles of the critical points from three transverse axle load positions of the light OSD variant are shown in Figures K.2-K.7.

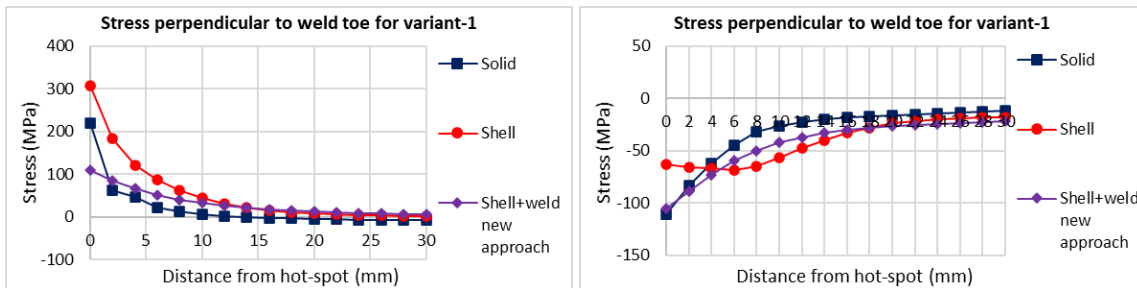


Figure K.2: Stress perpendicular to weld toe for maximum SHSS (left) and minimum SHSS (right) in crossbeam for axle load path 1 of variant 1 with new approach of weld modelling

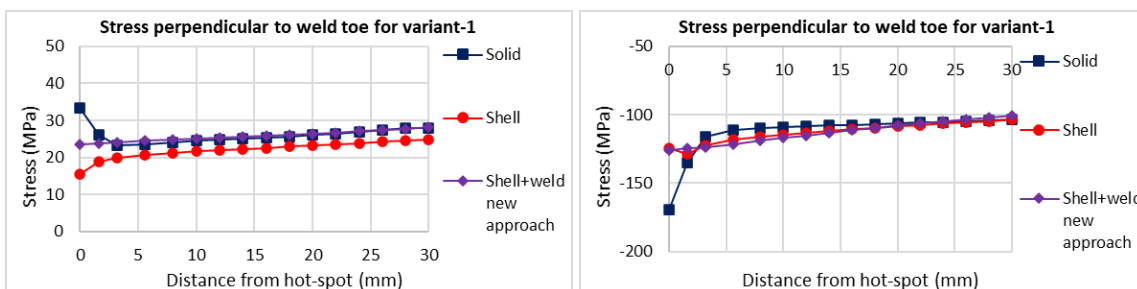


Figure K.3: Stress perpendicular to weld toe for maximum SHSS (left) and minimum SHSS (right) in stiffener for axle load path 1 of variant 1 with new approach of weld modelling

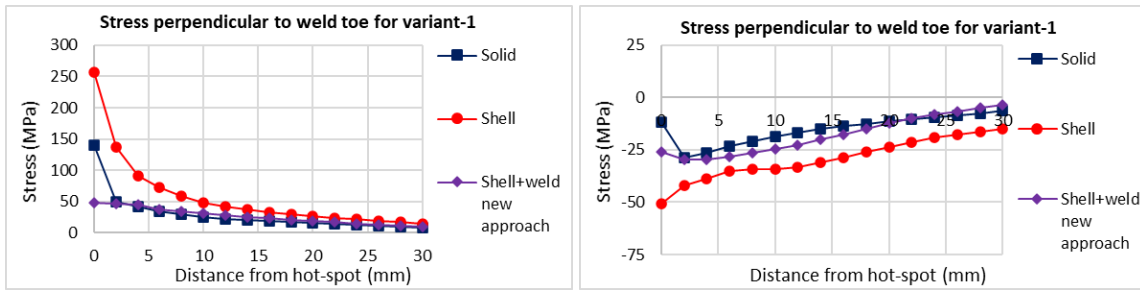


Figure K.4: Stress perpendicular to weld toe for maximum SHSS (left) and minimum SHSS (right) in crossbeam for axle load path 2 of variant 1 with new approach of weld modelling

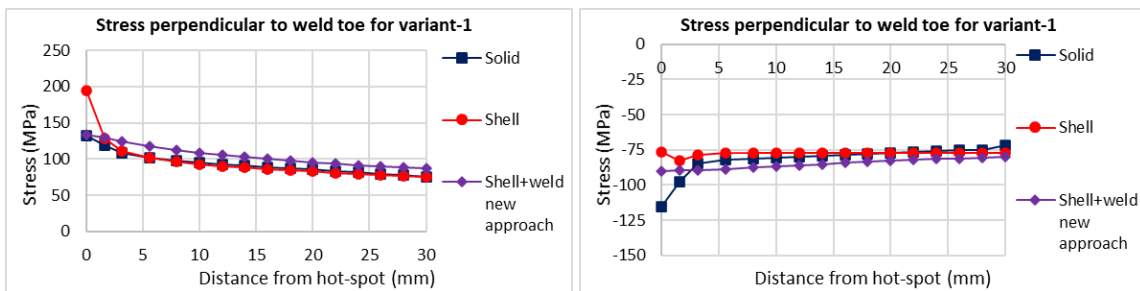


Figure K.5: Stress perpendicular to weld toe for maximum SHSS (left) and minimum SHSS (right) in stiffener for axle load path 2 of variant 1 with new approach of weld modelling

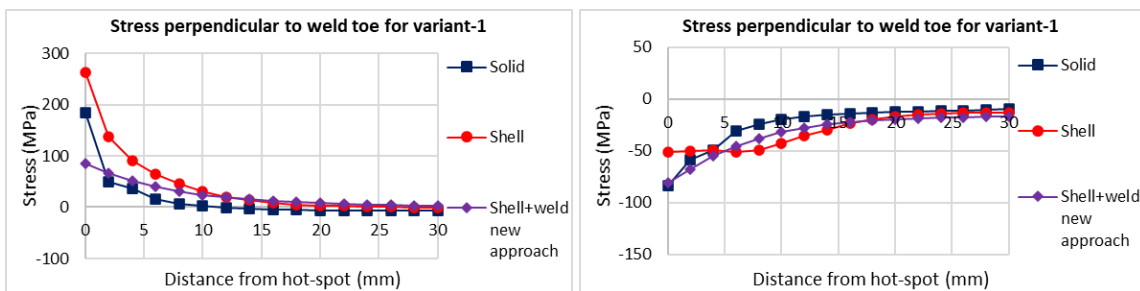


Figure K.6: Stress perpendicular to weld toe for maximum SHSS (left) and minimum SHSS (right) in crossbeam for axle load path 3 of variant 1 with new approach of weld modelling

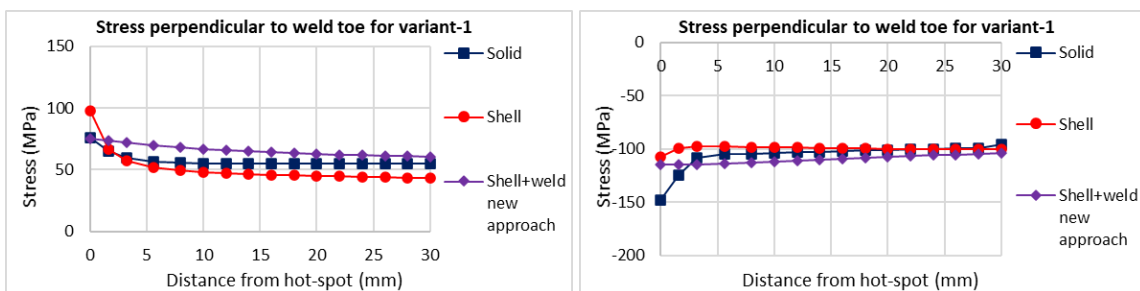


Figure K.7: Stress perpendicular to weld toe for maximum SHSS (left) and minimum SHSS (right) in stiffener for axle load path 3 of variant 1 with new approach of weld modelling

Heavy OSD variant: The stress profiles of the critical points from three transverse axle load positions of the heavy OSD variant are shown in Figures K.8-K.13.

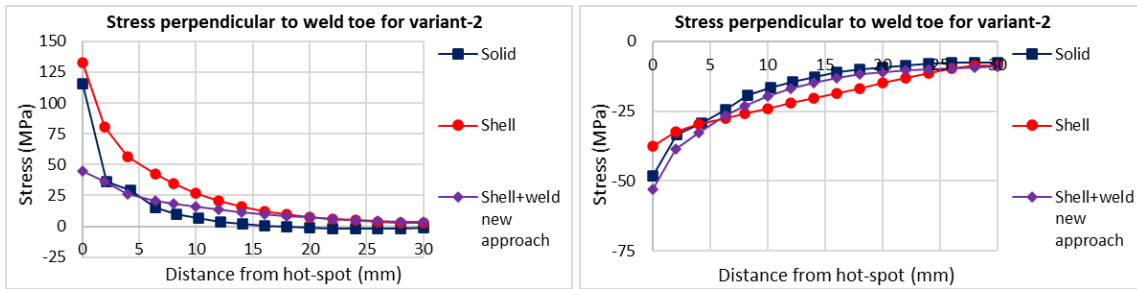


Figure K.8: Stress perpendicular to weld toe for maximum SHSS (left) and minimum SHSS (right) in crossbeam for axle load path 1 of variant 2 with new approach of weld modelling

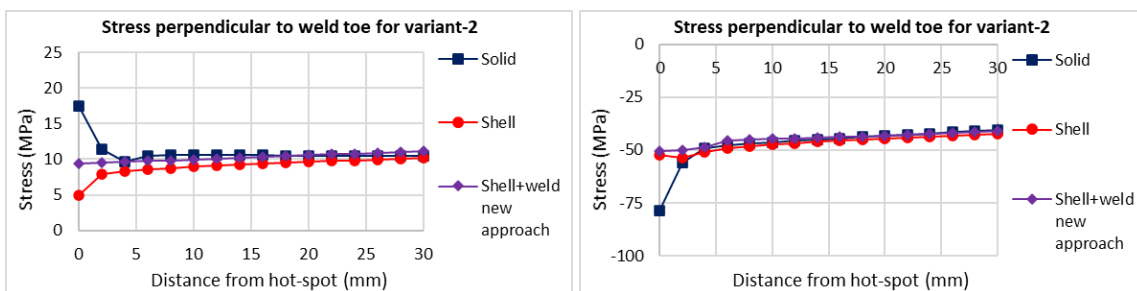


Figure K.9: Stress perpendicular to weld toe for maximum SHSS (left) and minimum SHSS (right) in stiffener for axle load path 1 of variant 2 with new approach of weld modelling

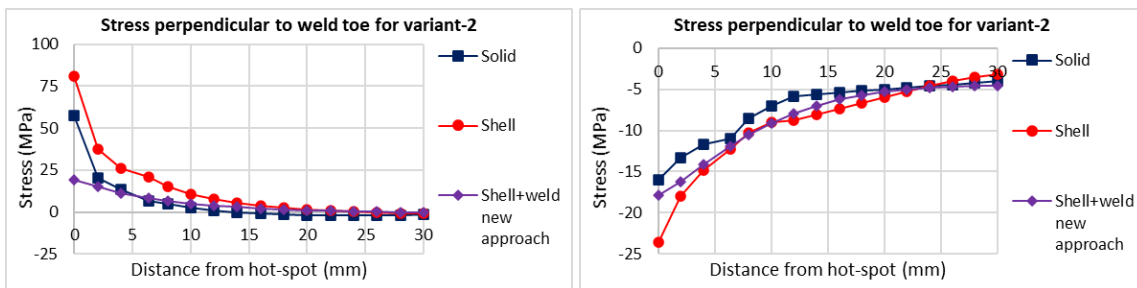


Figure K.10: Stress perpendicular to weld toe for maximum SHSS (left) and minimum SHSS (right) in crossbeam for axle load path 2 of variant 2 with new approach of weld modelling

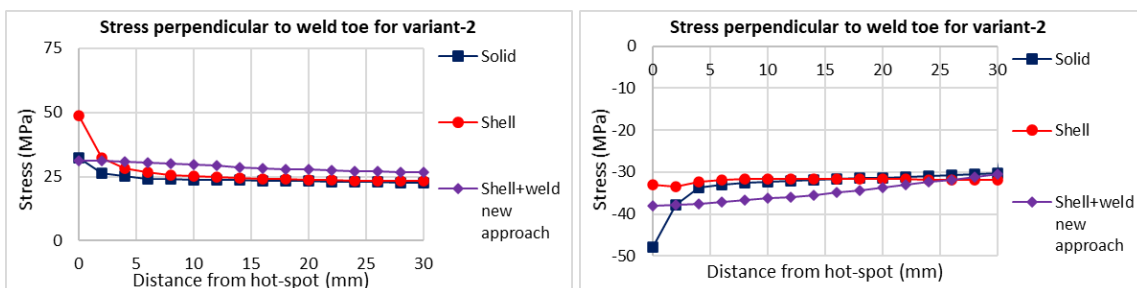


Figure K.11: Stress perpendicular to weld toe for maximum SHSS (left) and minimum SHSS (right) in stiffener for axle load path 2 of variant 2 with new approach of weld modelling

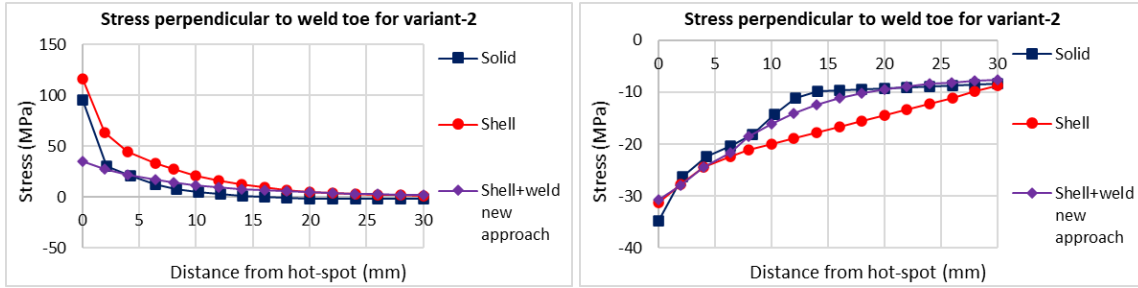


Figure K.12: Stress perpendicular to weld toe for maximum SHSS (left) and minimum SHSS (right) in crossbeam for axle load path 3 of variant 2 with new approach of weld modelling

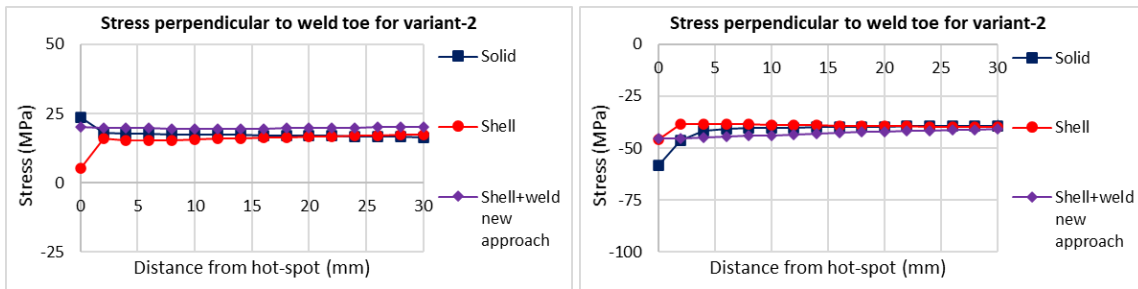


Figure K.13: Stress perpendicular to weld toe for maximum SHSS (left) and minimum SHSS (right) in stiffener for axle load path 3 of variant 2 with new approach of weld modelling

K.2. Tabulated results

From Table K.1, it can be seen that the shell model with welds modelled with the new approach is always conservative compared to the solid model in terms of SHSS for the light variant OSD.

Table K.1: SHSS ratio using the new approach of weld modelling with shell elements for variant-1

OSD Variant	Numerical Model	Axle load path 1				Axle load path 2				Axle load path 3			
		Crossbeam		Stiffener		Crossbeam		Stiffener		Crossbeam		Stiffener	
		Maxima	Minima	Maxima	Minima	Maxima	Minima	Maxima	Minima	Maxima	Minima	Maxima	Minima
Variant 1 (Light OSD)	Solid	72.32	-86.02	22.78	-120.44	53.03	-31.56	114.54	-87.53	58.01	-68.54	62.23	-111.44
	Shell+weld new approach	88.22	-93.44	23.59	-126.57	53.51	-33.42	132.47	-90.74	68.67	-70.79	74.74	-115.72
	Ratio	1.22	1.09	1.04	1.05	1.01	1.06	1.16	1.04	1.18	1.03	1.20	1.04

From Table K.2, it can be seen that the shell model with welds modelled with the new approach is always conservative compared to the solid model in terms of SHSS for the heavy variant OSD.

Table K.2: SHSS ratio using the new approach of weld modelling with shell elements for variant-2

OSD Variant	Numerical Model	Axle load path 1				Axle load path 2				Axle load path 3			
		Crossbeam		Stiffener		Crossbeam		Stiffener		Crossbeam		Stiffener	
		Maxima	Minima	Maxima	Minima	Maxima	Minima	Maxima	Minima	Maxima	Minima	Maxima	Minima
Variant 2 (Heavy OSD)	Solid	24.76	-33.32	9.15	-51.19	11.59	-14.75	26.06	-34.78	20.57	-27.40	17.88	-42.52
	Shell+weld new approach	28.13	-36.30	9.34	-51.24	12.37	-15.69	31.33	-38.36	23.98	-28.73	19.90	-45.80
	Ratio	1.14	1.09	1.02	1.00	1.07	1.06	1.20	1.10	1.17	1.05	1.11	1.08

The mean value of SHSS ratio for crossbeam is **1.10** and for stiffener is **1.09**. The coefficient of variation (CV) of the SHSS ratios is **5.9%** for crossbeam and **6.4%** for stiffener. Thus, it can be concluded that with this approach of weld modelling, the SHSS values obtained is consistent with that from solid model.

Bibliography

- [1] Guide for fatigue strength assessment of tankers, part 3 steel vessel rules. american bureau of shipping, new york. *American Bureau of Shipping (ABS)*, 1992.
- [2] Eurocode 3: Design of steel structures – part 1-9 fatigue. *Eurocode 3 (EN-1993-1-9)*, 2005.
- [3] Fatigue design of offshore steel structures, recommended practice. *Det Norske Veritas (DNV-RP-C203)*, 2011.
- [4] Eurocode 3: Actions on structures, part 2: Traffic loads on bridges. *Eurocode 3 (EN-1991-2)*, 2012.
- [5] Manual for design, construction and maintenance of orthotropic steel deck bridges. *US Department of Transportation, Federal Highway Administration*, 2012.
- [6] Fatigue assessment of ship structures, recommended practice. *Det Norske Veritas and Germanischer Lloyd (DNVGL (DNVGL-CG-0129))*, 2016.
- [7] Plan of approach for the strain gauge measurements for the haringvliet bridge. *PvA Rekmetingen document, Project: Haringvlietbrug, Client: Rijkswaterstaat*, 2016.
- [8] Abaqus version 2019. *Dassault Systèmes Simulia Corp., Providence, RI, USA*, 2019.
- [9] F. Z. Akhlaghi. Fatigue life assessment of welded bridge details using structural hot spot stress method. *MSc Thesis. Chalmers University of Technology, Sweden*, 2009.
- [10] F. Z. Akhlaghi, M. Al-Emrani, L. Fryba, and S. Urushadze. Fatigue testing and analysis of an orthotropic bridge welded detail using structural hot-spot stress method. *Fatigue Design. Chalmers University of Technology, Gothenburg, Sweden and Institute of Theoretical and Applied Mechanics (ITAM), Prague, Czech Republic*, 2009.
- [11] H. Al-Karawi, A. Manai, and M. Al-Emrani. Fatigue life extension of welded structures by peening and tig dressing - literature review for the state of the art. *Department of architecture and Civil Engineering, Structural Engineering division, Chalmers University of Technology Gothenburg, Sweden*, 2019.
- [12] M. Aygül. Fatigue analysis of welded structures using the finite element method. *International Journal of Fatigue*, 2012.
- [13] M. Aygül and M. Al-Emrani. Fatigue design of steel and composite bridges. *Technical report. Chalmers University of Technology Göteborg, Sweden*, 2014.
- [14] M. Aygül, M. Al-Emrani, and S. Urushadze. Modelling and fatigue life assessment of orthotropic bridge deck details using fem. *International Journal of Fatigue*, 40:129–142, 2012.
- [15] H. Backer. Chapter 22 - orthotropic steel decks. *Innovative Bridge Design Handbook*, 2016.
- [16] P. Beld. Improvements for the prediction of the fatigue life of the deck plate in orthotropic steel decks - a design optimization study. *Master thesis, Delft University of Technology*, 1997.
- [17] P. Dong. A structural stress definition and numerical implementation for fatigue analysis of welded joints. *International Journal of Fatigue* 23 865–876, 2001.
- [18] P. Dong. A robust structural stress method for fatigue analysis of offshore/marine structures. *Journal of Offshore Mechanics and Arctic Engineering*, 2004. doi: 10.1115/1.1854698.

- [19] D.van der Ende. Finite element analysis of the closed stiffener to crossbeam connection in osds using the hot spot stress approach. *MSc thesis, Department of Structural Engineering, Delft University of Technology*, 2020.
- [20] Å. Eriksson, A. M. Lignell, and H. Olsson, C. Spennare. Weld evaluation using fem - a guide to fatigue-loaded structures. *Industrilitteratur AB, Gothenburg, Sweden*, 2003.
- [21] J.L. Fayard, A. Bignonnet, and K. D. Van. Fatigue design criterion for welded structures. *Fatigue & Fracture of Engineering Materials & Structures*, vol. 19, no. 6, pages 723–729, 1996.
- [22] J.W. Fisher and C.C. Menzemer. Fatigue cracking in welded steel bridges. *Transportation Research Board*, pages 111–117, 1990. doi: 10.1061/(ASCE)0733-9445(1992)118:2(582).
- [23] W. Fricke. Recommended hot spot analysis procedure for structural details of fpso's and ships based on round-robin fe analyses. *International Journal of Offshore and Polar Engineering*, 12: 1–8, 2001.
- [24] W. Fricke, H. Petershagen, and H. Paetzold. Fatigue strength of ship structures. *GL-Technology, 1/1998, Germanischer Lloyd, Hamburg, Germany*, 1998.
- [25] L. Fryba and L. Gajdos. Fatigue properties of orthotropic decks on railway bridges. *Institute of Theoretical and Applied Mechanics, Academy of Sciences of the Czech Republic*, 1997.
- [26] J. Gustafsson and J. Saarinen. Multi-axial fatigue in welded details - an investigation of existing design approaches. *MSc thesis, Department of Structural Engineering, Chalmers University of Technology, Goteborg Sweden*, 2007.
- [27] M. Heshmati. Fatigue life assessment of bridge details using finite element method. *Masters thesis. Chalmers University of Technology, Gothenburg, Sweden*, 2012.
- [28] A. Hobbacher. Iiw document iiw-1823-07, recommendations for fatigue design of welded joints and components. *International Institute of Welding (IIW) document*, 2008.
- [29] D. Hutton. *Fundamentals of Finite Element Analysis*. First edition, the mcgraw-hill companies inc, us. edition, 2004.
- [30] K. Jent, R. Bez, E. Bruhwiler, M. Hirt, and J. Vorstenbosch-Krabbe. Fatigue resistance of orthotropic steel bridge decks with open ribs. *Swiss Federal Institute of Technology, Lausanne, ICOM-Steel Structures*, 1995.
- [31] B. Karabulut, G. Lombaert, D. Debruyne, and B. Rossi. Experimental and numerical fatigue assessment of duplex welded transversal stiffeners. *International journal of Fatigue 134 (2020) 105498*, 2020. doi: doi.org/10.1016/j.ijfatigue.2020.105498.
- [32] M. Kolstein. Fatigue classification of welded joints in orthotropic steel bridge decks. *Delft University of Technology, Delft: PhD Thesis*, 2007.
- [33] H. Kyuba and P. Dong. Equilibrium-equivalent structural stress approach to fatigue analysis of a rectangular hollow section joint. *International Journal of Fatigue 27 85–94*, 2005.
- [34] J.S. Leendertz. Fatigue behaviour of closed stiffener to cross beam connections in orthotropic steel bridge decks. *PhD Thesis. Delft University of Technology*, 2008.
- [35] J. Maljaars, H. Kolstein, and F.v. Dooren. Fatigue assessment for deck plates in orthotropic bridge decks. *Steel Construction 5*, 2012.
- [36] G. Marquis and J. Samuelsson. Modelling and fatigue life assessment of complex structures. *Materialwissenschaft und Werkstofftechnik*, pages 678–684, 2005. doi: 36(11).
- [37] C. Miki and K. Tateishi. Fatigue strength of cope hole details in steel bridges. *Department of Civil Engineering, Tokyo Institute of Technology*, 1997.
- [38] E. Niemi. Stress determination for fatigue analysis of welded components. 1995.

- [39] E. Niemi. Stress determination for fatigue analysis of welded components. *The International Institute of Welding*, 1995. doi: IIWdoc.IIS/IIW-1221-93.
- [40] E. Niemi, W. Fricke, and S.J. Maddox. Structural hot-spot stress approach to fatigue analysis of welded components- designers guide. *International Institute of Welding (IIW) document*, 2016.
- [41] N. et al Osawa. Study on the preciseness of hot spot stress of web-stiffened cruciform welded joints derived from shell finite element analyses. *Marine Structures 24, Elsevier Ltd.*, 2011.
- [42] I. Poutiainen, P. Tanskanen, and G. Marquis. Finite element methods for structural hot spot stress determination - a comparison of procedures. *International journal of fatigue*, 2004. doi: 26(11): 1147–1157.
- [43] E.P. Swierstra. Fatigue assessment in finite element analysis – a post-processor to fea output for hot spot stress calculation. *MSc thesis. Delft University of Technology. The Netherlands*, 2017.
- [44] P. Wang, X. Pei, P. Dong, and S. Song. Traction structural stress analysis of fatigue behaviors of rib-to-deck joints in orthotropic bridge deck. *International Journal of Fatigue*, 2019. doi: 125(2019) 11-12.
- [45] R. Wolchuk. Steel orthotropic decks: Developments in the 1990s. *Transportation Research Board*, pages 30–37, 1999.
- [46] R. Wolchuk and A Ostapenko. Secondary stresses in closed orthotropic deck ribs at floor beams. *J. Structural Engineering*, pages 582–595, 1992. doi: 10.1061/(ASCE)0733-9445(1992)118: 2(582).
- [47] W. Wu, H. Kolstein, M. Veljkovic, R. Pijpers, and J. Vorstenbosch-Krabbe. Fatigue behaviour of the closed rib to deck and crossbeam joint in a newly designed orthotropic bridge deck. *CE/papers*, 1(2-3):2378–2387, 2017. doi: org/10.1002/cepa.285.
- [48] Z.G. Xiao and K. Yamada. A method of determining geometric stress for fatigue strength evaluation of steel welded joints. *International journal of fatigue*, 2004. doi: 26(12):1277–1293.
- [49] H. Yang, H. Qian, P. Wang, and P. Dong. Analysis of fatigue behaviour of welded joints in orthotropic bridge deck using traction structural stress. *Research Article: Structural Integrity and Lifetime Prediction of Engineering Materials and Structures*, 2019.
- [50] K. Yokozeki and C. Miki. Fatigue evaluation for longitudinal-to-transverse rib connection of orthotropic steel deck by using structural hot spot stress. *International Institute of Welding*, 2015.
- [51] K. Yokozeki and C. Miki. Fatigue assessment of various types of longitudinal-transverse rib connection in orthotropic steel decks. *International Institute of Welding*, 2017.
- [52] U. Zerbst, M. Madia, and D. Hellmann. An analytical fracture mechanics model for estimation of s–n curves of metallic alloys containing large second phase particles. *Engineering Fracture Mechanics*, pages 115–134, 2012.
- [53] S. Zhang, X. Shao, J. Cao, J. Cui, J. Hu, and L. Deng. Fatigue performance of a lightweight composite bridge deck with open ribs. *American Society of Civil Engineers*, 2016. doi: 10.1061/(ASCE)BE.1943-5592.0000905.
- [54] K. Śledziewski. Fatigue assessment for selected connections of structural steel bridge components using the finite elements method. *1Faculty of Civil Engineering and Architecture, Lublin University of Technology, Nadbystrzycka 40, 20-618 Lublin, Poland*, 2017.
- [55] K. Śledziewski. Numerical investigation of the cope hole shape impact on fatigue life of welded joints in steel bridges. *Department of Road and Bridges, Faculty of Civil Engineering and Architecture, Lublin University of Technology*, 2019.